Fluorescence close to Dielectric Interfaces

Dissertation zur Erlangung des akademischen Grades des Dr. rer. nat.

im Fachbereich Physik der Johannes Gutenberg-Universitaet Mainz

vorgelegt von

Andrea Pomozzi

geboren in Viterbo, Italien

Mainz

July 2008

Dekan:

1. Gutachter:

2. Gutachter:

Diese Arbeit wurde in der Zeit von Mai 2005 bis Juni 2008 am Max-Planck-Institut fuer Polymerforschung in Mainz angefertigt.

The work for this dissertation was carried out between May 2005 and June 2008 at the Max-Planck-Institute for Polymer Research in Mainz (Germany).

"*I have fought the good fight,*

I have finished my race,

I have kept the faith.

Now there is in store for me the crown of righteousness [...]"

Paul of Tarsus (8-67 a.C.)

Contents

Chapter 1

Introduction

Local field effects play a major role in the interaction of light with condensed matter and represent the connection point between macroscopic and microscopic electromagnetic phenomena. Classical calculations of the local field effects are based on a "dipole-like" description of the matter, considering a spherical cavity around each dipole (i.e. molecule) inside the dielectric and calculating the interaction of such a structure with the external field [1]. The cavity size is always assumed large with respect the molecular dimensions but small with respect the wavelength involved, while the material outside the cavity is considered as a homogeneous dielectric. The resulting Clausius-Mosotti model contains an unspecified parameter constituted by the spherical cavity radius [8], which could be determined in principle by experimental data [3]. Moreover the choice about the inside of such cavity is still a matter of debate nowadays [4], still no clear experimental evidence supporting the virtual cavity model (macroscopic field undisturbed by the cavity) or the real cavity model (empty spherical cavity) [5] is available. Spontaneous emission in dielectrics was investigated to discriminate among different local-field corrections and most experimental data support so far the real cavity approach [6], [7]. In these two studies, the radiative decay rate of an europium complex was studied as function of the host refractive index, by changing the nature of the solvent [6] or the pressure of a dense supercritical CO_2 gas [7]. Based on these experiments, it seems to be generally accepted that when the emitter expels the dielectric molecule (substitutional case) the spontaneous emission decay rate obeys the real cavity model, while when the emitters act as interstitial ions in the dielectric lattice, then the virtual cavity applies [8], [9]. Finally the complete equivalence between the classical and quantum appraoch was proven analytically for emitters embedded in uniform, isotropic dielectric [10, 11] and near an absorbing dielectric surface [12].

Additional efforts come into play when a molecular probe is placed in proximity of a dielectric interface. Here a spherical cavity model may be not adequate to describe local fields effects, for distances comparable to the (unknown) cavity radius. Moreover, the electromagnetic boundary conditions impose a discontinuity for the normal component of the electric field (at charged dielectric interfaces) as a consequence of the vacuum fluctuations perturbations [19]. In this manner the spontaneous emission rate of an emitter nearby the dielectric interface is changed [6], with respect to case when an unbound, homogeneous medium is present. Purcell [20] was the first to notice that the spontaneous emission process was not an intrinsic property of the emitting system and from a classical point of view the presence of a dielectric interface can be seen as a way to modify the photonic mode density [21]. After pioneering experimental [22] and theoretical [23] works in the early seventies, a complete classical theory describing the fluorescence emission close to the interfaces was developed few years later by Chance, R. R., Prock A. and Silbey R. [24]. Important theoretical contributions came also by W. Lukosz and R. E. Kunz [25]. They developed the expressions for the total power radiated by magnetic

and electrical dipoles of arbitrary orientations, located in proximity of a plane interface. It's possible in fact to proof [26], that the total radiated power of any current distribution with harmonic time dependence (i.e. an oscillating dipole) has the identical expression than the spontaneous decay rate of a two-level quantum system. In this context the work of Lukosz and Kunz represented a milestone for any classical modelling of fluorescence.

Additional interest in fluorescence close to interfaces resulted from few works where the classical theory did not fit the experimental data. A.P. Alivisatos and coworkers found a non-classical behavior of the energy transfer from molecules to metal surfaces [27], while M. I. Sluch and his team detected an anomalous distance dependence of fluorescence lifetime from a semiconductor substrate [28]. Other authors needed to introduce the presence of a fictious selvedge region, in order to obtain satisfactory agreement between experimental and theoretical data [29]. Barnes reports a comprehensive and nice review [21] about the subject of fluorescence near dielectric interfaces and about the role of the the photonic mode density.

The advent of single molecule spectroscopy [30] opened a completely new field of investigations and again fluorescence close to planar interfaces attracted much attention [10], [9]. In these studies, single molecules polarized fluorescence provided information on the molecules orientation with respect to an interface. Single molecule spectroscopy of fluorescent dyes was used also to analyze local field effects in bulk. Recent studies from Vallee and coworkers showed fluctuations of the fluorescence lifetime for dye molecules embedded in polymer films [13, 14], which were attributed to density fluctuations of the surrounding polymer. In order to explain such fluctuations Vallee et al. proposed a microscopic model [15], where the emitter polarizability and the discrete structure of the polymer around the dye were taken in account. They suggest eventual discrepancies with the classical theory on the length scale of $\approx 2\,\mathrm{nm}$. Nevertheless when single molecules spectroscopy is applied to probe molecules nearby interfaces, difficulties come from the excitation of dipoles forming angles smaller than ≈ 30 degrees, with respect to the normal to the interface [6]. Moreover inevitable statistic limitations and blinking issues have to be taken in account.

In this work, the excited-state lifetimes and fluorescence intensities of an ensemble of dye molecules close to a dielectric interface were studied. Analogously to the established polarized fluorescence technique [20], the measurements were performed for several excitation-detection polarization combinations, by an "home made" surface plasmon fluorescence setup. A detection scheme was developed that enhances the difference among different polarizations, while photobleaching or blinking problems are avoided. To study the fluorescence characteristics of dyes in thin films, a new optical investigation method was introduced, called Polarization Combination Method (PCM). The PCM provides information about the micro-environment surrounding the dye and allows to determine the central photophysical parameters of surface bound dyes. In this way, averaged information on the local nano-environment surrounding the emitters was obtained, specifically close to the interface between two dielectric media. For the first time, the electric field discontinuity was experimentally probed in a few nanometres region across the interface. The systems investigated are constituted of different organic dyes deposited onto thin films or embedded in a matrix of polyelectrolytes. In general, polyelectrolytes provide an accurate thickness control down to few nanometres by the layer-by layer technique [33], an interface roughness of few nanometers [21, 30] and the possibilty of chain functionalization by chromophores. Moreover the polymer thickness and the chains conformations can be changed by varying parameters like pH [31, 37] or salt concentration [17, 44, 45], in the deposition solution. In such way the polyelectrolytes can be used as spacer or as host for the emitters and the fluorescence characteristics at the polymer-air interface can be studied, also as a function of the polymer chains conformation. The PCM was applied to dye molecules embedded in a thin polymer film ("in-polymer") and the calculated parameters were successively used to study the behaviour of the same dyes deposited as close as possible to the film's surface ("in-air").

In chapter 2 a description of the home-built experimental apparatus used for time resolved fluorescence measurements is given. The theory behind the numerical simulation is described in chapter 3, with details of the model and approximations used. In chapter 4, the PCM is described and applied to chromophores embedded in a polyelectrolytes matrix, at different distances from the air-polymer interface. Fluorescence characteristics of an ensemble of dyes deposited as close as possible to the surface of a thin polymer film is investigated in chapter 5.

Bibliography

[1] C. Kittel, *Introduction to Solid State Physics*, Ed. Wiley, New York, (1976).

[2] S. M. Barnett et al., *J. Phys. B: At. Mol. Opt. Phys.*, **29**, 3763-3781 (1996).

[3] S. Scheel et al., *Phys. Rev. A*, 60, No. 2, 1590 (1999).

[4] Chang-Kui Duan et al., *Physics Letters A*, **343**, 474-480 (2005).

[5] D. Toptygin, *J. of Fluorescence*, **13**, No. 3, 201 (2003).

[6] G. L. J. A. Rikken and Y. A. R. R. Kessener, *Phy. Rev. Lett.*, **74**, No. 6, 880 (1995).

[7] F. J. P. Schuurmans et al., *Phy. Rev. Lett.*, **80**, No. 23, 5077 (1998).

[8] P. de Vries and Ad Lagendijk, *Phy. Rev. Lett.*, **81**, No. 7, 1381 (1998).

[9] F. J. P. Schuurmans et al., *Physics Letter A*, **264**, 472-477 (2000).

[10] P. R. Berman and P. W. Milonni, *Phys. Rev. Lett.*, **92**, No. 5, 053601 (2004).

[11] Chang-qi Cao et al., *Physics Letters A*, **232**, 15-24 (1997).

[12] M. S. Yeung and T. K. Gustafson, *Phys. Rev. A*, Vol. **54**, No. 6, 5227 (1996).

[13] R.A.L. Vallee et al., *Chem. Phys. Lett.*, **372**, 282-287 (2003).

[14] R.A.L. Vallee et al., *Phys. Rev. Lett.*, **91**, No. 3, 038301 (2003).

[15] R.A.L. Vallee et al., *Chem. Phys. Chem.,* **6**, 81-91 (2005).

[16] R.A.L. Vallee et al., *Chem. Phys. Lett.,* **348**, 161-167 (2001).

[17] N. Danz et al., *Phys. Rev. A*, **66**, 063809 (2002).

[18] B. Valeur, *Molecular Fluorescence*, Wiley-VCH (2002).

[19] H. Khosravi and R. Loudon, Proceedings: Mathematical and Physical Sciences, Vol. 433, Issue 1888, 337-352 (1991).

[20] E. M. Purcell, *Phys. Rev.*, **69**, 681 (1946).

[21] Barnes W.L., *J. Mod. Opt.*, vol. **45**, no. 4, 661-699 (1998).

[22] Drexhage, K. H., *Prog. Optics*, **12**, 165 (1974).

[23] Kuhn, H., *J. Chem. Phys.*, **53**, 101 (1970).

[24] Chance, R. R., Prock A. and Silbey R., *Adv. Chem. Phys.*, **37**, 1 (1978).

[25] Lukosz W. and Kunz R. E., *J. Opt. Soc. Am.*, Vol. **67**, No. 12, December (1977), pagg. 1607-1615.

[26] Novotny L., Hecht B., *Principles of Nano-Optics*, Cambridge Univ. Press (2006).

[27] A.P. Alivisatos et al., *J. Chem Phys.*, **82**, 541 (1985).

[28] M. I. Sluch et al., *Physics Letters A*, 200, 61-64 (1995).

[29] F. Balzer et al., *Optics Letter*s, Vol. 22, No. **16**, 1262 (1997).

[30] W. P. Ambrose et al., *J. Chem Phys.*, **95**, 7150 (1991).

[31] J. J. Macklin, J. K. Trautman, T. D. Harris, and L. E. Brus, *Science,* **272**, 255 (1996).

[32] Kreiter M. et al., *J. Chem. Phys.*, vol. 117, **20**, (2002).

[33] G. Decher, J. D. Hong and J. Schmitt, *Thin Solid Films*, **210/211** 831-835 (1992).

[34] Y. Lvov et al., *Langmuir*, **9**, 481-486 (1993).

[35] Loesche et al. *Macromolecules*, Vol. 31, No. **25**, 8893 (1998).

[36] J. Choi and Michael F. Rubner, *Macromolecules*, **38**, 116-124 (2005).

[37] S. S. Shiratori and M. F. Rubner*, Macromolecules*, **33**, 4213-4219 (2000).

[38] H.G.M. van de Steeg et al., *Langmuir*, **8**, 2538-2546 (1992).

[39] S. A. Sukhishvili and S. Granick, *J. Chem. Phys.*, vol. 109, No. **16**, (1998).

[40] C.C. Buron et al., *J. Colloid and Interface Science*, **314**, 358-366 (2007).

Chapter 2

Experimental Apparatus

Time resolved fluorescence measurements in the far field were performed by a custom experimental apparatus, built following the concept of a Surface Plasmon Resonance (SPR) equipment, in the so called Kretschmann configuration [1]. The components were assembled onto an optical breadboard, with the sample holder and the detector placed within a metal "black-box", to reduce the background. The area containing the laser source and the required optics for chromophores excitation have been placed externally the "black-box". The laser beam impinged onto the sample through a $\sim 2\,\mathrm{cm}$ opening of a laser line filter (see figure 2.1.1 a)). A system of flipping mirrors and a $He-Ne$ laser were also installed for the optical alignment of the excitation and the detection devices. A diode laser at $532\,\mathrm{nm}$ was used for sample alignment to avoid chromophores photobleaching during this operation (dyes used through this work absorb mainly in the red region).

The electronic devices and the computer controlling excitation and detection processes were arranged in a separate rack, as it possible to see in picture 2.1.1 a). Figure 2.1.1 b) shows the optical components utilized for setup alignment and excitation, while in 2.1.1 c) images of the goniometer, sample holder and detector are reported. A sketch of the experimental setup with the optical paths is depicted in figure 2.1.2.

2.1 Excitation Source

The excitation source is constituted of an Hamamatsu high repetition picosecond light pulser (Model PLP10), with a laser diode head at wavelength $634\,\mathrm{nm}$ (M8903 PLP10-063) and a controller box (C8898).

Semiconductor lasers have usually wide angular spread and rectangular shaped emission beam (as it was verified experimentally). Besides collimation problems, this may bring difficulties in the theoretical simulation of the experiment. For this reason the LED laser source was coupled into a single mode fibre (Laser Components GmbH, model no. HCG200-ZZZZSS-FF-001.0) by a fiber coupler (New Focus, Mod. No. 9091-M) to obtain a narrow, collimated, Gaussian-shaped laser pulse, out of the fiber. Several single mode optical fibers from different manufacturers were tested, with different core diameters and materials, in order to obtain a point-like source and at the same time the highest possible output power. The fiber end was then set in the focus of a microscope objective lens (10X, 0.25, Spindler & Hoyer) and a collimated parallel beam (on the lenght scale of few metres) was obtained (diameter $\lesssim 5\,\mathrm{mm}$).

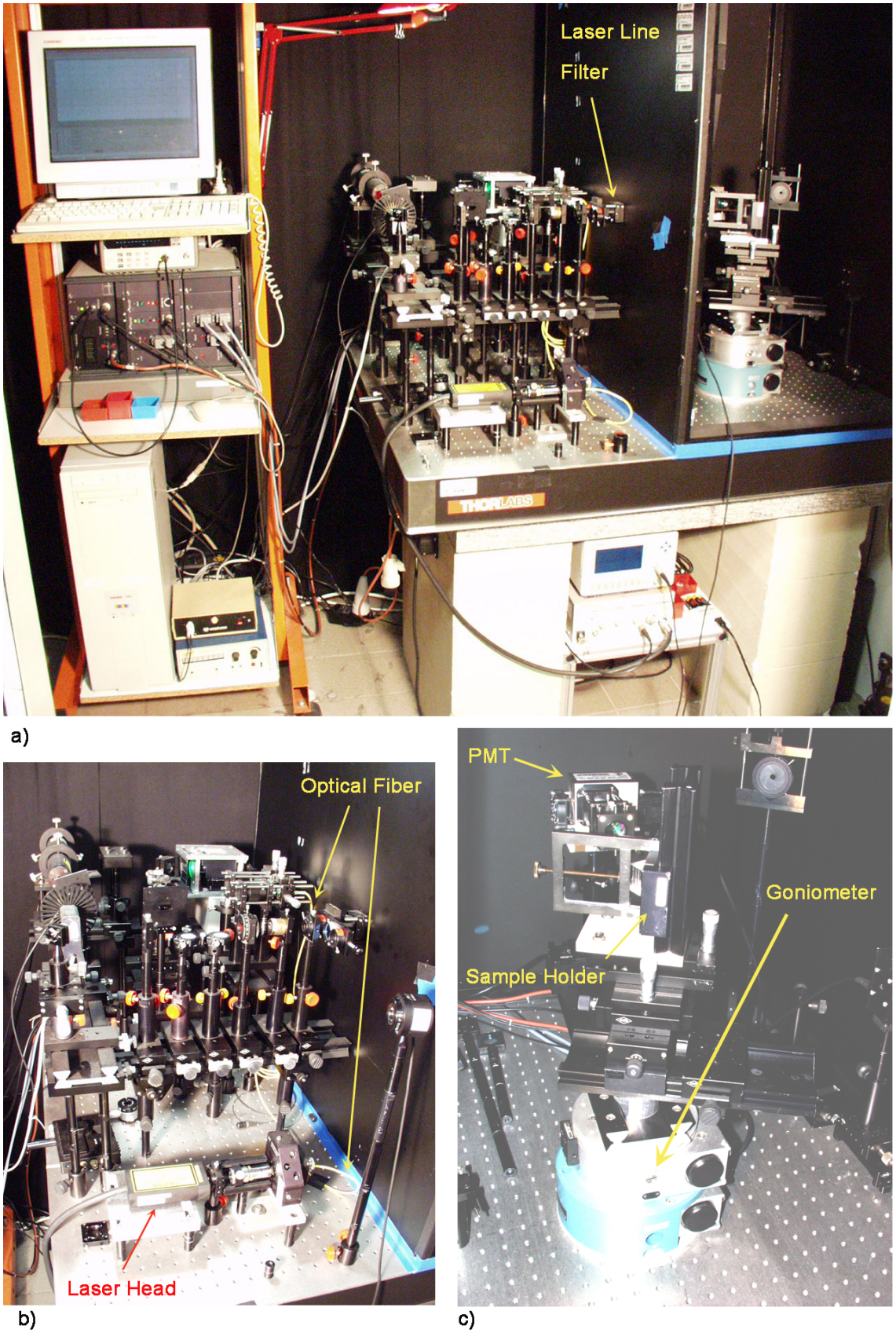

Figure 2.1.1: a) Overview of the designed experimental setup, with the electronic for goniometer motors and the controlling computer cards (left). b) Detail of the optics utilized for sample alignment and excitation. c) Overview of the goniometer, with the sample holder and the PMT.

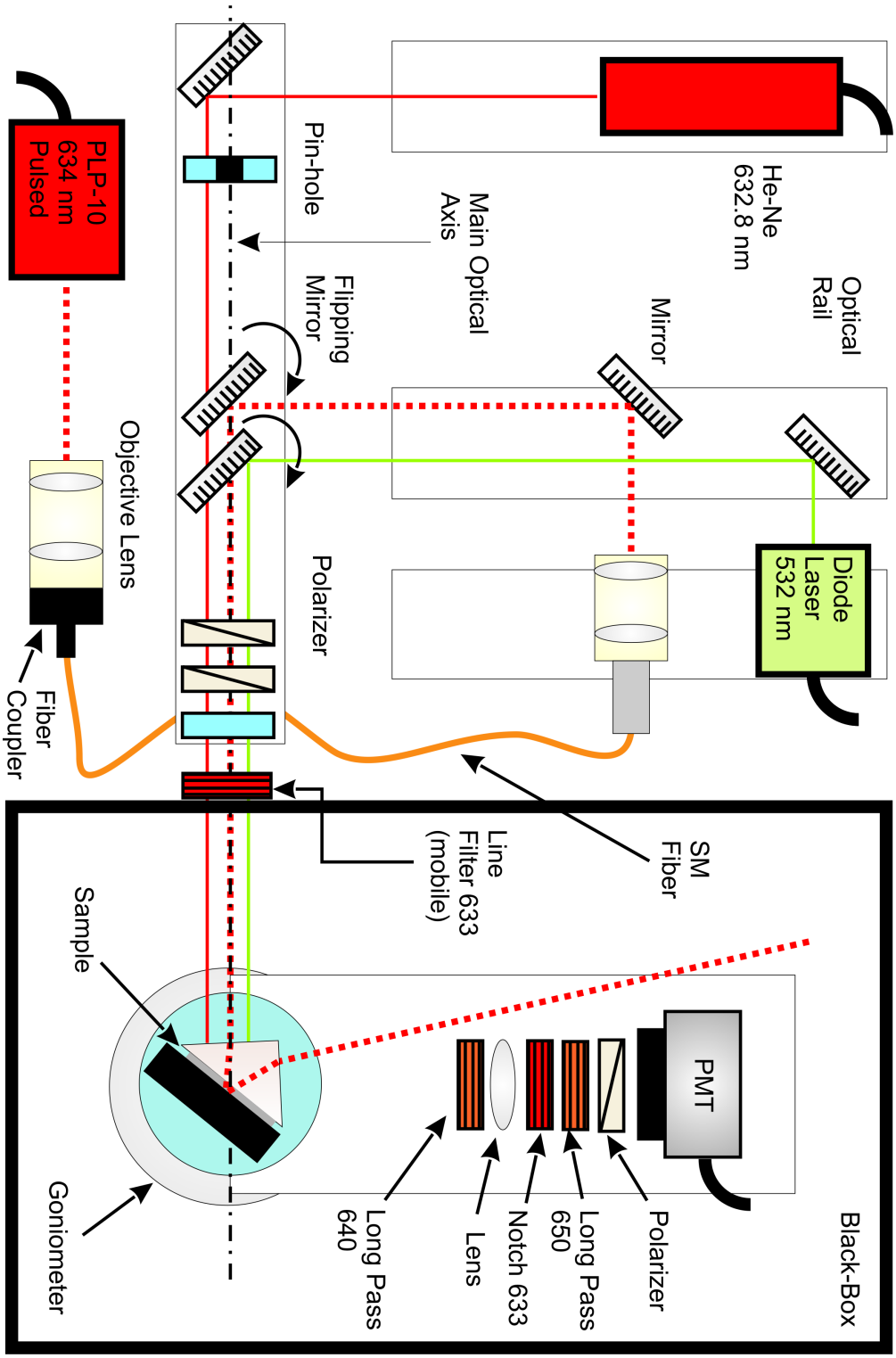

Figure 2.1.2: Simplified sketch of the custom experimental setup utilized for time resolved fluorescence measurements. In the drawing, the optical path used for the measurements is indicated by the red dotted line. The red and green lines represent the optical paths used respectively for optics and sample alignment (they are shifted from the main optical axis only for clarity reasons).

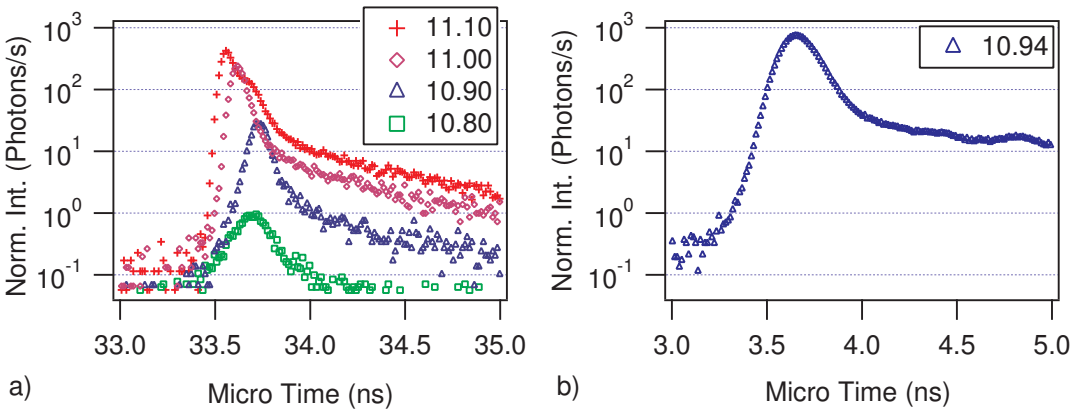

Figure 2.1.3: a) Pulse shape of the Hamamatsu PLP10 in time, as a function of the controller output power (power knob values in the legend), for a repetition rate of 20 MHz. The wavelength of the laser diode head was of 634 nm (M8903 PLP10-063). The measured FWHM values are ~ 90 ps, ~ 80 ps, ~ 86 ps and ~ 160 ps, respectively for power settings of 11.10, 11.00, 10.90 and 10.80. The test was performed by an APD detector (id100, id-Quantique SA). b) Hamamatsu PLP10 pulse shape in time, for a repetition rate of 20 MHz and power setting 10.94, as used in the experiments. The measured FWHM is ~ 195 ps, determined by a fast photomultiplier (PMC-100, Becker & Hickl GmbH).

The laser controller can provide several excitation frequencies and output powers, but the pulse shape is strongly dependent on these two parameters and the FWHM values change accordingly. The presence of a "tail" in the instrument response function is detected for higher excitation intensities, as a consequence of a broader laser pulse [2] and of the detector afterpulsing [5] (see figure 2.1.3 a). Real pulse width is an important variable in the instrument response function and for broader pulses, the influence of excitation on fluorescence decay signal is stronger[1]. The chosen repetition rate for measurements was 20 MHz, providing a time window between pulses of 50 ns, while the expected excited state lifetime for these dyes is on the time scale of few ns. After the frequency selection, a compromise between maximum excitation intensity and FWHM was reached by several tests, with a power setting of 10.94 for the laser controller knob (see figure 2.1.3 b). The time FWHM of the laser beam shape was measured as high as ~ 195 ps, while the wavelength tolerance is $< \pm 10$ nm and the spectral half-width < 5 nm, as provided by the manufacturer [3]. By using a linear polarizer (B. Halle) and a 633 nm line filter (MaxLineâ„¢ Laser-line Filter, SEMROCK Inc., part no. LL01-633-12.5), the detected power at the sample site resulted to be as high as $\sim 20 - 30\,\mu$W. The same power for *p*-polarized and *s*-polarized excitation radiation was approximatively achieved, by taking advantage of the birefringence phenomenon inside the fiber (i.e. changing the position of the fiber body). The incident power was recorded, for each excitation-detection polarization combination, by a digital power meter (Newport GmbH, Single-Channel, Model No. 1930-C, detection head 918-SL).

2.2 Excitation-Detection Scheme

The excitation beam was impinging the sample surface with an angle of 39.37Â° (θ_{ex} in figure 2.2.1), by passing through a linear polarizer and a 633 nm laser-line filter (MaxLineâ„¢ Laser-line Filter, SEMROCK, part no. LL01-633-12.5). The detector had a 90Â° inclination respect the laser beam

[1]The ideal excitation pulse has a "δ-like" character and this approximation will be used through all the theoretical calculations for simulation of the experiments.

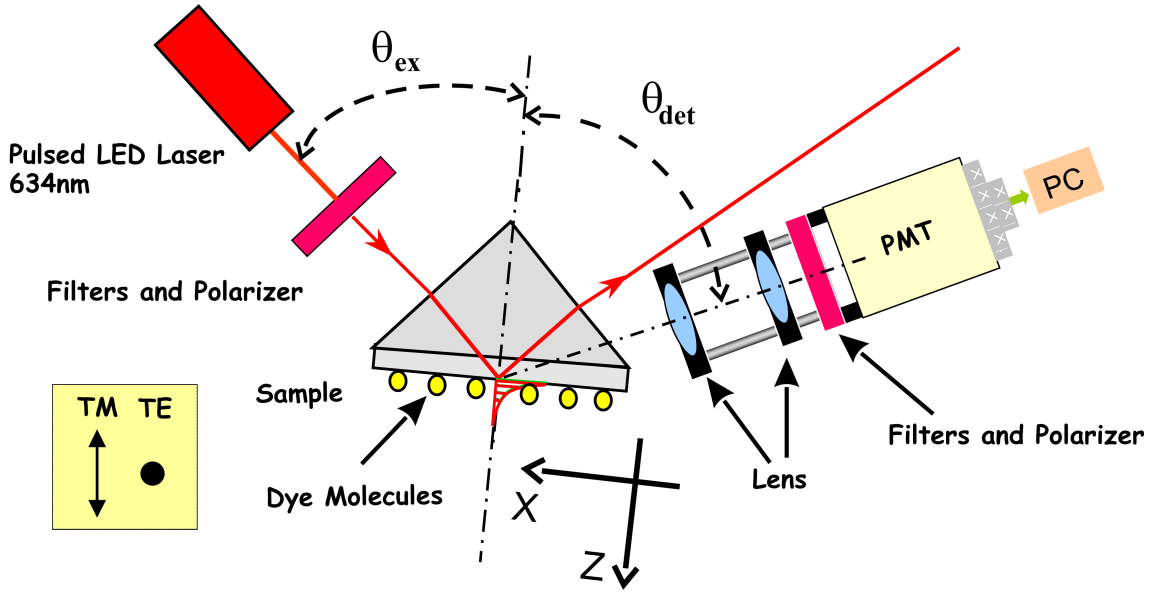

Figure 2.2.1: Schematic representation of the most general configuration for the measurements set-up. Indication of the electric field polarization modes TM and TE is reported, the plane of incidence is represented by the (x,z) plane.

to avoid direct reflection and maximize fluorescence collection (detection angle $\theta_{det} = 50.63$Â° in figure 2.2.1). The samples were constituted of polymer films with organic dyes deposited on top or embedded, supported by a fused silica substrate (as described in chapters 4 and 5). The glass slide was successively coupled, by the blank side, to a 90Â° fused silica prism (Melles Griot, no. 01PQB002, A = B = C = 25.4 mm), making use of a non-fluorescent immersion oil[2] (n = 1.515, Type NF550-NIKON Inc.). By this geometry the samples were excited with the evanescent wave of the local electric field at glass-air interface. θ_{ex} and θ_{det} were determined by the theoretical considerations reported in section 4.4 (chapter 4).

Briefly summarizing: the choice of the geometry came from an optimization of the excitation and detection electric field components. In this way, for lifetimes and intensities of an ensemble dye molecules, it was possible to enahnce the differences among different excitation-detection polarization combinations.

2.3 Detection System

A fast photo multiplier cooled with a Peltier system (PMC-100-20, Becker & Hickl GmbH) was used as detector. The PMT was driven by a computer card (DCC-100 Becker & Hickl GmbH) and controlled by a software (Detector Control Card, Vers. 1.23, Becker & Hickl GmbH). The detector nominal time resolution is around 200 ps and the measured dark count rate, after 10 minutes of cooling (regime condition), was $\sim$ 140 counts/s. The "high-voltage gain" parameter for the PMT was set at 85%, for all the measurements.

To avoid scattered light and maximize the signal to background ratio, a 633 nm Notch Filter (StopLineâ„¢ Notch Filters, SEMROCK Inc., part no. NF01-633U-25), coupled to a 650 nm long pass

[2]This particular immersion oil used for optical microscopy was chosen for its properties of low background fluorescence.

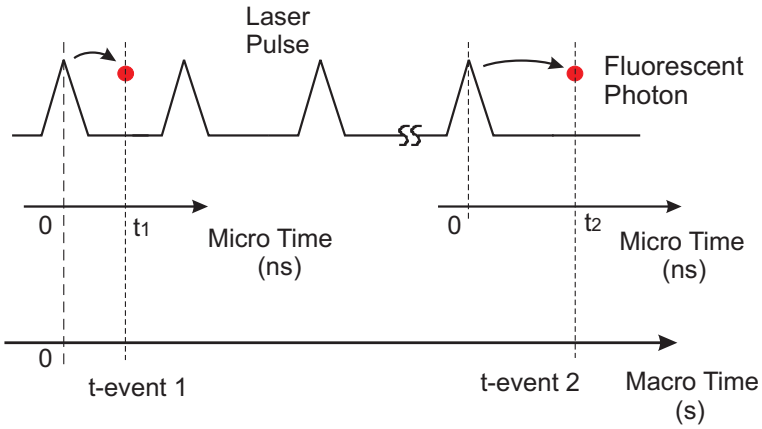

Figure 2.3.1: Time correlated Single Photon counting scheme.

	ZC Level (mV)	Low Limit (mV)
CFD	0.00	-70.59

	Range (ns)	Gain	Limit High	Limit Low	Offset (ns)
TAC	50	1	100	9.80	3.50

	ZC Level (mV)	Threshold (mV)	Holdoff (ns)	Freq. Divid.
SYNC	0.00	-400	7.50	1

Table 2.3.1: TCSPC card software parameters for TAC, SYNC and CFD. The values indicated are used for time correlated fluorescence measurements. An exhaustive explanation of parameters and acronymous is reported in [5].

filter (LP3D 650LP 28527, Omega Optical Inc.) were placed in front of the PMT detector. Then a linear polarizer (B. Halle) was set as the last optical component before the detector active area (see figure 2.2.1). Before the notch filter, a lens (f = 70 mm, OWIS) and an additional Long Pass filter (XR3003 640LP 134 0346, Omega Optical Inc.) were utilized to collect more effectively fluorescence photons (see figure 2.1.2).

The detector output and the pulsed laser controller synchronization signal were both sent, by opportune interface devices, to a Time Correlated Single Photon Counting card (TCSPC card: Becker&Hickl SPC630). This computer card and associated software (Single Photon Counter software, Version 8.50, Becker&Hickl) allow single photons counting. They record photons arrival time with respect to the begin of the experiment (called also Macro Time) and the time lag between each fluorescence photon and the previous excitation pulse (called also Micro Time, see figure 2.3.1). Collecting number of photons, Macro and Micro Time over many excitation cycles, it is possible to build an histogram representing the number of photons in each time interval (also called "bin") as function of Micro Time. The histogram then constitutes the so called "decay curve" (see also figure 2.4.1). For the chosen card parameters (50 ns time window and 4096 bins) the histogram time resolution (bin width) was of $\Delta t_b \simeq 12$ ps. The other card parameters were set after several optimization tests, changing accordingly also the BNC cables length between laser controller and TCSPC card, in order to introduce time delays. In this way, the laser pulse was placed at the beginning of the time window of the card and the complete decay curve was displayed within the same time window. The software parameters of the computer card used for measurements are reported in table 2.3.1.

The TCSPC technique requires that the probability to detect more than a photon between two excitation pulses is close to zero, while the maximum number of photons per second detectable by the utilized card is $\sim 2 \cdot 10^4$. The two conditions establish an upper limit for fluorescence intensity detection, while a lower limit is set by the background signal.

2.4 Data Collection and Analysis

For each single decay curve about $\sim 5 \cdot 10^5$ fluorescence photons were stored, together with Micro Time and Macro Time (see also figure 2.3.1). Recorded data were converted to ASCII format by the card in-built software and then analyzed with a specific software procedure, that has been realized by IgorPro package (Wavemetrics Inc.). By this custom software program was possible to load data from the ASCII files, build directly the histograms as function of Micro Time and perform the fit of the decay curve, for all polarization combinations. In figure 2.4.1 an example of the characteristic histogram for fluorescence emission from an organic dye is reported. In the inset, the decay curves for different excitation-detection polarization combinations are shown, together with a fit for *pp*.

In order to have a reliable fit of the fluorescence signal, the first 0.7 ns of the decay curve (4.5 ns from Micro Time origin) were not considered in the curve fitting, due to the finite excitation laser pulse width and presence of scattered light. A statistical error on photons count as high as $\sqrt{n}$ was considered in each histogram bin, with n the number of photons detected.

For a single non interacting dye, the fluorescence decay curve is exponentially decreasing with time (see chapter 3) and in the semi-log graph the slope of the curve represents directly the decay rate of the dye (Γ). The reciprocal provides directly the fluorescence lifetime value (τ). Moreover, the total number of fluorescence photons collected during the experiment, normalized by the excitation intensity and measurement time, is directly related to the fluorescence intensity of the sample (i.e. normalized integral of area under the decay curve). To properly extract fluorescence lifetime and intensities values from experimental decay curves, a correct estimation of background and of the systematic errors has to be done before the data fitting.

In general the background depends on diode laser stability in time, PMT detector characteristics and optical setup alignment. Several tests showed that different fused silica slides (substrates for the samples) and different samples holders do not affect the background signal in a significant way. On the other hand, the PMT dark counts are rather constant within the statistical error, after temperature stabilization ($\sim$ 10 minutes). Different optical prisms can generate an appreciable different background and fluctuations on room temperature strongly affect the diode laser emission. To investigate the latter effect a reproducibility study on laser pulse shape was performed. The evaluation of the background was performed, for each polarization combination, by the identical setup geometry described in section 2.2 (see in detail figure 2.2.1). The same prism used for the fluorescence measurements was then coupled to a bare fused silica slide (no fluorophores) and finally photons detected. The instrument background was measured several times in the same conditions after 1 hour and after 1 day: the results showed an averaged difference among the different curves of $\sim 18\%$ in both cases.

Figure 2.4.2 depicts the instrument background stability versus time, it is possible to observe the main contributions to IRF characteristics coming from:

- scattered light reaching the detector (not "delayed" light): peak around ~ 3.5 ns.
- Optics fluorescence and detector afterpulsing: curve slope between ~ 3.5 ns and ~ 20 ns.

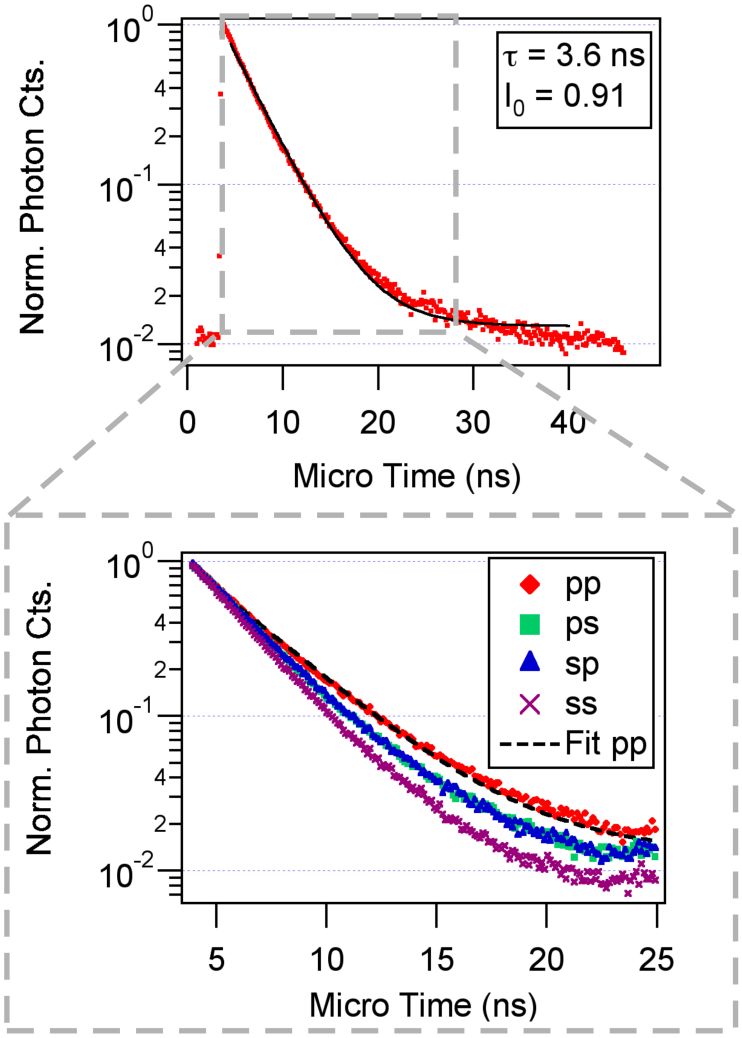

Figure 2.4.1: Typical histogram reporting normalized number of collected photons as a function of the micro time. In the magnified inset the decay curves for different excitation and detection polarizations are reported as an example. Relative fit by a single exponential function for "pp" is also shown.

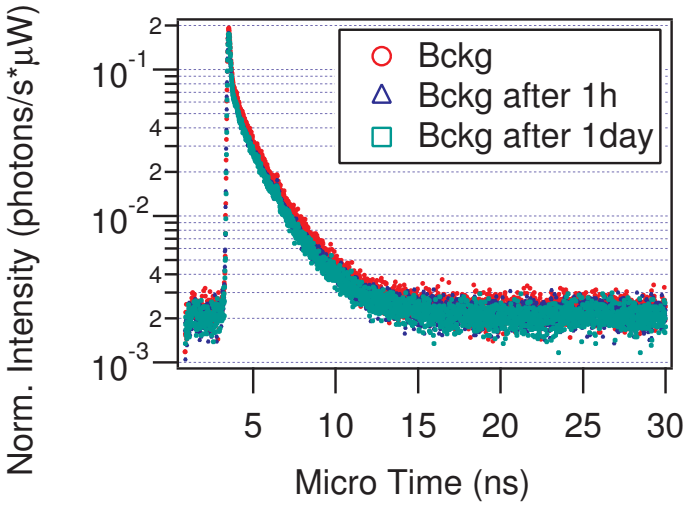

Figure 2.4.2: Instrument background stability versus time. The measurements were performed each time removing the prism from set-up and re-aligning the instrument again. For the "day after" measurement the laser was kept off during the night and $\sim$ 1 hour of warming up time was applied, on the next morning.

- Detector dark-counts: before laser excitation pulse ($\lesssim 3$ ns) and in the curve tail $\gtrsim 20$ ns.

To overcome problems of reproducibility, for each sample, the background was recorded directly after the fluorescence measurements. For each excitation-detection polarization combination $\sim 5 \cdot 10^5$ were collected[3] and then subtracted from the correspondent decay curves.

In figure 2.4.3 we report time correlated fluorescence measurements (full markers), with relative background data (crosses), for all excitation-detection polarization combinations. The measurements are for FR636 Red Reactive dyes embedded in a polymer matrix at ~ 60 nm from the polymer-air interface. By empty markers the decay curves with bckground subtracted.

Figure 2.4.3 shows that the experimental decay curve for *ss* polarization does not level off to the background value as for the other cases, after fluorescence emission. From further measurements (not shown here) the presence of a signal-dependent background was detected. The dependence is a well know effect: single photon counting detectors are in general affected by afterpulsing, while the filters used in detection may have some intrinsic fluorescence [5].

2.5 Dynamic Light Scattering Measurements

The samples were prepared by using ultra pure water (resistivity of 18.2 M$\Omega \cdot$cm, MilliQ) and DMF (Sigma Aldrich) and filtered twice by 0.22 μm syringe filters in dust-free cuvettes. To avoid fluorescence excitation, an infrared laser (Schaefter & Kirchhoff, excitation wavelength = 831.5 nm) was utilized, coupled to an equipment (ALV Langen GmbH) with a integrated fitting capability (ALV-5000 correlator) for the calculus of an apparent hydrodynamic radius (R_{app}). For the measurements in water and relative fits, the following physical parameters were utilized: solution temperature = 293.20 K; solution viscosity = 1.00041 cp; solution refractive index = 1.33200; scattering

[3] The same number of photons recorded for the fluorescence measurements.

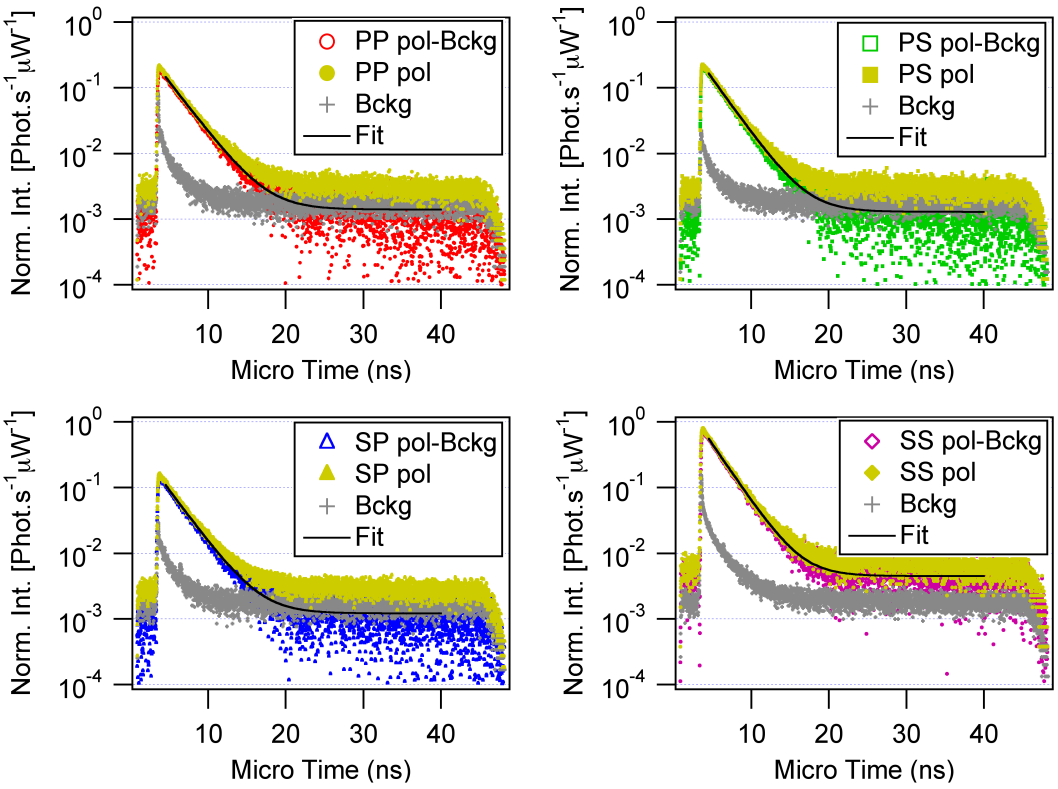

Figure 2.4.3: Lifetime decay curves for different excitation-detection polarization combinations (pp, ps, sp and ss) for FR636 red reactive dye embedded in a polymer matrix (PSS/PAH) at ~ 60 nm from polymer-air interface. The yellow full markers represent the original measured data and the grey crosses indicate the background. The differently coloured empty markers are the experimental data with background subtracted. Single exponential fits are also reported with lines.

detection angle = 90Â°, measurements time = 30 s. Analogously for the measurements in DMF and relative fits: solution temperature = 293.18 K; solution viscosity = 0.802 cp; solution refractive index = 1.4300; scattering detection angle = 90Â°, measurements time = 30 s. The fits to estimate the apparent hydrodynamic radius were performed by an inbuilt software (ALV-Correlation Software 3.0, ALV GmbH).

Bibliography

[1] E. Kretschmann, *Z. Phys.*, **241**, 313 (1971).

[2] T. Niedereichholz, Hamamatsu Photonics Deutschland GmbH, private communication.

[3] Hamamatsu PLP-10 technical data sheet (Hamamatsu Photonics K.K., System Division).

[4] R J Potton, "Reciprocity in optics", *Rep. Prog. Phys*. **67**, 717-754 (2004).

[5] "*The bh TCSPC Handbook*", W. Becker, Becker & Hickl GmbH.

Chapter 3

Simulation of Fluorescence Lifetime and Intensity

3.1 Abstract

A physical model for a dye molecule is developed, which assume the emitter as a couple of classical point-like electrical dipoles. The model relies on the equivalence between the radiated power of an electrical dipole and the fluorescence decay rate of a molecule. By using the Transfer Matrix Algorithm, the local electric field in a multilayer system is calculated and consequently the dipole excitation rate is obtained. The dipole emission into space was then evaluated by using the symmetry properties of the electromagnetic field, as indicated by the Reciprocity Theorem. In order to achieve a a full simulation of the time resolved fluorescence experiments, the expression for the fluorescence decay curves for a single and an ensemble of dyes were reported. Mathematical details are given in the following and they will be spilt in four main steps, for clarity reasons:

- Local electric fields calculation.
- Radiative decay rates evaluation.
- Simulation of a decay curve for a single dye
- Simulation of a decay curve for an ensemble of dyes.

Results and discussion about the relative numerical integration will be given at the end of each section.

3.2 Local Field in Multilayer Systems

Electromagnetic radiation interacting with a multilayer system is a phenomenon frequently encountered in most of the optical spectroscopy experiments. In the microscopy, plasmonic or fluorescence area it may be important to know the value of the local electromagnetic field and several techniques have been developed to accomplish such task. In the context of classical electromagnetic theory, an interesting method for such theoretical evaluation is the Transfer Matrix Algorithm (or TMA). It represents a compact analytical tool to calculate the electric and the magnetic field amplitudes by means of 2×2 matrices [1]. TMA will be utilized to calculate numerically the electromagnetic fields within a multilayer system. First a short introduction on TMA will be given and after the consistency of the simulation code verified.

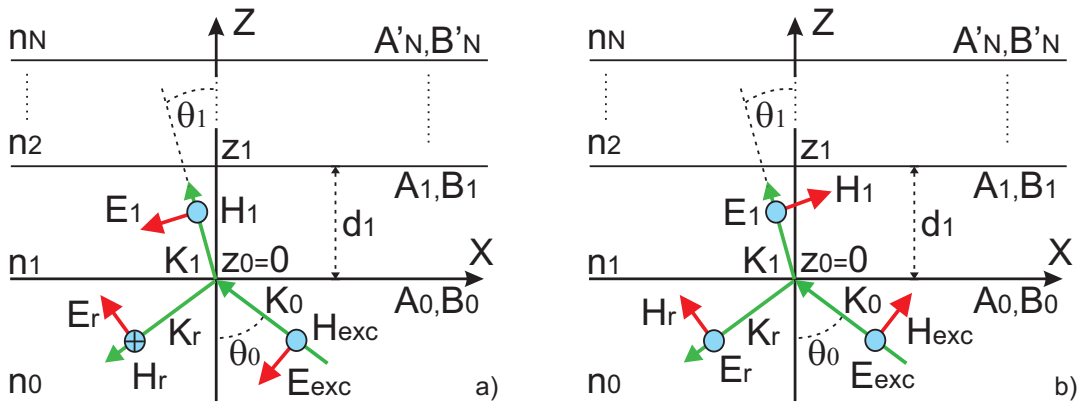

Figure 3.2.1: Schematic of multilayer system with N layers. a) Conventions for directions of electromagnetic field in TM mode in the multilayer. b) Conventions for directions of electromagnetic field in TE mode in the multilayer. The (x,z) represents the incidence plane and the Y axis enters into the drawing plane. Blue circles represent vectors perpendicular to incidence plane and having opposite direction with respect to Y axis. Circles with cross inside represent vectors parallel and with same direction of the Y axis .

3.2.1 The Transfer Matrix Algorithm

For a multilayer system and a given incident planewave, it is possible to decompose the expression of the electromagnetic field inside each single layer by a superposition of incident and reflected plane waves, by using opportune coefficients. Plane waves will be considered as excitation fields and the contributions of s-waves (TE mode) and p-waves (TM mode) to local fields will be calculated separately, due to their orthogonality. TE and TM are acronyms for respectively transverse electric field and transverse magnetic field, with respect to the plane of incidence.

Figure 3.2.1 depicts a multilayer system, constituted by N layers, where n_l is the refractive index and d_l the relative thickness of the l^{th} layer, while z_l is the coordinate of the interface between the l^{th} and the $(l+1)^{th}$ layers. The first $(l=0)$ and last $(l=N)$ layers are considered having infinite thickness and in the chosen reference system the origin of coordinates correspond to z_0. In figure 3.2.1 a) the propagation directions and the directions of the excitation electromagnetic field vectors are plotted, for TM-mode. Figure 3.2.1 b) shows the analogous directions, but for TE-mode.

Following the notation reported in figure 3.2.1, the expressions for the local fields in a generic point with coordinate z inside the l^{th} layer are, for TM mode:

$$\begin{aligned}
\vec{H}_{ly}(z) &= -n_l[-A_l e^{-ik_{lz}(z-z_l)} + B_l e^{ik_{lz}(z-z_l)}]\hat{u}_y \\
\vec{E}_{lx}(z) &= -\frac{k_{lz}}{k_l}[A_l e^{-ik_{lz}(z-z_l)} + B_l e^{ik_{lz}(z-z_l)}]\hat{u}_x \\
\vec{E}_{lz}(z) &= -\frac{\beta}{k_l}[A_l e^{-ik_{lz}(z-z_l)} + B_l e^{ik_{lz}(z-z_l)}]\hat{u}_z
\end{aligned} \tag{3.2.1}$$

while for TE mode

$$\begin{aligned}
\overrightarrow{E}_{ly}(z) &= -[A_l e^{-ik_{lz}(z-z_l)} + B_l e^{ik_{lz}(z-z_l)}]\hat{u}_y \\
\overrightarrow{H}_{lx}(z) &= +n_l \frac{k_{lz}}{k_l}[A_l e^{-ik_{lz}(z-z_l)} + B_l e^{ik_{lz}(z-z_l)}]\hat{u}_x \\
\overrightarrow{H}_{lz}(z) &= n_l \frac{\beta}{k_l}[A_l e^{-ik_{lz}(z-z_l)} + B_l e^{ik_{lz}(z-z_l)}]\hat{u}_z
\end{aligned} \tag{3.2.2}$$

In equations 3.2.1 and 3.2.2, k_l is the modulus of the wave vector in the l^{th} layer and k_{lz} its z-components. β is the wave vector component parallel to the interfaces, which is preserved through the multilayer system (i.e. $\beta_l = \beta$ in each layer). n_l and z_l have been already defined above. The fields amplitudes for the l^{th} layer (coefficients A_l and B_l) are always calculated *at* the interface with the *next* $(l+1)^{th}$ layer, on the side of the l^{th} layer. An exception has to be made for the last layer which is considered as semi-infinite: in this case the fields amplitudes $A_N^{'}, B_N^{'}$ are calculated infinitivally close to the interface with the previous $(N-1)^{th}$ layer, but on the side of layer N. This convention is necessary due to the refractive index discontinuity from one layer to the other and in figure 3.2.1 we drew the coefficients A_l and B_l for each layer, in the place where they should be calculated. By using the expression 3.2.1 and 3.2.2, the calculation of the electromagnetic field within a multilayer system is reduced to the evaluation of coefficients A_l and B_l for plane waves inside the specific layer l considered. The TMA has been designed to provide these coefficients and in general for multilayer system with N layers:

$$\begin{bmatrix} A_l \\ B_l \end{bmatrix} = D_l^{-1} D_{l+1} P_{l+1} \begin{bmatrix} A_{l+1} \\ B_{l+1} \end{bmatrix} \quad for \quad (0 < l < N) \tag{3.2.3}$$

l indicates the layer number inside the multilayer system, while for the last semi-infinite layer the following it is valid:

$$\begin{bmatrix} A'_N \\ B'_N \end{bmatrix} = D_N^{-1} D_{N-1} \begin{bmatrix} A_{N-1} \\ B_{N-1} \end{bmatrix}$$

In the expression 3.2.3, P_{l+1} represents the propagator matrix:

$$P_{l+1} = \begin{bmatrix} e^{i\phi_l} & 0 \\ 0 & e^{-i\phi_l} \end{bmatrix}$$

describing the evolution of the phase $\phi_l = k_{lz} d_l$ inside the l^{th} layer. The matrices D_l are called "dynamical matrices" and they contain information about the transmission and reflection of the fields at the interface between the the l^{th} and $(l+1)^{th}$ layers. As a consequence of the boundary conditions for the electromagnetic fields, A_l and B_l have different values for p or s waves and therefore the dynamical matrices depend on the fields polarization. In detail for TM and TE waves respectively:

$$D_{l_p} = \begin{bmatrix} \cos\theta_l & \cos\theta_l \\ n_l & -n_l \end{bmatrix} \tag{3.2.4}$$

$$D_{l_s} = \begin{bmatrix} 1 & 1 \\ n_l \cos\theta_l & -n_l \cos\theta_l \end{bmatrix} \tag{3.2.5}$$

where θ_l is the angle between the wave vector $\vec{k}_l$ and the normal vector to the interface in the l^{th} layer (see also figure 3.2.1). This angle can be calculated observing that the parallel component of the wave

vector (β) is preserved through the system. Moreover $|\vec{k}_l|^2 = (\frac{n_l\omega}{c})^2$, where c is the light speed in the vacuum and ω the oscillation frequency of the excitation plane wave. Thus:

$$n_l \cdot cos(\theta_l) = (n_l^2 - n_1^2 \cdot sin^2(\theta_1))^{1/2} \tag{3.2.6}$$

In equation 3.2.3 the coefficients A_{l+1} and B_{l+1} are not known. Therefore this equation have to be iteratively applied, in order to express A_l and B_l as a function of the excitation field amplitude coefficients (i.e. A_0 and B_0). This can be done for the specific multilayer system considered, by defining the so called Transfer Matrix M:

$$M = \begin{bmatrix} M_{11} & M_{12} \\ M_{21} & M_{22} \end{bmatrix} = D_0^{-1} \left[\prod_{i=1}^{N-1} D_l P_l D_l^{-1} \right] D_N \tag{3.2.7}$$

and in this way

$$\begin{bmatrix} A_0 \\ B_0 \end{bmatrix} = M \begin{bmatrix} A'_N \\ B'_N \end{bmatrix}. \tag{3.2.8}$$

The transfer matrix depends on the fields polarization through the dynamical matrices (equations 3.2.4 and 3.2.5), while by M is possible to calculate directly also the reflection and transmission coefficients for p and s waves [1]:

$$r = \left(\frac{B_0}{A_0}\right)_{B_{N+1}=0} = \frac{M_{21}}{M_{11}} \tag{3.2.9}$$

$$t = \left(\frac{A_{N+1}}{A_0}\right)_{B_{N+1}=0} = \frac{1}{M_{11}} \tag{3.2.10}$$

Finally taking in account the notation in figure 3.2.1 and considering $|\overrightarrow{E}_{exc}| = E_0$, the electromagnetic excitation field for TM modes is:

$$\begin{aligned} \overrightarrow{E}_{exc}(z) &= -E_0(\cos\theta_0 \hat{u}_x + \sin\theta_0 \hat{u}_z) \\ \overrightarrow{H}_{exc}(z) &= -E_0 n_0 \hat{u}_y \\ \overrightarrow{k}_0 &= k_0(\cos\theta_0 \hat{u}_z - \sin\theta_0 \hat{u}_x) \end{aligned}$$

while for TE modes

$$\begin{aligned} \overrightarrow{E}_{exc}(z) &= -E_0 \hat{u}_y \\ \overrightarrow{H}_{exc}(z) &= -n_0 E_0(\cos\theta_0 \hat{u}_x + \sin\theta_0 \hat{u}_z) \\ \overrightarrow{k}_0 &= k_0(\cos\theta_0 \hat{u}_z - \sin\theta_0 \hat{u}_x) \end{aligned}$$

For the relations above, given a monochromatic excitation with wavelenght λ_{vac} in vacuum, then $k_0 = \frac{2\pi}{\lambda_{vac}} n_0$ and by the system definition it follows that: $A_0 \equiv E_0$ and $B_0 \equiv r_p A_0$ for TM modes, whereas $B_0 \equiv r_s A_0$ for TE modes. The coefficients r_p and r_s are the reflection coefficients, calculated by the relations 3.2.9 and by using the dynamical matrices for p and s-waves, respectively (see 3.2.4 and 3.2.5). Knowing A_0 and B_0, A_l and B_l can be determined by using the equations 3.2.8 and 3.2.3. Finally, the local electromagnetic field inside the multilayer is obtained by the sets of equations 3.2.1 and 3.2.2.

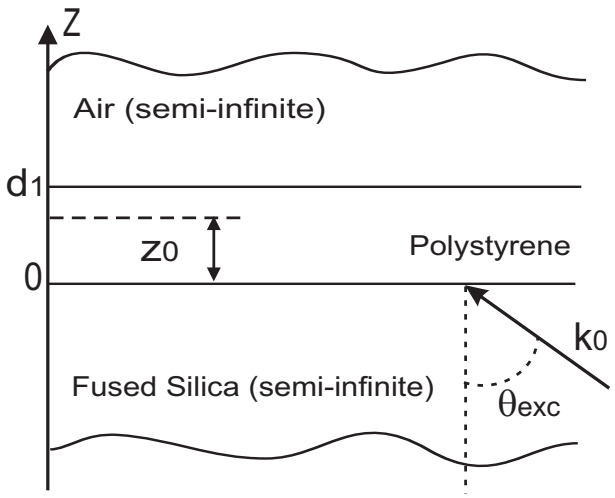

Figure 3.2.2: Three layers system used to test our simulation code. The multilayer characteristics are described in the text.

3.2.2 Numerical Simulation

To calculate numerically the expressions 3.2.1 and 3.2.2 within a multilayer system a code which implements the TMA method for a 5 layers multilayer system was realized. The code was written by , by the software package IGOR Pro (Wavemetrics Inc.) and it can be easily extended to multilayers with arbitrary number of layers. For sake of simplicity initially the algorithm was tested on a three layers system, like in figure 3.2.2. The multilayer system has the following characteristics:

- first layer with "infinite" thickness, representing the part of the space where the excitation radiation comes from. The material considered is fused silica with refractive index n = 1.45702 at a wavelength of 632.8 nm (the same material of the prism used in the experiments).
- The second layer is a 20 nm thick Polystyrene film (refractive index n = 1.58 at wavelength 632.8 nm).
- The third layer has again an "infinite" thickness and is vacuum with a refractive index equal to 1.

The origin of coordinates is placed, as also shown in figure 3.2.2, at the interface between the first two layers (layer 0 and layer 1). In order to verify the validity of the *Igor* code the electromagnetic field distribution was calculated in the middle layer. Successively the output was compared for the the same multilayer system with an reference software available on the market (i.e. *Winspall* - Ver. 2.90 Rel:0.1 by J. Worm - MPIP 2004).

Figures 3.2.3 and 3.2.4 show the electromagnetic fields components (real and imaginary parts) versus the distance z_d with respect to the origin in the multilayer system of figure 3.2.2. The fields components are calculated by the two software programs *Igor*-based code and *Winspall* for TM mode (figure 3.2.3) and for TE mode (figure 3.2.4). The two software give exactly the same results and the curves perfectly overlap for both *p* and *s* waves. The incident angle for excitation was 39.37Â° while the excitation wavelength was 632.8 nm.

To extensively check the code two additional tasks were accomplished:

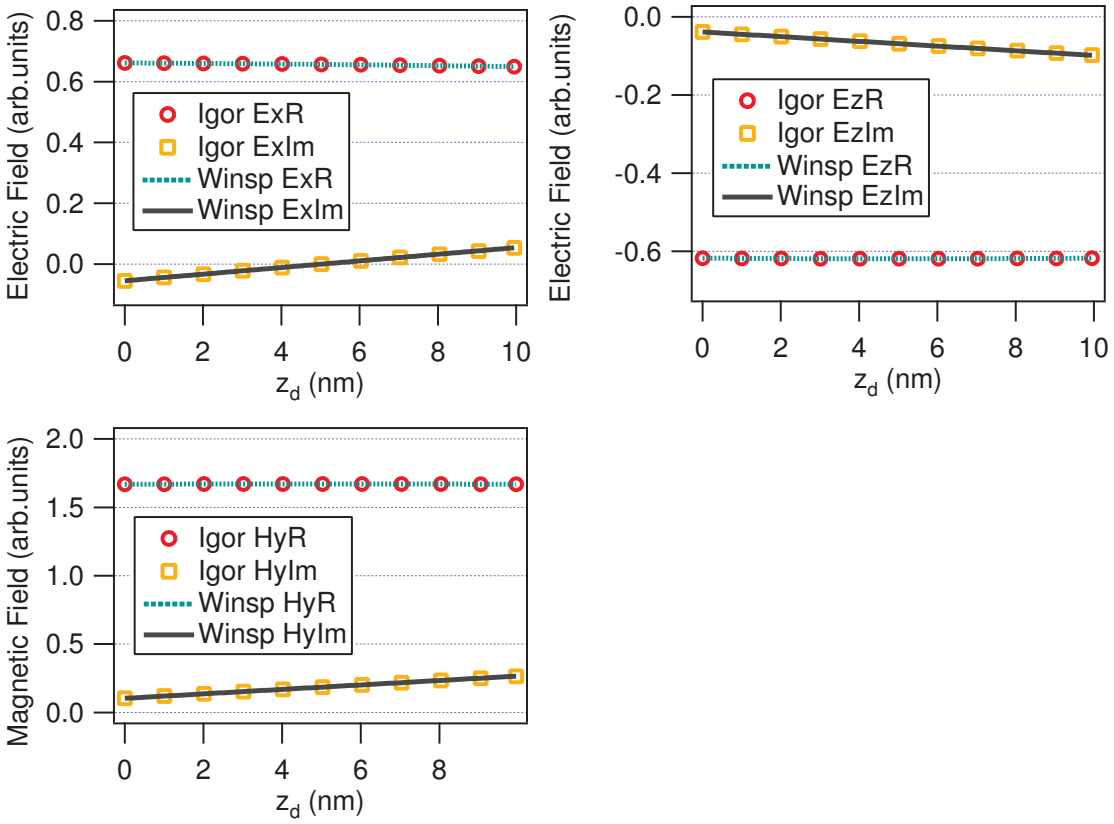

Figure 3.2.3: Local electromagnetic fields components (real R and imaginary parts Im) for TM-mode versus distance z_d inside a polystyrene layer, for the multilayer system in figure 3.2.2. In the legends, the curves named by *Igor* are generated by our code, the ones named *Winsp* by the reference sotware *Winspall*.

- the modulus of the local field components was calculated at one specific position inside the polystyrene layer ($z_0 = 10\,\text{nm}$), for different excitation angles (θ_{exc} in figure 3.2.2).

- The reflection coefficient for p-waves (r_p given by equation 3.2.9) was evaluated, in the case of a gold layer replacing the polystyrene layer.

Figure 3.2.5 a) shows the local electromagnetic field components modulus calculated at $z_d = 10\,\text{nm}$ inside the poystyrene layer, as function of the excitation angle θ_{exc}, for the multilayer system in figure 3.2.2. The fields components are plotted as obtained by the two software. *Winspall* and our *Igor*-based codes provide same results.

Figure 3.2.5 b) shows the reflection coefficient r_p as function of the excitation angle θ_{exc}, for the multilayer in figure 3.2.2, where polystyrene has been replaced by gold: the characteristic plasmon curve is observed. The value of r_p has been calculated by our *Igor*-based code (by using equation 3.2.9) and by the reference software *Winspall*. Again identical results are obtained. Once the validity of our simulation program was verified, it was possible to proceed to the next task: calculate the radiative decay rates of a dipole emebedded in a multilayer system.

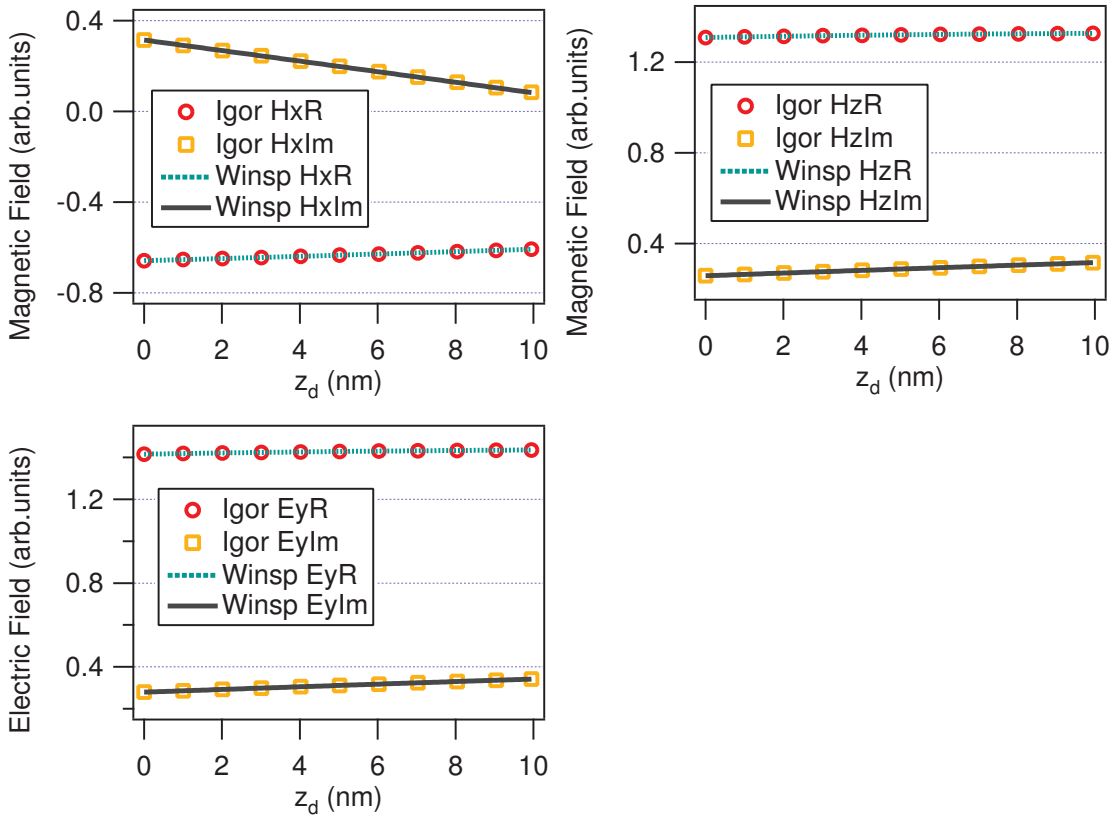

Figure 3.2.4: Local electromagnetic fields components (real *R* and imaginary parts *Im*) for TE-mode versus distance z_d inside the polystyrene layer for the multilayer system in figure 3.2.2. In the legends, curves named by *Igor* are generated by our code, the ones named *Winsp* by the reference sotware *Winspall*.

3.3 Decay Rates

For a molecular chromophore we model the fluorescence as a radiative de-excitation process involving two molecular states: a lower energy ground state and an higher energy excited state. The excitation process by electromagnetic absorption brings the molecule in an excited state. After a charateristic time τ (excited state lifetime) the molecule goes back to the ground state releasing the energy through radiative (fluorescence) and non radiative channels (intra-molecular phenomenon). As a consequence of the photon absorbtion and emission processes between two energy levels of a molecule, it is possible to associate a transition dipole moment [3] to the fluorescence phenomenon. The probability for the two-states transition to happen is then intimately related to the transition dipole moment (in first approximation, that is dipole approximation). Hence, the fluorescence intensities and the excited state lifetime are also related to the dipole moment.

It's also possible to define in complete parallelism a classical physics equivalent: the electric dipole moment. Thus a fluorescent system (i.e. a chromophore or dye molecule) can be modeled classically as a couple of oscillating point-like electric dipoles, being the point-like approximation well satisfied in our far-field studies. Magnetic effects at microscopic scale are in general orders of magnitue weaker for non magnetic materials [5] and they will be neglected. It is possible to define this couple of oscillating point-like dipole as excitation dipole moment and emission dipole moment, each one associated to a specific physical process. The two dipoles may coincide if the excitation and emission

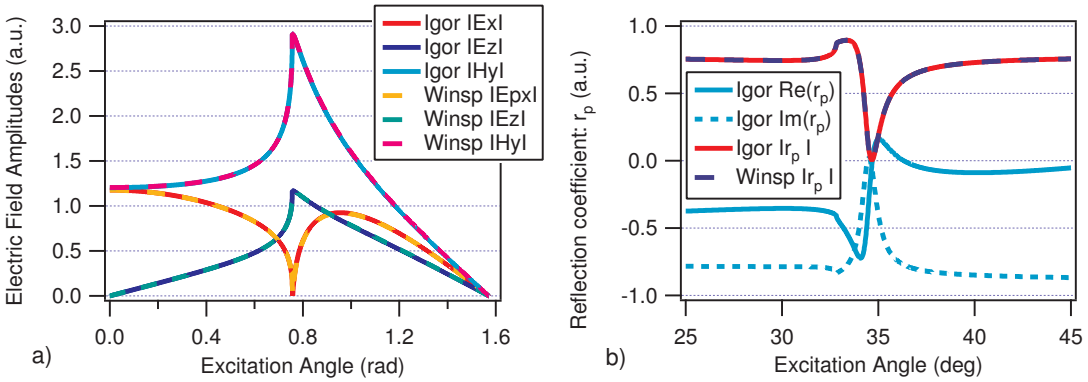

Figure 3.2.5: a) Local electromagnetic field amplitudes at $z_d = 10\,\text{nm}$ inside polystyrene layer, as a function of the excitation angle θ_{exc}, for the multilayer system described in figure 3.2.2. Two different software were employed for the simulation. b) Reflection coefficient for p-waves (r_p), as a function of the excitation angle θ_{exc}, for the multilayer system in figure 3.2.2, but with gold replacing polystyrene. The curves indicated by *Igor* in the graphs are generated by our code, while the others by the *Winspall* program.

processes occur from the same energy levels, while they are in general different when different levels are involved. Within this model the excitation dipole is considered initially at rest and then irradiated by an excitation pulse δ-like in time. As a consequence the dipole starts to oscillate trasferring part of this energy to the emission dipole moment. The latter, analogous to an optical antenna, will lose its energy coming back to rest by damped harmonic oscillations and emitting electromagnetic radiation in space, i.e. fluorescence radiation. The emission dipole has not any driving force and the energy emitted will decrease in an exponential way. The time after which the emitted fluorescence intensity is $1/e$ of the initial value (at time $t = 0$) is called fluorescence lifetime *(τ).* For organic molecules in general τ is of the order of few nanoseconds.

Through the whole following work, the organic dye molecule will be modeled as a couple of point-like electrical dipoles $\vec{d}_{exc}$ and $\vec{d}_{em}$, interacting with electromagnetic radiation and surrounding matter.

3.3.1 Decay Rates and Lifetimes

The typical lifetime of a molecule in its excited state depends on the nature of the molecule itself and on the environment where it is embedded (geometry and material). It is particularly interesting, for the following study, the situation when the molecule is in proximity of an interface, between two different dielectric media. For a single molecule a characteristic total decay rate can be defined in the following way:

$$\Gamma_{tot} = \frac{1}{\tau} \tag{3.3.1}$$

where τ is the fluorescence lifetime introduced in the previous section. The decay rate is a frequency and it is related to the probability that the excited molecule will decay to the ground state after a certain time. In general the total normalized fluorescence decay rate for a molecular dye can be written as:

$$\Gamma_{tot} = \Gamma_r + \Gamma_{nr} \tag{3.3.2}$$

where Γ_r is the the radiative contribution, while the non radiative contribution Γ_{nr} in general is unknown. The non radiative contribution is given by $\Gamma_{nr} = \Gamma_{nr,em} + \Gamma_{nr,i}$ [4], where the first term is relative to radiative emission in the near field without propagation in the far field and the second term is relative to non radiative de-excitation channels like collisional and intra-molecular relaxation processes. In the case where only dielectric materials are considered, absorption can be neglected and as a consequence the first term $\Gamma_{nr,em}$ vanishes. The non radiative contribution is related to two main phenomena: internal conversion *(ic)* and intersystem crossing *(isc)*. Hence, the non radiative contribution could be further split in two contributions: $\Gamma_{nr,i} = \Gamma_{nr,ic} + \Gamma_{nr,isc}$ [4]. The first kind of process is due to non-radiative process between two electronic states of same spin multiplicity (i.e. $S_1 \rightarrow S_0$), while the latter type of process is a non-radiative transition between two isoenergetic vibrational levels belonging to electronic states of different multiplicities (i.e. $S_1 \rightarrow T_1$).

Spontaneous decay is a pure quantum effect and it requires a quantum electrodynamic treatment. It is possible anyway to derive a classical physics analogy based on an oscillating point-like electrical dipole model. To show the connection between a quantum mechanical approach and a classical treatment of a fluorescent dye molecule a second quantization procedure is needed, even in its simplest model of two level system. It's possible to proof that the total radiated power of any current distribution with harmonic time dependence (i.e. an oscillating dipole) has the identical expression than the spontaneous decay rate of a two-level quantum system (see for example [5]). As a consequence, for an oscillating electric dipole at the same position of the dye molecule and parallel to the transition dipole moment of the dye molecule, the radiative decay rate is [7]:

$$\left[\frac{\Gamma(z_0,n_1,n_2)}{\Gamma_0}\right]_r = \left[\frac{\Gamma(z_0,n_1,n_2)}{\Gamma_0}\right]_\perp \cdot \cos^2(\theta_{em}) + \left[\frac{\Gamma(z_0,n_1,n_2)}{\Gamma_0}\right]_\parallel \cdot \sin^2(\theta_{em}) \tag{3.3.3}$$

The subscipt r is indicating the radiative part of the decay rate, while θ_{em} is the emission dipole polar angle (figure 3.3.1). $\Gamma_{\perp,N} = \left[\frac{\Gamma(z_0,n_1,n_2)}{\Gamma_0}\right]_\perp$ and $\Gamma_{\parallel,N} = \left[\frac{\Gamma(z_0,n_1,n_2)}{\Gamma_0}\right]_\parallel$ are the normalized radiative decay rates for perpendicular and parallel dipoles, respectively. The orientatation is with respect to the interface, while thay have the same dipole strenght and position. In the expression 3.3.3 the decay rates are normalized with respect to Γ_0: the oscillator decay rate in vacuum. In the theoretical model the decay rates are always normalized to $\Gamma_0 = 8.378$, where the value was obtained by our simulation code, calculating the average power emitted by a dipole in the vacuum. The ratios in 3.3.3 make the radiative decay rates independent from the dipole (oscillator) strenght, but on the other side the resulting calculated lifetimes are only defined up to a factor Γ_0. By using equation 3.3.3, the determination of the total decay rate for an arbitrary oriented electrical dipole with respect to an interface is reduced to the calculus of decays rates for two identical dipoles. These are placed at the same position but perpendicular and parallel with respect to the interface.

Figure 3.3.1 a) depicts a dye molecule modeled as a couple of excitation and emission dipole, $\vec{d}_{exc}$ and $\vec{d}_{em}$ respectively. Figure 3.3.1 b) shows a plot for equation 3.3.3 as a function of the dipole orientation with respect to the interface. The interface is in between air and polystyrene, with the dipole in air.

Reciprocity Theorem and Decay Rates

The calculus of $\Gamma_{\perp,N}$ and $\Gamma_{\parallel,N}$ for an oscillating dipole can be simplified making use of the Reciprocity Theorem in optics. The theorem can be proved to be a direct consequence of the time-space properties of the classical Maxwell equations and it is valid in presence of non absorbing media [2]. A short formulation of the theorem could be: "*the probability that an excited system will undergo a transition to the ground state, emitting a photon in a certain direction in the space is the same than*

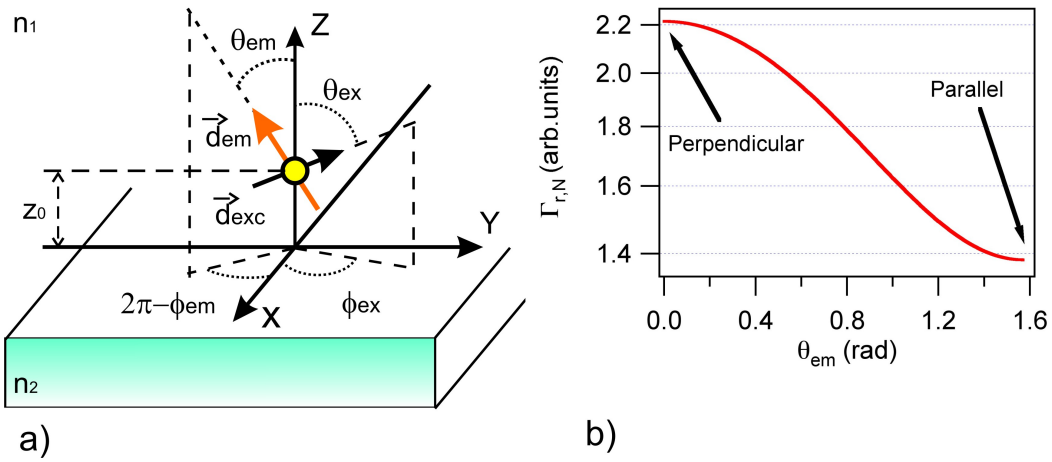

Figure 3.3.1: a) Sketch of a dye molecule modeled as a couple of excitation and emission dipole, $\vec{d}_{exc}$ and $\vec{d}_{em}$ respectively in figure. The point like dipoles are at distance z_0 from an interface separating two semi-infinite and homogeneous media with refractive index n_1 and n_2. Orientations are given in polar coordinates : $\vec{d}_{exc} \equiv (\theta_{ex}, \phi_{ex})$ and $\vec{d}_{em} \equiv (\theta_{em}, \phi_{em})$. b) Radiative decay rate $\Gamma_{r,N}$ in equation 3.3.3, as a function of the emission dipole orientation with respect to the interface. The arrows in the graph indicate values for $\Gamma_{\perp,N}$ (perpendicular) and $\Gamma_{\parallel,N}$ (parallel).

the probability to excite that system in the ground state by a photon coming from the same direction in the *space*". This means it is possible calculate the emission probability toward a certain direction, like the excitation probability from the same direction. Remembering that the fluorescence radiation is related to the emission electrical dipole $\vec{d}_{em}$, the radiative decay rate for a specific direction $\vec{l}$ is:

$$\Gamma_r(\theta_{em}, \phi_{em}, \vec{l}) \propto |\vec{d}_{em} \cdot \overrightarrow{E}^{pol}_{em,loc}(\vec{l})|^2 \tag{3.3.4}$$

having used the Reciprocity Theorem within classical electromagnetic theory frame [5]. θ_{em}, ϕ_{em} are defined as in figure 3.3.1 a), n_m is the refractive index of the medium where the fluorescence emission is detected. $\vec{d}_{em}$ is the emission dipole and $\overrightarrow{E}^{pol}_{em,loc}$ the local electric field at the dipole site, having polarization *pol* and calculated by the Reciprocity Theorem. To obtain an exact relation for 3.3.4 a model for the so called *Lorentz-Onsager* sphere [6] should be defined. In this manner an expression for the molecule polarizability α_m is obtained. Defining $\hat{u}_{em}$ the unit vector along the dipole $\vec{d}_{em}$ direction, $Im\{\alpha_m\}$ the imaginary part of polarizability and ω the electric field oscillation frequency, it is possible to show that [5]:

$$\Gamma_r = \frac{\omega}{2} \cdot Im\{\alpha_m\} \cdot \mid \hat{u}_{em} \cdot \overrightarrow{E}^{pol}_{em,loc}(z_0, \hat{l}, n_1, n_2) \mid^2 \tag{3.3.5}$$

In general the electric dipole moment associated to the molecule ($\vec{d}_{em}$) is not known, while the local electric field ($\overrightarrow{E}^{pol}_{em,loc}$) can be calculated by the TMA approach (see section 3.2.1). One advantage of using the Reciprocity Theorem is to explicit clearly the dependance of the decay rate from the possible decay channels (also called Photonic Mode Density), i.e. from the dipole orientation in the space and from the dipole-interface distance as well. Equation 3.3.4 shows that for dipoles perpendicular to the interface between the two media only the contribution of E_z^p must be considered, while for dipoles parallel to the interface only E_x^p and E_y^s give a non zero term in the scalar product. p and s denote TM and TE polarization respectively, while the Cartesian components are referred to the system in

figure 3.3.1 a), having set the plane (x,z) as plane of incidence. By equation 3.3.4 the radiative decay rate for a single specific direction $\vec{l}$ is calculated, while $\Gamma_{\perp,N}$ and $\Gamma_{\parallel,N}$ in equation 3.3.3 are relative to emitted fluorescence radiation into the whole space. It is therefore necessary to integrate 3.3.4 over all possible directions $\vec{l}$ in the space. In our simple model the whole space is divided by the two different media: in the specific case the first medium is air (refractive index n_{air}) and the second one is glass (refractive index n_{glass}). Matematically in polar coordinates the integration over all directions in space gives:

$$\begin{aligned}\Gamma_{\perp,N} &= \Gamma^{air}_{\perp,N}+\Gamma^{glass}_{\perp,N}= && (3.3.6)\\ & && (3.3.7)\\ &= \frac{\int_0^{\pi/2} d\vartheta \int_0^{2\pi} d\varphi \{n_{air}\cdot |\overrightarrow{d}_{em,\perp}\cdot \overrightarrow{E}^{air}_{loc,em}|^2\cdot sin\theta\}}{\int_0^{\pi} d\vartheta \int_0^{2\pi} d\varphi \{n_{vac}\cdot |\overrightarrow{d}_{em,\perp}\cdot \overrightarrow{E}^{vac}_{loc,em}|^2\cdot sin\theta\}}+\\ &+ \frac{\int_{-\pi/2}^{0} d\vartheta \int_0^{2\pi} d\varphi \{n_{glass}\cdot |\overrightarrow{d}_{em,\perp}\cdot \overrightarrow{E}^{glass}_{loc,em}|^2\cdot sin\theta\}}{\int_0^{\pi} d\vartheta \int_0^{2\pi} d\varphi \{n_{vac}\cdot |\overrightarrow{d}_{em,\perp}\cdot \overrightarrow{E}^{vac}_{loc,em}|^2\cdot sin\theta\}}.\end{aligned}$$

The local electric fields vectors are calculated at the dipole position close to the interface in the air side ($\overrightarrow{E}^{air}_{loc,em}$), close to the interface in the glass side ($\overrightarrow{E}^{glass}_{loc,em}$) or in the unbound vacuum ($\overrightarrow{E}^{vac}_{loc,em}$). Detailing the scalar products in the integrals then, regardless of the medium:

$$|\overrightarrow{d}_{em,\perp}\cdot \overrightarrow{E}_{loc,em}|^2 = (|\overrightarrow{d}_{em,\perp}|\cdot|\overrightarrow{E}_{loc,em}|\cdot sin\beta)^2 = |\overrightarrow{d}_{em,\perp}|^2\cdot(E^p_z)^2 \qquad (3.3.8)$$

where β is the angle in between the electric field vector and the dipole moment. E^p_z has axial symmetry and does not depend on φ. Hence, the integrals over φ bring only a factor 2π that cancels out between numerator and denominator. The same for the dipole moment modules. As a consequence:

$$\begin{aligned}\Gamma_{\perp,N} &= \Gamma^{air}_{\perp,N}+\Gamma^{glass}_{\perp,N}= && (3.3.9)\\ &= \frac{\int_0^{\pi/2} d\vartheta \{n_{air}\cdot (E^{p,air}_z)^2\cdot sin\theta\}}{\int_0^{\pi} d\vartheta \{n_{vac}\cdot (E^{p,vac}_z)^2\cdot sin\theta\}}+\\ &+ \frac{\int_{-\pi/2}^{0} d\vartheta \{n_{glass}\cdot (E^{p,glass}_z)^2\cdot sin\theta\}}{\int_0^{\pi} d\vartheta \{n_{vac}\cdot (E^{p,vac}_z)^2\cdot sin\theta\}};\end{aligned}$$

For the parallel case by using the same notation used above for the electric fields:

$$\begin{aligned}\Gamma_{\parallel,N} &= \Gamma^{air}_{\parallel,N}+\Gamma^{glass}_{\parallel,N}= && (3.3.10)\\ &= \frac{\int_0^{\pi/2} d\vartheta \int_0^{2\pi} d\varphi \{n_{air}\cdot |\overrightarrow{d}_{em,\parallel}\cdot \overrightarrow{E}^{air}_{loc,em}|^2\cdot sin\theta\}}{\int_0^{\pi} d\vartheta \int_0^{2\pi} d\varphi \{n_{vac}\cdot |\overrightarrow{d}_{em,\parallel}\cdot \overrightarrow{E}^{vac}_{loc,em}|^2\cdot sin\theta\}}+\\ &+ \frac{\int_{-\pi/2}^{0} d\vartheta \int_0^{2\pi} d\varphi \{n_{glass}\cdot |\overrightarrow{d}_{em,\parallel}\cdot \overrightarrow{E}^{glass}_{loc,em}|^2\cdot sin\theta\}}{\int_0^{\pi} d\vartheta \int_0^{2\pi} d\varphi \{n_{vac}\cdot |\overrightarrow{d}_{em,\parallel}\cdot \overrightarrow{E}^{vac}_{loc,em}|^2\cdot sin\theta\}}=\end{aligned}$$

Detailing again the scalar products as before:

$$\begin{aligned}\Gamma_{\parallel,N} &= \Gamma^{air}_{\parallel,N}+\Gamma^{glass}_{\parallel,N}= \qquad (3.3.11)\\ &= \frac{\int_0^{\pi/2} d\vartheta \int_0^{2\pi} d\varphi \{n_{air}\cdot[(E_y^{s,air})^2+(E_x^{p,air})^2]\cdot sin\theta\cdot cos^2(\varphi-\phi_{em})\}}{\int_0^{\pi} d\vartheta \int_0^{2\pi} d\varphi \{n_{vac}\cdot[(E_y^{s,vac})^2+(E_x^{p,vac})^2]\cdot sin\theta\cdot cos^2(\varphi-\phi_{em})\}}+\\ &+ \frac{\int_{-\pi/2}^{0} d\vartheta \int_0^{2\pi} d\varphi \{n_{air}\cdot[(E_y^{s,glass})^2+(E_x^{p,glass})^2]\cdot sin\theta\cdot cos^2(\varphi-\phi_{em})\}}{\int_0^{\pi} d\vartheta \int_0^{2\pi} d\varphi \{n_{vac}\cdot[(E_y^{s,vac})^2+(E_x^{p,vac})^2]\cdot sin\theta\cdot cos^2(\varphi-\phi_{em})\}}=\end{aligned}$$

The quantity $[(E_y^{s,glass})^2+(E_x^{p,glass})^2]$ is independent from the azimuthal angle, it is therefore possible to integrate over φ and select $\varphi_{em}=0$ without any loss of generality. As a consequence, a factor π cancels out between numerator and denominator and finally:

$$\begin{aligned}\Gamma_{\parallel,N} &= \Gamma^{air}_{\parallel,N}+\Gamma^{glass}_{\parallel,N}= \qquad (3.3.12)\\ &= \frac{\int_0^{\pi/2} d\vartheta \{n_{air}\cdot[(E_y^{s,air})^2+(E_x^{p,air})^2]\cdot sin\theta\}}{\int_0^{\pi} d\vartheta \{n_{air}\cdot[(E_y^{s,vac})^2+(E_x^{p,vac})^2]\cdot sin\theta\}}+\\ &+ \frac{\int_{-\pi/2}^{0} d\vartheta \{n_{glass}\cdot[(E_y^{s,glass})^2+(E_x^{p,glass})^2]\cdot sin\theta\}}{\int_0^{\pi} d\vartheta \{n_{air}\cdot[(E_y^{s,vac})^2+(E_x^{p,vac})^2]\cdot sin\theta\}}.\end{aligned}$$

In the equations above, the local electric fields $\overrightarrow{E}^{glass}_{loc,em}$ and $\overrightarrow{E}^{air}_{loc,em}$ were decomposed in their Cartesian components, based on the reference system indicated in figure 3.3.1, with (x,z) always the plane of incidence.

Once the decay rates $\Gamma_{\perp,N}$ and $\Gamma_{\parallel,N}$ are determined for the specific system, it is necessary to know the orientation of the emission dipole moment respect the surface (i.e. θ_{em} in figure 3.3.1). In this way, it is possible to calculate the total radiative decay rate by equation 3.3.3. In general for a specific chromophore, $\vec{d}_{ex}$ and $\vec{d}_{em}$ are unkown and by quantum chemistry calculations only their orientations with respect to the molecular structure are determined. By single molecule spectroscopy, it would be possible in principle to determine experimentally the excitation and emission dipoles directions in the space, but in practice the dye molecules photobleach quickly, not allowing appropriate measurements.

Numerical Integration

The equations 3.3.9 and 3.3.12 can be applied to a practical case, considering the same three layer system described previously in section 3.2.2 (see also figure 3.2.2). The electrical dipole (i.e. the fluorescent molecule) is then placed at an infinitesimal distance from the polystyrene-air interface, in the air side. Integrals are numerically performed by discretizing the space of variables and as first step thus the integrals convergence has to be proved. In the simulation code the polar angle range ($\theta\in[0,\pi]$) was divided in a number of intervals $m-1$ (with m the number of integration points). Successively 3.3.9 and 3.3.12 were calculated for different values of m. The multilayer-dipole system is symmetric under variations of φ, thus no real integration is necessary for this variable. Figure 3.3.2

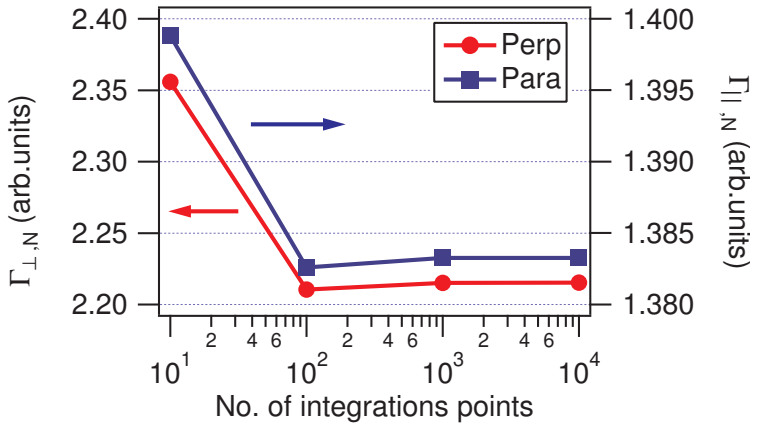

Figure 3.3.2: Normalized decay rate values for a perpendicular ($\Gamma_{\perp,N}$) and parallel ($\Gamma_{\parallel,N}$) dipoles close an interface, based on the system described in the text.

shows the results of the numerical integration for equations 3.3.9 and 3.3.12, as a function of the number of integration intervals. From the trend plotted in figure 3.3.2 the convergence of the integrals 3.3.9 and 3.3.12 is achieved around 10^3 integration points, within the intrisic software numerical error.

Considering 10^4 points in the final numerical integration, for the dipole at the interface: $\Gamma_{\perp,r} \cong 18.559 \cdot \mid \overrightarrow{d}_{em} \mid^2$ and $\Gamma_{\parallel,r} \cong 11.589 \cdot \mid \overrightarrow{d}_{em} \mid^2$. Whereas considering the dipole embedded in infinite vacuum space the decay rate is $\Gamma_0 \cong 8.378 \cdot \mid \overrightarrow{d}_{em} \mid^2$. In such way the normalized factors are calculated as:

$$\Gamma_{\perp,N} = \frac{\Gamma_{\perp,tot}}{\Gamma_0} \cong 2.215$$

$$\Gamma_{\parallel,N} = \frac{\Gamma_{\parallel,tot}}{\Gamma_0} \cong 1.383$$

To test the correctness of the decay rates calculus, the obtained results are compared against another software code written on the base of Back Reacted Field approach. From the last one: $\Gamma_{\perp,N} = 2.207$ and $\Gamma_{\parallel,N} = 1.340$, with a difference of $\sim 0.4\%$ and $\sim 3\%$ respectively.

3.4 Fluorescence Decay Curves for Single Dye

In the standard time-resolved fluorescence spectroscopy, the measured quantity is the number of fluorescence photons detected as a function of the time lag between excitation laser pulse and fluorescence photon arrival time (for more details see chapter 2). The resulting experimental data set can be plot as an histogram which is approximated by a fluorescence decay curve. The approximation comes by the fact the electronic cards used for single photon counting have a finite time resolution. In this way the relative width of histograms bins show a minimum value and the representation by a continuous function in time is clearly an approximation. For a single dye molecule, the measured decay curve is represented well by a decreasing exponential function:

$$\mathrm{D}_s(t) \propto Ae^{-t/\tau} \tag{3.4.1}$$

where the decay time constant τ represents exactly the chromophore fluorescence lifetime. The exponential factor in the relation 3.4.1 comes from the assumption that in stationary conditions the lifetime should not change with time. Once the problem geometry is fixed (i.e. the excitation conditions and the environment where the dipole is embedded into), the decay rate and so the lifetime is constant with respect to the time. In this case, the exponential factor comes out from the first order linear differential equation describing the depletion of the excited state. The function $\mathrm{D}_s(t)$ is related by some proportionality factors (summarized in A) to the istantaneous fluorescence intensity detected. These factors are the excitation efficiency, the molecule fluorescence quantum yield and the detection efficiency. The fluorescence quantum yield is usually defined as [4]:

$$\Phi_F = \frac{\Gamma_r}{\Gamma_r + \Gamma_{nr}} \tag{3.4.2}$$

where Γ_r and Γ_{nr} are respectively the radiative and non-radiative decay rate for the chromophore (see also section 3.3.1). The fluorescence quantum yield as defined is not an absolute intrinsic property of the dye only, but it depends also on the specific chromophore's surrounding environment by Γ_{nr}.

The lifetime τ can be extracted by a fitting procedure from an experimental fluorescence decay curve, and afterwards its value can be compared with the theoretical value in equation 3.4.1. In order to give a more precise expression to equation 3.4.1, a single dye molecule is embedded in a multilayer system and excited by a monochromatic plane waves impinging from a generic direction $\vec{l}$. The emitted fluorescence radiation is detected from a different direction $\vec{m}$ (see figure 3.4.1). In the following simulations, the excitation radiation will be always constituted of electromagnetic plane waves. This is an approximation, but it does not remove validity to our model, due to the Fourier theorem.

For a physical system like the one reported in figure 3.4.1, the fluorescence probability density function $\mathrm{D}_s(t)$ (equation 3.4.1) will be evaluated. The probability to detect a fluorescence photon, at a certain time t after excitation, will depend on the excitation probability for the generic excitation direction $\vec{l}$, i.e. $P_{exc}(\vec{l})$, on the emission rate in the space $R_{em}(t)$ at time t and on detection probability P_{det} for the specific detector considered. In this manner it is possible to write the fluorescence probability density for a single dipole:

$$\mathrm{D}_s(t) \propto P_{exc} \cdot R_{em}(t) \cdot P_{det} \tag{3.4.3}$$

The function $\mathrm{D}_s(t)$ has the dimensions of a rate and is also called probability density, because its integral over a generic time interval (t_1, t_2) provides the number of photons detected in that interval (intensity).

3.4.1 Excitation Probability P_{exc}

The process of selective excitation for a single dye, called also photoselection [4], is achieved by changing the excitation radiation polarization with respect to the interface. Considering the excitation source constituted by plane waves impinging the interface at certain direction, defined by the unit vector $\hat{l}$, and referring to figure 3.4.1:

$$P_{exc}(\theta_{ex}, \phi_{ex}, z_0, \hat{l}, n_1, n_2, pol) \propto \mid \overrightarrow{d}_{exc} \cdot \overrightarrow{E}^{pol}_{exc,loc}(z_0, \hat{l}, n_1, n_2) \mid^2 \tag{3.4.4}$$

$\overrightarrow{d}_{exc}$ is the associated excitation dipole moment and $\overrightarrow{E}^{pol}_{exc,loc}$ is the excitation local electric field experienced by the dipole itself. *pol* is relative to the field polarization mode: TM (p) or TE (s).

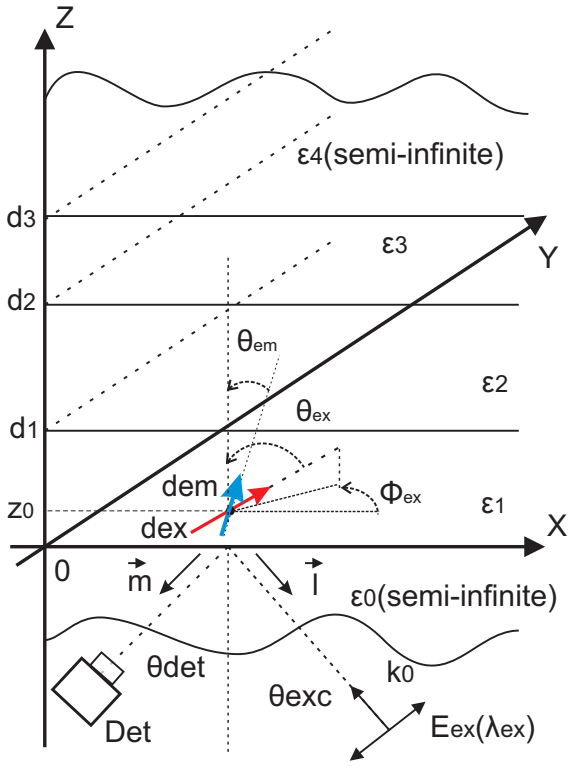

Figure 3.4.1: Schematic representation of a 5 layers system, where the first and the last layer are considered semi-infinite. In figure the different variables used in the text are indicated. The dielectric constants of the layers are: $\varepsilon_k = n_k^2$, with n_k the refractive index.

The local field is for the incident radiation made up of electromagnetic plane waves with momentum parallel to $\vec{l}$ and the calculus of such local field was treated extensively in section 3.2.1.

The equation 3.4.4 is valid for weak excitation, i.e. $I_{exc} \ll I_s$, where I_s is the saturation intensity. For single dyes at room temperature $I_s \sim 3\,\mathrm{KW/cm^2}$ [5], much larger than our typical excitation intensities $I_{exc} \sim 20\,\mu\mathrm{W/cm^2}$.

3.4.2 Emission Rate R_{em}

The total fluorescence emission rate in the whole space at time t is defined as:

$$R_{em}(t) = \Gamma_0 \cdot \Gamma_{r,N} \cdot e^{-\Gamma_{tot,N} \cdot \Gamma_0 \cdot t} \tag{3.4.5}$$

where $\Gamma_{r,N}$ is given by 3.3.3, $\Gamma_{tot,N}$ by 3.3.2 and again Γ_0 is the fluorescence decay rate in vacuum. The exponential behavior comes out from the differential equation for a harmonic damped oscillator equations. The factor $\Gamma_{tot,N}$ normalize the expression 3.4.5: integrating over the time between 0 and ∞ the expression for the fluorescence quantum yield Φ_F is recovered (equation 3.4.2).

3.4.3 Detection Probability P_{det}

The expression in 3.4.5 is relative to the whole space, but in the real experiment the photons can be collected only within a limited solid angle, depending on the detection geometry and the specific de-

tector utilized. By using the Reciprocity Optical Theorem [2] (see section 3.3.1) and always referring to figure 3.4.1, it is possible to explicit the probability that an emitted photon is detected along the direction $\hat{m}$:

$$P_{det}(\hat{m}) \propto \mid \overrightarrow{d}_{em} \cdot \overrightarrow{E}^{pol}_{em,loc}(z_0, \hat{m}, n_1, n_2) \mid^2 \tag{3.4.6}$$

$\overrightarrow{d}_{em}$ is the associated emission dipole moment (see figure 3.3.1), $\overrightarrow{E}^{pol}_{em,loc}$ the emitted fluorescence local field with indication of its polarization in the superscript *pol*. The local field is relative to emission radiation made up of electromagnetic plane waves with momentum parallel to $\vec{m}$ and the calculus of such local field was treated extensively in section 3.2.1. The correct normalization factors come by integrating equation 3.4.6 over all space and imposing the detection probability equal to 1. Therefore, it is obtained:

$$P_{det}(\Omega_d) \propto \frac{1}{\Gamma_{r,N} \cdot \Gamma_0} \cdot \int_{\Omega_d} \mid \overrightarrow{d}_{em} \cdot \overrightarrow{E}^{pol}_{em,loc}(z_0, \hat{m}, n_1, n_2) \mid^2 d\hat{m} \tag{3.4.7}$$

where again $\Gamma_{r,N}$ is given by 3.3.3, while Ω_d represents the solid angle under which we collect the fluorescence photons are collected. The expression 3.4.7 can be verified by using the following relation:

$$\Gamma_r \propto \int_{Space} \mid \overrightarrow{d}_{em} \cdot \overrightarrow{E}^{pol}_{em,loc}(z_0, \hat{m}, n_1, n_2) \mid^2 d\hat{m} \tag{3.4.8}$$

Integrating the equation 3.4.7 over the whole space, a probability equal one is obtained. In real experimental conditions, the detector has a finite detection area, while the detector quantum efficiency (η_d) is different from unity. For a proper simulation of the measured fluorescence decay curves, it is thus necessary to integrate the detection probability over the corresponding solid angle and multiply it for η_d.

3.4.4 Decay curve for a single dye

By using the expressions 3.4.4 and 3.4.7, the total probability to detect a fluorescence photon in the detector is obtained. Once the dye molecule has been excited by a laser pulse, for single emission wavelength, the probability density of emission is:

$$\begin{aligned} \mathrm{D}_s^{\sigma\delta}(z_0, \theta_{ex}, \phi_{ex}, \theta_{em}, \phi_{em}, \Gamma_{nr}, \Gamma_0, n_1, n_2, \hat{l}, \Omega_d, t) &= \\ = \alpha \cdot \mid \overrightarrow{d}_{exc} \cdot \overrightarrow{E}^{\sigma}_{exc,loc}(z_0, \hat{l}, n_1, n_2) \mid^2 &\cdot \\ \cdot e^{-\Gamma_{tot,N}(\theta_{em}, \phi_{em}, z_0, n_1, n_2, \Gamma_{nr}) \cdot \Gamma_0 \cdot t} &\cdot \\ \cdot \int_{\Omega_d} \mid \overrightarrow{d}_{em} \cdot \overrightarrow{E}^{\delta}_{em,loc}(z_0, \hat{m}, n_1, n_2) \mid^2 d\hat{m} & \end{aligned} \tag{3.4.9}$$

The variables are explained in figure 3.4.1, while α includes several multiplying factors:

- the unknown excitation (η_e) and detection (η_d) efficiency.
- A factor Γ_0 coming from correct normalization of equation 3.4.7.

- N_c indicating the number of the excitation-emission cycles during the experiment. The number of photons collected in a certain time interval Δt is proportional also to the number of excitation cycles that the molecule undergoes in Δt.
- Other constants related to the optical paths of the experimental setup (filters, lenses,...).

The superscripts σ and δ in equation 3.4.9 indicate the polarizations of the excitation and emission local fields respectively, where the possible independent combinations are $(\sigma\delta) = pp, ps, sp, ss$. In general organic dye molecules have a broad emission spectrum, not limited to a single emission wavelength and the correct expression for equation 3.4.9 should therefore include an integral over the measurable part of the emission band B_ω[1] . In the case of broad fluorescence emission spectrum also the detector quantum efficiency (η_d) should assume different values: $\eta_d = \eta_d(\lambda)$. Nevertheless, for the photomultiplier used in the experiments, η_d is constant over a wide range of wavelenghts through the visible spectrum [8]. As a consequence, a monochromatic emitted radiation will be considered, with the wavelength value corresponding to the maximum of the fluorescence emission spectrum.

The fluorescence probability density in equation 3.4.9 is related to the fluorescence intensity by its integral over time intervals. Considering an inifinitely short excitation pulse at time $t = 0$ (i.e. delta-like excitation), then the number of photons collected in a time interval Δt, at generic time t after excitation pulse is:

$$\mathrm{I}_{\sigma\delta}(t, \Delta t) = \int_{t}^{t+\Delta t} D_s^{\sigma\delta}(t) \cdot dt \tag{3.4.10}$$

from which it is shown that the fluorescence intensity depends on the excitation-detection polarization combinations.

In an experimental design the variables defining the sample characteristics (z_0, n_1, n_2) and the geometry of the experimental setup ($\hat{l}$ excitation direction, Ω_d solid angle of detector's active area) are known, while the variables related to the molecular structure of the dye $(\theta_{ex}, \phi_{ex}, \theta_{em}, \phi_{em}, \Gamma_0)$ and its interaction with the surroundings (Γ_{nr}) are unknown. To highlight the relationship between the probability density $D_s(t)$ (eq. 3.4.9) and the physical variables of the model, it may be convenient to define some *sets of variables*. For a single dipole emebedded in a multilayer system with n layers:

$$\begin{aligned} \{ML\} &= \{\varepsilon_0, \varepsilon_1, ..., \varepsilon_{n-1}, d_1, d_2, ..., d_{n-2}\} \\ \{EX\} &= \{\hat{l}, \lambda_{ex}\} \\ \{EM\} &= \{\hat{m}, \lambda_{em}\} \\ \{\mu ex\} &= \{d_{ex}, \theta_{ex}, \phi_{ex}, z_0\} \\ \{\mu em\} &= \{d_{em}, \theta_{em}, \phi_{em}, z_0\} \end{aligned} \tag{3.4.11}$$

$\{ML\}$ is the set of variables related to the multilayer physical system (dielectric functions and thicknesses of the several layers). $\{EX\}$ is relative to the incidence direction and wavelength of the excitation radiation. $\{EM\}$ represents the detection direction and wavelength of the emitted radiation from the dipole. $\{\mu ex\}$ and $\{\mu em\}$ describe the magnitude and the position in spherical coordinates of the excitation and emission transition dipoles (associated to the chromophore), respectively. As

[1] During the experiment, part of the dye emission spectrum is cut usually by a Long Pass optical filter, to avoid detection of scattered light caused by the excitation source.

an example figure 3.4.1 depicts the sketch for a multilayer system with $n = 5$, where the previous mentioned physical variables are indicated.

By the electromagnetic field properties, it is possible to decompose the analysis considering TE (s-waves) and TM (p-waves) components, separately. Defining for simplicity the following quantities

$$R^{\sigma}_{exc} = |\overrightarrow{d}_{ex} \cdot \overrightarrow{E}^{\delta}_{loc,ex}|^2 \quad \text{and} \quad R^{\delta}_{em} = |\overrightarrow{d}_{em} \cdot \overrightarrow{E}^{\sigma}_{loc,em}|^2$$

the final expression for the fluorescence probability is:

$$\begin{aligned} \mathrm{D}^{\sigma\delta}_{s}(t) &\propto \\ &= \alpha \cdot R^{\sigma}_{exc}(\{\mu ex\},\{EX\},\{ML\}) \cdot \\ &\cdot \quad e^{-\Gamma_{tot}(\{ML\}\{\lambda_{em}\}\{\mu em\})\cdot t} \cdot \int_{\Omega_d} R^{\delta}_{em}(\{\mu em\},\{EM\},\{ML\})\, d\hat{m} \end{aligned} \tag{3.4.12}$$

where $\sigma\delta$ indicates one possible combination of excitation and emission fields polarizations (i.e. *pp, ps, sp* or *ss*). Equation 3.4.12 shows that there are different decay curves for different excitation-detection polarization combinations, even in the case of a single dipole. On the other hand, the fluorescence lifetime of the dye molecule is independent from polarizations combinations, once the geometry of the system is determined.

3.4.5 Numerical Test

The equation (3.4.12) can be verified numerically considering, for sake of simplicity, the emission and detection dipoles coincident ($\vec{d}_{ex} \equiv \vec{d}_{em} \equiv \vec{d}$). In the case of a multilayer system (figure 3.4.1), the simulated decay curves can be plotted for several dipole orientations (θ, ϕ). Figure 3.4.2 shows, for different excitation-detection polarization combinations, the fluorescence probability density as a function of the time, according to 3.4.12 normalized with respect to α.

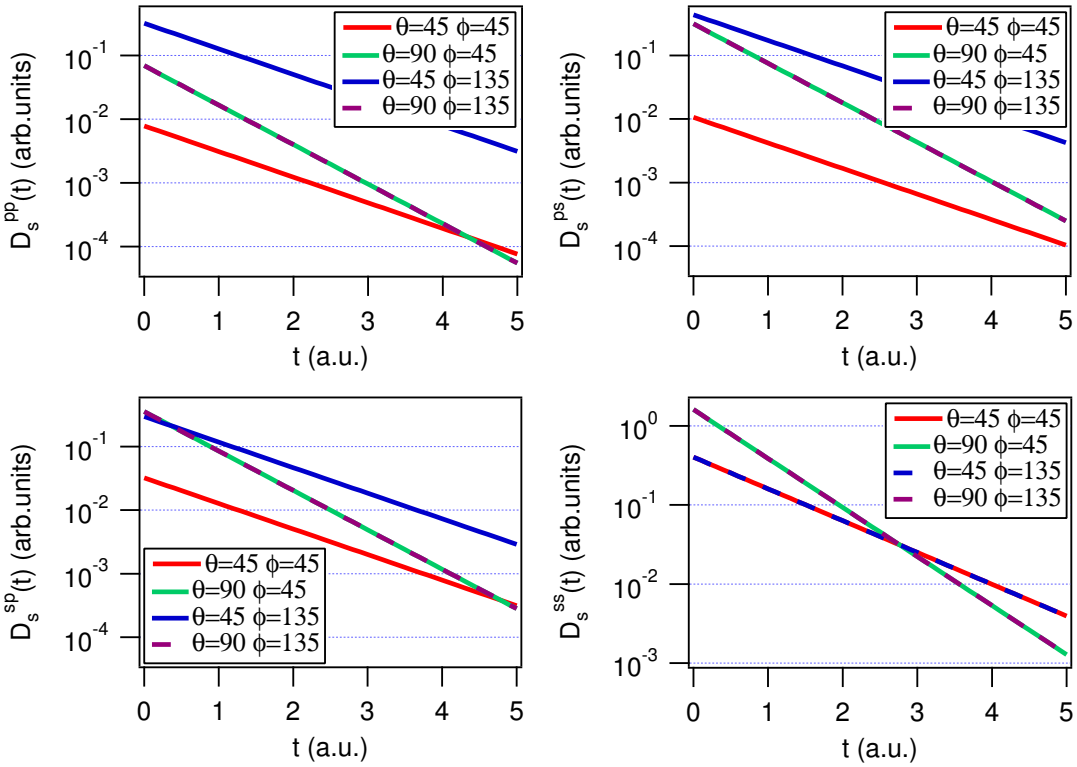

Figure 3.4.2: Decay curves $D_s^{\sigma\delta}(t)$ for different dipole orientations and different excitation-detection polarizations (clockwise from top left: *pp, ps, ss, sp*). The excitation and emission dipoles are considered identical and for each dipole orientation. The angular coordinates are shown in the legends: θ polar angle, ϕ azimutal angle. The multilayer system used for the simulation is schematically represented in figure 3.4.1, with: $\vartheta_{ex} = 39.37\hat{A}°$, $\vartheta_{det} = 50.63\hat{A}°$, $\varepsilon_0 = 2.12291$, $\varepsilon_1 = 2.4964$, $\varepsilon_2 = \varepsilon_3 = \varepsilon_4 = 1$, $z_d = 10\,\text{nm}$. The excitation and emission wavelength are 632.8 nm and 660 nm, respectively.

Figure 3.4.2 indicates that dipoles having the same polar angle (θ), independently from the value of the azimutal angle (ϕ), have decay curves with same slope. The exponential function $D_s^{\sigma\delta}(t)$ versus t is represented by a straight line whose slope is the molecule fluorescence lifetime $\tau = \frac{1}{\Gamma_{tot}}$ (see equation 3.4.12). Remembering equation 3.3.3 for the total radiative decay rate and having assumed $\Gamma_{nr} = 0$, then Γ_{tot} depends only on θ. The simulation results in figure 3.4.2 show correctly this symmetry with respect to φ. Among all dipole orientations in figure 3.4.2, two cases are studied in detail as an example of analysis:

- $(\theta = 90, \phi = 45)$ and $(\theta = 90, \phi = 135)$ give correctly the same decay curves because for dipoles lying in the (x,y) plane there is no z components and the modulus of the expressions (3.4.4), (3.4.6) cancels relative signs differences.
- $(\theta = 45, \phi = 45)$ and $(\theta = 45, \phi = 135)$: for *ss* polarization the relative decay curves overlap because $\sin(\phi) = \sin(\pi - \phi)$. For *pp, ps* and *sp* polarizations the two curves are different since $\cos(\phi) = -\cos(\pi - \phi)$ and thus the presence of the z component introduces different signs.

By similar arguments (i.e. by symmetries analysis), it is possible to discuss the behavior of other decay curves for other dipole orientations. In any case the consistency of our simulation code is proven.

3.5 Fluorescence Decay Curves for an Ensemble of Molecules

For an ensemble of fluorescent molecules, the total fluorescence detected is the sum of the radiation from each emitting dye. Thus, in complete analogy with equation 3.4.1:

$$\mathrm{D}_e(t) \propto \sum_k A_k e^{-t/\tau_k} \tag{3.5.1}$$

Different values of excitation efficiency, detection efficiency and radiation quantum yield, for each single molecule, are taken into account through the coefficients A_k. As a consequence of equation 3.5.1, the decay curve is not a single exponential function anymore, in the case of an ensemble of chromophores. Hence, it is not possible to define a single decay constant, i.e. an unique fluorescence lifetime τ. By fitting the decay curve resulting from equation 3.5.1, an average value for the lifetime of the ensemble is obtained. On the other hand, the evaluation of $D_e(0)$ provides information about the global excitation-detection process over many molecules.

When an ensemble of identical molecules is considered, additional assumptions are needed in order to simplify the expression for the fluorescence probability density and make the calculus possible, in detail:

- the molecules are distributed over the sample surface in such way they do not interact each other: no molecular aggregation effects are presents.
- Associated electrical dipoles are all at the same distance from the interface. Practically the real microscopic roughness of the interfaces and eventual molecular diffusion inside the layers are not taken into account. Anyway, the theory shows this approximation is not critical: by the simulation code was possible to check that a change of the dye-interface distance, within a range of $\sim 10\,\mathrm{nm}$ inside the same medium[2], corresponds to an indetermination of $\sim 2 \div 5\%$ on the lifetimes (depending on excitation-detection polarization combinations considered).
- All dyes are identical: same excitation quantum efficiency (η_a) and same excitation and emission dipole moments strenght ($\mid \vec{d}_{ex} \mid$ and $\mid \vec{d}_{em} \mid$ respectively). Therefore each molecule emits fluorescence radiation at the same wavelength.
- The dipole orientations are uniformly distributed over all the directions, as a continuum. Therefore the dipole density in the space can be written $n(\phi_{ex}, \theta_{ex}, \phi_{em}, \theta_{ex}) = n_{ex}(\phi_{ex}, \theta_{ex}) = n(\phi, \theta) = \rho = \text{constant}$. Thus, within a solid angle $d\Omega$ the number of dipoles is $dN = n(\phi, \theta) \cdot \sin\theta \, d\theta \, d\phi = \rho \cdot \sin\theta \, d\theta \, d\phi$. In the experiment performed $\sim 10^{11}$ dye molecules were estimated on the sample, within the laser spot. Hence, the continuum approximation can be considered reasonable, in first instance. If A is the spot of the excitation laser beam and c the concentration of the molecules over the sample surface, then $N = cA$ dyes molecules can be excited on the sample:

$$N = c \cdot A = \int_0^{\pi} d\vartheta \int_0^{2\pi} d\phi \, \rho \cdot \sin\vartheta = 4\pi\rho$$

The emission probability density (or decay curve) for an ensemble of identical dye molecules at the same distance z_0 from an interface of a multilayer system, can be obtained from the expression of

[2] Far above our experimental ability to control the dye position within the samples.

$\mathrm{D}_s^{\sigma\delta}(t)$ for a single dipole (equation 3.4.12). Considering for each dye molecule the excitation and emission transition dipole moments coincidents ($\vec{d}_{ex} \equiv \vec{d}_{em}$) and integrating $\mathrm{D}_s^{\sigma\delta}(t)$ over all possible excitation dipole orientations in the space:

$$\begin{aligned} \mathrm{D}_e^{\sigma\delta}(z_0,t) &= \\ &= \alpha \cdot \int_0^{\pi} d\theta_{ex} sin(\theta_{ex}) \int_0^{2\pi} d\phi_{ex} R_{exc}^{\sigma}(\{\mu ex\},\{EX\},\{ML\}) \cdot \\ &\cdot \quad e^{-\Gamma_{tot}(\{ML\},\{EM\},\{\mu ex\})\cdot t} \int_{\Omega_d} R_{em}^{\delta}(\{\mu ex\},\{EM\},\{ML\})\, d\hat{m} \end{aligned} \tag{3.5.2}$$

$\sigma\delta$ refers to the excitation-detection polarization combination (i.e. *pp, ps, sp* or *ss*), while the "sets of variables" are defined in 3.4.11. Now α includes also a factor related to the dyes concetration on the sample: $\left(\frac{cA}{4\pi}\right)$.

3.5.1 Emission Dipole Moment

Until now the dye excitation and emission dipoles have been considered identical. From a quantum mechanical point of view, the excitation and the emission were regarded as single-frequency transitions involving the same pair of dye molecule energy levels. Even representing a reasonable approximation, the fluorescence excitation and emission spectra of any chromophore show broad bands over a wide region of wavelengths, indicating the reality is more complex. Due to the definition of the transition dipole moments and the energy levels structure of a dye molecule, $\vec{d}_{ex}$ and $\vec{d}_{em}$ are not independent. It is therefore appropriate to express, for example, the latter in function of the first. In this manner the emission dipole moment lies on a cone surface: the cone has as main axis the excitation dipole moment and a definite semi-opening angle $\Delta\theta$ (see figure 3.5.1). To simulate correctly the fluorescence decay curve for an ensemble of dye molecules the exact direction of $\vec{d}_{em}$ respect $\vec{d}_{ex}$ for each chromophore would be necessary. However, in this wirk an uniform orientation of the dye molecules in space (i.e. uniform orientation of $\vec{d}_{ex}$) was assumed and $\Delta\theta$ was considered as an intrinsic property of the emitter. As a consequence, it is possible to integrate over the cone perimeter (over the angle ξ in the figure 3.5.1) to take in account of distinct emission dipole from the excitation dipole.

According to figure 3.5.1, for the emission dipole moment:

$$\theta_{\mathrm{em}} = \theta_{\mathrm{em}}(\theta_{ex}, \Delta\theta, \xi)$$

$$\phi_{\mathrm{em}} = \phi_{\mathrm{em}}(\phi_{ex}, \Delta\theta, \xi)$$

but working in spherical coordinates there is no univocal relation between ξ and $\Delta\phi = \phi_{\mathrm{ex}} - \phi_{\mathrm{em}}$. To correct the ambiguity in the integration over ξ, the dipole moment cartesian components can be used. First the original coordinates system (x,y,z) are rotated in such manner tha $\vec{d}_{\mathrm{ex}}$ is parallel to z-axis in the new reference system (x',y',z') and then by a second rotation the two x axis are made coincident ($x \equiv x'$). In this way in the new reference system: $\theta_{\mathrm{em}}^{'} = \Delta\theta$ and $\phi_{\mathrm{em}}^{'} = \xi$ (see also figure 3.5.2).

Using the rotation matrices for the cartesian axes in a 3-dimensional space, for an angle α:

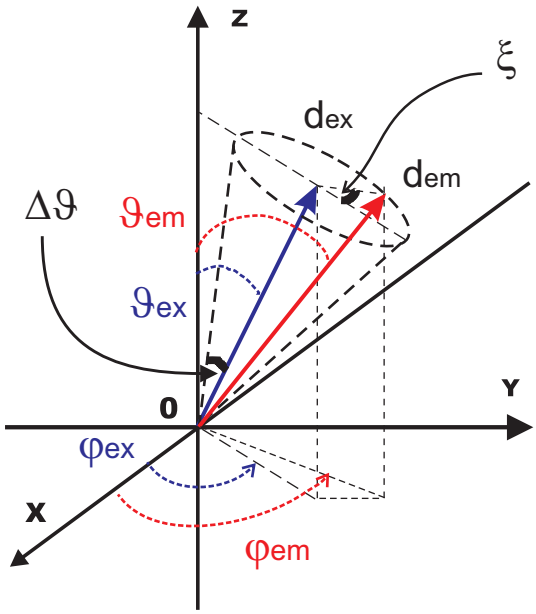

Figure 3.5.1: Schematic representation of associated excitation ($\vec{d}_{ex}$ - blue) and emission ($\vec{d}_{em}$ - red) transition dipole moments for an organic dye molecule. Relative polar and azimutal angles are also reported.

$$R_{\mathrm{x}}(\alpha) = \begin{bmatrix} 1 & 0 & 0 \\ 0 & \cos\alpha & \sin\alpha \\ 0 & -\sin\alpha & \cos\alpha \end{bmatrix}$$

$$R_{\mathrm{y}}(\alpha) = \begin{bmatrix} \cos\alpha & 0 & -\sin\alpha \\ 0 & 1 & 0 \\ \sin\alpha & 0 & \cos\alpha \end{bmatrix}$$

$$R_{\mathrm{z}}(\alpha) = \begin{bmatrix} \cos\alpha & \sin\alpha & 0 \\ -\sin\alpha & \cos\alpha & 0 \\ 0 & 0 & 1 \end{bmatrix}$$

To find the total rotation matrix for the wanted transformation:

$$R_{\mathrm{T}}(\theta_{\mathrm{ex}},\phi_{\mathrm{ex}}) = R_{\mathrm{y}}(\theta_{\mathrm{ex}}) \cdot R_{\mathrm{z}}(\phi_{\mathrm{ex}}) = \begin{bmatrix} \cos\phi_{\mathrm{ex}}\cos\theta_{\mathrm{ex}} & \sin\phi_{\mathrm{ex}}\cos\theta_{\mathrm{ex}} & -\sin\theta_{\mathrm{ex}} \\ -\sin\phi_{\mathrm{ex}} & \cos\phi_{\mathrm{ex}} & 0 \\ \sin\theta_{\mathrm{ex}}\cos\phi_{\mathrm{ex}} & \sin\theta_{\mathrm{ex}}\sin\phi_{\mathrm{ex}} & \cos\theta_{\mathrm{ex}} \end{bmatrix}$$

Using this matrix to transform the emission dipole moment then:

$$\overrightarrow{d'}_{\mathrm{em}} = R_{\mathrm{T}}(\theta_{\mathrm{ex}},\phi_{\mathrm{ex}})\,\overrightarrow{d}_{\mathrm{em}} \tag{3.5.3}$$

and by orthogonality of rotation matrices and looking at figure 3.5.2 finally:

$$\overrightarrow{d}_{\mathrm{em}} = {}^{\mathrm{t}}R_{\mathrm{T}}(\theta_{\mathrm{ex}},\phi_{\mathrm{ex}})\,\overrightarrow{d}'_{\mathrm{em}} \tag{3.5.4}$$

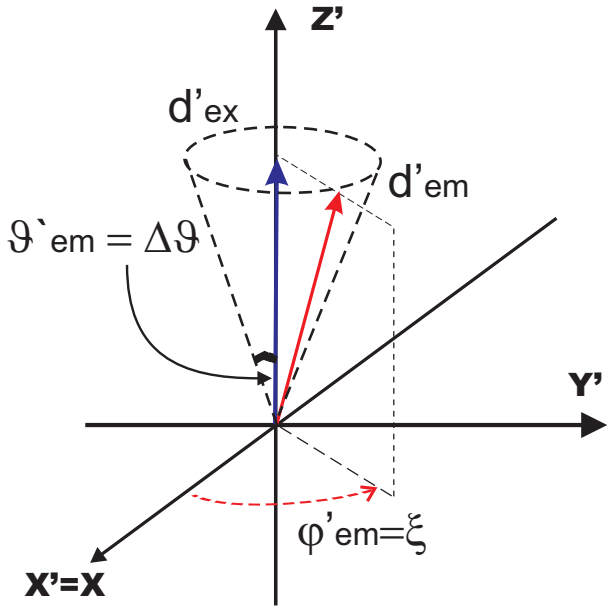

Figure 3.5.2: Schematic representation of excitation ($\vec{d}'_{\text{ex}}$ - blue) and emission ($\vec{d}'_{\text{em}}$ - red) transition dipole moments for an organic dye molecule in the new reference system (x',y',z'), as explained in the text.

By detailing the cartesian components of 3.5.4:

$$\begin{aligned} d^{\text{x}}_{\text{em}} &= d_{\text{em}} \cdot \{\sin\Delta\theta\cos\xi\cos\theta_{\text{ex}}\cos\phi_{\text{ex}} - \sin\Delta\theta\sin\xi\sin\phi_{\text{ex}} + \cos\Delta\theta\sin\theta_{\text{ex}}\cos\phi_{\text{ex}}\} \\ d^{\text{y}}_{\text{em}} &= d_{\text{em}} \cdot \{\sin\Delta\theta\cos\xi\cos\theta_{\text{ex}}\sin\phi_{\text{ex}} + \sin\Delta\theta\sin\xi\cos\phi_{\text{ex}} + \cos\Delta\theta\sin\theta_{\text{ex}}\sin\phi_{\text{ex}}\} \\ d^{\text{z}}_{\text{em}} &= d_{\text{em}} \cdot \{-\sin\Delta\theta\cos\xi\sin\theta_{\text{ex}} - \sin\Delta\theta\sin\xi\sin\phi_{\text{ex}} + \cos\Delta\theta\cos\theta_{\text{ex}}\} \end{aligned} \tag{3.5.5}$$

The components of the emission dipole moment expressed in 3.5.5 can be introduced directly in the calculus of the detection probability. For an ensemble of dyes the integral over the cone perimeter (over ξ), has to be performed after the value of $\Delta\theta$ is determined. In this way, starting from equation 3.5.2, the fluorescence probability for an ensemble of dyes can be generalized to the case of distinct excitation and emission dipoles:

$$\mathrm{D}_e^{\sigma\delta}(\bar{z}_0,\Delta\theta,\Gamma_{nr},\Gamma_0,n_1,n_2,\hat{l},\Omega_d,t) = \alpha\cdot\int_0^{\pi} d\theta_{ex} A\cdot B\cdot C \tag{3.5.6}$$

having set for clarity of notation

$$\begin{aligned} A = &\quad \sin(\theta_{ex})\cdot\textstyle\int_0^{2\pi} d\phi_{ex} R^{\sigma}_{exc}(\{\mu ex\},\{EX\},\{ML\}) \\ B = &\quad \textstyle\int_0^{2\pi} d\xi\, e^{-\Gamma_{tot}(\{ML\},\{\lambda_{em}\},\{\mu ex\},\xi,\Delta\theta,\Gamma_{nr})\cdot t} \\ C = &\quad \textstyle\int_{\Omega_d} d\hat{m} R^{\delta}_{em}(\{\mu ex\},\{EM\},\{ML\},\xi,\Delta\theta) \end{aligned} \tag{3.5.7}$$

The polar coordinates of the excitation $(\theta_{ex},\varphi_{ex})$ and emission $(\Delta\theta,\xi)$ dipoles are showed in figure 3.5.1 and now $\bar{z}_0$ represents the mean distance of all dyes from the interface. Here the superscripts σ

and δ denote the polarization of the excitation and emission local fields respectively and the possible combinations are $\sigma\delta = pp, ps, sp, ss$. The variables related to the multilayer system $(\bar{z}_0, \mathrm{n}_1, \mathrm{n}_2)$ and to the geometry of experimental setup $(\hat{l}, \Omega_d)$ are known and displayed in figure 3.4.1. The variables connected to the molecular structure of the dye $(\Delta\theta, \Gamma_0)$ and its interaction with the surroundings (Γ_{nr}) are unknown and constitute the free parameters of the model. $\mathrm{D}_e^{\sigma\delta}(z_0,t)$ is not single exponential decay curve like $\mathrm{D}_s^{\sigma\delta}(z_0,t)$ for the single dipole, because now $\Gamma_{tot}(\{ML\},\{EM\},\{\mu ex\})$ depends on excitation dipole moment and has to be integrated over all the possible orientations for $\vec{d}_{\mathrm{ex}}$.

Once the decay curve for an ensemble of dipoles is obtained by expression 3.5.6, it is possible to evaluate the average lifetime either anatically by calculating the first moment of the probability distribution

$$< \tau^{\sigma\delta} >= \frac{\int_0^\infty \mathrm{D}_e^{\sigma\delta}(z_0,t)\cdot t\, dt}{\int_0^\infty \mathrm{D}_e^{\sigma\delta}(z_0,t)\, dt} = \frac{1}{\Gamma_{tot}} = \tau_{sim}^{\sigma\delta} \tag{3.5.8}$$

or by least squares fitting of the resulting simulated decay curve. The integrals in 3.5.6 and thus in 3.5.8 can be calculated only numerically and the space of the variables have to be discretized. Thus, it turns out that the least squares fitting is the most suitable method for theoretical lifetime evaluation. From equation 3.5.8 it is important to notice that the mean average lifetime depends on the polarization combinations. As a consequence, the quantity $\tau_{sim}^{\sigma\delta}$ can be compared to experimental fluorescence lifetime values.

On the other hand the emission probability density, $\mathrm{D}_e^{\sigma\delta}(t)$ in equation 3.5.6, is related to the detected fluorescence intensity by its integral over time intervals. For an infinitely short excitation pulse at time $t = 0$ (i.e. delta-like excitation), the number of photons collected in a time interval Δt, at time t after excitation pulse is given by:

$$\mathrm{I}_{sim}^{\sigma\delta}(t,\Delta t) = \int_t^{t+\Delta t} \mathrm{D}_e^{\sigma\delta}(t')\cdot dt' \tag{3.5.9}$$

Equation 3.5.9 shows that the fluorescence intensity depends on excitation-detection polarization combinations as well. The theoretical values by the equation 3.5.9 can be compared with experimental decay curves. The fluorescence intensity evaluated at time $t = 0$ (i.e. $\mathrm{I}_{sim}^{\sigma\delta}(0)$) will assume particular importance in the PCM method (chapter 4).

3.5.2 Numerical Evaluation

To evaluate the final emission probability density expressed by the equation 3.5.6 numerical methods are necessary and specific procedures were created by the *Igor Pro* software (Wavemetrics Inc.). *Igor Pro* is a package for data waves manipulation which includes several subroutines for graphical applications and data fitting. Key points are the numerical convergence for the integrals involved through all the simulations steps and the effect of discretization process on the calculated physical quantities for each single integral in 3.5.6. The convergence of each integral included in equation 3.5.6 was checked:

- integrals in θ_{ex} and ϕ_{ex}: the polar and azimutal angular ranges (π and 2π respectively) were divided in different number of intervals (number of points of integration). On a discrete base

this number corresponds exactly to the number of dipoles considered in our simulation and distributed symmetrically through space. Figure 3.5.3 depicts the theoretical emission probability density of an ensemble of dipoles $D_e^{\sigma\delta}(t)$, according to equation 3.5.6, for different excitation-detection polarization combinations (*pp, ps, sp,* ss*)*. Here a different number of dipoles forming the ensemble: 16, 10^2, 10^3 and 10^4 are considered.

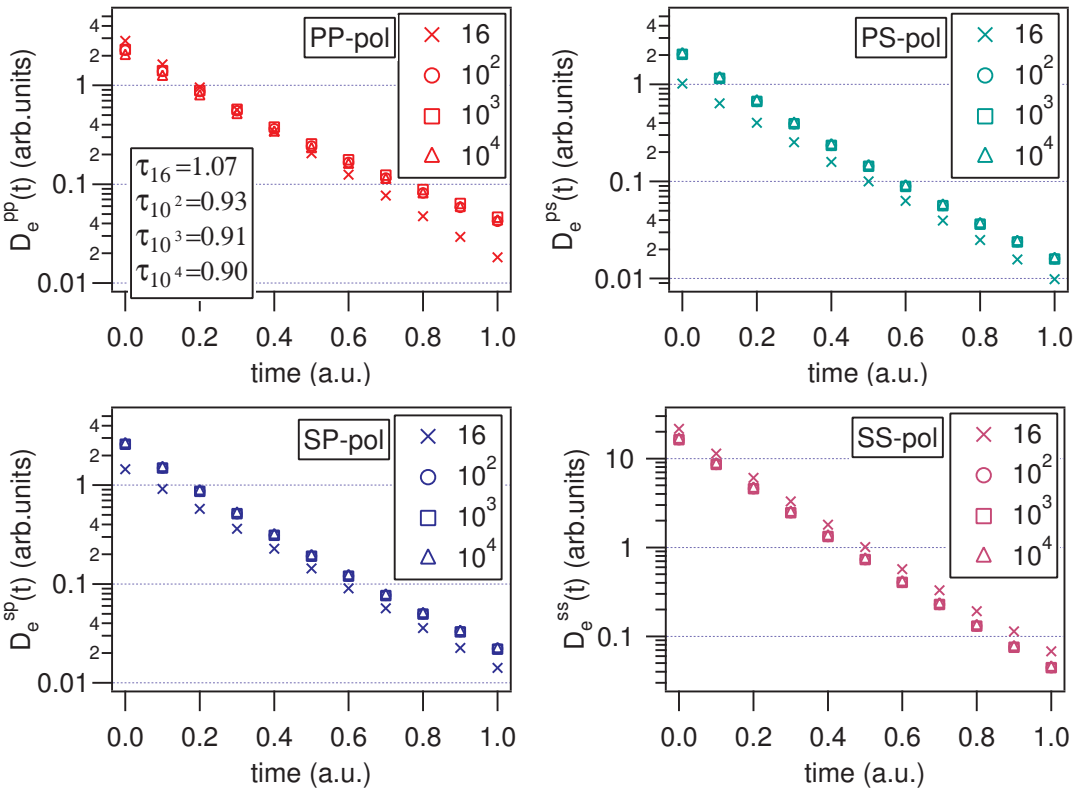

Figure 3.5.3: Simulated emission probability density of an ensemble of dipoles $D_e^{\sigma\delta}(t)$, according to equation 3.5.6, for different excitation-detection polarization combinations (*pp, ps, sp,* ss*)* and as function of a different number of dipoles constituting the ensemble*:* 16, 10^2, 10^3 and 10^4. The dipoles are placed close to an interface air-polymer, in the air side. As an example, the lifetime values for pp polarization combination obtained by graphical fit are reported in the inset.

Figure 3.5.3 indicates that already with $\sim 10^3 \div 10^4$ dipoles, the numerical oscillations for lifetime values are below 2% (see the inset in figure, for the case of *pp* polarization). Hence, the numerical convergence is reached within the software code accuracy. As a consequence a dipole-mesh with vectors every 6Â° on polar range (θ) and every 12Â° on azimutal scale (φ) already gives good numerical results respect the analytical integration. 900 dipoles in the simulation can represent a good compromise between numerical accuracy and machine time.

- Integral in $\hat{m}$: estimating the size of the detector's active area and its distance from the sample, the solid angle associated to the detector's area was determined as high as $d\Omega = A_d/r^2 \sim 3.5 \cdot 10^{-3}$ steradians. A_d is the detector active area with a corresponding cone angular opening of $\sim$ 3.82Â°. Figure 3.5.4 shows the simulated fluorescence lifetime ($\tau_{sim}^{\sigma\delta}$) and intensity ($I_{sim}^{\sigma\delta}(0)$) of an ensemble of 900 dipoles uniformly oriented through space, according to equations 3.5.8 and 3.5.9. Figure 3.5.4 shows the values for different excitation-emission polarization combinations ($\sigma\delta$) and different number of integration points across the detector active area.

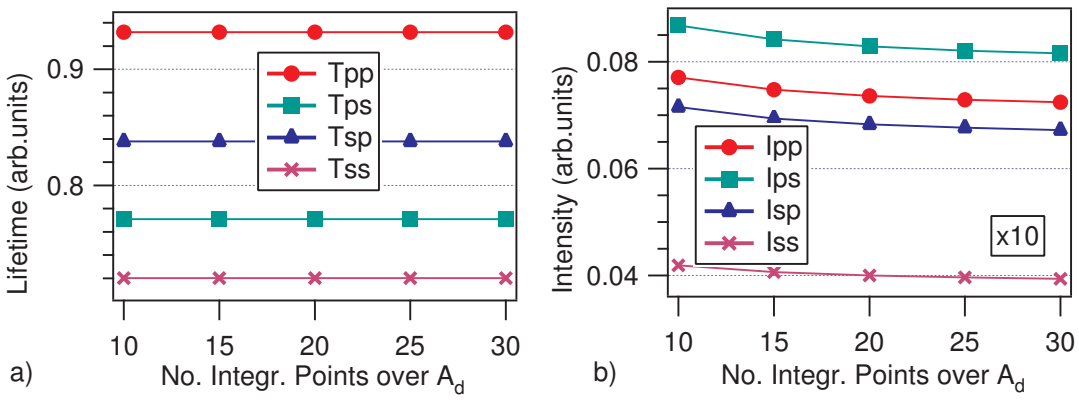

Figure 3.5.4: Simulated fluorescence lifetime ($\tau_{sim}^{\sigma\delta}$) a) and intensity ($I_{sim}^{\sigma\delta}(0)$) b) of an *ensemble* of 900 dipoles uniformly distributed through space, according to equations 3.5.8 and 3.5.9. In figure the values for different excitation-emission polarization combinations ($\sigma\delta$) are reported, as a function of the different number of integration points across the detector active area (A_d).

Figure 3.5.4 indicates that the fluorescence lifetime is practically not affected from the discretization of the detector area, for all polarization combinations. On the other hand, the intensities get approximatively their limit values (error $\lesssim 0.6\%$ between two successive points) after 30 integration intervals. In the final code 30 integration intervals over the detector area A_d, will be considered.

- Integral in ξ: the average over all possible emission dipole orientations on the surface of the cone, for a fixed excitation dipole (i.e. a well oriented organic dye molecule). It may depend on the number of integration points chosen across the cone perimeter (see figure 3.5.2).

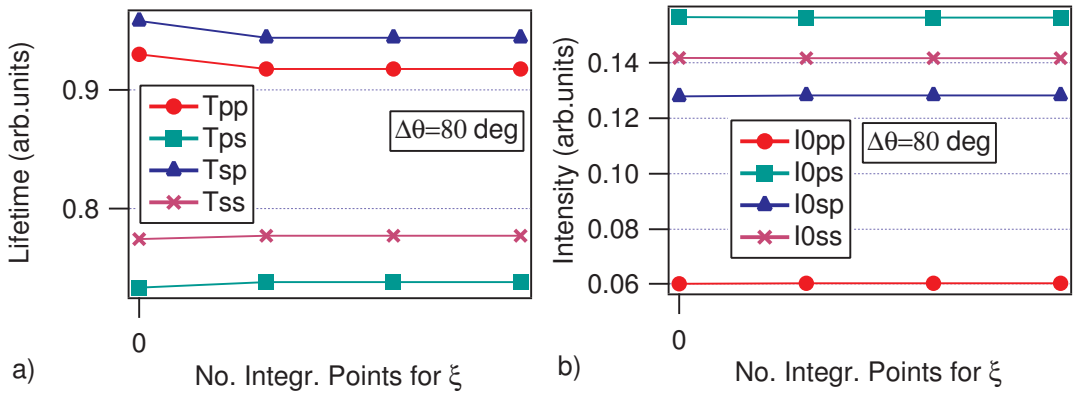

Figure 3.5.5: Simulated fluorescence lifetime ($\tau_{sim}^{\sigma\delta}$) a) and intensity ($I_{sim}^{\sigma\delta}(0)$) b) of an ensemble of 900 dipoles uniformly distributed through space, according to equations 3.5.8 and 3.5.9. In figure, the values for different excitation-emission polarization combinations and different number of integration points on the perimeter of the cone are reported.

In figure 3.5.5 the simulated fluorescence lifetime $\tau_{sim}^{\sigma\delta}$ and intensity $I_{sim}^{\sigma\delta}(0)$ of an ensemble of 900 dipoles uniformly oriented through space are plotted (according to equations 3.5.8 and 3.5.9). The curves are relative to different polarization combinations as a function of the number of integration points chosen over the perimeter of the cone (i.e. over the variable ξ in figure 3.5.2). The chosen semi-opening for the cone is $\Delta\theta = 80\hat{A}^\circ$. For smaller values of $\Delta\theta$, the variation in lifetimes and intensities

is smaller than the numerical error of the software code. Figure 3.5.5 shows that the summatory convergence is quite fast and after integrationg over 10 different orientations no changes within the software numerical precision are obtained. Therefor, 15 integration intervals in all successive data simulations will be used.

Simulation Time

By using numerical methods computational time is definitively an issue. On the other hand the integrals convergence studies in the previous section show how the discretization process can affect the final result. The integration over the detector area (A_d) represents the most "internal" integral: it has to be calculated for each single dipole in the system (see term C in equations 3.5.6 and 3.5.7). An optimization of this integral would be beneficila in terms of simulation time. Two different methods of calculus were tested:

- the fluorescence radiation field emitted by the ensemble of chromophores was calculated on each single point of the grid, which defines the discretized detector area A_d.
- The electric field value evaluated at the centre of the detector was taken for all points of the grid, which defines the discretized detector area A_d.

Figure 3.5.6 displays a comparison among theoretical decay curves obtained by calculating fluorescence far-field values at each point of the grid within the detector area and by using a mean value of the fluorescence far-field calculated in the center of the detector area. The curves in figure 3.5.6 are plotted for different polarization combinations, according to equation 3.5.2.

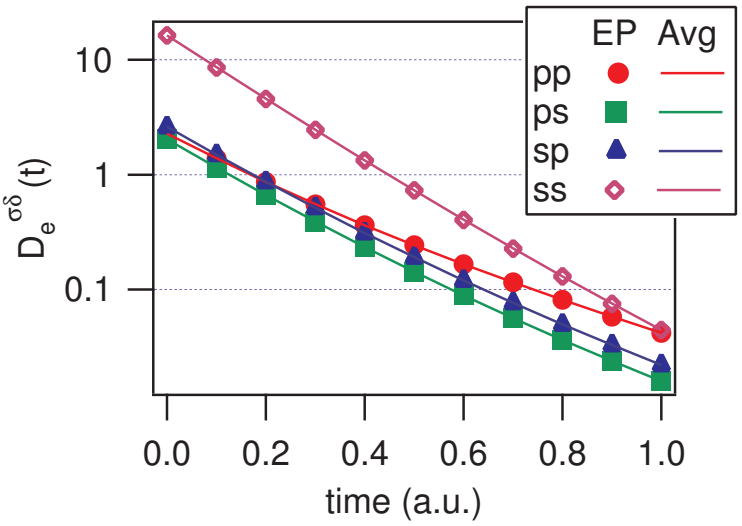

Figure 3.5.6: Comparison among the simulated decay curves obtained by calculating emission far-field values at each point of the grid within the detector area (markers in the plot, EP in the legend) and by using a mean value for the emission far-field, calculated in the center of the detector area (lines in the plot, AVG in the legend). The curves are plotted for different polarization combinations, according to equation 3.5.2.

From figure 3.5.6, it is possible to conclude that the two methods do not show significant differences. Lifetimes changes are within an interval between 0.2% and 0.5% for different polarization combinations. On the other hand by using the mean value of electric field over the whole detector active area A_{d}, the simulation time was reduced of a factor ~ 200 (from many hours to few minutes).

3.6 Conclusions

A numerical method to calculate excitation and emission of an ensemble of dye molecules embedded in a multilayer system was presented in this chapter. The method models the chromophores as point-like electrical dipoles and it makes use of the:

- Transfer Matrix Algorithm, by which it is possible to calculate the local electric fields within a multilayer system, by using plane waves and classical (electromagnetism) boundary conditions.
- Reciprocity Theorem, for the evalutation of the dipoles emission into space.
- Equivalence between the radiated power by an electrical dipole and the fluorescence decay rate of a molecule.

The method was numerically implemented by a software code, specifically built for a 5 layer system, with the purpose to simulate the experimental conditions met during the measurements. The numerical convergence of the integrals involved in the theoretical calculations was explored and verified for the discretized variables. The code was also optimizated in order to reduce computational time. The method here developed can be easily extended to a multilayer with an arbitrary number of layers and it provides the theoretical fluorescence decay curve for single dye or for an ensemble of dyes embedded within a multilayer system. In this manner a full simulation of the time resolved fluorescence experiments is obtained.

Bibliography

[1] Pochi Y., *Optical Waves in Layered Media,* Ed. Wiley (1988)

[2] Potton R.J., *Rep. Prog. Phys*. **67** (2004) 717â€“754.

[3] Herzberg G., *Spectra of Diatomic Molecules, Vol.1, 2nd ed.; Krieger Publishing Co., (1989).*

[4] Valeur B., *Molecular Fluorescence,* WILEY-VCH Verlag GmbH (2002).

[5] Novotny L., Hecht B., *Principles of Nano-Optics*, Cambridge Univ. Press (2006).

[6] Dmitri Toptygin, *Journal of Fluorescence*, Vol. 13, No. 3, May 2003 (2003).

[7] Lukosz W. and Kunz R. E., *J. Opt. Soc. Am.*, Vol. **67**, No. 12, December 1977.

[8] See datasheet for PMC-100-20 photomultiplier, Becker&Hickl, at the web adress http://www.becker-hickl.de/).

Chapter 4

The *Polarizations Combination* Method

Abstract

An optical investigation method for chromophores close to an interface, analogous to polarized fluorescent emission in solvent is presented. It discriminates between transition dipoles parallel and perpendicular to a dielectric interface. The technique analyzes the fluorescence lifetime and the intensity of a dye molecule close to an interface, as a function of the polarization of the exciting radiation and of the detection. Orientation dependent lifetimes can be measured and they allow for the determination of the angle between excitation and emission dipoles, non-radiative decay rate and vacuum lifetime of the chromophores. In the following, some theoretical concepts about the fluorescence decay curves expressed in the previous chapter will be repeated. The purpose of such choice is to focus on key physical ideas.

4.1 Introduction

4.1.1 The background

Since earlier work of Purcell at radio frequencies [16], it is well established that the spontaneous emission probability of a quantum system is affected by the surrounding. Fluorescence is a spontaneous emission process and the related decay rate is not only an intrinsic property of the emitting system itself, but is influenced also by the so called Photonic Mode Density (PMD) [17]. Fluorescence lifetime as a function of the fluorophore distance from an interface between two dielectric media was already subject of the pioneering work of Drexhage and coworkers. In this study an emitter was spaced from a metallic substrate by varying the number of organic Langmuir-Blodgett monolayers. Consequently, the distance between the emitter and the mirror surface was then changed in a controlled way (for a nice summary see [1]). Kuhn [2] was the first to develop theoretical model trying to explain Drexhage's results. Kuhn was able to evaluate correctly the far field, but the model failed in predicting quenching at short distances from the surface. A fully correct and comprehensive theory was then developed by Chance, Prock and Silbey [5], the so called CPS theory. This included naturally the metal surface plasmon polariton by considering the full optical response of the surface, that is the complex dielectric permittivity of the metal. Several years later, the equivalence between the classical model used in the CPS treatment and a full quantum-mechanical calculation was established by Yeung and Gustafson [6]. Lukosz and Kunz studied the light emission by magnetic and electric

dipoles close to a plane interface, for loss-free dielectric media. They gave an expression for the total emitted power and calculated the relative radiation patterns [3]. The developed theory indicates a dependency of the emitted radiation from the dipole orientation with respect to the interface. Experimental proof of this result came from the work of Macklin [8] and Kreiter [7], where was shown that single molecules have different lifetimes for distinct orientations. Excited state lifetimes near interfaces attracted much attention in the following years, from a theoretical perspective and as a potential technique for sensing applications, opening the doors also to single molecule experiments. In this context, Brokmann and coworkers [9] found a method to determine the radiative and non-radiative decay rate of individual fluorescent emitters at room temperature. Single CdSe nanoparticles were placed on a glass cover slip and covered by polymer films of different thickness (i.e. close and far from a dielectric interface). By measuring the photoluminescence decay and the orientation of the quantum dots, Brokmann et al. were able to measure the quantum dots fluorescence quantum efficiency in an unbounded medium. Besides the large amount of information provided, single molecule experiments may have some drawbacks like photobleaching (limiting the photon statistics for each single emitter) or in the case of quantum dots fluorescence intermittency. Moreover, single molecule measurements are necessarily biased by the choice of some molecules during the experiment (for example the brighter ones) which may not provide representative information on the system under investigation. Finally, single molecule experiments are time consuming, if a good sample statistic for the number of molecules analyzed is required. In this respect fluorescence lifetime experiments on an ensemble of molecules are advantageous: a simpler and cheaper experimental setup is necessary and photobleaching is not relevant at the local excitation power densities involved. Moreover, the measurements for specific excitation and detection polarization can take from few seconds to several minutes. Finally, far field fluorescence experiments do not suffer from limitations on photon statistics. For these reasons, time correlated fluorescence spectroscopy of an ensemble of dyes may provide useful information for microscopic electromagnetic phenomena, possibly giving insights in understanding the local environment of the dye molecules. As an interesting example, a possible application comes from the electromagnetic field boundary conditions. Through a charged interface between two dielectric media, with refractive index n_1 and n_2, the perpendicular component of the electric field undergoes a discontinuity, while the parallel component is preserved from one medium to the other [19]. In detail:

$$\begin{aligned} (n_1)^2 \cdot E_{\perp,1} &= (n_2)^2 \cdot E_{\perp,2} \\ E_{\parallel,1} &= E_{\parallel,2} \end{aligned} \tag{4.1.1}$$

Placing therefore an ensemble of dye molecules in proximity either side of the interface, in principle it would be possible to verify the field discontinuity down to the nanometer range. At this length scale, much smaller than the wavelength, the continuous media approximation may be questionable.

A new optical investigation technique based on far field polarized fluorescence experiments for an ensemble of organic dyes in proximity to a dielectric interface was developed. Lifetimes and intensities were measured for several excitation-detection polarization combinations, in order to obtain averaged information on the local environment surrounding the emitters. It is the first time that the fluorescence characteristics of chromophores near a dielectric interface are analyzed in the far field, for all possible excitation-detection combinations. The suggested detection scheme also enhances the difference among different polarizations. By this technique no photobleaching or blinking issues are encountered, numerical aperture of observation does not constitute a limitation and no restrictions on excitation-detection angular range of dipoles are experienced. The method, called Polarization Combination Method (PCM), provides information about the micro-environment surrounding the dye and about the connection between fluorescence properties and local environment. It allows in fact a mea-

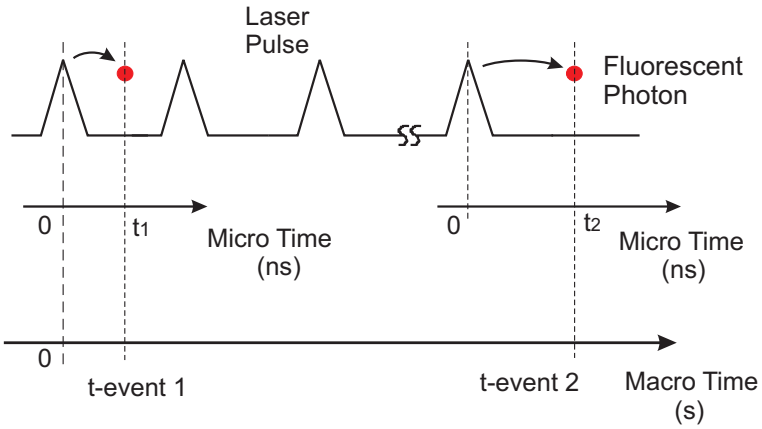

Figure 4.2.1: Schematic representation of the Micro Time and Macro Time for a time resolved fluorescence experiment. The Micro Time is also called TCSPC time, while the latter is also called Tag Time or real time.

surement of the angle-dependent PMD (section 4.2). Finally, the PCM gives some insights about intrinsic properties of the dye.

In the following the theoretical background of the technique is first introduced, then the method is applied to organic dye molecules embedded in a polyelectrolyte matrix. The preparation of a dye ensemble is described in section 4.3, while details of the experimental setup are given in section 4.4. The samples are characterized in section 4.5 and the PCM details are discussed in the data analysis section 4.6. Finally, conclusions will be given in section 4.7.

4.2 The Theoretical Bases behind PCM

Spontaneous decay is a pure quantum effect and requires a quantum electrodynamic treatment. Then the quantum mechanics pictures involves the concept of transition dipole moment, as a physical quantity associated to a photon absorption-emission process between two energy levels of a molecule [18]. It is also possible to derive a classical analogy based on an oscillating point-like electrical dipole. Hence, a fluorophore can be modeled as a couple of oscillating point-like dipole moments, describing the excitation and emission processes. The dipoles are called excitation and emission dipole moments and the point-like dipole approximation is well satisfied for far-field studies. To show rigorously the connection between a quantum mechanical approach and a classical treatment, even in its simplest model of two level system, a second quantization procedure is needed and it is out of the purposes of this work [23] (see also chapter 3).

In the experiments the dye molecule is excited by a pulsed laser and the fluorescence radiation is detected in the time interval between two successive pulses. This acquisition method is called time-tagged time-resolved or equivalently time correlated single photon counting and a maximum of one photon between two laser pulses is detected ([25]). The arrival time of the photon with respect to the excitation pulse is called Micro Time (see figure 4.2.1). In general, an experiment of photoluminescence involves as many excitation cycles as necessary to reach a good photon statistics for the detected fluorescence intensity. The relative time required is defined as Macro Time, i.e. the time of the experiment also called Tag Time or real time.

For adequate time-spaced excitation pulses (i.e. excitation frequency $\ll$ emitter decay rate) the system can be considered always in the same physical condition at the arrival of each excitation pulse

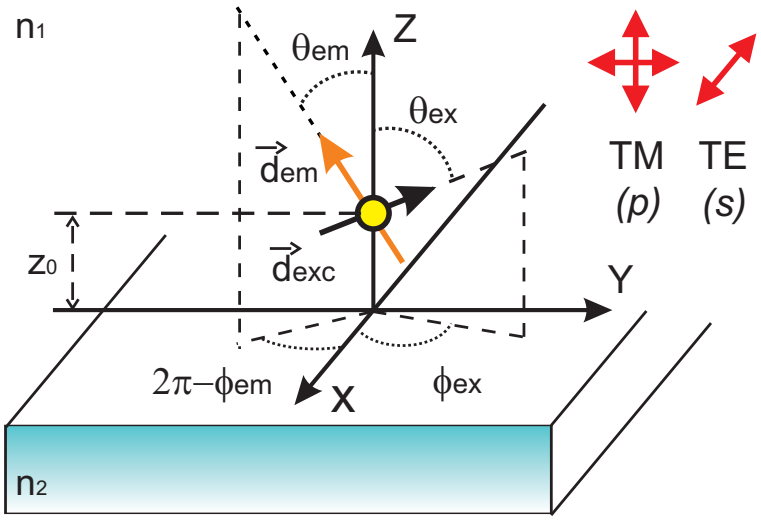

Figure 4.2.2: Sketch of a dye molecule modeled as a couple of excitation and emission dipole, $\vec{d}_{exc}$ and $\vec{d}_{em}$ respectively in figure. The point-like dipoles are at distance z_0 from an interface separating two semi-infinite and homogeneous media with refractive index n_1 and n_2 and orientations in polar coordinates are given: $\vec{d}_{exc} \equiv (\theta_{ex}, \phi_{ex})$ and $\vec{d}_{em} \equiv (\theta_{em}, \phi_{em})$. The plane of figure represents the plane of incidence and electric field vectors for TM and TE modes are reported.

front. Therefore, for simulation purposes, it is convenient to consider a photoluminescence measurement of an emitter like a fictitious one-excitation-pulse experiment after which *all* the photons are collected. The resulting intensity curve, as a function of the Micro Time, is represented by the Probability Density Function $\mathrm{D}_s(t)$. When this function is integrated over a generic time interval, it provides the number of fluorescence photons in that interval (fluorescence intensity). The emission characteristics of a fluorescent system are thus analyzed by comparing the experimental and the theoretical decay curves. In the next sections, a brief overview is given about the calculation of the Probability Density Function for a single dipole and for an ensemble of identical dipoles. A more comprehensive treatment is reported in chapter 3.

4.2.1 Single dipole

It is useful to consider the whole space filled with two semi-infinite media divided by an interface and a couple of classical point-like oscillating electric dipoles embedded in one of the two media, at a fixed distance z_0 from the interface. It is possible to regard them as excitation ($\vec{d}_{exc}$) and emission ($\vec{d}_{em}$) dipoles having a certain orientation with respect to the interface (see figure 4.2.2). The probability to detect a fluorescence photon at certain time t after excitation will depend on the excitation probability P_{exc} of the dye molecule, the emission rate $R_{em}(t)$ at time t and on the detection probability P_{det} for the specific detector considered. In this manner, it is possible to write the fluorescence probability density for a single dipole as:

$$\mathrm{D}_s(t) \propto P_{exc} \cdot R_{em}(t) \cdot P_{det} \tag{4.2.1}$$

The function $\mathrm{D}_s(t)$ has the dimension of a rate and integrated on a time interval it provides the number of photons detected. In the next sections P_{exc}, $R_{em}(t)$ and P_{det} will be evaluated separately, detailing their dependence on the system variables.

a) Excitation Probability P_{exc}

The excitation rate depends both on dye orientation and on excitation polarization. The process of selective excitation for a single dye (i.e. photoselection [15]) is achieved by changing the polarization of the excitation radiation with respect to the interface. Considering the excitation source constituted by plane waves impinging the interface at a certain direction, defined by the unit vector $\hat{l}$, then:

$$P_{exc}(\theta_{ex},\phi_{ex},z_0,\hat{l},n_1,n_2,pol) \propto \mid \overrightarrow{d}_{exc} \cdot \overrightarrow{E}^{pol}_{exc,loc}(z_0,\hat{l},n_1,n_2) \mid^2 \tag{4.2.2}$$

where $\overrightarrow{d}_{exc}$ is the associated excitation dipole moment and $(\theta_{ex},\phi_{ex},z_0)$ its coordinates. $\overrightarrow{E}^{pol}_{exc,loc}$ is the excitation local electric field experienced by the dipole itself, while *pol* indicates the field polarization as indicated in figure 4.2.2). TM mode is relative to transverse magnetic vector field with respect to the plane of incidence or *p* polarized radiation, while TE means transverse electric vector field with respect to the the plane of incidence or *s* polarized radiation.

b) Total Emitted Radiation and Decay Rates

Once the excitation dipole $\overrightarrow{d}_{exc}$ has been excited, an immediate and complete transfer of all energy to the emission dipole $\vec{d}_{em}$ takes place. In general, the emission dipole has a different orientation than the excitation dipole (see figure 4.2.2). Then, $\vec{d}_{em}$ represents a damped harmonic oscillator which loses its energy emitting radiation in the space and through non-radiative channels. The total time-averaged power $S(z_0)$ radiated by an oscillating (i.e. excited) dipole can be expressed by [3]:

$$\left[\frac{S(z_0,n_1,n_2)}{S_{n_1,\infty}}\right] = \left[\frac{S(z_0,n_1,n_2)}{S_{n_1,\infty}}\right]_{\perp} \cdot \cos^2(\theta_{em}) + \left[\frac{S(z_0,n_1,n_2)}{S_{n_1,\infty}}\right]_{\parallel} \cdot \sin^2(\theta_{em}) \tag{4.2.3}$$

where $S_{n_1,\infty}$ is the total power when the dipole is at infinite distance from the interface in the medium with refractive index n_1. θ_{em} is the relative angle between the dipole vector and the normal to the interface (figure 4.2.2). The media are considered semi-infinite, linear, isotropic and non magnetic. The subscripts $\perp$ and $\parallel$ denote dipoles perpendicular and parallel to the interface, respectively. For a generical dipole orientation, it is always possible to decompose the dipole vector in a component parallel and in a perpendicular one to the surface, but these components are not completely independent and they oscillate with the same phase factor: as a result the $\sin^2$ and $\cos^2$ functions appear in equation 4.2.3.

Radiative decay rate Γ_r It is possible to proof that the total radiated power of any current distribution with armonic time dependence (i.e. an oscillating dipole) has the identical expression than the spontaneous decay rate of a two-level quantum system (compare [23]). As a consequence of this equivalence, an identical expression to 4.2.3 can be written for decay rates. In the classical picture an oscillating electric dipole is assumed to be at the same position of the dye molecule and parallel to the transition dipole moment of the chromophore. Defining Γ as the fluorescence decay rate:

$$\left[\frac{\Gamma(z_0,n_1,n_2)}{\Gamma_0}\right]_r = \left[\frac{\Gamma(z_0,n_1,n_2)}{\Gamma_0}\right]_{\perp} \cdot \cos^2(\theta_{em}) + \left[\frac{\Gamma(z_0,n_1,n_2)}{\Gamma_0}\right]_{\parallel} \cdot \sin^2(\theta_{em}) \tag{4.2.4}$$

where the subscipt r is indicating the radiative part of the decay rate. In the expression 4.2.4 the decay rates are normalized with respect to Γ_0: the dipole decay rate at an infinite distance from the interface in vacuum. The oscillator decay rate in vacuum Γ_0 was obtained by the simulation code, calculating the average power emitted by a dipole in the unbound vacuum space (see chapter 3). The ratios in 4.2.4 make the radiative decay rates independent from the unknown dipole strength. As a drawback, the calculated lifetimes are only defined up to a multiplying factor. Therefore, for a direct comparison between experimental values and theoretical data the value of Γ_0 is necessary. In section 4.6.3, it will be explained how to extract a value for Γ_0 by the PCM method .

Non-radiative decay rate Γ_{nr} In general the total normalized fluorescence decay rate for a molecular dye can be written as:

$$\Gamma_{tot,N} = \Gamma_{r,N} + \Gamma_{nr,N} \tag{4.2.5}$$

where the radiative contribution $\Gamma_{r,N}$ is given exactly by eq. 4.2.4, while the non-radiative contribution $\Gamma_{nr,N}$ (here normalized by the same quantity Γ_0) in general is unknown. In equation 4.2.5, the physical variable $\Gamma_{tot,N} = \Gamma_{tot}/\Gamma_0$ is dimensionless and in the following treatment all the variables with subscript N are normalized with respect to the same value Γ_0. In section 4.6.2 it will be shown that with the PCM method it is possible to determine Γ_{nr}, under the important assumption of Γ_{nr} constant for different polarization combinations. Basically the non-radiative decay rate will be considered independent from the emission dipole orientation (with respect to the interface).

The total fluorescence emission rate in the whole space at time t is defined:

$$R_{em}(t) = \Gamma_0 \cdot \Gamma_{r,N} \cdot e^{-\Gamma_{tot,N} \cdot \Gamma_0 \cdot t} \tag{4.2.6}$$

where $\Gamma_{r,N}$ is given by 4.2.4, $\Gamma_{tot,N}$ by 4.2.5 and again Γ_0 is the fluorescence decay rate in vacuum. The exponential behavior comes out from the differential equations for a damped harmonic oscillator, while the factor $\Gamma_{tot,N}$ is necessary to normalize the expression 4.2.6. Integrating equation 4.2.6 over time between 0 and ∞, the fluorescence quantum yield is obtained:

$$\Phi_F = \frac{\Gamma_r}{\Gamma_r + \Gamma_{nr}}$$

Looking at equation 4.2.6 and remembering the classical definition of fluorescence lifetime given in chapter 3, it is possible to define the single dye molecule lifetime as:

$$\tau = \frac{1}{\Gamma_{tot,N} \cdot \Gamma_0} \tag{4.2.7}$$

Through equations 4.2.7, 4.2.5 and 4.2.4, the fluorescence lifetime for a single dye is well determined (except for a normalization factor Γ_0), once the geometry of the whole system is set (θ_{em}, z_0) and the material properties are known (n_1, n_2).

c) Detection Probability P_{det}

The expression in 4.2.6 yields the emission in the entire space, but in a real experiment the photons can be detected only within a limited solid angle. By using the Reciprocity Optical Theorem [24] (see for more details chapter 3), it is possible to show that the probability that an emitted photon is detected along the direction $\hat{m}$ is:

$$P_{det}(\hat{m}) \propto \mid \overrightarrow{d}_{em} \cdot \overrightarrow{E}^{pol}_{em,loc}(z_0, \hat{m}, \mathrm{n}_1, \mathrm{n}_2) \mid^2 \tag{4.2.8}$$

where $\overrightarrow{d}_{em}$ is the associated emission dipole moment (see figure 4.2.2). $\overrightarrow{E}^{pol}_{em,loc}$ is the emitted fluorescence local field with indication of its polarization in *pol*. The correct normalization factors come by integrating equation 4.2.8 over all space and imposing the detection probability equal to 1. Thus, the detection probability is:

$$P_{det}(\Omega_d) \propto \frac{1}{\Gamma_{r,N} \cdot \Gamma_0} \cdot \int_{\Omega_d} \mid \overrightarrow{d}_{em} \cdot \overrightarrow{E}^{pol}_{em,loc}(z_0, \hat{m}, \mathrm{n}_1, \mathrm{n}_2) \mid^2 d\hat{m} \tag{4.2.9}$$

where $\Gamma_{r,N}$ is given by 4.2.4, while Ω_d represents the solid angle under which fluorescence photons were collected.

Decay Curve for a Single Dye

Using the expressions 4.2.2 and 4.2.9, the total probability to detect a fluorescence photon in the detector is obtained. It is possible to write equation 4.2.1 in detail:

$$\begin{aligned} D_s^{\sigma\delta}(z_0, \theta_{ex}, \phi_{ex}, \theta_{em}, \phi_{em}, \Gamma_{nr}, \Gamma_0, \mathrm{n}_1, \mathrm{n}_2, \hat{l}, \Omega_d, t) \quad &= \\ = \alpha \cdot \mid \overrightarrow{d}_{exc} \cdot \overrightarrow{E}^{\sigma}_{exc,loc}(z_0, \hat{l}, \mathrm{n}_1, \mathrm{n}_2) \mid^2 \cdot & \\ \cdot e^{-\Gamma_{tot,N}(\theta_{em}, \phi_{em}, z_0, n_1, n_2, \Gamma_{nr}) \cdot \Gamma_0 \cdot t} \cdot & \\ \cdot \int_{\Omega_d} \mid \overrightarrow{d}_{em} \cdot \overrightarrow{E}^{\delta}_{em,loc}(z_0, \hat{m}, \mathrm{n}_1, \mathrm{n}_2) \mid^2 d\hat{m} & \end{aligned} \tag{4.2.10}$$

with α including the unknown factors connected to the excitation and detection efficiency. It contains a factor Γ_0 coming from correct normalization of equation 4.2.9, the number of excitation cycles per time unit and other constants related to the optical paths. The superscripts σ and δ denote the polarization of the excitation and emission local fields, respectively. Then the possible independent polarization combinations are $(\sigma\delta) = pp, ps, sp, ss$. The fluorescence probability density in equation 4.2.10 is then related to the fluorescence intensity by its integral over time intervals. Considering a generic time $t = t_0$, then the number of photons collected for a single dye molecule after a time $t = t_0 + \Delta t$ is given by

$$\mathrm{I}_{\sigma\delta}(t_0, \Delta t) = \int_{t_0}^{t_0+\Delta t} \mathrm{D}_s^{\sigma\delta}(t) \cdot dt \tag{4.2.11}$$

from which it is clear that the fluorescence intensity depends on excitation-detection polarization combinations. In an experimental design the variables defining the samples characteristics (z_0, n_1, n_2) and the geometry of experimental setup $(\hat{l}, \Omega_d)$ in equation 4.2.10 are known. Whereas the variables related to the molecular structure of the dye $(\theta_{ex}, \phi_{ex}, \theta_{em}, \phi_{em}, \Gamma_0)$ and to its interaction with the surroundings (Γ_{nr}) are unknown.

4.2.2 Dipoles Ensemble

An ensemble of identical dye molecules will be considered through this work. Each fluorophore has its own characteristic fluorescence lifetime and intensity, as expressed by the fluorescence probability density in equation 4.2.10. Moreover, following the previous section, each fluorophore is characterized by a couple of dipoles (excitation-emission dipole). Two additional assumptions were made:

- the dipoles of the ensemble are randomly oriented in space.
- All the dipoles are at the same distance $\bar{z}_0$ from the interface.

In chapter 3 the validity of the assumption is discussed. The total fluorescence radiation for the ensemble will be then the sum of the single dipoles radiation: non-interacting dipoles are independent and there is no phase relation among the light emitted by different dye molecules. Therefore, to calculate the fluorescence emission probability D_e for an ensemble of dyes, the expression 4.2.10 has to be integrated over all the dye molecules within the ensemble and over all possible excitation dipole orientations. Regarding the emission dipoles directions, an additional integral is needed over all the possible emission dipoles orientations in relation to the correspondent excitation dipoles. More details will be given in the next section.

a) Emission Dipole Moment

In the calculation of excitation (eq. 4.2.2) and detection (eq. 4.2.9) rates for a single dye molecule it was necessary to know the directions for excitation and emission dipole moments. Nevertheless for a specific chromophore, $\vec{d}_{ex}$ and $\vec{d}_{em}$ are in general unkown and by quantum chemistry calculations it is possible to know their orientations only with respect to the molecular structure. For a given dye molecule, $\vec{d}_{ex}$ and $\vec{d}_{em}$ are not independent: the emission dipole moment lies on a cone having as main axis the excitation dipole moment and a defined semi-opening angle $\Delta\theta$ (see figure 4.2.3).

Within an ensemble of dyes, it is necessary to consider all possible directions of the excitation dipoles in space and for every excitation dipole there is a certain emission dipole associated. As a consequence, even if the exact position of the emission dipole moment on the cone surface is not known, it is possible to integrate over the angle ξ (see figure 4.2.3). As it will be done in the next section.

b) Decay curve for an ensemble of dyes

In this way, integrating over excitation dipoles orientations (θ_{ex}, ϕ_{ex}) and on emission dipoles related orientation (ξ), it is possible to generalize the fluorescence probability density for single dye (eq. 4.2.10):

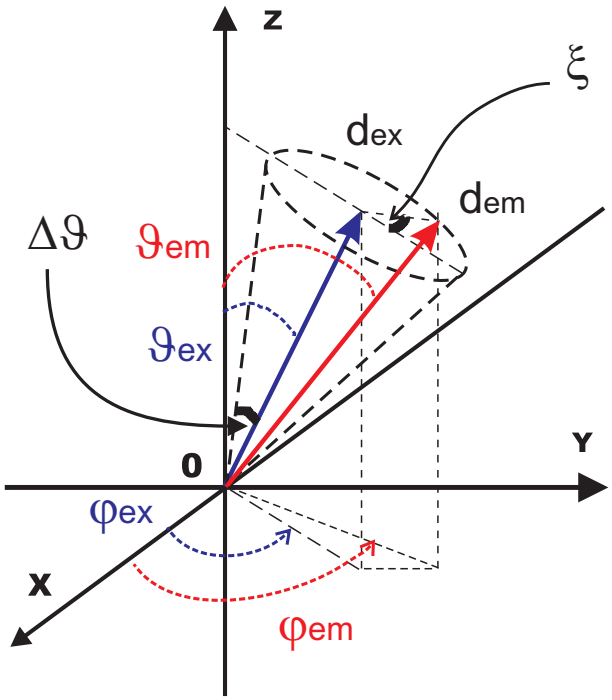

Figure 4.2.3: Schematic representation of associated excitation ($\vec{d}_{ex}$ - blue) and emission ($\vec{d}_{em}$ - red) transition dipole moments for an organic dye molecule. Relative polar and azimutal angles are also reported.

$$\mathrm{D}_e^{\sigma\delta}(\bar{z}_0,\Delta\theta,\Gamma_{nr},\Gamma_0,n_1,n_2,\hat{l},\Omega_d,t) = \alpha\cdot\int_0^{\pi} d\theta_{ex} A^{\sigma}\cdot B\cdot C^{\delta} \tag{4.2.12}$$

having set for clarity of notation:

$$\begin{aligned} A^{\sigma} &= sin(\theta_{ex})\cdot\textstyle\int_0^{2\pi} d\phi_{ex} \mid \vec{d}_{ex}\cdot\overrightarrow{E}^{\sigma}_{exc,loc}(z_0,\hat{l},\mathrm{n}_1,\mathrm{n}_2)\mid^2 \\ B &= \textstyle\int_0^{2\pi} d\xi\, e^{-\Gamma_{tot,N}(\theta_{ex},\phi_{ex},\Delta\vartheta,\xi,\Gamma_{nr})\cdot\Gamma_0\cdot t} \\ C^{\delta} &= \textstyle\int_{\Omega_d} \mid \vec{d}_{em}(\theta_{ex},\phi_{ex},\Delta\theta,\xi)\cdot\overrightarrow{E}^{\delta}_{em,loc}(z_0,\hat{m},\mathrm{n}_1,\mathrm{n}_2)\mid^2 d\hat{m} \end{aligned} \tag{4.2.13}$$

The polar coordinates of the excitation (θ_{ex},ϕ_{ex}) and emission $(\Delta\theta,\xi)$ dipoles are shown in figure 4.2.3 and $\bar{z}_0$ represents the distance of all dyes from the interface. Again the superscripts σ and δ denote the polarization of the excitation and emission local fields, respectively ($\sigma\delta = pp, ps, sp, ss$). The variables related to the multilayer system ($\bar{z}_0, \mathrm{n}_1, \mathrm{n}_2$) and to the experimental geometry ($\hat{l},\Omega_d$) are known, while the ones connected to the molecular structure of the dye ($\Delta\theta,\Gamma_0$) and its interaction with the surroundings (Γ_{nr}) are unknown and constitute the free parameters of the model. It is possible to calculate the detected fluorescence intensity by integrating the fluorescence probability density in equation 4.2.12 over time. An analogous equation to 4.2.11 can be written for an ensemble of dye molecules. Setting without loss of generality $t_0 = 0$, then the number of photons collected at time t after excitation is given by:

$$\mathrm{I}_{sim}^{\sigma\delta}(t) = \int_0^{t} \mathrm{D}_e^{\sigma\delta}(t')\cdot dt' \tag{4.2.14}$$

From 4.2.14, it is clear that the fluorescence intensity depends on excitation-detection polarization combinations. The theoretical curves obtained by the equation 4.2.14 can be then compared with experimental decay curves. The fluorescence intensity evaluated at time $t_0 = 0$ ($I^{\sigma\delta}_{sim}(0) \equiv I^{\sigma\delta}_{0sim}$).

c) Numerical Simulation

Equations 4.2.12 and 4.2.14 can only be evaluated numerically and for such purpose a software code (Igor, Wavemetrics Inc.) has been realized. In the software program the space of variables was discretized and integrals replaced by sums. The simulation of the fluorescence probability density of an ensemble of dyes was performed in three steps:

- simulation of the electric field distribution inside a multilayer system.
- Calculus of radiative decay rates $\Gamma_{r,N}$, based on equation 4.2.4.
- Generation of decay curves in equation 4.2.12.

The mathematical details, including discretization process and convergence issues, are reported in chapter 3, while the theoretical results so generated are compared in the next sections with experimental data.

d) Theoretical Decay Curves Fit

Equation 4.2.12 indicates that different fluorescence decay curves are obtained for different polarizations. The reason is seen in equation 4.2.13, as a consequence of the scalar products between the dipoles directions and the local electric field vectors. Hence different fluorescence intensities and lifetimes can be obtained, by photoselection. Experimentally this means that the dye ensemble can be excited by TM (p) or TE (s) and the fluorescence radiation detected selectively by polarizers. The measured intensity curves ($I^{\sigma\delta}_{exp}(t)$) can be compared with the corresponding theoretical curves ($I^{\sigma\delta}_{sim}(t)$), for different excitation-detection polarization combinations ($\sigma\delta = pp, ps, sp, ss$).

The geometry and the parameters utilized in the simulation are shown in figure 4.2.4. Here an ensemble of dipoles is represented close to an interface between two dielectric media. Fields components for p (TM) and s (TE) polarization are also indicated. The excitation radiation is constituted by plane waves coming from the medium 2 (n_2), having a propagation momentum forming an angle θ_{ex} with respect to the normal of the interface. Analogously, the fluorescence is detected in the medium 2, in a direction forming an angle θ_{det} with respect to the normal of the interface. The plane of incidence coincides with the (x,z) plane and the dipoles are at an average distance from the interface as high as $\bar{z}_0$. Further details are given in chapter 3.

Figure 4.2.5 shows the simulated fluorescence probability density for an ensemble of dyes versus time, according to equation 4.2.12 and using the geometry sketched in figure 4.2.4. There $D^{\sigma\delta}_e(t)$ is reported in logarithmic scale for different excitation-detection polarization combinations (i.e. *pp, ps, sp* and *ss*) by markers, while the lines are single exponential fits. In the inset of figure 4.2.5 the first part of the decay curves is magnified, indicating the values of fluorescence intensity at time $t = 0$ for different polarization combinations. The single exponential function fits the simulated decay curves quite well, even if a slight deviation can be observed in the last part of the curves, for higher values of t. $D^{\sigma\delta}_e(t)$ is in fact not properly a single exponential curve due to the integrals on ξ and θ_{ex}. However, it is possible to approximate it as a single exponential function because perpendicular

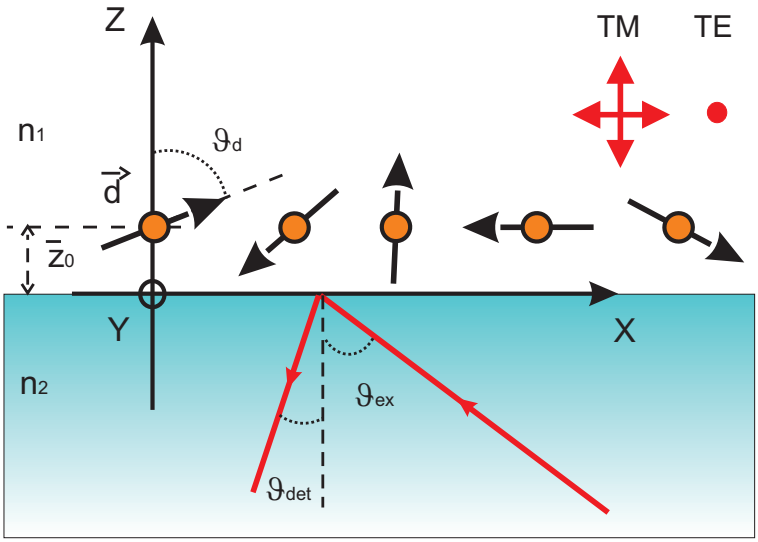

Figure 4.2.4: Dipoles ensemble in proximity of an interface between two media, with indication of dipole orientation θ_d, distance from interface $\bar{z}_0$, media refractive index values n_1 and n_2. The electric fields components for TM (p) and TE (s) polarization are also reported, while θ_{ex} and θ_{det} represent the excitation and the detection angles, respectively.

and parallel dipoles to the interface have not very different radiative decay rates, in the specific case reported in figure 4.2.5. In detail $\left[\frac{\Gamma(z_0,n_1,n_2)}{\Gamma_0}\right]_\perp \simeq 0.39$ and $\left[\frac{\Gamma(z_0,n_1,n_2)}{\Gamma_0}\right]_\parallel \simeq 1.49$, respectively. For the others possible directions the values are in between weigthed by the polar angle, according to equation 4.2.4. Moreover, a model for the non-radiative decay rate as a function of the dipole orientation was not found and therefore Γ_{nr} was assumed constant, regardless of dipole orientation with respect to the interface. As consequence, $\Gamma_{tot,N}$ depends on the dipole orientation only through the radiative decay and the slope difference among different dyes is not large enough to provide a strong multiexponential behavior in $D_e^{\sigma\delta}(t)$.

It is possible to employ numerical methods to evaluate fluorescence lifetime and intensity from $D_e^{\sigma\delta}(t)$ in equation 4.2.12: by plotting $D_e^{\sigma\delta}(t)$ versus time and then fitting the curve by a single exponential curve. In a logarithmic scale representation, the inverse of the curve slope provides directly the value of fluorescence lifetime ($\tau_{sim}^{\sigma\delta}$), averaged over all dipoles with scalar products not vanishing. On the other hand the intercept with Y axis represents directly the fluorescence intensity at time $t = 0$ (i.e. $I_{sim}^{\sigma\delta}(0) \equiv I_{0sim}^{\sigma\delta}$, in figure 4.2.5). The procedure can be applied for every polarizations combination ($\sigma\delta$) and a full comparison between theory and experiment can be done.

4.2.3 Fluorescence through an interface

In figure 4.2.6 fluorescence lifetimes and intensities (at time $t = 0$) are plotted, as extracted from theoretical decay curves. Here an ensemble of dye molecules close to an interface between two semi-infinite media (air (n_1) and polymer (n_2)) is considered. Values for the limiting cases of perpendicular (dotted line) and parallel (dashed line) single dipoles with respect to the interface are also shown. Figure 4.2.6 shows that an ensemble of dipoles at the interface has lifetimes close to the limiting values of single dipole case, for *pp* and *ss* polarizations. Whereas when the dipoles are embedded in a polymer matrix, this is true only in the case of the *ss* polarization. The difference with respect to the single dipole situation is due to the averaging process over the excitation and emission dipoles directions, in the case of many dipoles. When the dyes are in the medium with lower refractive index

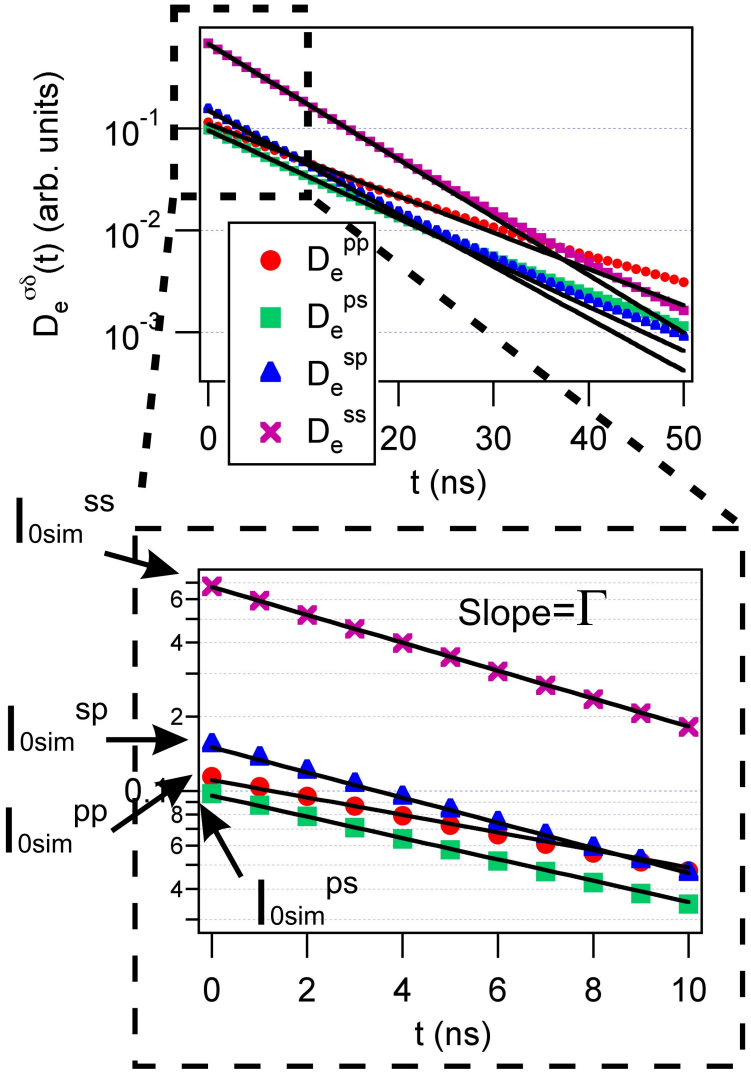

Figure 4.2.5: Simulated fluorescence probability density for an ensemble of 900 dyes versus time, according to equation 4.2.12, where $\Delta\theta = \Gamma_{nr} = 0$, $n_1 = 1$, $n_2 = 1.6$ and $\bar{z}_0 = -0.5\,\text{nm}$, on the base of figure 4.2.4. $D_e^{\sigma\delta}(t)$ is reported for different excitation-detection polarization combinations (i.e. $\sigma\delta = pp, ps, sp, ss$) and lines represent single exponential fits. In the inset the first part of the decay curves is magnified, with indication of the intensity for time $t = 0$: $I_{0sim}^{\sigma\delta}$.

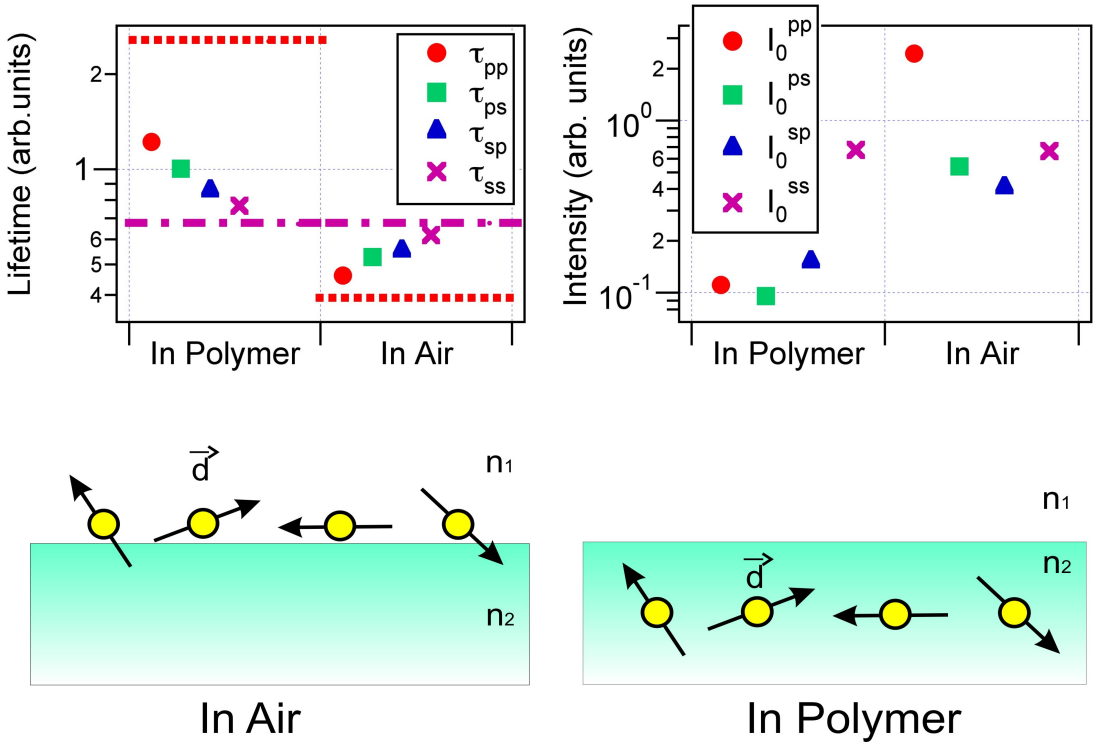

Figure 4.2.6: Simulated fluorescence lifetimes ($\tau_{sim}^{\sigma\delta}$) and intensities at time $t = 0$ ($I_{0sim}^{\sigma\delta}$), for an ensemble of 900 dye molecules at the interface between two semi-infinite media: air ($n_1 = 1$) and polystyrene ($n_2 = 1.6$). In the figure two situations are sketched, where all dipoles (dyes) are in the air side at the interface ("*At Interface*") or embedded in the polymer matrix ("*In Polymer*"). Fluorescence lifetime values for limit cases of perpendicular (dotted lines) and parallel (dashed lines) single dipole with respect to the interface are shown.

(n_1), from figure 4.2.6 results that $\tau_{pp} < \tau_{ps} < \tau_{sp} < \tau_{ss}$. In the case of dyes embedded in the medium with higher refractive index (n_2) the opposite lifetime behaviour is obtained: $\tau_{pp} > \tau_{ps} > \tau_{sp} > \tau_{ss}$. These inequalities turn to be valid in general and related only to the ratio between the two refractive indices and not on their absolute values. In figure 4.2.6 the theoretical intensities show higher values when the dyes are embedded in the medium with lower refractive index (n_1), except for the case of *ss* polarization for which the intensity has the same value regardless of the difference between n_1 and n_2. Moreover, it is possible to observe in figure 4.2.6 that I_0^{pp} is subjected to a large change across the interface.

By using the relations 4.1.1 it is possible now to explain the invariance of I_0^{ss} across the interface and the large difference between I_0^{pp} in the two media. The coefficients $[\frac{\Gamma(z_0)}{\Gamma_{n,\infty}}]_\perp$ and $[\frac{\Gamma(z_0)}{\Gamma_{n,\infty}}]_\parallel$ in equation 4.2.4 depend in fact on the local electric field the dipole experiences. Hence, the decay rate of a single dye molecule close to an interface is necessarily affected by the electromagnetic field boundary conditions, expressed by equations 4.1.1. Practically, even for identical orientation of the transition dipole and same distance from the interface, a chromophore has in general different decay rates across the interface, except for the case of orientation parallel to the interface. Finally, the relation between fluorescence lifetimes and intensities in figure 4.2.6 can be understood considering the equivalence between quantum mechanical decay rate and classical averaged emitted radiation by a dipole [23]. In figure 4.2.6, it is possible to observe that higher intensities correspond to higher decay rates (i.e. lower lifetimes) and viceversa.

4.3 Sample Preparation

Fluorescent organic dyes represent real molecular probe*s* of local electromagnetic fields and when coupled to polymers they constitute a suitable system for costs effectiveness, sample preparation and flexibility. At the same time, adsorption of polyelectrolytes can be controlled well down to a thickness of a few nanometers using the layer-by-layer technique.

4.3.1 Substrate preparation

UV-grade fused silica slides, both sides optically polished and with dimensions 25 mm x 25 mm x 1 mm (PGO GmbH) have been used. They were cleaned with a 2% solution detergent (Hellmanex - Hellma GmbH) in an ultrasound bath for 15 minutes and rinsed with ultrapure water twice (MilliQ resistivity, $18.2\,M\Omega \cdot cm$). After successive rinsing with ethanol (Fischer Scientific), the slides were dried by a N_2 flow and successively immersed in a bath of $H_2O_2 : NH_3 : H_2O$ (10 ml : 10 ml : 50 ml). There, NH_3 solution 32% and H_2O_2 solution 34% have been used. The slides were left in the solution for 45 minutes at 80Â°C. After rinsing 20 times with ultrapure H_2O and ethanol, the slides were carefully dried by a N_2 flow and put in a closed flask with 0.5 ml (3-Aminopropyl)-triethoxysilane (3-APTES, CAS: 919-30-2, Sigma Aldrich Inc.). The closed flask was then put in a oven, under vacuum, at 130Â°C for 3 hours [10]. After cooling down the slides were rinsed two times with ethanol to remove physisorbed silane aggregates from the surface and rinsed additionally 20 times with ultrapure water. At the end, the substrates were dried by N_2 and used as first charged layer for deposition of polyelectrolytes.

4.3.2 Polyelectrolytes deposition

3-APTES guarantees a positively charged surface, covering the glass slide in a fairly uniform manner [11]. In order to have a more uniform fully charged surface a polymer spacer constituted by 2.5 bilayers of PSS/PAH [poly(styrene sulfonate) / poly(allylamine hydrochloride)] and terminated by PSS was used. To prepare the PSS solution 50 mL of ultrapure water (resistivity of $18.2\,M\Omega \cdot cm$) was put in a flask with 4.049 g of $MnCl_2$ salt (Alfa Aesar). After complete solving by shaking, 0.207 g of PSS (CAS: 25704-18-1, $M_w \sim 70000$, Sigma Aldrich) were added and the ultrasound bath was utilized for complete solubilization of the polymer. The solution was then filtered in an empty slide-container (Faerbebox, Assistent) by a 200 nm pores size syringe filter. Finally, 0.5 mL of HCl 0.1 N was added to adjust the pH to 3. To prepare the PAH solution, 50 mL of ultrapure water were put in a flask with 10.29 g of NaBr (Alfa Aesar), after complete solving by shaking 0.0935 g of PAH (CAS: $71550-12-4$, $M_w \sim 15000$, Sigma Aldrich) was added and the ultrasound bath helped complete solubilizations of the polymer in water. The solution was then filtered in an empty slide-container (Faerbebox, Assistent) by a syringe filter 200 nm pore size and afterward 0.5 ml of HCl 0.1 N was added to adjust the pH to 3.

The fused silica slides were immersed in the PSS and PAH solution, alternately for 20 minutes, to deposit polyelectrolyte layers on the substrate. The samples were rinsed after each deposition step 10 times with ultrapure water. At the end of the desired number of deposition cycles, the slides were dried with a N_2 flow and stored under room conditions.

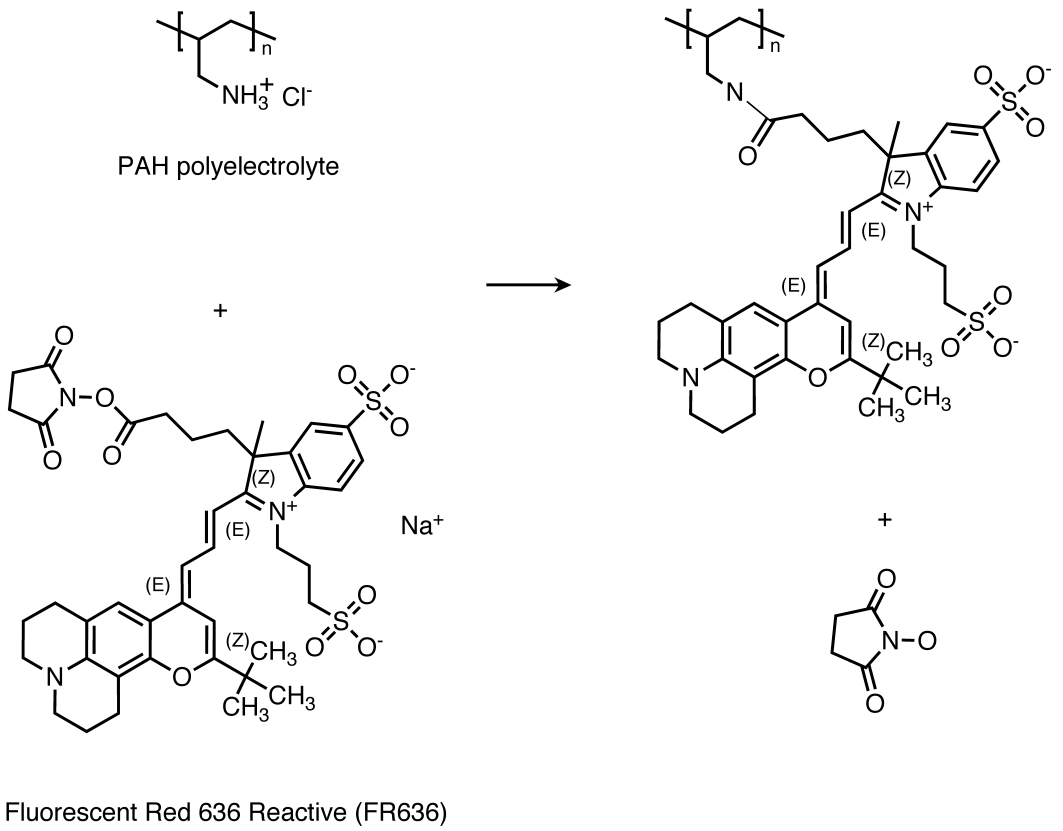

Figure 4.3.1: Scheme of functionalization of PAH with Fluorescent Red 636 reactive dye.

4.3.3 PAH functionalization

In order to chemically bond the organic dye to PAH (CAS: 71550-12-4, $M_w \sim 15000$, Sigma Aldrich), a condensation reaction was used (see figure 4.3.1). Initially 24.5 mg of PAH ($2.63 \cdot 10^{-4}$ mol) were dissolved in 5 ml of bicarbonate buffer ($NaHCO_3, 50\,mM, pH = 9.0$). To this solution 50 μl of NHS-modified fluorescent red dye FR (FR636 Red Reactive organic dye - Sigma Aldrich Inc., product no. 69296) in DMF was added ($5 \cdot 10^{-5}$ mol). The solution was incubated in the dark for one hour. The FR-functionalized PAH was then purified by adding acetone (200 ml) to precipitate the polymer and the solution was filtered to collect the functionalized polymer as powder. After drying, the polymer was diluted in ultrapure water to obtain a concentration of $\sim 2\,mg/ml$ and the pH adjusted by adding HCl to a value $pH = 3$.

4.3.4 Dyes at controlled distance from the air-polymer interface

The substrates with PSS/PAH layers were dipped in the water based solution containing PAH chains functionalized with the FR organic dye at $pH = 3$ for about one hour. The low pH value guarantees that the PAH chains are fully ionized [14]. Fully charged polymer chains assume a rod-like shape that provides smoother layer-to-layer transition interfaces. After dye deposition, the glass slides were gently rinsed with ultrapure water (resistivity of $18.2\,M\Omega \cdot cm$) for five times and then dried by a N_2 stream. In this manner samples with dye on top of the surface were obtained.

The samples were then reimmersed in the PSS solution and in the PAH solution, repeating the cycle PSS/PAH different times for different samples depending on how many polyelectrolytes bilayers had

to be deposited on top of the dyes. By using the layer-by-layer technique, it was possible to control the polymer film thickness deposited on top of the chromophores with an accuracy of a few nanometers. Hence, the fluorescence lifetimes and intensities could be studied, as a function of the distance z_0 between the dyes and the air-polymer interface (see figure 4.3.2).

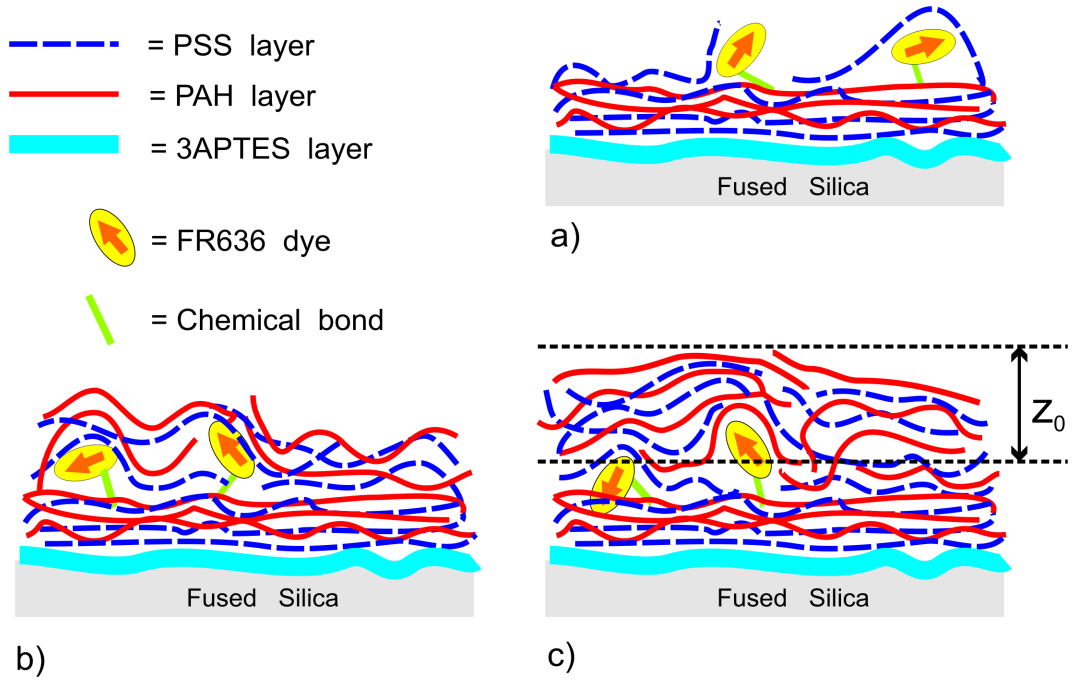

Figure 4.3.2: Scheme of samples for in-polymer case: (a) with one monolayer of PSS on top of FR636 dye, (b) with two PSS/PAH bilayers on top and (c) with four bilayers of PSS/PAH covering the dyes. All layers were deposited by immersion technique. Increasing the number of layers deposited, the distance between the molecular dyes and the polymer-air interface increased (z_0 in figure).

The samples were left overnight at room temperature to remove part of the water trapped in the polymer film during the dipping process (see also chapter 5). Finally characterization by ellipsometry for PSS/PAH bilayers thickness and optical inspection (see section 4.5 for more details) were done.

4.3.5 Dyes embedded in a polystyrene matrix

To prepare samples with dye molecules deeply embedded in a polymer matrix, a solution of polystyrene (Polysciences, Inc. - $M_W = 45000$) at 15%wt in toluene was spin coated on top of the fused silica glass slides (cleaned as detailed in section 4.3.1). The samples were left for two hours in a vacuum oven at 50Â°C and afterwards the polystyrene film surface was activated by plasma treatment (for plasma process detail see Appendix A.5). Right after the plasma process, the chromophores were deposited onto the polystyrene film by using the drop casting technique, starting from two different water solutions:

- the activated surface was covered with a few drops of an aqueous solution of polymer chains functionalized with the FR636 dye (see figure 4.3.1) at $\sim 10^{-7}$ M and pH ~ 7.
- The activated surface was covered with a few drops of an aqueous solution containing the free FR636 dyes at $\sim 10^{-7}$ M and pH ~ 7.

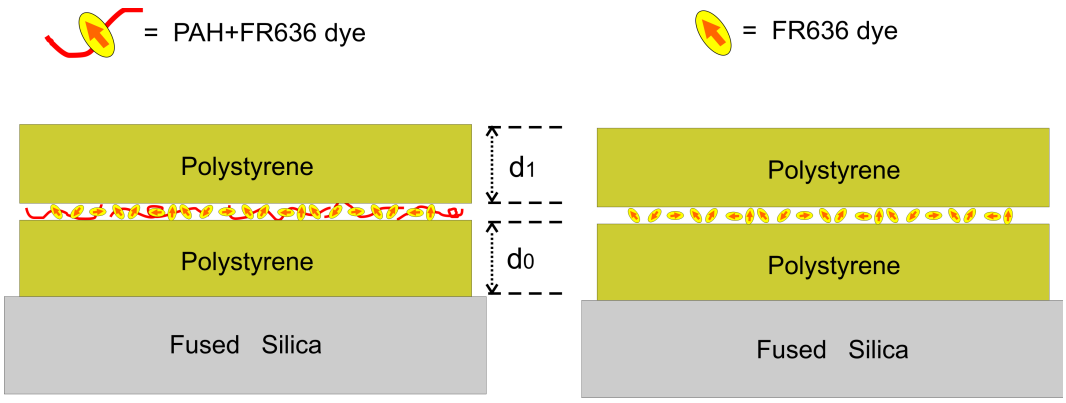

Figure 4.3.3: Sketch of sample with PAH polymer chains functionalized by FR636 red reactive dye molecules (left) and only FR636 dye molecules (right) embedded in a polystyrene sandwich. In figure $d_0 \sim 1.7\,\mu$m, while $d_1 \sim 1.9\,\mu$m for the sample with dye loaded polymer (left) and $d_1 \sim 0.3\,\mu$m for the sample with only dye molecules whitin the sandwich (right).

Finally, the samples were left overnight at room temperature for drying. The next layer of polystyrene was deposited the day after by spin coating and the samples were left another day at room temperature for solvent removal. The solvent removal step, like the dye solution drying process, could only be performed at room temperature because already at temperatures as high as 50Â°C, for two hours, it was proved that the fluorescent chromophores were deactivated in an irreversible way. No appreciable differences were detected in fluorescence characteristics before and after drying process by using medium vacuum environment (10^{-5} bar) for two hours. A sketch of the samples after the preparation process is depicted in figure 4.3.3.

4.4 Experimental Setup

The excitation source is constituted by a Hamamatsu PLP10 pulsed laser with a wavelength of 634 nm and a repetition rate of 20 MHz. This frequency gives a time window between pulses of 50 ns, while the expected lifetime for the organic dyes employed is on the time scale of a few ns. The LED laser source was coupled into a single mode fibre (HCG200-ZZZZSS-FF-001.0, Laser Components GmbH) and then by an objective lens a narrow, collimated, Gaussian-shaped laser pulse was obtained. The temporal FWHM (Full Width Half Maximum) of the laser beam shape was $\sim$ 110 ps and the excitation power at the sample site was determined for each single measurements to be always in the range between 10 and 20 μW (laser controller power knob at 10.94).

The samples were coupled to the prism by a non-fluorescent immersion oil (n = 1.455, NF550-NIKON Inc.), keeping the surface with the chromophore facing towards the air side (figure 4.4.1). In this way under the total internal reflection condition, it was possible to generate an evanescent wave at the glass-air interface to excite the dye molecules in the sample. The excitation beam was impinging on the sample surface at an angle of $\theta_{exc} = 39.4$Â° (figure 4.4.1), by passing through a linear polarizer and a 633 nm line filter. The detector had a 90Â° inclination with respect to the laser beam to avoid direct reflection and maximize fluorescence collection (this corresponds to a detection angle of $\theta_{det} = 50.6$Â° in figure 4.4.1). The detector used was a fast Peltier cooled photo multiplier (PMC-100-20 from Becker & Hickl GmbH), with a time resolution around 200 ps and a dark count rate 200 s^{-1}. The overall time resolution for the whole measurement system was calculated as high as 240 ps. To avoid scattered light a 633 nm Notch Filter (Semrock Inc.) was used, coupled to a

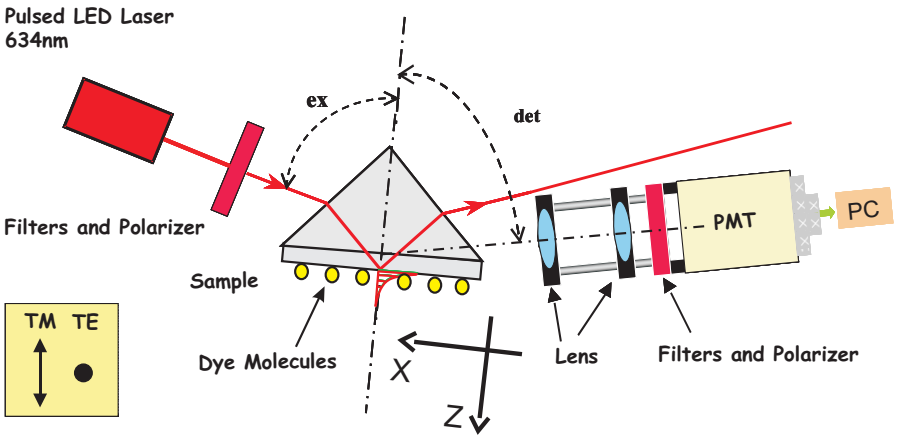

Figure 4.4.1: Schematic representation of the general configuration for the measurements set-up, in the inset the directions of electric field components for TM and TE mode are shown. For samples showing intense fluorescence signal, only one lens was utilized.

650 nm long pass filter (Omega Inc.) in front of the PMT detector. A linear polarizer was set as the last optical component before the active area (see figure 4.4.1). The detector output and the pulsed laser controller synchronization signal were sent to a Time Correlated Single Photon Counting card: TCSPC-SPC630 (Becker & Hickl). In order to adapt the detector output signal to the TCSPC card input, a home-made resistors-network was realized to reduce the voltage. The excitation intensity was measured by a digital power meter (Newport 1930-C Single-Channel) right in front of the prism.

4.4.1 Different Polarizations Detection Enhancement

In figure 4.4.2 a dipole in proximity to an interface between two different media is sketched. Relative reference system and indication of the electric field components directions for TM and TE mode are depicted. The plane of incidence coincides with the (x,z) plane and TM (or p polarized) mode contains one component perpendicular and one parallel with respect to the interface. It has already been shown in section 4.2.1 that fluorescence intensity and lifetime for different excitation-detection polarization combinations depend also on the local electric field. In order to enhance experimentally the differences among different polarization combinations in excitation and detection, a specific geometry that minimizes the TM component parallel to the interface was chosen. In this way, the dipoles lying parallel to the interface were only excited by TE mode.

Figure 4.4.3 shows the calculated electric fields, as a function of internal excitation angles, for TM (E_{px}, E_{pz}) and TE (E_{sy}) modes, respectively. There, the field components are relative to the reference system in figure 4.4.2. The angle at which $\mid E_{px} \mid = 0$ is the critical angle, also called total internal reflection angle. In the case of a fused silica prism $\theta_{TIR} \simeq 43.3\hat{A}^\circ$ (0.76 rad). In figure 4.4.3, the values set for the excitation and the detection internal angles $\theta_{exc} = 41.1\hat{A}^\circ$ (0.72 rad) and $\theta_{det} = 48.9\hat{A}^\circ$ (0.85 rad) are plotted by dashed vertical lines. The angles are measured with respect to the normal at the prism base (see also figure 4.4.1). By using right-angle prism, the relation between internal (θ_{exc}) and external angle (θ_{exc}^{ext}) is given:

$$\theta_{exc} = \frac{\pi}{4} \cdot \arcsin\left[\left(\frac{n_1}{n_2}\right) \cdot \sin\left(\frac{\pi}{4} - \theta_{exc}^{ext}\right)\right] \tag{4.4.1}$$

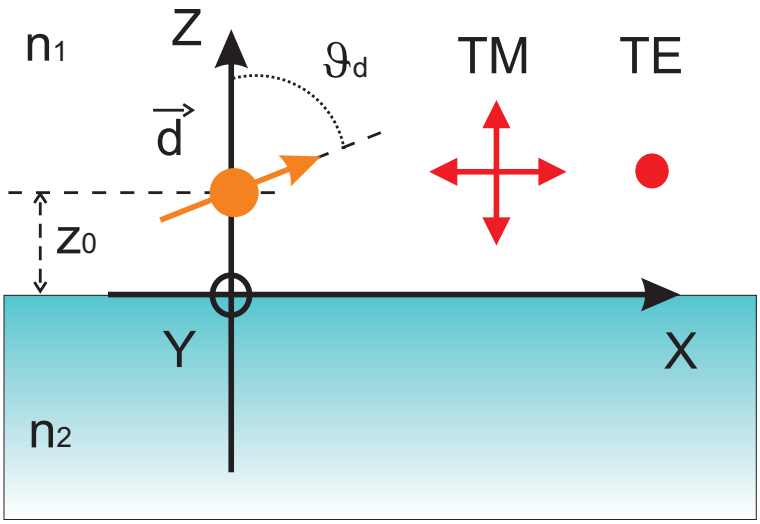

Figure 4.4.2: Dipole in proximity of an interface between two media with indication of the directions of the electric field components for TM and TE mode. The plane of incidence coincides with the (x,z) plane.

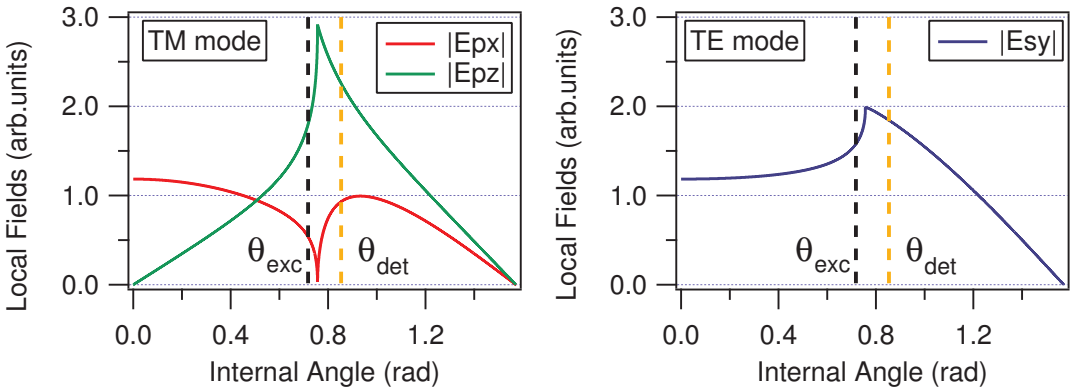

Figure 4.4.3: Simulated electric field components for the local excitation and detection fields. The excitation and detection internal angles (incidence angle at interface) are indicated by the left and right vertical dashed lines. The z component is the one perpendicular to the sample's surface.

where n_1 and n_2 are the refractive indices of air and fused silica, respectively (at a wavelength of 633 nm). The same relation is valid for the detection angle and by using 4.4.1, the external excitation angle is $\theta_{exc}^{ext} = 39.7\hat{A}°$ (0.69 rad) and the external detection angle is $\theta_{det}^{ext} = 50.6\hat{A}°$ (0.88 rad). The angles are always given with respect to the normal at the prism base. Thus the perpendicular component (to the interface) of the local excitation electric field is enhanced and the parallel component is strongly suppressed, for TM mode. The same arguments are valid for local excitation and emission fields by the Reciprocity Theorem (see chapter 3). Hence, the detection angle θ_{det} was chosen close to the TIR condition as well. In this way the detection of the normal component of the local emitted field is ehnanced. At the same time the contribution to the detection given by the component parallel to the interface is suppressed. The particular set-up geometry was chosen to avoid the direct detection of excitation laser beam, reflected at the fused silica slide-polymer interface: for this reason it was not possible to set θ_{exc} and θ_{det} equal to θ_{TIR}. Moreover, at θ_{TIR} infinitely quick variations of the fields are obtained with respect to the small variations of the excitation and detection angle.

In summary: the choice of the measurement geometry came from the theoretical calculations of excitation and detection local fields (see figure 4.4.3). For TM mode, at the total internal reflection angle for the prism-air interface, the excitation field in the direction normal to the sample surface is maximized, while the parallel component is strongly suppressed (see figure 4.4.3). In this manner, for an ensemble of dye molecules and for different excitation-detection polarization combinations, the differences among measured lifetimes are enhanced. The calculations performed for the excitation local field are still valid for the emission field, as consequence of the Reciprocity Optical Theorem [24]. It is then possible to determine excitation and detection angles from the plot reported in figure 4.4.3.

4.4.2 Data Collection

For each single measurement: the number of fluorescence photons, the Micro Time for each photon (time lag between the excitation laser pulse and the photon time of arrival at the detector) and Macro Time (absolute time of arrival at the detector with respect to the beginning of the experiment) were recorded. Due to the finite time resolution of the TCSPC card, the number of fluorescence photons detected were collected in a histogram as a function of the Micro Time. A 50 ns time window was divided in 4096 bins having a time width of $\Delta t_b \simeq 12$ ps. Data were converted to ASCII format and then analyzed by a custom procedure, which was realized with the IgorPro package (Wavemetrics Inc.). In order to have a reliable fit of the fluorescence signal, the first 0.7 ns of the decay curve were not considered in the curve fitting due to the finite excitation laser pulse width (4.5 ns from Micro Time origin), while a statistical error on photons count as high as $\sqrt{n}$ was considered in each histogram bin, being n the number of photons detected.

Figure 4.4.4 shows an experimental decay curve for fluorescence emission of an organic dye embedded in a polymer matrix with exponential fit. In the upper part of figure 4.4.4 the histogram reports the number of normalized photons as a function of the Micro Time. The magnified inset shows a detail of several decay curves for the same sample, but for different excitation and detection polarization combinations. In figure 4.4.4 the curves were normalized to 1, only to enhance the slope differences. Whereas, in general, the number of fluorescence photons detected in each bin was divided by the collection time (time of experiment) and by the excitation power. This normalization guarantees a correct intensity evaluation.

Figure 4.4.4 suggests that the experimental decay curves can be fitted by a single exponential function like:

$$\mathrm{D}_{exp}^{\sigma\delta}(t) = \mathrm{D}_{bckg} + \mathrm{D}_{0exp}^{\sigma\delta} \cdot e^{-\frac{t-t_0}{\tau_{exp}}} \tag{4.4.2}$$

where D_{bckg} represents the background signal given mainly by the photomultiplier dark counts and was left as free parameter in the fit. $\sigma\delta = pp, ps, sp, ss$ are the possible excitation-detection polarization combinations used in the measurements. The experimental curve is a histogram with a finite bin width, thus the fluorescence intensity is constant within the i^{th} bin and it is related to the probability density by:

$$\mathrm{I}_{exp}^{\sigma\delta}(t_i, t_{i+1}) = \mathrm{I}_{exp}^{\sigma\delta}(t_i, t_i + \Delta t_b) = \mathrm{D}_{exp}^{\sigma\delta}(t_i) \cdot \Delta t_b \tag{4.4.3}$$

By looking at equation 4.4.2, it is clear that the slope of the decay curves in a logarithmic scale provides directly the decay rate of the dye. Therefore the reciprocal value is the fluorescence lifetime

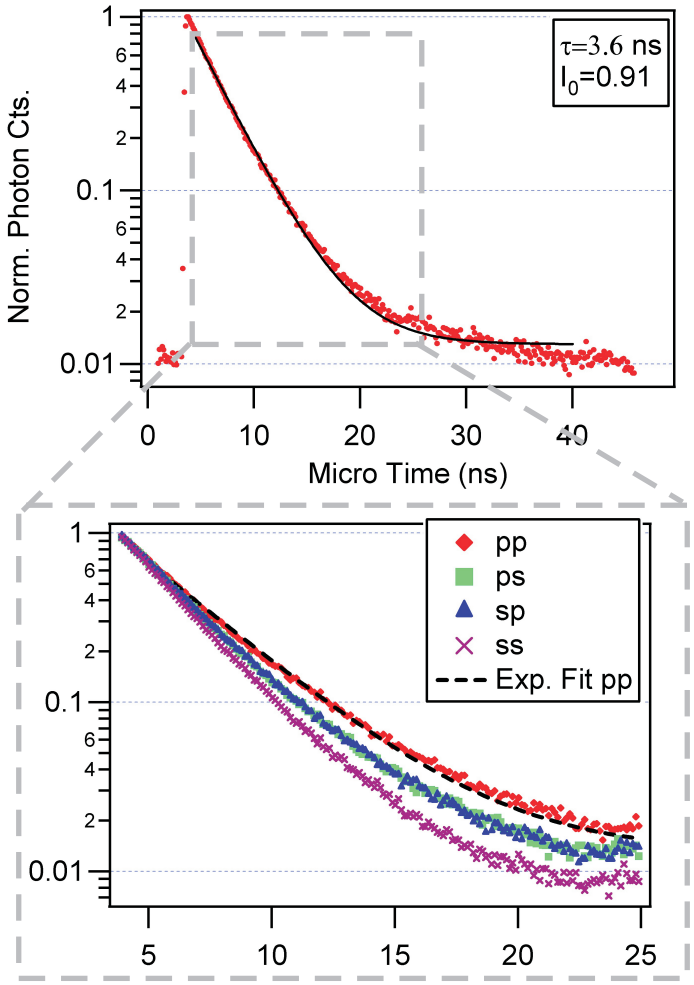

Figure 4.4.4: Typical histogram reporting a normalized number of collected photons versus micro time. In the magnified inset decay curves for different excitation and detection polarizations are reported as example and a relative fit by a single exponential function.

for a specific excitation-detection polarizations combination, $\tau_{exp}^{\sigma\delta}$. At $t = t_0$, the probability density is the quantity:

$$\mathrm{D}_{exp}^{\sigma\delta}(t_0) = \mathrm{D}_{bckg} + \mathrm{D}_{0exp}^{\sigma\delta} \tag{4.4.4}$$

For the performed measurements $D_{0exp}^{\sigma\delta}$ resulted in 2 or 3 orders of magnitude larger than D_{bckg} (also see figure 4.4.4) and within the experimental error:

$$\mathrm{I}_{exp}^{\sigma\delta}(t) \sim \mathrm{I}_{0exp}^{\sigma\delta} \cdot e^{-\frac{t-t_0}{\tau_{exp}}} \tag{4.4.5}$$

Here t_0 represents the time when the dyes start to emit fluorescence radiation in the Micro Time scale (as a consequence of the excitation pulse) and it corresponds to $t = 0$ in the simulation code (see in detail term B in equation 4.2.13). The absorption process is very fast ($\sim 10^{-15}$ s), while the vibrational relaxation has charactristic times of $\sim 10^{-12} - 10^{-10}$ s and the lifetime of the excited state is $\sim 10^{-10} - 10^{-7}$ s [15]. In principle, the chromophores may start to emit during the rise front of the excitation pulse. Thus, a correct determination of t_0 is not straightforward and by the instrument response function (IRF) analysis, $t_0 = 3.8$ ns was chosen as best guess. Figure 4.4.5 depicts the IRF of the equipment used for the measurements with indication of the value of t_0 used to fit the experimental curves. The tail following the pulse is due to afterpulsing (characteristic for photomultiplier detectors), optical filters and prism residual fluorescence [25]. The difference between $t_0 = 3.8$ ns and the IRF maximum at $t_0 = 3.54$ ns brings a difference in the intensity ratios, among different polarization combinations, smaller than 1%. In this respect, t_0 is not a critical parameter in the fit process within the range of few tenth of nanoseconds around the IRF maxima.

In figure 4.4.6 an example of experimental decay curves used to evaluate lifetimes and intensities by a fit procedure is reported for all the possible excitation-detection polarization combinations (i.e. $\sigma\delta = pp, ps, sp, ss$). In figure 4.4.6, the number of the photons detected by the PMT was normalized to the collection time (time of experiment) and to the excitation intensity, for a proper evaluation of the experimental fluoresecence intensities. Finally, the intensities $\mathrm{I}_{0exp}^{\sigma\delta}$ were evaluated at time $t_0 = 3.8$ ns.

Figure 4.4.6 suggests that the statistical errors on the fit results are quite small, while an experimental error has to be considered to take into account systematic errors, measurements reproducibility and samples uniformity. The error bars on experimental lifetimes were set to ± 0.05 ns while on intensity a relative error of $\pm 10\%$ was applied. The error values were determined by both a sample-to-sample repeatability test for a set of identical samples and by a reproducibility test measuring different spots within the same sample. At the end, the maximum deviations coming from the two tests were considered as experimental errors.

Finally the experimental data $\tau_{exp}^{\sigma\delta}$ and $\mathrm{I}_{0exp}^{\sigma\delta}$ were compared to the results of the theoretical calculations $\tau_{sim}^{\sigma\delta}$ and $\mathrm{I}_{0sim}^{\sigma\delta}$.

4.5 Sample characterization

4.5.1 FR636 dyes embedded in PSS/PAH polymer matrix

The polymer layers thickness was measured by two different techniques:

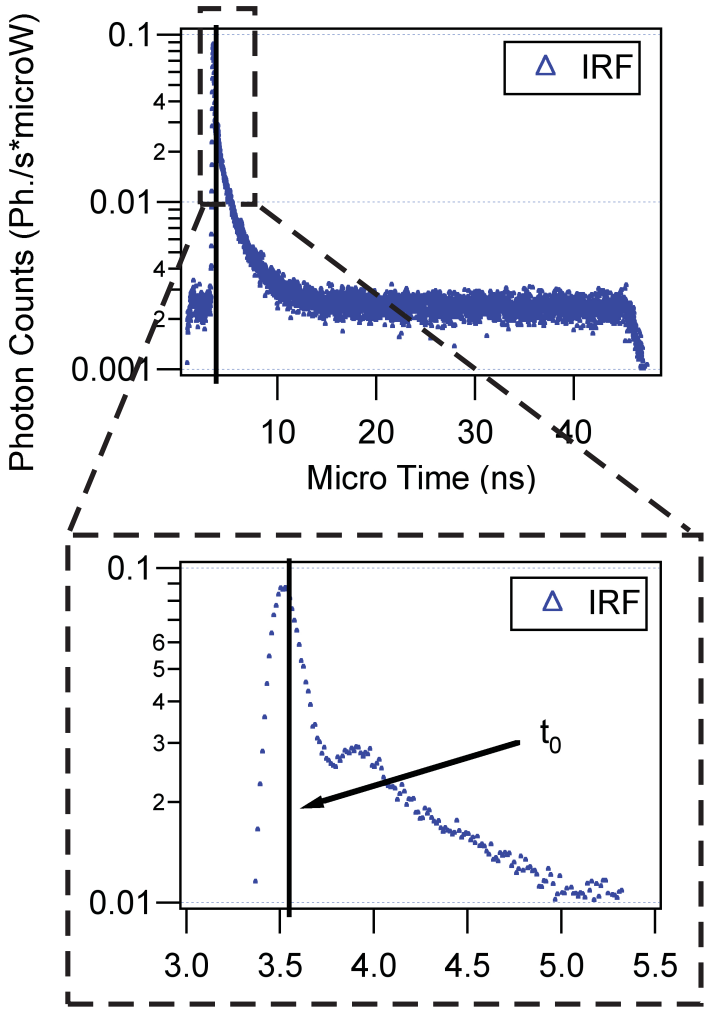

Figure 4.4.5: Instrument Response Function (IRF) for the measurements setup used. The arrow indicates the value of t_0 chosen for the experimental curves fitting.

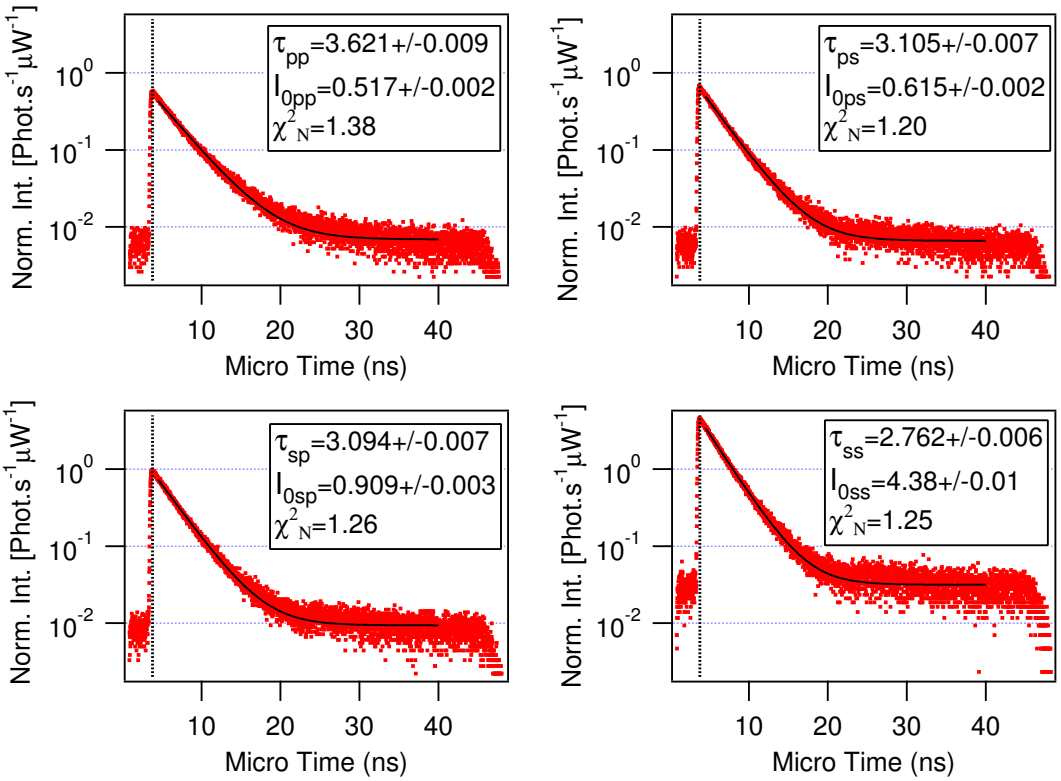

Figure 4.4.6: Experimental decay curves for different excitation-detection polarization combinations, normalized to the excitation intensity and collection time (time of the experiment). In the legends, the lifetimes and the intensities obtained by a fit are indicated ($\tau_{exp}^{\sigma\delta}$ and $I_{0exp}^{\sigma\delta}$ in the text), together with the normalized χ^2 values. The time at which $I_{0exp}^{\sigma\delta}$ is evaluated (i.e. t_0 in the text) is also reported by vertical dotted lines.

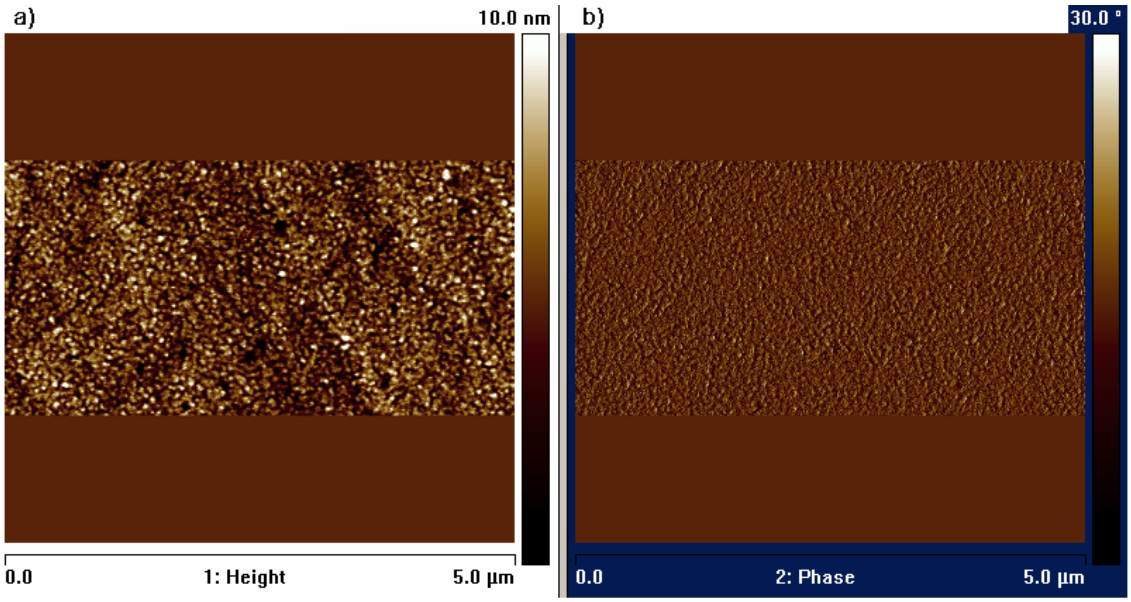

Figure 4.5.1: AFM image of a sample with three bilayers of PSS/PAH deposited on a fused silica glass slide: the last layer is PAH functionalized with the FR636 chromophore. a) Morphology of the surface (height) is shown. b) Relative phase is reported. RMS â€“ roughness: 2.02 nm

- ellipsometry (NANOFILM EP3 tool - software EP3Viewer V233 with integrated modelling capability) by fitting experimental data on a 3-layers model: SiO_2-amorphous (refractive index n =1.46), polymer (refractive index $n_p = 1.56$) and air (refractive index n = 1). For the measurements four angles (51Â°, 53Â°, 60Â° and 62Â°) were used and a 532 nm wavelength laser served as excitation source. Measurements down to five PSS/PAH polyelectrolyte bilayers gave good fit results for the thickness, with fit quality parameter[1] MSE $\sim 0.8 \div 2$. For thinner polymer films a value of MSE ~ 7 was obtained, indicating a non-appropriate fit by the model used. The statistical error obtained by the software was around ~ 0.5 nm, while no indication for an experimental error was derived directly from the tool. An average roughness of RMS ~ 2 nm was obtained by AFM measurements, performed on a sample with three PSS/PAH bilayers deposited on a glass. This quantity was considered as experimental error on thickness measurements (see figure 4.5.1). The resulting thickness values for $5, 7, 9, 11$ and 13 bilayers above the glass were: 14.9 nm, 36.7 nm, 49.7 nm, 64.5 nm and 88.5 nm, respectively.

- step profiler (TENCORÂ® P-10 Surface Profiler - KLA TENCOR). The polymer film was scratched with a syringe needle and the resulting step was measured. For each sample four different measurements were performed and the mean value was taken. The maximum deviation from the average was considered as experimental error. The resulting thickness values for $3, 5, 7, 9, 11$ and 13 bilayers above the glass were: 6.0 ± 1.2 nm, 13.5 ± 2.4 nm, 29.4 ± 0.7 nm, 43.3 ± 1.0 nm, 69.9 ± 1.5 nm and 81.9 ± 1.9 nm, respectively.

In figure 4.5.1 an AFM scan (Dimension 3100 CL NS IV Controller - Cantilever Typ: Olympus non-contact mode OMCL-AC160TS-W2 K = 42 N/m Range: $33.5 \div 94.1$ N/m) of a sample constituted

[1]The parameter MSE is the equivalent of the χ^2 value in the least squares method. Values of MSE ~ 1 indicates good quality fits.

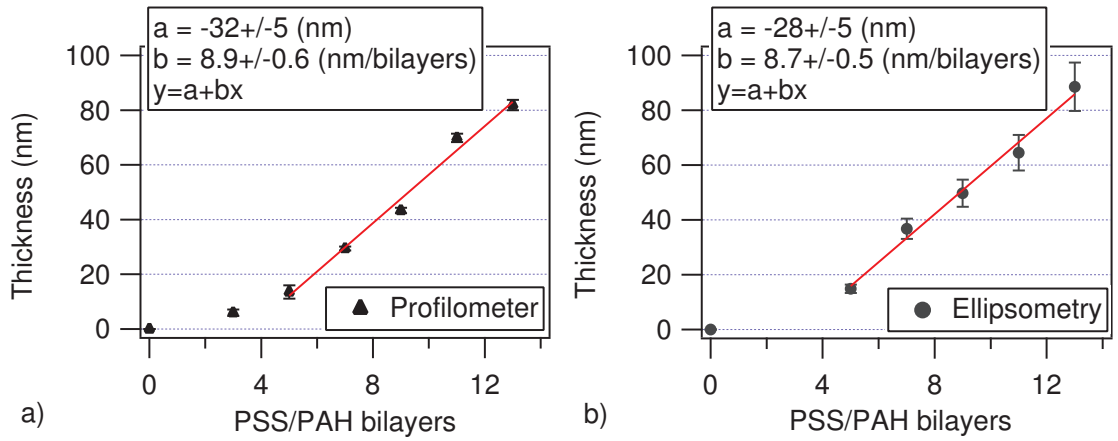

Figure 4.5.2: Thickness of PSS/PAH polyelectrolytes films, for different number of bilayers deposited on top of the fused silica glass slide. Measurements were performed by a profilometer (a) and by ellipsometry (b). In the figures, the relative fits are drawn and the results are reported in the insets. In figure (a) the value for 3 bilayers is 6 nm.

of three PSS/PAH bilayers deposited on top of the fused silica slide is shown. The last PAH layer is functionalized with the dye FR636. In figure 4.5.1 a) the morphology of the sample surface is shown, while in b) the relative phase image is displayed. The measurement was performed using tapping mode and the surface roughness was ~ 2 nm. On a $5\,\mu$m scale, the surface shows a fair good uniformity without presence of large voids.

Figure 4.5.2 shows the experimental thickness for PSS/PAH polyelectrolyte films for different numbers of bilayers, obtained by the step profiler 4.5.2 a) and by ellipsometry 4.5.2 b). The fits of the experimental points are also shown as a continuous straight line. The two methods are in quite good agreement within the experimental error. The polyelectrolyte deposition rate is constant above $\sim 10 \div 20$ nm and has a value of ~ 8.8 nm/bilayer for the specific polyelectrolytes deposition recipe. Step profile or ellipsometry are used to obtain the total polymer thickness on the fused silica substrate. However the relevant parameter for the study is the thickness of the polymer above the dye molecules: i.e. the distance z_0 between the chromophore and the polymer-air interface (figure 4.3.2). To obtain a value for z_0: the measurements obtained by the two techniques were averaged and afterward the thickness value for the first three bilayers subtracted. The last one is the distance of the the dye molecules with respect to the fused silica slide. In this way for $2, 4, 6, 8$ and 10 bilayers above the chromophores, the values for z_0 are: 8.2 nm, 27.1 nm, 40.5 nm, 61.2 nm and 79.2 nm, respectively.

As a remark, in figure 4.5.2 a), a change in the deposition rate is observed around ~ 5 bilayers. The effect is due to the intrinsic absorption properties of chain polymers on a surface and it is well known in the literature [12, 13]. The deposition regime for the first few layers is substrate dependent and the deposition rate changes with the number of layers adsorbed until it stabilizes to a constant value after the first $\sim 4-5$ bilayers. Here, the constant deposition rate indicates that the substrate does not play any role on successive layers depositions.

Figure 4.5.3 reports measured fluorescence intensities (fit at time $t = 0$ of experimental decay curves) of FR636 dye molecules, as a function of the number of the PSS/PAH layers deposited on top of the chromophore. The data are for different excitation-detection polarization combinations. The correspondent experimental decay curves and relative fits are included in the Appendix A.1. From figure 4.5.3 a large intensity drop is noticed, for all polarizations combinations, for progressive number of PSS/PAH layers deposited above the dye molecules, up to ~ 4 bilayers. The intensity oscillations

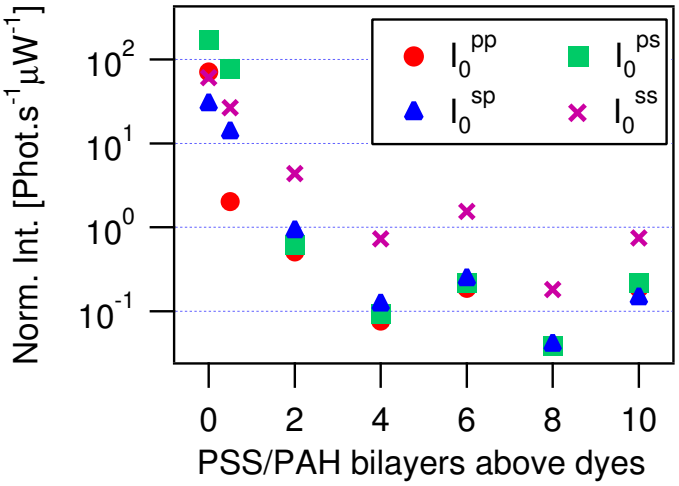

Figure 4.5.3: Fluorescence intensities $I_{0exp}^{\sigma\delta}$, as function of number of PSS/PAH layers deposited on top, for different excitation-detection polarization combinations. The experimental error was estimated as $\pm 10\%$. Error bars are not shown for clarity.

for more than ~ 4 bilayers deposited above the chromophores are probably related to different dye concentrations on the different samples.

The intensity drop in figure 4.5.3 may be due to mainly two physical effects:

- displacements of dye loaded chains.
- pH effect on the dye molecules.

The first effect gives a small contribution and it may be responsible for the drop of the intensity after one monolayer of PSS has been deposited on top of the chromophores. During the deposition of the very first layers above the chromophore, some chains functionalized with the dye may be exposed to the water solution containing PSS or PAH. A chain displacement of the polymer loaded with dye may take place, in favour of small ions or other polymer chains present in the solution. As a result, the displaced chains go in to the solution depleting the sample and lowering, therefore, the dye concentration on the surface. In some extent, the rinsing steps in between successive layer depositions are proved to remove some polyelectrolyte chains from the surface (see Appendix A.4). The depletion effect is drastically reduced with the increase of the number of layers on top of the dye molecules. When a fairly uniform polymer film is formed and the chains functionalized with the dyes are protected (i.e. by $\gtrsim 4$ bilayers on top of the dyes), the fluorescence intensity stabilizes.

Nevertheless, from figure 4.5.3, it is seen that after the deposition of first 4 bilayers the signal decreased ~ 2 orders of magnitude. In this regard, the chain displacement effect is not sufficient to explain such a large variation. This would imply that about $\approx 99\%$ of the chains loaded with a dye are lost during the deposition of successive layers. This result is not compatible with the layer-by-layer technique and the film growth. In successive investigations regarding the specific chromophore used, a strong influence of pH on the fluorescence properties is found. For acidic solutions pH $\lesssim 4$ the water solution containing PAH functionalized with the dye became clear, loosing thus the characteristic light blue color, indicating a change on the absorbance spectrum.

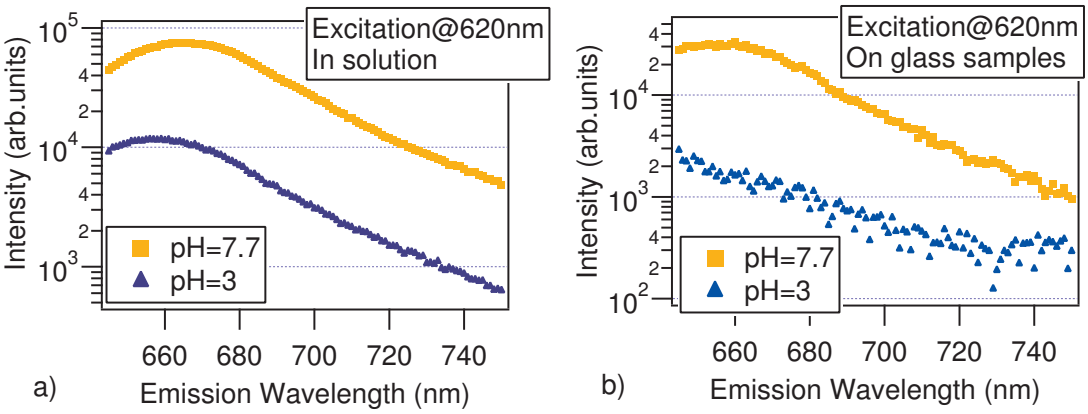

Figure 4.5.4: a) Fluorescence spectra of PAH functionalized with FR636 chromophore in water solution for two different pH values, at same dye concentration $\sim 10^{-8}$M. b) Fluorescence spectra for 1 monolayer of PAH functionalized with FR636 chromophore deposited by dipping technique above fused silica substrate, for two different pH values of the deposition solution.

Figure 4.5.4 a) shows the fluorescence spectra of FR636 dye molecules, chemically bond to PAH chains, in water solution at $\sim 10^{-8}$M. The spectra are measured for two different pH values. The excitation wavelength was chosen at 620 nm and all detection parameters were left the same (slit opening, integration time and detector voltage). Figure 4.5.4 b) shows the the fluorescence spectra of FR636 dye molecules, chemically bond to PAH chains, on a fused silica slide, at two different pH values of the water solution used for deposition on the substrate. The excitation wavelength was chosen at 620 nm and all detection parameters left the same (slit opening, integration time and detector voltage). From the analysis of figure 4.5.4 a) and b) it becomes clear that for low pH the fluorescence is strongly inhibited. This effect may be explained by the protonation of the lone pairs responsible for the fluorescent process in the dye molecule. Figure 4.5.5 depicts the molecular structure of FR636 chemically bond to a PAH chain with n monomers, showing also the lone pairs associated to the oxygen and nitrogen atoms which are believed to be protonated at low pH values. The resonant structure responsible for the dye fluorescence emission is the one enclosed between N^+ and the N, O atoms within benzene rings (see figure 4.5.5). When N and O are protonated, the fluorescence is inhibited. The two SO_3^- groups are believed to make the molecule soluble in water.

The PSS and PAH solutions employed have pH $= 3$ to allow a degree of ionization for PAH close to 100% [14]. In this way the PAH chains assume a fully stretched conformation minimizing the roughness at the layer-to-layer interface during PSS/PAH bilayers deposition. The chromophores are immersed in a water solution at pH $= 3$ during the PSS/PAH bilayers deposition and the thicker the polymer film deposited (i.e. the higher the number of bilayers) the longer the time the dye molecules are immersed in the acidic solution. This may protonate progressively a higher number of dye molecules until $\sim 4 \div 5$ bilayers are deposited on top. Afterwards the dyes may be protected by the bilayers. The comparison between the spectra in figure 4.5.4 b) shows that at pH $= 3$ about 10% of the chromophores are still active, indicating a probable equilibrium condition of the system. It is believed that the low pH environment combined with the displacement of the chains for the first bilayers deposition above the chromophores explain the fluorescence intensity trend showed in figure 4.5.3.

The layer-by-layer technique was found to be suitable for deposition of relatively thin polyelectrolytes bilayers (i.e. up to few tens of nanometres) due to the time required for deposition: ≈ 1 hour/bilayer. In the case of thick polymer films (hundreds or thousands of nanometres) a different technique may

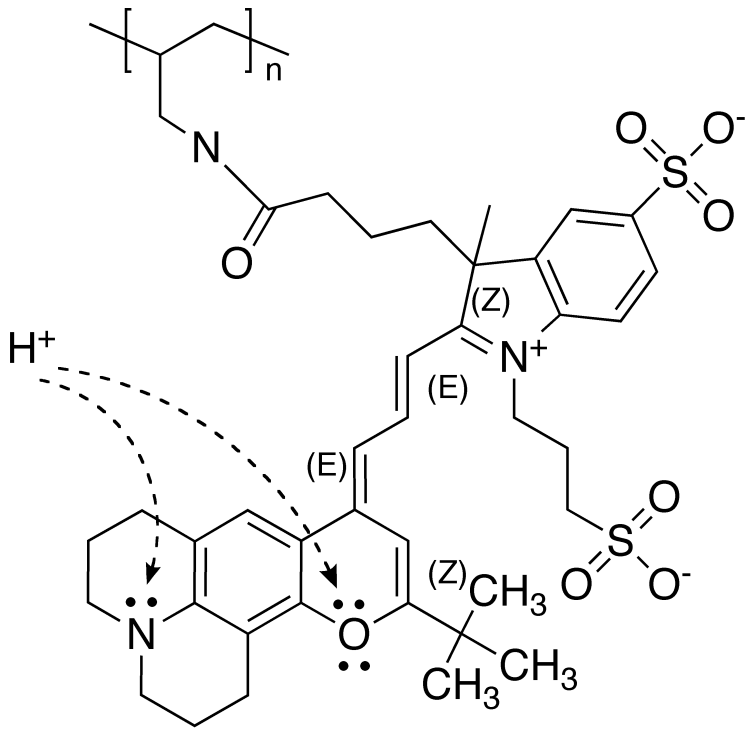

Figure 4.5.5: Chemical structure of FR636 dye molecule (FR636 Red Reactive organic dye - Sigma Aldrich Inc., product no. 69296) bond to the PAH polymer chain. In the figure the lone pairs associated to the oxygen and nitrogen atoms are indicated and the process of protonation due to H^+ ions in acidic environment.

be used. As an alternative, the spin coating technique was utilized to fabricate samples with organic dyes deeply embedded in polymer (hundreds of nanometers up to several microns). In general, spin coating provides good film uniformity, accurate control of thickness and robust fabrication process, for layers on the order of tens of nanometers or thicker. The purpose was to obtain an experimental evaluation of the specific chromophore decay rate in a homogeneous and isotrope medium, quite important for correct simulations of experiments. On the other hand, the fluorescence characteristics in bulk are directly related, by the refractive index, to the dye decay rate in vacuum (Γ_0). The realized sample was sandwich-like, where the chromophores were embedded between two thick slabs (thicker than wavelength) of polystyrene, like in figure 4.3.3. For optimum adhesion to the substrate, the spin coated film should have a certain chemical affinity with it or being electrostatically attracted. Glass, 3-APTES or PSS/PAH substrates did not have such affinity in common with the polystyrene film. As a consequence, it was not possible to deposit the organic dyes by a dipping process on top of the polystyrene film. During the deposition step in aqueous solutions, the polystyrene film detached from the substrate and it was washed away. Thus a drop-casting technique for dye deposition had to be used.

4.5.2 FR636 dyes embedded in a Polystyrene Matrix

The spin coated samples were characterized by a step profiler (TENCORÂ® P-10 Surface Profiler - KLA TENCOR) after plasma treatment and before polymer functionalization with dye deposition. The measured thickness was as high as $1743 \pm 120\,\text{nm}$ (d_0 in figure 4.3.3), with the largest thickness differences between the centre ($\sim 1802\,\text{nm}$) and the edge ($\sim 1624\,\text{nm}$) of the sample. After deposition of a second polystyrene layer the total polymer film was characterized again by profilometry. The thickness was $3672 \pm 130\,\text{nm}$ for samples with dye-loaded PAH polymer chains, whereas the total thickness for the sample with free chromophores embedded in the polystyrene sandwich was $2027 \pm 62\,\text{nm}$. In this way the distance between the chromophores and the polymer-air interface could be determined as $\sim 1929\,\text{nm}$ for the first kind of sample and $\sim 284\,\text{nm}$ for the latter (d_1 in figure 4.3.3).

4.6 Data Analysis by PCM

After sample preparation and characterization, fluorescence decay curves were measured for every sample and for each excitation-detection polarization combination. Details on data collection and fitting are in section 4.4.2. Figure 4.6.1 a) and b) report respectively fluorescence lifetime and intensity measurements for a set of samples with FR636 dye molecules covered by different numbers of PSS/PAH bilayers.

In 4.6.1 a) it is observed that the ratios among lifetimes for several polarization combinations tend to be smaller and the absolute values decrease with dye-interface distance, as predicted from the theory [7]. In 4.6.1 b) fluorescence intensities for $4, 6, 8$ and 10 bilayers above the dyes show slight fluctuations most probably due to different dye concentrations for different samples. The large deviation with the 2 bilayers case was already explained in section 4.5. By analyzing the experimental data of dyes embedded in polymer two tasks can be accomplished:

- determine the unknown parameters in the model: Γ_0, Γ_{nr} and $\triangle\theta$ (see section 4.2.2).
- Check the validity of the model.

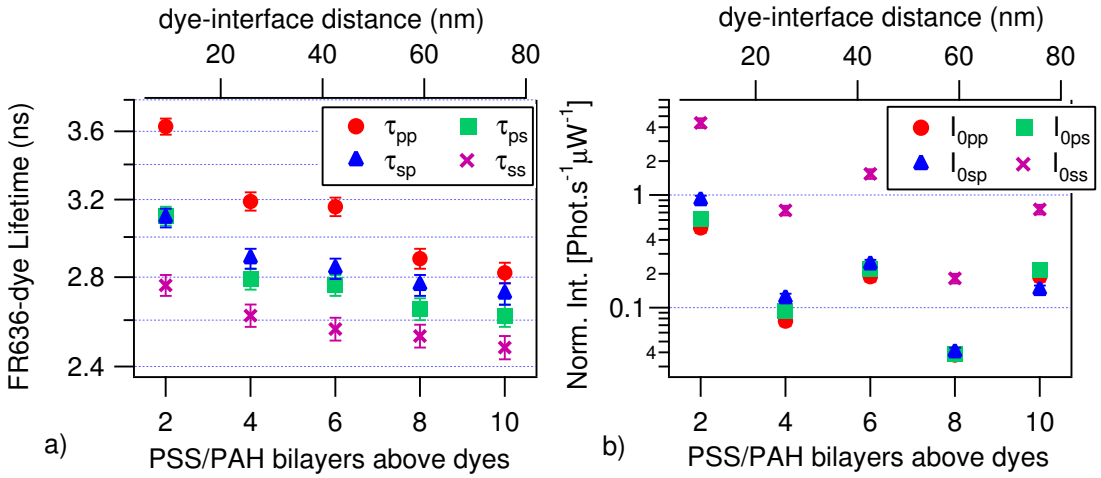

Figure 4.6.1: a) Fluorescence lifetime for FR6363 dye covalently bond to PAH and covered by different number of PSS/PAH bilayers b) Fluorescence intensity normalized by excitation power and photons acquisition time for the same samples. In the top horizontal axis of a) and b) mean distances between dyes and air-polymer interface are reported, based on ellipsometry and profilometer measurements. Errors on lifetime and intensity measurements were estimated to be 0.05 ns and 10% of value respectively.

In principle it is possible to fix a number of unknown parameters in the model as high as the number of independent physical variables measured. For each sample, 8 independent measurements are obtained: fluorescence lifetime and intensity for all 4 excitation-detection polarization combinations. The fitting process for the variables can then be split in two main steps:

- Determination of $\triangle\theta$ by using fluorescence intensities at time $t = 0$ (section 4.6.1).
- Determination of Γ_{nr} by using fluorescence lifetime and $\triangle\theta$ calculated in the previous point (section 4.6.2).

Once Γ_{nr} and $\triangle\theta$ are fixed, it is possible to simulate the full set of experimental data apart from a proportionality factor: Γ_0. If the classical approach correctly describes electromagnetism at the nanometer scale, the ratio between the simulated normalized lifetimes and the experimental ones should provide always the same value, i.e. the characteristic decay rate of the dye in vacuum Γ_0 (section 4.6.3). After obtaining the value of Γ_0, the result can be double checked by comparison with the same quantity from the same organic dyes deeply embedded in a polystyrene matrix (section 4.6.4) .

4.6.1 Determination of $\triangle\theta$

The expression for the fluorescence probability density for an ensemble of dipoles can be written as (see also chpater 3):

$$D_e^{\sigma\delta}(\bar{z}_0, \Delta\theta, \Gamma_{nr}, \Gamma_0, n_1, n_2, \hat{l}, \Omega_d, t) = \alpha \cdot \int_0^{\pi} d\theta_{ex} A \cdot B \cdot C \tag{4.6.1}$$

where the three functions in the integrand are:

$$\begin{aligned} A = &\quad sin(\theta_{ex}) \cdot \int_0^{2\pi} d\phi_{ex} \mid \vec{d}_{ex} \cdot \overrightarrow{E}^{\sigma}_{exc,loc}(z_0, \hat{l}, n_1, n_2) \mid^2 \\ B = &\quad \int_0^{2\pi} d\xi \, e^{-\Gamma_{tot,N}(\theta_{ex},\phi_{ex},\Delta\vartheta,\xi,\Gamma_{nr})\cdot\Gamma_0\cdot t} \\ C = &\quad \int_{\Omega_d} \mid \vec{d}_{em}(\theta_{ex}, \phi_{ex}, \Delta\theta, \xi) \cdot \overrightarrow{E}^{\delta}_{em,loc}(z_0, \hat{m}, n_1, n_2) \mid^2 d\hat{m} \end{aligned} \tag{4.6.2}$$

At time $t = 0$, $D_e^{\sigma\delta}$ in equation 4.6.1 depends only on the excitation-emission dipoles relative angle $\Delta\theta$ by the function C and on Γ_0 linearly through the overall multiplicative factor α (i.e. for $t = 0$ then $B = 2\pi$). If a factor 2π is included in α:

$$D_e^{\sigma\delta}(\bar{z}_0, \Delta\theta, \Gamma_0, n_1, n_2, \hat{l}, \Omega_d, 0) = \alpha \cdot \int_0^{\pi} d\theta_{ex} A \cdot C = \alpha \cdot \mathrm{I}_{0sim}^{\sigma\delta} \tag{4.6.3}$$

where the quantity $\mathrm{I}_{0sim}^{\sigma\delta}$ was re-defined except for a constant α. The fluorescence intensity at time $t = 0$ (eq. 4.6.3) is independent from the total decay rate $\Gamma_{tot,N}$. Using the comparison among theoretical ($\alpha \cdot \mathrm{I}_{0sim}^{\sigma\delta}$) and experimental values ($\mathrm{I}_{0exp}^{\sigma\delta}$), for different polarization combinations, it is possible to determine separetely and independently the excitation-emission relative angle $\Delta\theta$. To remove the unknown factor α in equation 4.6.3, the sum of the squared differences between measured and calculated values for different polarization combinations is minimized, by using α as variable:

$$\triangle \mathrm{I}(\triangle\theta, \alpha) = \sum_{pol} (\mathrm{I}_{0exp}^{pol} - \alpha \cdot \mathrm{I}_{0sim}^{pol})^2 \rightarrow minimum \tag{4.6.4}$$

Here the sum is over possible excitation-detection polarization combinations *pp, ps, sp, ss.* As a result:

$$\alpha_{min} = \frac{\sum_{pol} \mathrm{I}_{0exp}^{pol} \cdot \mathrm{I}_{0sim}^{pol}}{\sum_{pol} (\mathrm{I}_{0sim}^{pol})^2} \tag{4.6.5}$$

and replacing back in 4.6.4 only $\triangle\theta$ is left:

$$\triangle I(\triangle\theta) = \sum_{pol} (\mathrm{I}_{0exp}^{pol} - \alpha_{min} \cdot \mathrm{I}_{0sim}^{pol})^2 \tag{4.6.6}$$

A fit of the latter equation allows to determine the best value for the angle between excitation and emission dipoles $\triangle\theta$ of the single organic dye molecule within the model.

Figure 4.6.2 reports $\triangle$I as a function of $\triangle\theta$ following equation 4.6.6, for five samples with polyelectrolytes films of different thickness deposited on top of the dye molecules. The minimum of the curves in figure 4.6.2 corresponds to minimal differences between simulation and experiment. Hence, a graphical determination of $(\triangle\theta)_{min}$ can be performed. Then, by statistical considerations (appendix A.2), it is also possible to determine graphically an error on $(\triangle\theta)_{min}$ for each sample, in figure 4.6.2. The error is the difference between the abscissa value of the curve minima and the abscissa of the intersection between the curve and a value 2 times the ordinate minima (see figure 4.6.3). It is possible to show (appendix A.2) that such a difference corresponds to a abscissa variation as large as twice the standard deviation ($\triangle_i \sim 2 \cdot \sigma$). Figure 4.6.3 shows $\triangle$I as a function of $\triangle\theta$ around the curves minima for different samples, according to equation 4.6.6. The error ($\triangle_i$) on $(\triangle\theta)_{min}$ is also

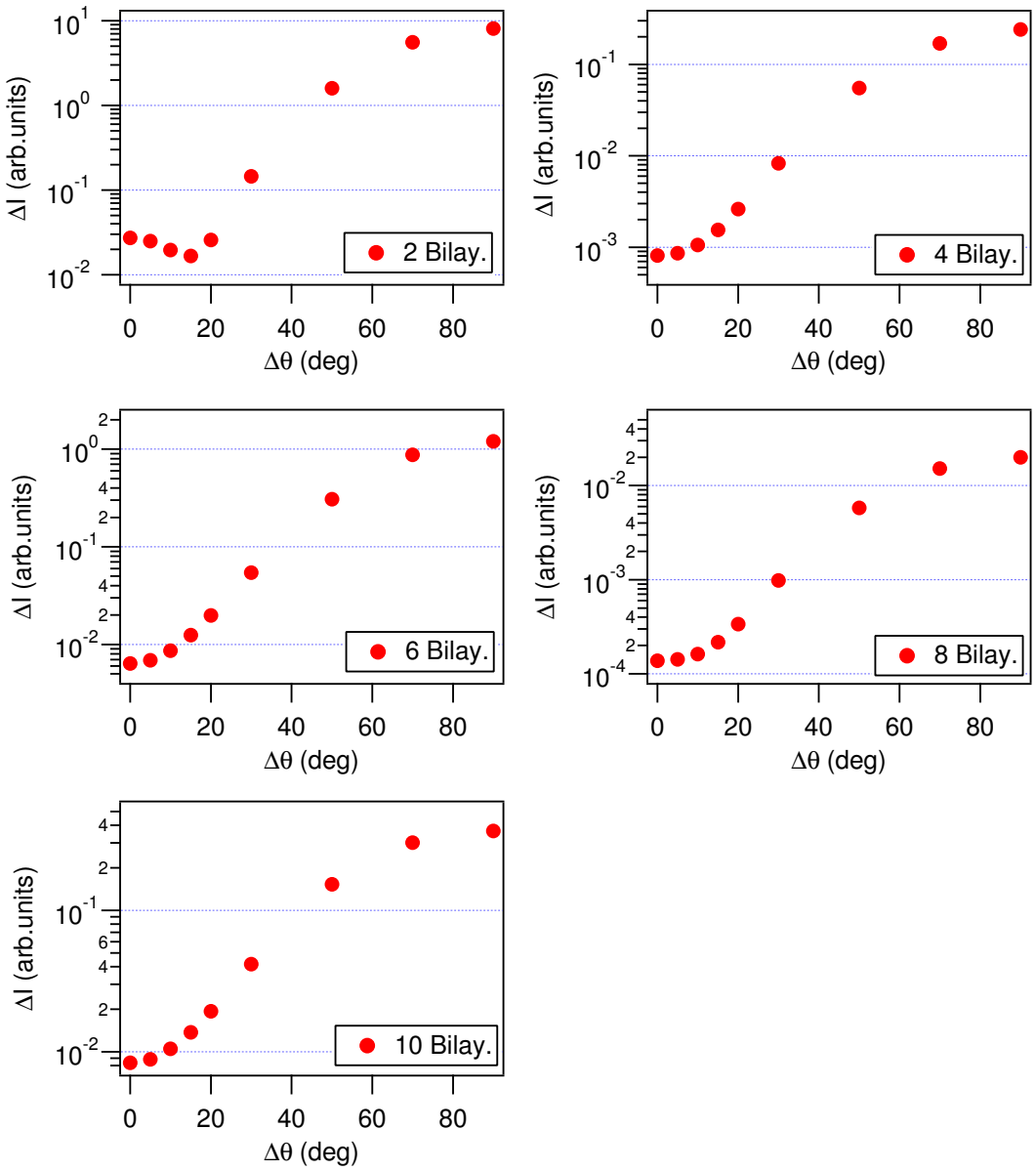

Figure 4.6.2: Sum of the squared differences between measured and calculated intensities values at time t=0. Data are for different polarization combinations, as a function of dye molecule's angle between excitation and emission dipoles. In the legend the number of PSS/PAH bilayers deposited above the molecular chromophores are indicated. Markers size indicate an error of 10% on experimental intensities.

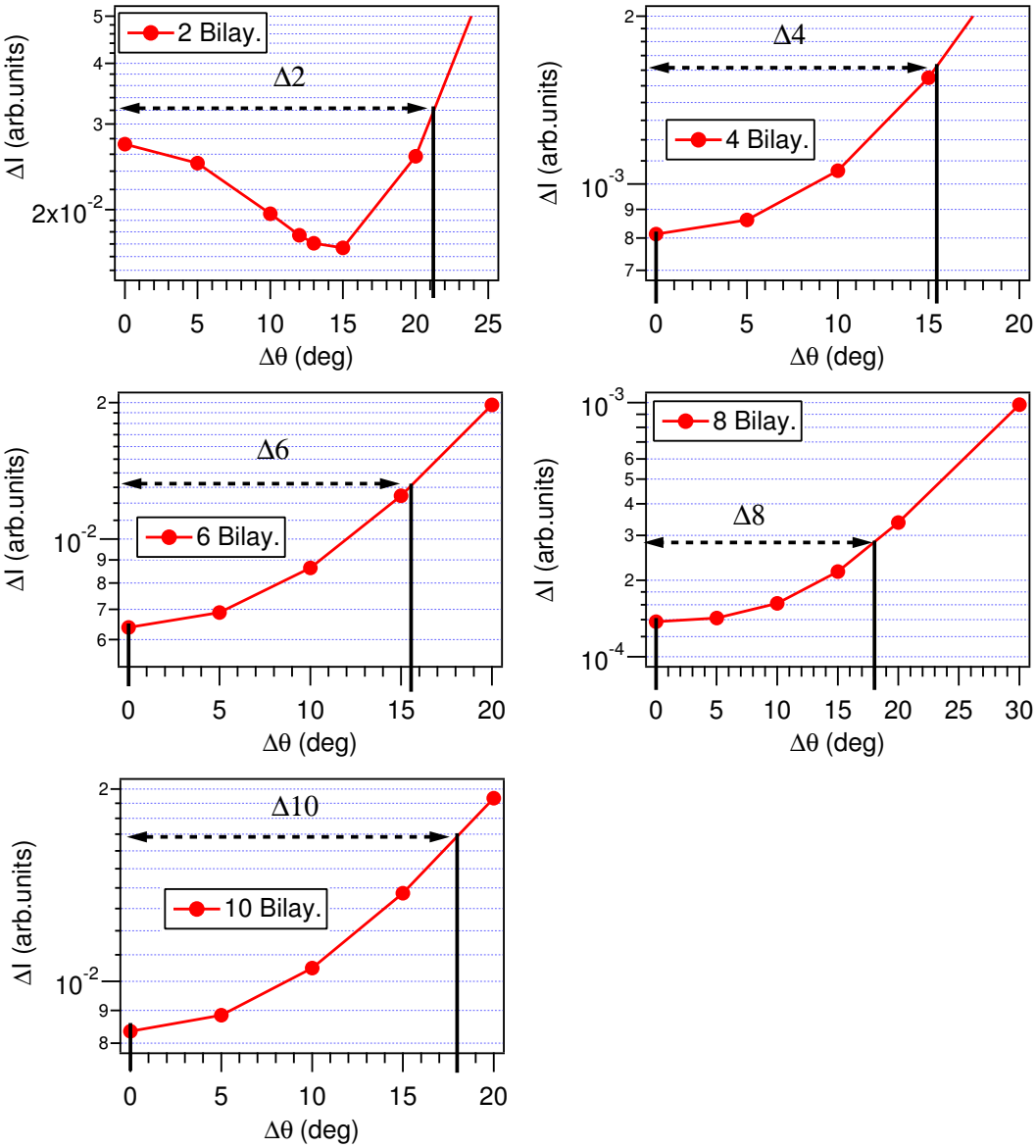

Figure 4.6.3: Graphical representation of $\triangle$I as a function of $\triangle\theta$ around the curves minima for different samples, according to equation 4.6.6. Vertical lines correspond to minima and to a value 2 times minima ordinate. $\triangle 2, \triangle 4, \triangle 6, \triangle 8$ and $\triangle 10$ are the estimated errors for $(\triangle\theta)_{min}$, representing an interval of $\sim 2 \cdot \sigma$. In the legends, the number of PSS/PAH bilayers deposited above the molecular chromophores are indicated. Markers size indicates an error of 10% on experimental intensities.

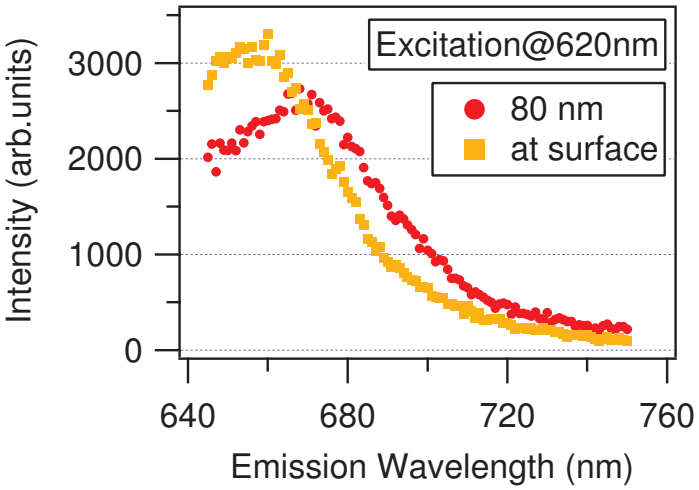

Figure 4.6.4: Fluorescence spectra of FR636 red reactive dyes covalently bound to PAH chains for the two extreme cases of dyes fully-embedded in polymer and at surface.

graphically estimated. For different samples (in degree): $\triangle 2 \gtrsim 21, \triangle 4 \simeq 15, \triangle 6 \simeq 15, \triangle 8 \simeq 18$ and $\triangle 10 \simeq 18$ and averaging only the last four samples, at the end $\sigma \simeq 8\hat{A}°$.

In figures 4.6.2 and 4.6.3, for all samples the optimal value for $(\triangle\theta)_{min}$ is $0\hat{A}°$, except for the case with 2 PSS/PAH bilayers covering the emitters, which shows the best fit for values around $15\hat{A}°$. The difference in $(\triangle\theta)_{min}$ may rise from different dye-local environment interactions, due to not uniform dye molecule coverage with 2 PSS/PAH bilayers. In fact the polymer film thickness on top of the dye for 2 PSS/PAH bilayers is 8 ± 2 nm (section 4.5) and the dye molecules have an average size of ≈ 3 nm (see also figure 4.5.5). Moreover, the position of the chromophore with respect to the PAH chain is unknown. Moreover, the chain-chain interdigitation between adjacent polymer layers (internal roughness) of ~ 2 nm should be also considered [21]. Therefore for the sample with 2 PSS/PAH bilayers the chromophores still experience the polymer matrix as optical environment (see lifetimes in figure 4.6.1), like the ones fully embedded in the polymer (4, 6, 8 and 10 bilayers), but the non-radiative interactions of the dyes with the local environment could be different with respect to the other samples. One of the possible explanations of the relative angle difference could be that, for such a thin layer, many dye molecules are outside the polymer matrix and, therefore, their contribution is not included within the model. Another possible reason may come from a quantum mechanical view: the contributions to fluorescence may come from different vibrational energy levels of the molecule, in the case of very thin layers covering the dye molecules. In figure 4.6.4, two measured fluorescence spectra are reported: for dye molecules at surface and embedded in the polymer matrix at ~ 80 nm from the air-polymer interface (a sketch of the samples is in figure 4.3.2). The chromophores were excited at fixed wavelength of 620 nm and the fluorescence spectra recorded by scanning over the wavelenghts range.

Figure 4.6.4 shows that, when the dyes are covered by a thick polymer film, the fluorescence emission band peak is red-shifted with respect to the case of dyes at surface. This indicates that the emission occurs mainly from different levels when the dyes are fully-embedded in polymer. Nevertheless, a conclusive and univocal explanation for the difference in $\triangle\theta$ for thin layers covering the dye molecules could not be found.

To gain more insight, it is useful to check the sensitivity of the model with respect to the $\triangle\theta$ param-

eter. Therefore the intensity and the lifetime trends as a function of the emission-excitation dipole angle were calculated. Figure 4.6.5 shows the simulated fluorescence intensities I_{0sim}^{pol} for different excitation-detection polarizations combinations, as a function of the excitation-emission dipoles relative angle $\triangle\theta$. For $\triangle\theta$ values below $\sim 30\hat{A}^\circ$ the maximum variation of I_{0sim}^{pol} is less than 20%, indicating a weak dependence of fluorescence intensity (at time $t = 0$) from the relative angle $\triangle\theta$. Figure 4.6.5 shows that for TM excitation radiation (*pp* and *ps*), the theory overestimates the intensities values even for $\triangle\theta = 0\hat{A}^\circ$, especially for thicker polymer films. The field components perpendicular to the interface depend on the media refractive indices, while the parallel components are preserved according to the equations 4.1.1. In this respect, it is believed that the mismatch between experiment and theory is caused by a not correct estimation of the polyelectrolytes refractive index at the excitation wavelenght, in the model.

A reason for the inaccurate estimation of the refractive index could be the presence of residual water trapped within the polyelectrolytes film [20]. To verify such hypothesis, the refractive index of the polymer layer above the dye molecule was changed in the theoretical calculations. For the sample with 10 bilayers, where the discrepancy is larger, the refractive index was changed from $n = 1.523$ to $n = (1.523 + 1.33)/2 = 1.426$, with $n = 1.33$ the value for water. Figure 4.6.6 shows the comparison among theoretical and experimental curves when using the new refractive index value: a good agreement for $\triangle\theta = 0\hat{A}^\circ$ can be observed also for the *pp* and *ps* polarizations.

In figure 4.6.7 the simulated fluorescence lifetimes τ_{sim}^{pol} for different excitation-detection polarizations combinations are plotted versus the angle $\triangle\theta$, with the assumption of $\Gamma_{nr} = 0$. There it is possible to observe that the fluorescence lifetime is weakly dependent on the excitation-emission dipole, and that the change of τ_{sim}^{pol} is smaller for larger dyes-interface distances. For example, for small angles ($\Delta\theta \lesssim 30\hat{A}^\circ$) the lifetime changes are maximum $\sim 10\%$.

4.6.2 Determination of Γ_{nr}

Once $\Delta\theta$ is determined by a fitting procedure, its value is put back in equation 4.6.1 and $\Gamma_{nr,N}$ is now extracted by using the comparison among experimental and theoretical lifetime values. In the calculation of the fluorescence probability density of an ensemble of dyes, the decay rate values were always normalized to the dye fluorescence decay rate in vacuum, to eliminate the dependence on the dipole strenght. As a consequence, the theoretical decay curves contain an exponential function of the type (see *B* in equation 4.2.13):

$$e^{(-\Gamma_{tot,N}\cdot\gamma\cdot t)} \equiv e^{(-\frac{1}{\tau_{sim}}\cdot\gamma\cdot t)} \tag{4.6.7}$$

$\Gamma_{tot,N}$ is normalized to the decay rate in vacuum Γ_0 and γ is a scaling factor with physical dimensions of a frequency (ns^{-1}). $\Gamma_{tot,N}$ and τ_{sim} are dimensionless. The simulated lifetime is normalized to the vacuum value because $\tau_{sim} = 1/\Gamma_{tot,N}$. Assuming the theoretical model is valid, it is possible to write:

$$e^{(-\frac{1}{\tau_{sim}}\cdot\gamma\cdot t)} = e^{(-\frac{\tau_0}{\tau_{exp}}\cdot t)} \tag{4.6.8}$$

The ratio between the experimental and the simulated lifetimes represents the value of dye lifetime in vacuum in nanoseconds, except for a scaling factor. In fact, from equation 4.6.8: $\frac{\tau_{exp}}{\tau_{sim}} = \frac{\tau_0}{\gamma}$. Following the procedure of the previous section (4.6.1) it is possible to define a similar quantity for lifetimes values to minimize:

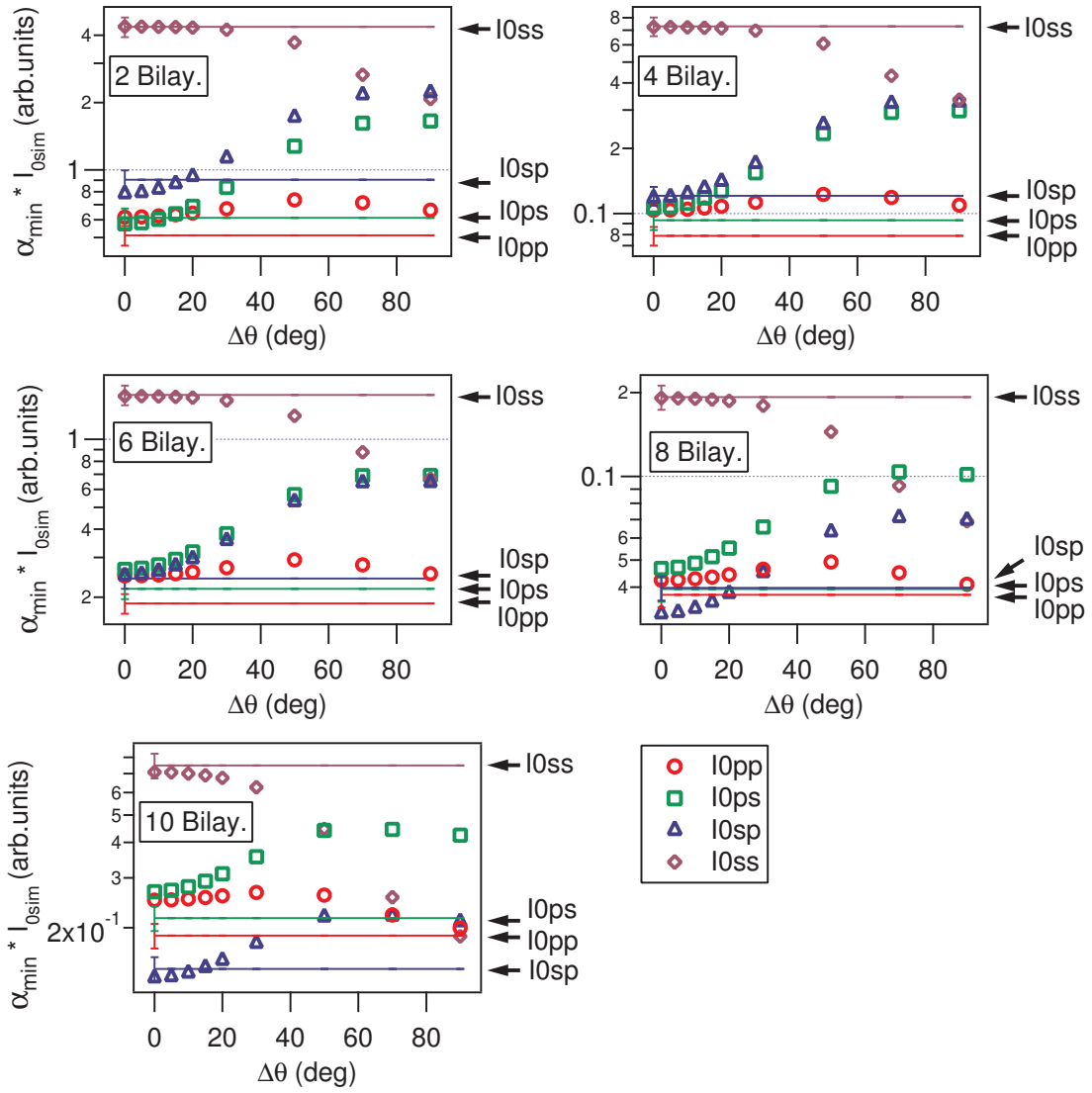

Figure 4.6.5: Simulated fluorescence intensities (I_{0sim}), for different excitation-detection polarizations combinations as a function of the excitation-emission dipoles relative angle ($\triangle\theta$). Five different samples with different numbers of PSS/PAH polyelectrolytes bilayers deposited above dyes are reported (indicated in the figures legends) .

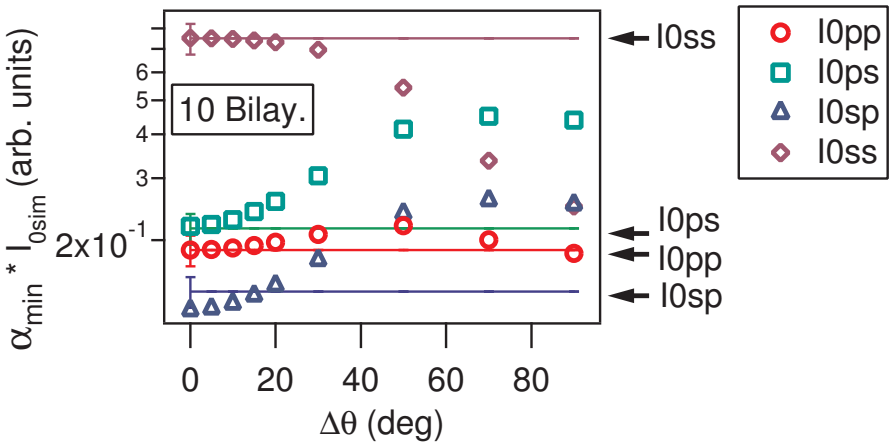

Figure 4.6.6: Simulated fluorescence intensities (I_{0sim}), for different excitation-detection polarizations combinations as a function of the excitation-emission dipoles relative angle ($\triangle\theta$). The sample with 10 PSS/PAH polyelectrolytes bilayers deposited on top of the dyes is here considered. A refractive index value $n = 1.426$ was used for the polymer in the simulation.

$$\triangle\tau(\frac{\tau_0}{\gamma}, \frac{\Gamma_{nr}}{\Gamma_0}, \triangle\theta) = \sum_{pol}(\tau_{exp}^{pol} - \frac{\tau_0}{\gamma} \cdot \tau_{sim}^{pol})^2 \rightarrow minimum \tag{4.6.9}$$

For the dimensionless scaling factor $\frac{\gamma}{\tau_0}$, the value that minimize the sum of the squared differences between the measured fluorescence lifetime and the calculated ones is

$$(\frac{\tau_0}{\gamma})_{min} = \frac{\sum_{pol} \tau_{exp}^{pol} \cdot \tau_{sim}^{pol}}{\sum_{pol}(\tau_{sim}^{pol})^2}. \tag{4.6.10}$$

After substitutuing the expression 4.6.10 in the equation 4.6.9 and using the value for $\triangle\theta$ calculated in the previous section, Γ_{nr} is the only variable left. Its value can be determined by the minima of the function:

$$\triangle\tau(\Gamma_{nr}, \frac{\Gamma_{nr}}{\Gamma_0}, \triangle\theta) = \sum_{pol}(\tau_{exp}^{pol} - (\frac{\tau_0}{\gamma})_{min} \cdot \tau_{sim}^{pol})^2 \tag{4.6.11}$$

In figure 4.6.8, $\triangle\tau(\Gamma_{nr}/\Gamma_0, \triangle\theta)$ is plotted as a function of normalized non-radiative decay rate and for different values of $\triangle\theta$, according to equation 4.6.11. The normalized non-radiative values $(\Gamma_{nr}/\Gamma_0)_{min}$ can be determined graphically for each sample from figure 4.6.8, even if the depth of the minima is quite different for several samples, implying a different quality of the fit. For samples with 4 and 6 bilayers above the dyes, the well pronounced minima represent a good quality fit. On the other hand for 8 and especially 10 bilayers above the dyes, the $\triangle\tau(\Gamma_{nr}, \triangle\theta)$ function minima are not pronounced thus providing more questionable fit results. A possible explanation of different fits quality may consider residual trapped water in thicker polymer films as a consequence of the layer-by-layer deposition technique. From successive studies (see Appendix A.3), in fact, the water resulted to be a strong quencher for the FR636 dye molecule, while on the other hand it is well known the high degree of hydrophilicity of polyelectrolytes films [20]. The amount of water in polyelectrolytes films deposited by layer-by-layer method depends on the number of deposition cycles (i.e. the number of

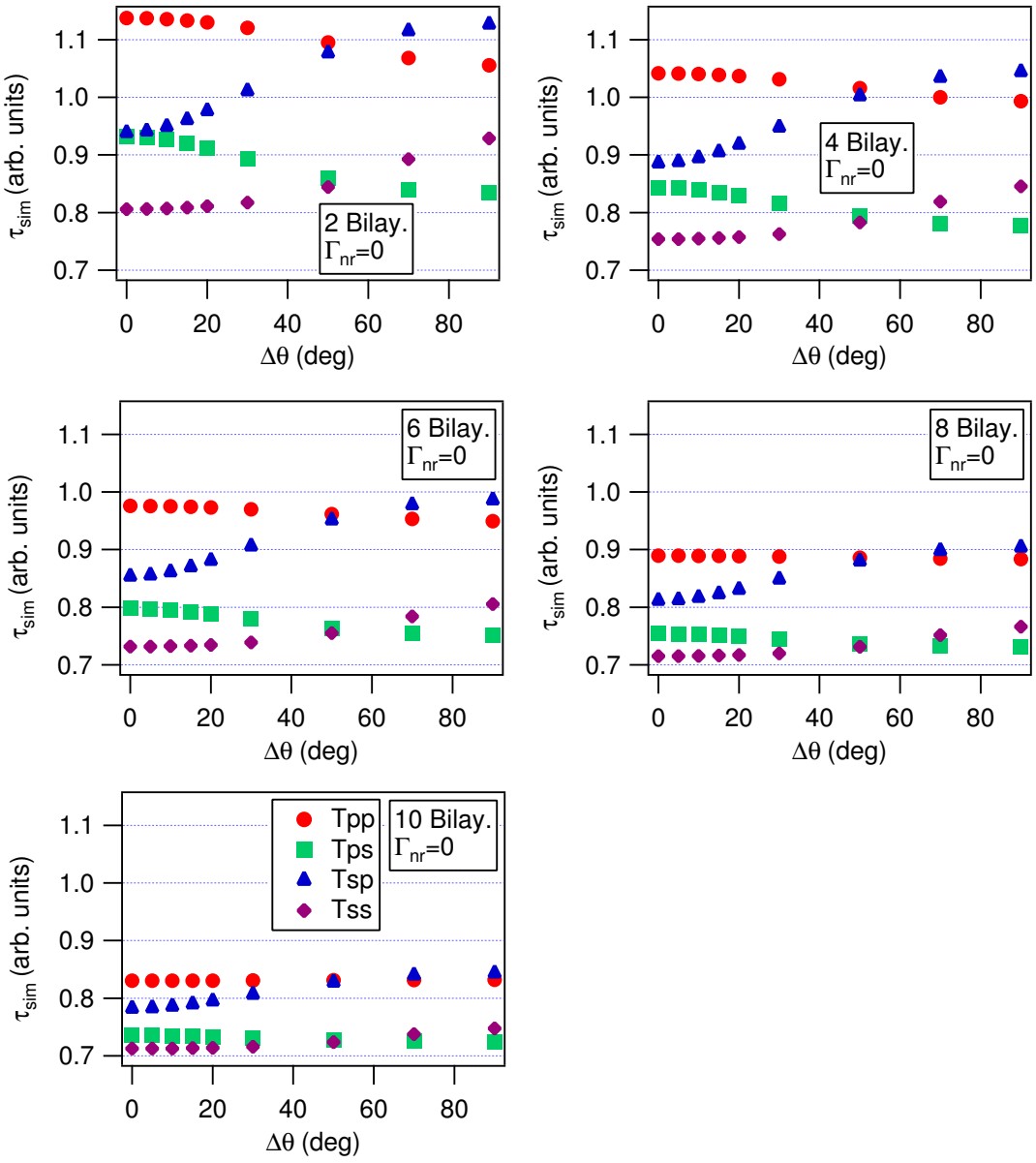

Figure 4.6.7: Simulated fluorescence lifetimes τ_{sim}^{pol} for different excitation-detection polarizations combinations as a function of the excitation-emission dipoles relative angle ($\triangle\theta$). Five different samples with different numbers of polyelectrolyte layers deposited on top of the dyes are considered.

layers deposited). In general thicker films trap higher amount of water molecules, which are very difficult to remove without any thermal treatment. For this purpose a drying process was attempted at 50Â°C in oven for an hour. However, afterwards the fluorescence was deactivated permanently at the available excitation wavelength.

From figure 4.6.8, the sample with 2 PSS/PAH bilayers shows the smallest non-radiative decay rate (with a pronounced minimum). Apparently, the chromophores experience different non-radiative decay channels, even if the optical environment seems to be the same with respect to the other samples (as it is observed from figure 4.6.1). The small value of $(\Gamma_{nr}/\Gamma_0)_{min}$ could be explained by the same argument used in section 4.6.1 to justify a different value of $\triangle\theta$, that is poor polymer coverage of the dye molecules.

In figure 4.6.8 the minimum position (i.e. $(\Gamma_{nr}/\Gamma_0)_{min}$) is fairly independent of the value of $\triangle\theta$ used in the simulation within an interval $\sim 0 \div 15\hat{A}^\circ$, for the sample with 2 PSS/PAH bilayers. It can be proved that the same conclusion is valid for all the samples. The reason may be seen in the weak dependence of the fluorescence lifetime on $\triangle\theta$, for small angle values, especially for thicker polymer films covering the emitters (figure 4.6.7).

The weighted average of the $(\Gamma_{nr}/\Gamma_0)_{min}$ values may be taken into account the consider the different quality of the fits for the non-radiative decay rate. In this manner an optimum estimate for a true value of Γ_{nr}/Γ_0 may be obtained. By statistical considerations detailed in appendix A.2, for each sample it is also possible to determine a statistical error on $(\Gamma_{nr}/\Gamma_0)_{min}$. In figure 4.6.9, the difference between the abscissa value of the curve minima and the abscissa of the intersection between the curve and a value 2 times the ordinate minima is graphically estimated. It is possible to show (appendix A.2) that such a difference corresponds to a (Γ_{nr}/Γ_0) variation as large as the standard deviation (σ).

In figure 4.6.9 a) - e) the plot region under the minima of curves reported in figure 4.6.8 have been enlarged, respectively for samples with $2,4,6,8$ and 10 PSS/PAH bilayers above the dye molecules. For each sample in figure 4.6.9, the minimum ordinate of the $\triangle\tau(\Gamma_{nr},\triangle\theta)$ function and the ordinate for a value double the minimum are indicated by horizontal dashed lines. The abscissae corrispondent to the intersection with the function $\triangle\tau(\Gamma_{nr},\triangle\theta)$ are pointed to by continuous vertical lines. The distances between the abscissa of intersections for different samples indicate how pronounced the minima of the $\triangle\tau(\Gamma_{nr},\triangle\theta)$ function are. The values of $\Delta 2 = 0.3, \Delta 4 = 0.13, \Delta 6 = 0.13, \Delta 8 = 0.46$ and $\Delta 10 = 0.84$ in figure 4.6.9 correspond to a statistical error of $\sim 2\cdot\sigma$. Therefore, the quantities

$$\frac{1}{\sigma_k^2} = \left(\frac{2}{\Delta_k}\right)^2 \tag{4.6.12}$$

can be considered as weights to calculate the average among the different values of $(\Gamma_{nr}/\Gamma_0)_{min}$.

By using the weighted average and excluding the data from the sample with 2 bilayers (poor coverage):

$$< (\Gamma_{nr}/\Gamma_0)_{min} >= \frac{\sum_k \left(\frac{2}{\Delta_k}\right)^2 \cdot (\Gamma_{nr}/\Gamma_0)^k_{min}}{\sum_k \left(\frac{2}{\Delta_k}\right)^2} = 0.56 \pm 0.05 \tag{4.6.13}$$

where the error corresponds to the standard deviation σ_N calculated as

$$\sigma_N = \left\{\sum_k \left(\frac{2}{\Delta_k}\right)^2\right\}^{-1/2} \tag{4.6.14}$$

If the sample with two bilayers is included in the averaging process, the final result is $< (\Gamma_{nr}/\Gamma_0)_{min} >= 0.52 \pm 0.05$, which is within the error range of the result obtained from equation 4.6.13.

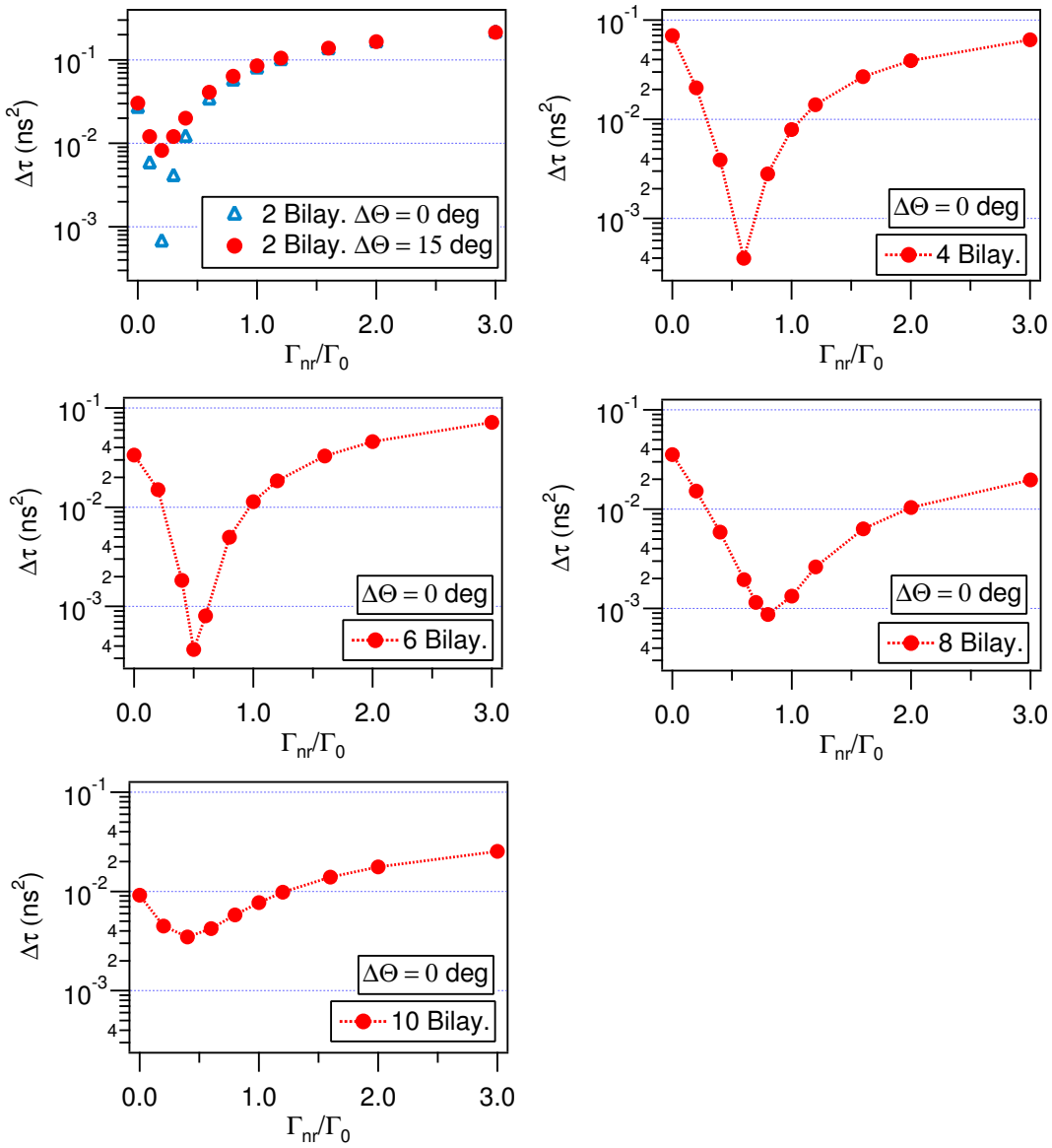

Figure 4.6.8: Graphical representation of $\triangle\tau(\Gamma_{nr}, \triangle\theta)$ according to equation 4.6.11. The number of the PSS/PAH bilayers deposited on top of the chromophores are shown in the legend together with of $\triangle\theta$ values used for simulation. The estimated error on $\triangle\tau(\Gamma_{nr}, \triangle\theta)$ is $\sim 2\%$, smaller than marker size. The Γ_{nr}/Γ_0 abscissa values for the $\triangle\tau$ minima are $0.2, 0.6, 0.5, 0.8$ and 0.4 respectively for $2, 4, 6, 8$ and 10 bilayers.

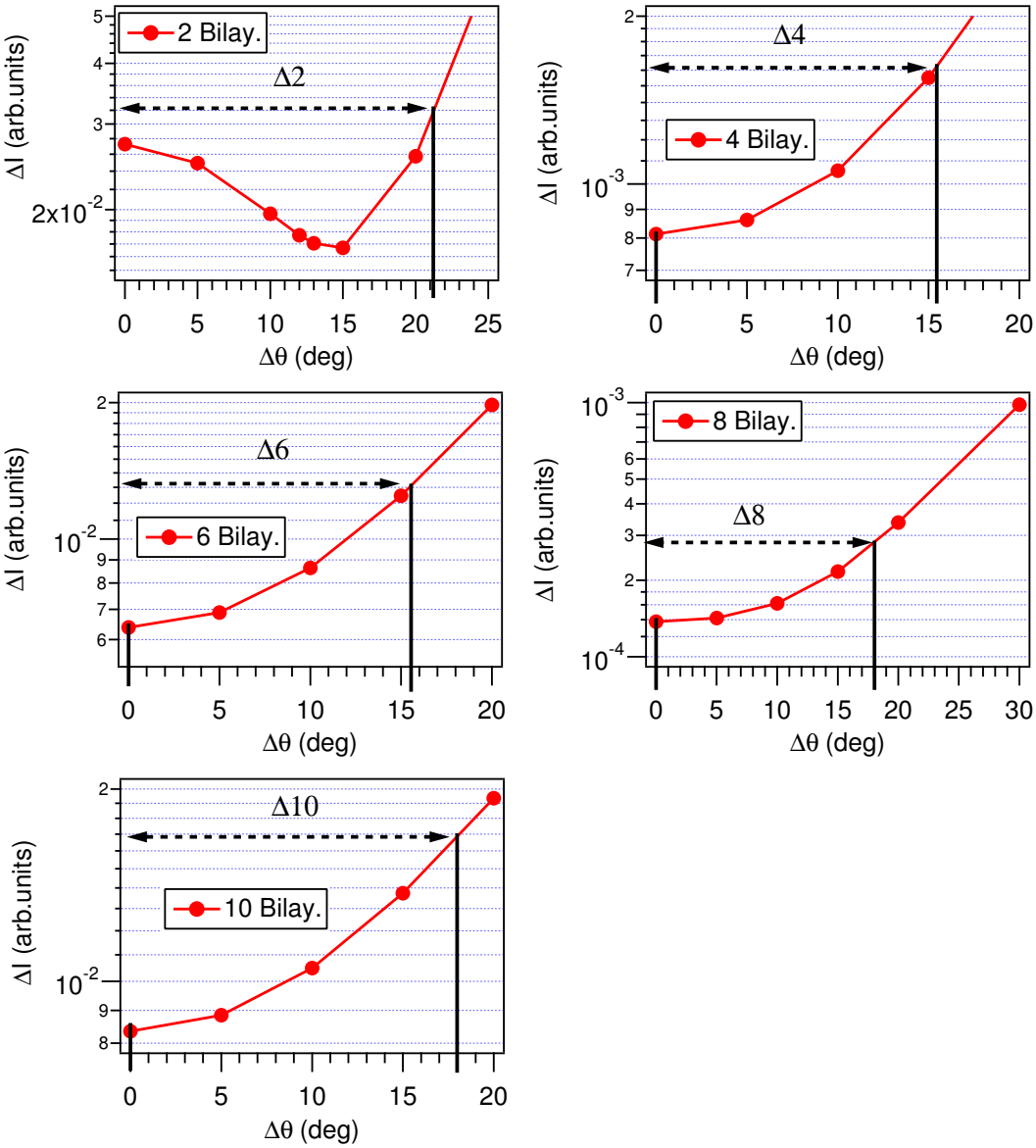

Figure 4.6.9: a) - e) Graphical representation of function $\triangle\tau(\Gamma_{nr}, \triangle\theta)$ plotted around the minimum, according to equation 4.6.11. The number of the PSS/PAH bilayers deposited above the chromophores are shown in the legend together with the values of $\triangle\theta$ used for simulation. Horizontal dashed lines represent the minimum ordinate and 2 times the minimum value ordinate. The quantities $\Delta 2, \Delta 4, \Delta 6, \Delta 8$, and $\Delta 10$ represent an interval around the minima of $\sim 2 \cdot \sigma$.

No. of PSS/PAH bilayers	$(\Gamma_{nr}/\Gamma_0)_{min}$	$\triangle_k \sim 2 \cdot \sigma$
2	0.2	0.3
4	0.6	0.13
6	0.5	0.13
8	0.8	0.46
10	0.4	0.84

Table 4.6.1: Values of $(\Gamma_{nr}/\Gamma_0)_{min}$ for the different samples extracted by graphical minimization of the function $\triangle\tau(\Gamma_{nr}, \triangle\theta)$, according to equation 4.6.11, by using $\triangle\theta = 0\hat{A}^\circ$. The statistical error for each value of $(\Gamma_{nr}/\Gamma_0)_{min}$, as derived graphically from figure 4.6.9, is also indicated.

Figure 4.6.10 shows the theoretical fluorescence lifetime $\left(\frac{\tau_0}{\gamma}\right)_{min} \cdot \tau_{sim}^{pol}$ (equation 4.6.7) for different samples and different excitation-detection polarizations, as a function of the normalized non-radiative decay rate Γ_{nr}/Γ_0. In the same figure, the relative experimental lifetimes and the value $(\Gamma_{nr}/\Gamma_0)_{min}$ for which the function $\triangle\tau$ has a minimum are also plotted. From figure 4.6.10 a good agreement among theory and experiment is observed, within the experimental error, for all the samples at the value of Γ_{nr}/Γ_0 that minimizes $\triangle\tau$. It is interesting also to notice that lower fluorescence quantum efficiency values (i.e. larger non radiative decay rate) bring smaller differences among lifetimes, for different excitation-detection polarization combinations.

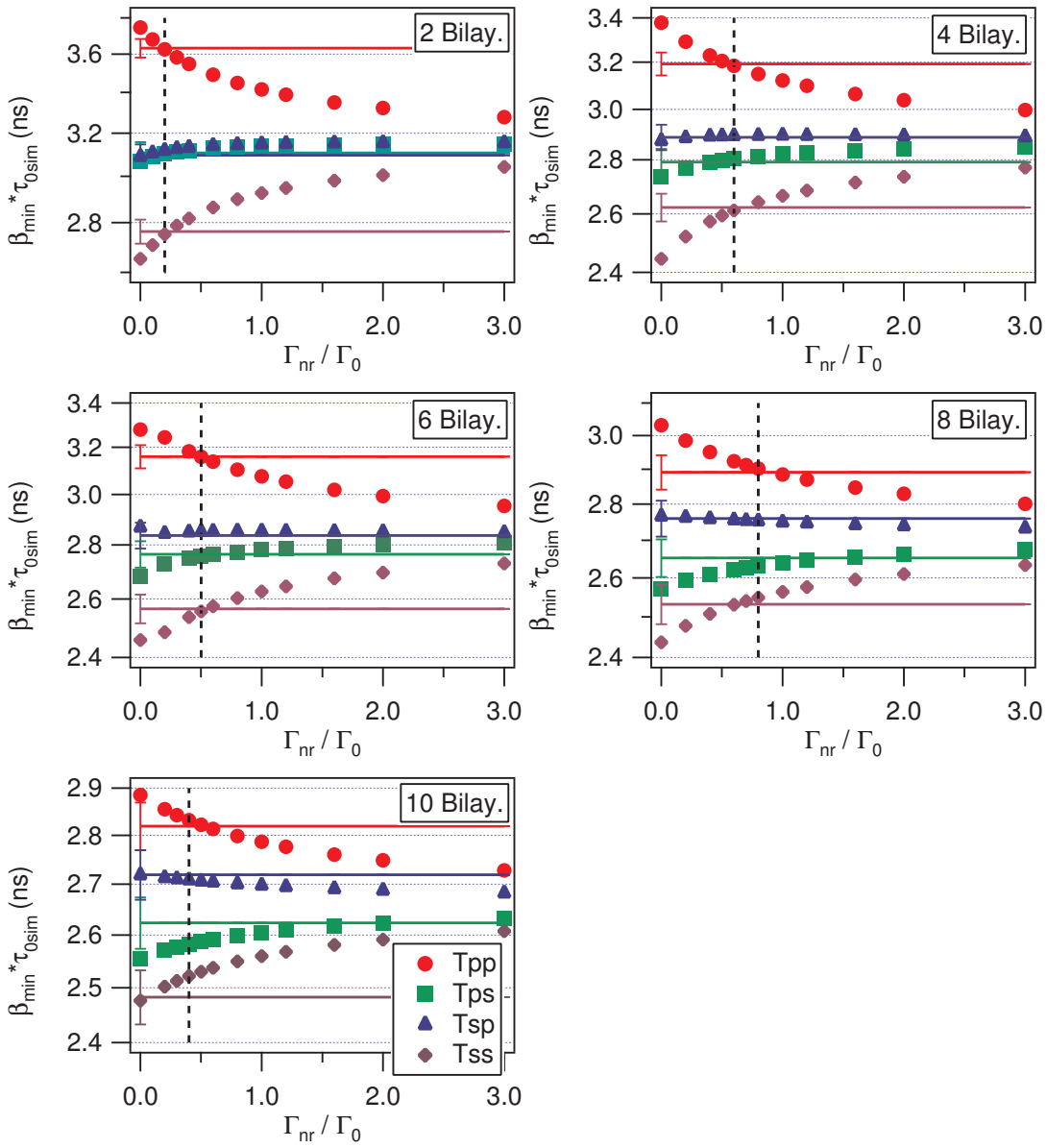

Figure 4.6.10: Simulated fluorescence lifetime ($(\frac{\tau_0}{\gamma})_{min} \cdot \tau_{sim}^{pol}$) for different samples and different excitation-detection polarization (i.e. *pp, ps, sp, ss*) as a function of the normalized non-radiative decay rate Γ_{nr}/Γ_0 (full markers). In the graph $(\frac{\tau_0}{\gamma})_{min} \equiv \beta_{min}$ for graphical convenience. Experimental lifetimes are reported as horizontal lines. Same colours indicate same polarization combinations. The experimental error is ± 0.05 ns and the numbers of bilayers deposited above the dyes are reported in the legends. In the graphs it is also shown the value (as vertical dashed line) of the normalized non-radiative decay as a result of the best fit for the data (see table 4.6.1). Error bars are drawn for experimental horizontal lines only at $\Gamma_{nr}/\Gamma_0 = 0$ for clarity reasons.

4.6.3 Determination of τ_0

With the values for $\Delta\theta$ and $(\Gamma_{nr}/\Gamma_0)_{min}$ previously determined, equation 4.6.1 can be used once more to simulate the whole set of experimental data. By using ratios bewteen simulated and measured lifetimes values, the normalization factor Γ_0 is obtained. Successively, τ_{sim} and I_{0sim} are calculated, for

each sample and for each excitation-detection polarization combination. In the comparison between theory and experiment, after equation 4.6.8 with the scaling factor $\gamma = 1$, the following expression can be written:

$$\frac{\tau_{exp}^{\sigma\delta}}{\tau_{sim}^{\sigma\delta}} = \tau_0^{\sigma\delta} \tag{4.6.15}$$

From which the fluorescence lifetime in vacuum is obtained, in nanoseconds, for each polarization combination and for each sample . If the model describes correctly the experiment, the different ratios in expression 4.6.15 should provide the same value for $\tau_0^{\sigma\delta}$ within the error range. To calculate the error on τ_0, the error propagation law can be applied to expression 4.6.15 and considering the average over different polarization combinations:

$$\Delta\tau_0 = \frac{1}{\tau_{sim}} \cdot \Delta\tau_{exp} + \frac{\tau_{exp}}{(\tau_{sim})^2} \cdot \Delta\tau_{sim} \tag{4.6.16}$$

Remembering that

$$\tau_{sim} = \frac{1}{\Gamma_{tot,N}} = \frac{1}{\Gamma_{rad,N} + \Gamma_{nr,N}} \tag{4.6.17}$$

then

$$\Delta\tau_0 = \frac{1}{\tau_{sim}} \cdot \Delta\tau_{exp} + \tau_{exp} \cdot \left[\Delta\Gamma_{rad,N} + \Delta\Gamma_{nr,N}\right] \tag{4.6.18}$$

where $\Delta\Gamma_{nr,N}$ corresponds to the σ_k value determined by the equation 4.6.12, while $\Delta\Gamma_{rad,N}$ is the error on the numerically calculated $\Gamma_{rad,N}$ and can be neglected ($\lesssim 10^{-5}$). $\Delta\tau_{exp}$ represent the experimental error. All the errors have the same value for different polarization combinations. In table 4.6.2 the lifetime values calculated from equation 4.6.15 are reported, for different polarization combinations and different samples. The associated error, estimated according to expression 4.6.18, is also indicated. From table 4.6.2, for each sample the values of τ_0 obtained from different polarizations are identical within the statistical error. Instead a difference is seen among different samples. The main reason for different values of vacuum lifetime is due to different values of $(\Gamma_{nr}/\Gamma_0)_{min}$ used in the simulation. Different errors on τ_0 are the consequence of different indetermination on the values of $(\Gamma_{nr}/\Gamma_0)_{min}$.

Nevertheless, it is possible to average different values of vacuum lifetime in the sense of least squares method: giving a weight to the single entries equal to the reciprocal of the error. In this way, more weight is given to entries with smaller error:

$$< \tau_0 >= \frac{\sum_k \left(\frac{1}{\Delta\tau_0}\right)^2 \cdot \tau_0}{\sum_k \left(\frac{1}{\Delta\tau_0}\right)^2} = 4.9 \pm 0.2 \tag{4.6.19}$$

The error is calculated as

$$\sigma_\tau = \left\{\sum_k \left(\frac{1}{\Delta\tau_0}\right)^2\right\}^{-1/2} \tag{4.6.20}$$

No. of PSS/PAH bilayers	τ_0^{pp}	τ_0^{ps}	τ_0^{sp}	τ_0^{ss}	$\Delta\tau_0$
2	4.0	4.0	4.0	3.9	0.5
4	5.1	5.0	5.1	5.0	0.3
6	4.9	4.9	4.8	4.8	0.3
8	5.6	5.6	5.6	5.6	0.7
10	4.5	4.6	4.5	4.6	1.2

Table 4.6.2: Vacuum lifetime values, calculated according to equation 4.6.15, for different polarization combinations and different samples. In the simulation, for each sample, different values of $(\Gamma_{nr}/\Gamma_0)_{min}$ have been used, according to the graphical fits in figure 4.6.9. The associated error evaluated by averaging over the different polarization combinations (equation 4.6.18) is also reported.

where the subscript k denotes different samples. Figure 4.6.11 a) depicts the vacuum lifetimes values of table 4.6.2 plotted against the correspondent values of $(\Gamma_{nr}/\Gamma_0)_{min}$ used in the simulation, from table 4.6.1. The value for the weighted average $<(\Gamma_{nr}/\Gamma_0)_{min}>$ with relative error, from equation 4.6.13, is also plotted (dotted line). Figure 4.6.11 b) reports, the values of $<\tau_0>\pm\sigma_\tau$, as indicated in table 4.6.2, and the weighted average for vacuum lifetime according to equation 4.6.19.

Once all parameters $\triangle\vartheta = 0\pm 8\hat{A}^\circ$, $\Gamma_{nr}/\Gamma_0 = 0.56\pm 0.05$ and $\tau_0 = 4.9\pm 0.2$ ns have been determined, it is possible to simulate the whole set of measurements and have a global comparison with the experimental data. Figure 4.6.12 draws the comparison among calculated and experimental fluorescence lifetimes and intensities, for FR6363 dye molecules covered by a different number of PSS/PAH polyelectrolytes bilayers. Data is relative to different excitation-detection polarization combinations.

For the simulation in figure 4.6.12, $\triangle\vartheta = 0\hat{A}^\circ$ and $\Gamma_{nr} = 0.56$ were used for all the samples. Theoretical and measured intensities have been scaled for each sample respectively by the following factors:

$$I_{tot,sim} = I_{0sim}^{pp} + I_{0sim}^{ps} + I_{0sim}^{sp} + I_{0sim}^{ss} \tag{4.6.21}$$

and

$$I_{tot,exp} = I_{0exp}^{pp} + I_{0exp}^{ps} + I_{0exp}^{sp} + I_{0exp}^{ss}. \tag{4.6.22}$$

In this way a different scaling factor for each experiment has been introduced. This procedure is anyway justified since the unknown proportionality factor in the equation 4.2.12 (α) is directly proportional to the dye molecules concentration per unit area on the sample (c). Due to the limits of reproducibility in the sample preparation and mainly to the pH effect on the chromophores (see section 4.5) it is not possible, to achieve exactly the same dye concentration for different samples.

From figure 4.6.12 a) a good agreement between experiment and theory can be observed, except for a slight deviation in the case of 2 PSS/PAH bilayers. The mismatch may come from an undefined local environment of the dye molecules (details in section 4.6.1). In this case, therefore, the model is not able to fully take into account the non-radiative decay channels and at the same time provide a correct

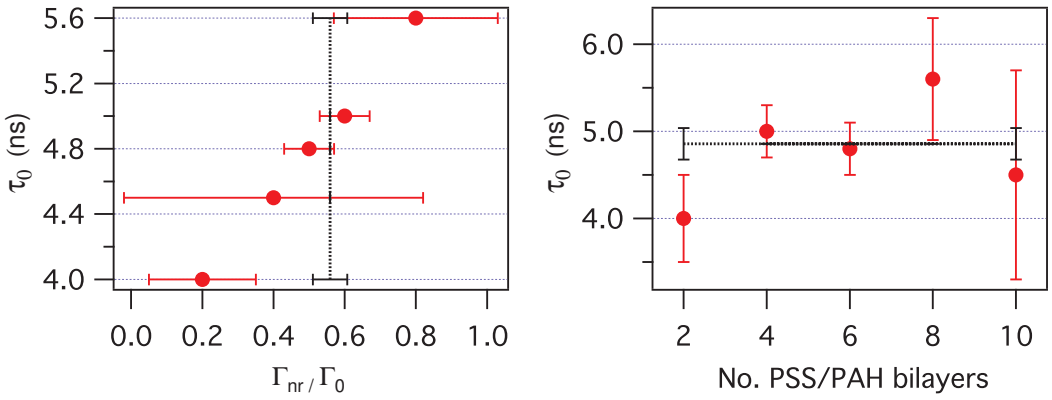

Figure 4.6.11: a) Value of vacuum lifetime τ_0, calculated according to eq. 4.6.15, for different values of $(\Gamma_{nr}/\Gamma_0)_{min}$ extracted by graphical fits in figure 4.6.9. Relative errors corresponding to the quantities σ_k in eq. 4.6.12 are also reported. The average $<(\Gamma_{nr}/\Gamma_0)_{min}>=0.56\pm0.05$ is indicated by a dotted line. b) Value of vacuum lifetime τ_0 calculated according to eq. 4.6.15 for different samples, by using $(\Gamma_{nr}/\Gamma_0)_{min}$ extracted by graphical fits in figure 4.6.9. The weighted average value $<\tau_0>=4.9\pm0.2$ ns is indicated by a line. Error bars are discussed in the text.

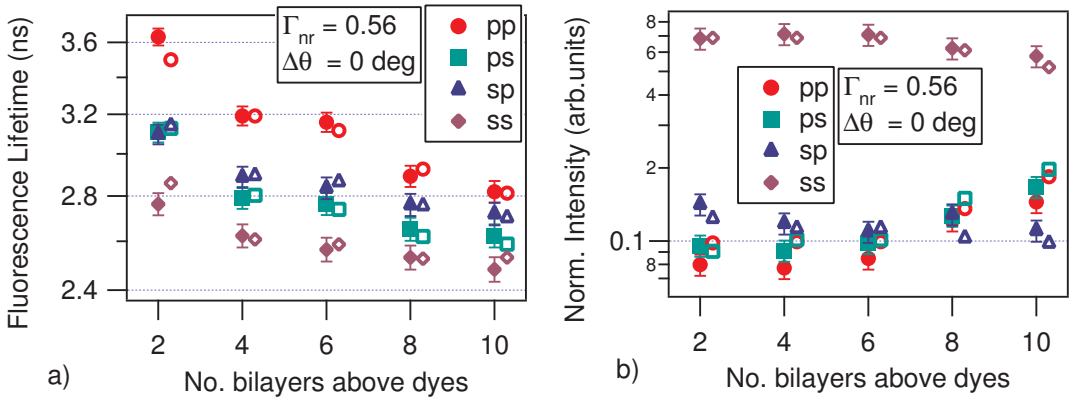

Figure 4.6.12: Comparison among calculated (empty markers) and experimental (full markers) fluorescence lifetimes values a) and intensities at time $t=0$ b). The data is for FR6363 dye covered by a different number of PSS/PAH polyelectrolytes bilayers (theoretical data are slightly shifted to the right *only* for clarity convenience). In the simulation $\triangle\vartheta=0\hat{A}^\circ$, $\Gamma_{nr}/\Gamma_0=0.56$ and $\tau_0=4.9$ ns were used for all the samples.

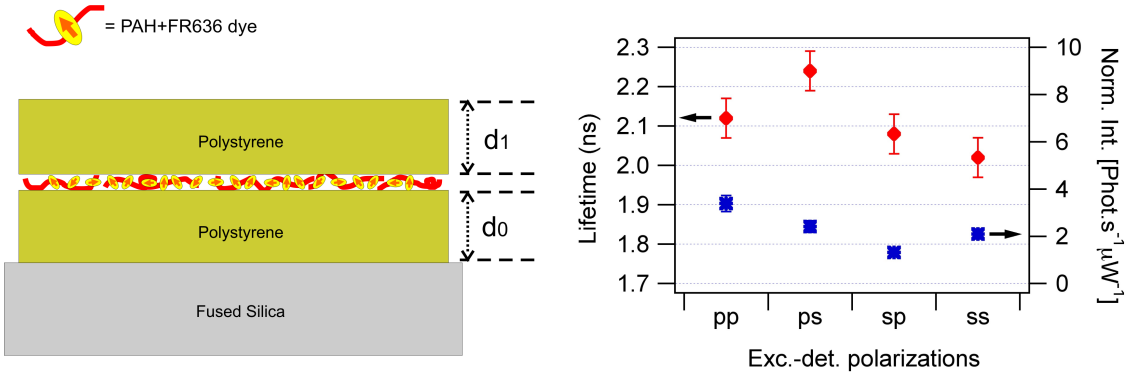

Figure 4.6.13: a) Sketch of sample with PAH polymer chains functionalized by FR636 red reactive dyes embedded in a polystyrene *sandwich*. The polystyrene slabs have thickness $d_0 \sim 1.7\,\mu$m and $d_1 \sim 1.9\,\mu$m. b) Relative fluorescence lifetimes and intensities for different excitation-detection polarization combinations.

value for τ_0. Figure 4.6.12 b) shows that the theoretical results reproduce well the measured fluorescence intensities. Differences up to $\approx 10\%$ are observed only for pp polarization: overestimation of experimental I_{0pp} could be related to an incorrect value of the polymer matrix refractive index used in the model. The presence of residual water molecules in the polymer film could slightly lower the refractive index value, thus decreasing the fluorescence intensity. The electric field component normal to the interface is the most sensitive to refractive index changes, as stated by equation 4.1.1. Other small deviations between theory and experiment in the intensities, could be explained considering the actual dipole distribution (i.e. dye molecule orientation inside the polymer). Due to the non fully symmetric structure of the chromophore and to the electrostatic interaction of the solubility groups (groups SO_3^- in figure 4.5.5) with PAH and PSS chains, the dipole distribution may not be uniform as assumed in the model.

4.6.4 Lifetime of dyes in an *infinite* medium

The value of the vacuum lifetime τ_0 obtained in section 4.6.3 can be verified by an independent experiment, where the PAH chains loaded by FR636 dye molecules are deeply embedded in the middle of a thick polystyrene film $\sim 3.6\,\mu$m (figure 4.6.13). In this way the PAH polymer chains preserve, for the dye molecules, the same sub-nanoenvironment of previous experiments with polyelectrolytes (i.e. the environment within the Lorentz-Onsager Sphere [22]). At the same time, they improve the adhesion of the second polystyrene layer spin coated above the chromophores.

Figure 4.6.13 a) shows a sketch for the PAH polymer chains functionalized by FR636 dyes embedded in a polystyrene sandwich. In figure 4.6.13 b) the relative experimental fluorescence lifetimes and intensities, for different excitation-detection polarization combinations, are reported. From figure 4.6.13, the lifetimes are similar (within the experimental error) for different excitation-detection polarization combinations. This indicates that the effect of the polymer-air interface is negligible and the dyes may be considered like embedded in an infinite homogenous dielectric medium, with a lifetime $\tau_{PS,exp} = 2.1 \pm 0.1$ ns. The slight lifetime difference for different polarization combinations is due to the presence of the fused silica substrate (see figure 4.6.14) while, an explanation for the anomalous deviation observed for *ps* polarization could not be found.

In general for dyes embedded in a homgeneous polystyrene matrix it is possible to write:

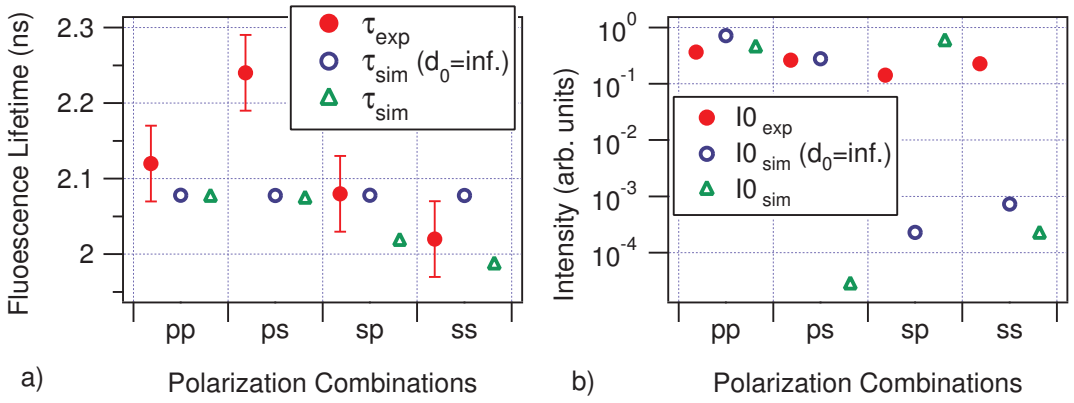

Figure 4.6.14: a) Comparison between simulated lifetimes for $d_0 = \infty$ (open circle) and $d_0 = 1.743\,\mu$m (open triangles), and experimental lifetimes (full circles) with d_0 as in figure 4.6.13. b) Comparison between simulated fluorescence intensities at time $t = 0$ with $d_0 = \infty$ (open circle), $d_0 = 1.743\,\mu$m (open triangles) and experimental values (full circles). In both cases the distance between dye molecules and polymer-air interface is $d_1 = 1.929\,\mu$m. The refractive index used is $n = 1.6$.

$$\Gamma_{tot,PS} = n \cdot \Gamma_0 + \Gamma_{nr} \tag{4.6.23}$$

where $n = 1.6$ is the refractive index of the polystyrene [26], Γ_0 is the vacuum decay rate of the dye and Γ_{nr} the non-radiative decay rate for the chromohores embedded in the polystyrene (which is unknown). Γ_{nr} can be roughly estimated from the non radiative values obtained for the dyes embedded in the polyelectrolytes matrix (section 4.6.2). In particular is possible to set $\Gamma_{nr}/\Gamma_0 = 0.8$, as obtained for the sample with 8 PSS/PAH bilayers above the dye (table 4.6.1). For this specific sample, it is believed that residual water trapped in the polyelectrolytes film was the cause of such higher non-radiative decay rate. In the same way, it is believed that residual solvent is present in the polystyrene film. By using equation 4.6.23:

$$\Gamma_{tot,PS} = n \cdot \frac{1}{\tau_0} + \left(\frac{\Gamma_{nr}}{\Gamma_0}\right) \cdot \Gamma_0 = 1.6 \cdot \frac{1}{4.9} + 0.8 \cdot \frac{1}{4.9} = 0.49 \pm 0.03\,\text{ns}^{-1} \tag{4.6.24}$$

and consequently

$$\tau_{PS,sim} = \frac{1}{\Gamma_{tot,PS}} = 2.04 \pm 0.15\,\text{ns} \tag{4.6.25}$$

where the errors were determined by propagation law. From equation 4.6.25, it is possible to observe a good agreement with the experimental data in figure 4.6.13.

Figure 4.6.14 a) shows the comparison, for different polarization combinations, between simulated lifetimes with $d_0 = \infty$ and $d_0 = 1.743\,\mu$m and the experimental lifetimes. There d_0 is the distance of the chromophores from the fused silica substrate (figure 4.6.13). It is possible to notice that the presence of the glass cover slip still has a slight effect on the fluorescence lifetimes as a function of the excitation-detection polarization combinations. On the other hand, a clear explanation for the experimental value of τ_{ps} was not found. The lifetimes comparison is the key point of this experiment for chromophores embedded in a polystyrene matrix. The self consistency of the model was proved

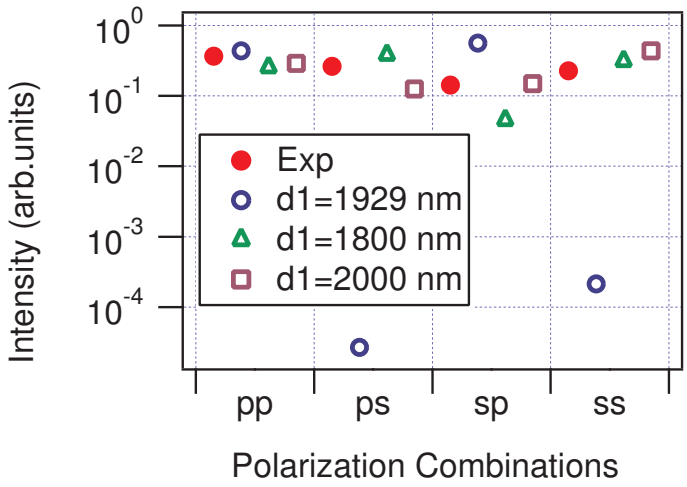

Figure 4.6.15: Comparison berween experimental fluorecence intensities (Exp) and theoretical values calculated for several d_1 values, $d_0 = 1.743\,\mu m$ and different excitation-detection polarization combinations. The data are for PAH chains functionalized by FR636 dye, embedded in a polystyrene matrix (for a sample sketch see figure 4.6.13).

by the result obtained in the expression 4.6.25. Nevertheless, in the following, a short analysis for fluorescence intensities is also reported, for completeness.

Figure 4.6.14 b) shows the comparison between simulated intensities (at time $t = 0$) with $d_0 = \infty$ and $d_0 = 1.743\,\mu$m, and experimental values. In both cases a large discrepancy between theoretical and measured values is observed. Nevertheless, considering the actual sample structure with the presence of the glass cover slip, and therefore $d_0 = 1.743\,\mu$m, the mismatch is found only for the *s* polarization in detection. Moreover, due to the structure of the multilayer, simulation of the experiment involves polymer layers with thickness of the same order of magnitude of the excitation wavelength. As a consequence, the interference effects may play a relevant role: *s* polarized plane waves, reflected at the polymer-air interface, may interfere generating spacial patterns with minima. To verify such hypothesis, theoretical values for fluorescence intensities have been calculated for slightly different values of d_1 (distance of the dyes from the air-polymer interface). Figure 4.6.15 shows the comparison among experimental and simulated intensities, where the theoretical values are for different film thicknesses (d_1) for the polystyrene layer covering the dye molecules. Measured and calculated intensities in figure 4.6.15 have been normalized to the corresponding sums of intensities for different polarization combinations (see equations 4.6.21 and 4.6.22). Figure 4.6.15 shows dramatic changes in the emitted radiation for slight variations of the value of d_1, as a function of distinct excitation-detection polarization combinations. This indicates the presence of an interference minimum around $d_1 \sim 1.9\,\mu$m, as it was suspected. There an experimental error on d_1 of ± 250nm it was considered, due to its indirect measurements from the difference between the total polystyrene film thickness ($d_0 + d_1$) and the first slab thickness (d_0). In such a way, the exact position of the dye molecules is unknown in a range of several hundreds of nanometers. Experimental values indicate a real value of d_1 much closer to $2\,\mu$m, away from the interference minimum.

4.7 Conclusions

A new optical investigation technique was introduced: the Polarization Combination Method (PCM). The method relies on the polarized fluorescence measurements for an ensemble of dye molecules at defined distance from an interface between two dielectric media. Dye molecules are modeled as classical electrical non-interacting point-like dipoles. Applying such method to organic dye molecules embedded in a PSS/PAH polyelectrolytes matrix, it was possible to determine the model free parameters: the non-radiative decay rate Γ_{nr}, the vacuum decay rate Γ_0 and the relative angle $\Delta\theta$ between the excitation and emission dipoles.

By making use of the PCM, the validity of a classical physics approach was tested down to dye-interface separation of a few nanometers range. A few layers of polyelectrolytes ($\sim 8\,\text{nm}$) are sufficient for the dye molecule to behave as predicted by point-like dipoles, embedded in a medium which is described by its refractive index.

As a drawback, the PCM requires a well defined geometry down to the nanometer scale and impurities-free samples to extract useful information from the comparison between simulation and experimental data. On the lenght-scale of few nanometers, the chromophores size, the interface roughness and the exact position of molecules may play a role in determining the non-radiative decay channels, thus limiting the accuracy of the analysis.

Bibliography

[1] Drexhage, K. H., *Prog. Optics*, **12**, 165 (1974).

[2] Kuhn, H., *J. Chem. Phys.*, **53**, 101 (1970).

[3] Lukosz W. and Kunz R. E., *J. Opt. Soc. Am.*, Vol. **67**, No. 12, December 1977, pagg. 1607-1615 and *J. Opt. Soc. Am.*, Vol. **67**, No. 12, December 1977 pagg.1615-1619.

[4] Lukosz, *J. Opt. Soc. Am.*, Vol. **69**, No. 11, November 1979.

[5] Chance, R. R., Prock A. and Silbey R., *Adv. Chem. Phys.*, **37**, 1 (1978).

[6] Yeung, M. S., and Gustafson, T. K., *Phys. Rev. A*, **54**, (1996).

[7] Kreiter M. et al., *J. Chem. Phys.*, vol. 117, **20**, (2002).

[8] J. J. Macklin, J. K. Trautman, T. D. Harris, and L. E. Brus, *Science* 272, 255 (1996).

[9] Brokmann X. et al., *Phy. Rev. Lett.*, vol. 93, **10**, 107403-1, (2004).

[10] W. J. Zhu, T. Song J.Q., Liu Z.F. *Thin Solid Films,* **327**, 591 (1998).

[11] M.C. Alvarez, private communication.

[12] Schmitt, J.; Grunewald, T.; Decher, G.; Pershan, P. S.; Kjaer, K.; Losche, M. *Macromolecules* 1993, **26**, 7058.

[13] Y. Lvov et al., *Langmuir*, **9**, 481-486 (1993).

[14] Choi J. and M.F. Rubner, *Macromolecules*, vol. **38**, No.1, (2005).

[15] Valeur B., *Molecular Fluorescence,* WILEY-VCH Verlag GmbH (2002).

[16] E. M. Purcell, *Phys. Rev.,* **69**, 681 (1946).

[17] Barnes W.L., *J. Mod. Opt.*, vol. **45**, no. 4, 661-699 (1998).

[18] Herzberg G., *Spectra of Diatomic Molecules, Vol.1, 2nd ed.; Krieger Publishing Co., (1989).*

[19] Khosravi H. and Loudon R., *Proc.:Math. and Phys. Science*, vol.433, issue 1888, 337-352 (1991).

[20] T. Farhat et al., *Langmuir*, 15, 6621-6623, (1999).

[21] Loesche et al. Macromolecules, Vol. 31, No. **25**, 8893 (1998).

[22] Dmitri Toptygin, *Journal of Fluorescence*, Vol. 13, No. 3, May 2003 (2003).

[23] Novotny L., Hecht B., *Principles of Nano-Optics*, Cambridge Univ. Press (2006).

[24] Potton R.J., *Rep. Prog. Phys.* **67** (2004) 717â€“754.

[25] *The bh TCSPC Handbook*, Becker & Hickl GmbH, http://www.becker-hickl.de/literature.htm

[26] http://www.polysciences.com/shop/product.asp?pf%5Fid=18544&dept%5Fid=300147

Chapter 5

Fluorescence of Organic Dyes at Dielectric Surfaces

Abstract

The fluorescence characteristics of organic dyes very close to dielectric surfaces are analyzed by using the Polarization Combination Method in the simulation of the experiments. Excited state lifetimes and fluorescence intensities of several organic dyes onto different substrates architectures were studied, in order to investigate microscopic electromagnetic phenomena at the interface. All dye molecules used exhibited clusters formation in most of the solvents utilized, down to a concentration of 10^{-7} M. Free chromophores ($\approx 2-3$ nm size) on thin polyelectrolyte films (≈ 6 nm) showed the same fluorescence characteristics as when embedded in a polymer matrix, indicating diffusion. The same results are obtained for a spacer constituted by 1 monolayer of PSS, deposited onto a fused silica substrate functionalized with 3-APTE silane. This shows that one polyelectrolyte monolayer is sufficient to define the optical environment surrounding the chromophores. To achieve better control over the emitters position and higher intensities without aggregation, organic dyes were chemically bound to PAH chains. When functionalized chains were deposited in a train-like conformation, on top of the polyelectrolyte spacer, the fluorescence had the characteristics of emitters embedded in a polymer matrix. Surface deposition in a loop-like conformation showed an intermediate behaviour between emitters embedded in polymer and on top of the surface (in air).

For all the organic dyes investigated onto a ≈ 6 nm polyelectrolyte spacer, a good agreement between theory and experiment was achieved, when considering the dyes in the polymer matrix at a distance of $\approx 2-3$ nm from the air-polymer interface. The validity of our model based on classical electromagnetism without any local field correction was shown for these samples. For chromophores covalently bound to polyelectrolytes and deposited onto negatively charged silanes, discrepancies were found between theory and experiment. Possible sensing applications for qualitative investigations of interface properties are suggested.

5.1 Introduction

Fluorescence lifetime studies of dyes embedded in a dielectric matrix have been extensively utilized to investigate segmental dynamics in polymers [1], conformational effects [2] and local density fluctuations [3]. Some theoretical [4] and experimental work [5] was also carried out to analyze dye-polymer

interactions and the contribution of local field effects on them. In these studies single molecule spectroscopy of fluorescent dyes was used to analyze lifetime fluctuations as function of the time, with all inevitable statistic limitations. Organic dyes can be modeled as electric dipoles and single molecules polarized fluorescence studies provided information on the molecules orientation with respect to an interface [9, 10]. For the cited works above, the samples were constituted generally by a blend of organic dyes and polymer, which was spin coated on a glass substrate, achieving film thicknesses of $\sim 20-200\,\mathrm{nm}$. By this technique little or no control is reached on dyes position within the polymer matrix and in general annealing procedures are necessary for stress and solvent removal, also for thinner films [6]. Finally, dye aggregation may be one of the main issues to be solved in sample preparation, in order to obtain reliable measurements [7]. In spite of the large amount of work done no experimental data is available for local electric fields in proximity of a dielectric interface, in the few nanometers range. Moreover macroscopic derivations of local field corrections imply the use of a cavity around the radiating atom/molecule and the specific choice of the cavity represents a subtle issue [8]. In this respect, the experimental study of molecular fluorescence near a medium discontinuity may provide insights in the cavity definition.

In the following work the PCM is applied to study organic dyes which are placed as close as possible to a polymer surface. Samples were prepared by very thin ($\approx 6\,\mathrm{nm}$) PSS/PAH polyelectrolytes layers [39] deposited onto glass cover slips or on top of functionalized glass substrates. Organic dyes were successively added on top. In general, the layer-by-layer technique guarantees an accurate thickness control down to few nanometers [13], low stress films ($\approx 3\,\mathrm{N/m}$ [14], against $\approx 10-30\,\mathrm{N/m}$ of polystyrene spin coated films [15]) and no necessity for annealing steps. Polyelectrolytes constitute also a flexible tool for different substrate architectures and layer thickness can be changed by varying deposition solution pH [31, 34] and salt concentration [21], in terms of amount and conformation [17]. On the other hand, polyelectrolyte films show an interface roughness of $\approx 2\,\mathrm{nm}$ [30] and they may be permeable to chromophore diffusion [18]. To overcome some of these issues a polymer functionalization process by a specific dye molecule was set, allowing a better control on dyes position.

In section 5.2, theoretical fluorescence lifetimes and intensities for an ensemble of chromophores in proximity of a dielectric interface are discussed. In 5.3, in order to obtain reliable fluorescence measurements, the main requirements for a "good" sample are described. In the sections 5.4 and 5.5, two different organic dyes are studied, with a focus on the samples preparation challenges and on the limitations by using free dyes. In order to overcome such limitations and explore other substrate architectures, in section 5.6 a process to functionalize polyelectrolyte PAH chains is introduced. Successively the measured fluorescence is analyzed for the dye loaded polymer deposited on top of different substrates.

5.2 In Air versus in Polymer Behaviour

At a charged interface between two dielectric media, the parallel component of the electric field is preserved, while the normal component undergoes a discontinuity depending on the refractive index ratio [19]. Organic dye molecules can be placed in proximity of the interface as local electric field probes and the emitted fluorescence can be studied to investigate microscopic electromagnetic effects. In detail, the fluorescence intensity and the excited state lifetime can be measured across the interface and in principle the predicted discontinuity verified experimentally. More generally it is possible to investigate the local field effects and verify the validity of the classical approach used, down to the nanometer range. In a simplified description, the dyes are modeled as non-interacting, point-like, identical electric dipoles, placed within a multilayer system at the same distance from an interface.

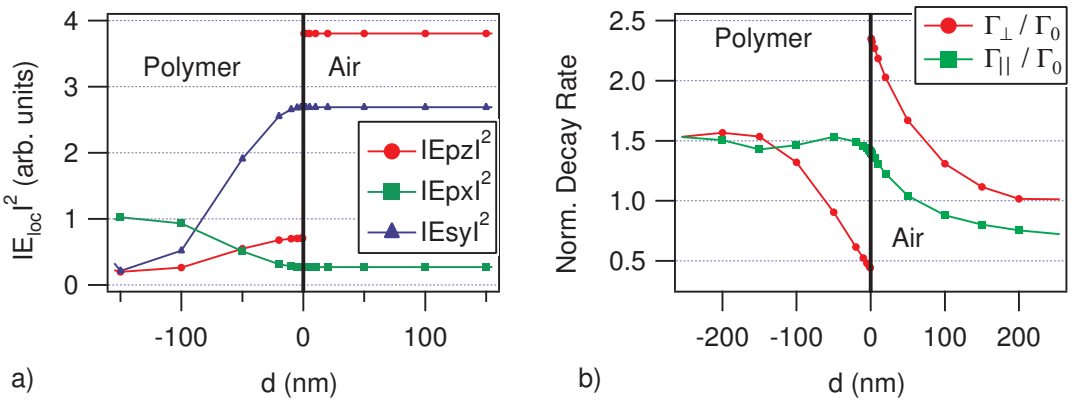

Figure 5.2.1: a) Moduli of Cartesian components for excitation electric field, as a function of the distance from the interface between two semi-infinite dielectric media: air (n = 1) and polymer (n = 1.53). The interface coincides with the plane (x,y), while the subscripts "p" and "s" in the legend indicate TM and TE excitation. b) Decay rates normalized to the in vacuum value (Γ_0), for a dipole normal ($\Gamma_\perp$) and parallel ($\Gamma_\parallel$) to the interface, as a function of the dipole distance from the interface. Excitation source and detection are in the polymer half-space at $\theta = 39.37\hat{A}°$ and $\theta = -50.63\hat{A}°$ (compare figure 4.2.2).

For such dipoles it is possible to calculate the excited state lifetime and the emitted radiation intensity (see chapter 3).

In figure 5.2.1 a) the local excitation field is plotted as a function of the distance from the interface between two semi-infinite dielectric media. The system geometry is described in the caption. The moduli of the Cartesian components are reported for TM ("p") and TE ("s") excitation mode. The interface coincides with the (x,y) plane and it is possible to notice the discontinuity of the perpendicular component of the electric field ($|\,E_{pz}\,|^2$).

Figure 5.2.1 b) shows the normalized decay rates for a dipole perpendicular ($\Gamma_\perp/\Gamma_0$) and parallel ($\Gamma_\parallel/\Gamma_0$) to the interface, as a function of the dipole distance from the interface. As a consequence of the "jump" in the electric field component normal to the interface, also the decay rate $\Gamma_\perp$ undergoes a discontinuity from a medium to the other. For an ensemble of dipoles, the total emitted radiation can be expressed as the sum of radiation from each emitting dipole and the associated fluorescence decay curve can be represented by a function like:

$$D_e(t) \propto \sum_k A_k \cdot e^{-t/\tau_k} \tag{5.2.1}$$

The coefficients A_k take into account different values of excitation efficiency, detection efficiency and radiation quantum yield for each single molecule[1]. As a consequence of equation 5.2.1, the decay curve is not a single exponential function. Nevertheless, by theoretical simulations (see chapter 3), it turns out that for emission from perpendicular and parallel dipoles (with respect to the interface), the difference in decay curves slope is about a factor ≈ 2. This difference can not be resolved experimentally and the equation 5.2.1 is well approximated by a single exponential function. For the whole ensemble, therefore, it is possible to define a single fluorescence lifetime and a single intensity value. Hence, for different excitation-detection polarization combinations ($\sigma\delta = pp, ps, sp, ss$):

$$D_e^{\sigma\delta}(t) \propto I_0^{\sigma\delta} \cdot e^{-t/\tau_{\sigma\delta}} \tag{5.2.2}$$

[1]More details on theoretical calculations are given in chapter 3

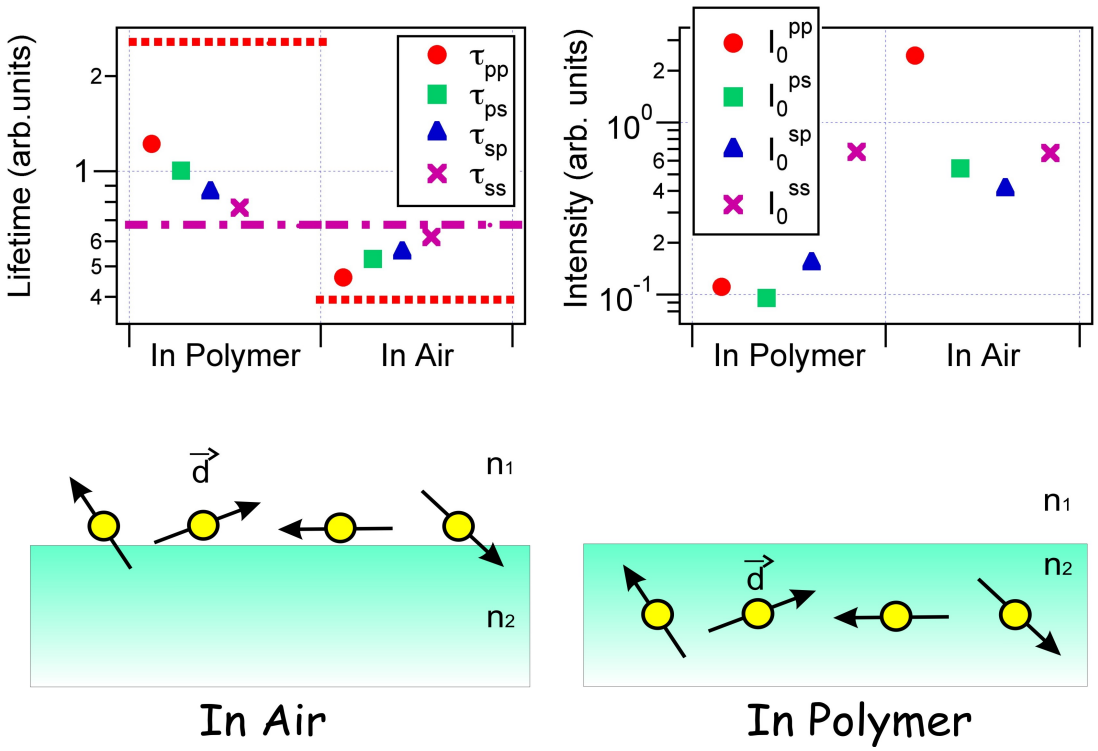

Figure 5.2.2: Simulated fluorescence lifetimes ($\tau_{\sigma\delta}$) and intensities at time $t = 0$ ($I_0^{\sigma\delta}$), for an ensemble of 900 dye molecules at the interface between two semi-infinite media: air ($n_1 = 1$) and polystyrene ($n_2 = 1.6$). Two limiting situations are sketched: all dipoles (dyes) are in the air side ("In Air") or embedded in the polymer matrix ("In Polymer"), in proximity of the interface. Fluorescence lifetime values for the limiting cases of a dipole perpendicular (dotted lines) and parallel (dashed lines) with respect to the interface are shown.

In equation 5.2.2, $\tau_{\sigma\delta}$ is the averaged lifetime of the ensemble and $I_0^{\sigma\delta}$ represents the fluorescence intensity at time $t = 0$. By fitting the decay curve in equation 5.2.2, the averaged value for the lifetime of the ensemble is obtained, while the evaluation of $D_e(0)$ will provide information about the global excitation-detection process over many molecules.

In figure 4.2.6 (chapter 4), the fitted fluorescence lifetimes ($\tau_{\sigma\delta}$) and intensities ($I_0^{\sigma\delta}$) are reported for different polarization combinations, for the case that all the chromophores of an ensemble are either in air or in polymer. For convenience, the results are shown again in figure 5.2.2, together with the limiting cases for the perpendicular (dotted line) and parallel (dashed line) single dipole with respect to the interface.

From figure 5.2.2 it is possible to notice that for an ensemble of dipoles "in air": $\tau_{pp} < \tau_{ss}$ and $I_0^{pp} > I_0^{ss}$. For dipoles "in polymer" the opposite relations are valid, with mixed polarization combinations (*ps* and *sp*) assuming always intermediate values. These inequalities, like the differences with the "in polymer" case, are the consequence of different local electric field values for different components, as shown in figure 5.2.1 a). On the other hand, the differences with respect to the single dipole situation are due to the averaging process over the excitation and emission dipoles directions, in case of many dipoles.

The characteristic ratios for the lifetime and the intensities for either "in air" and "in polymer" cases depend on the refractive indices. Nevertheless finite size dye molecules and real interfaces have to

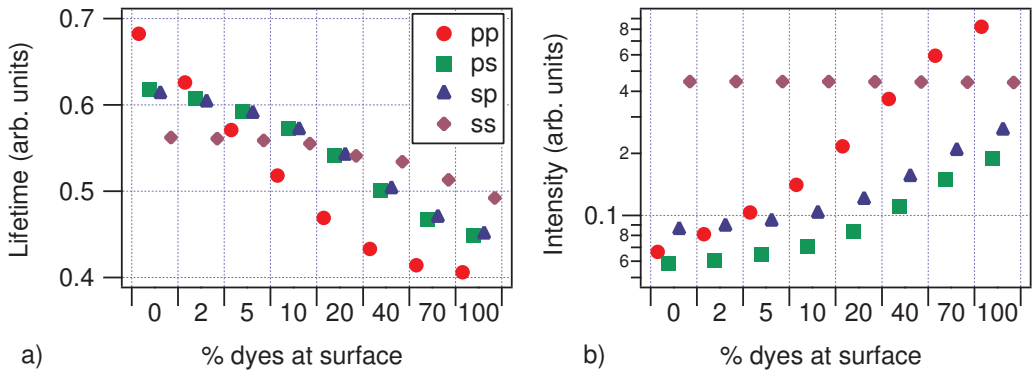

Figure 5.2.3: a) Simulated fluorescence lifetimes ($\tau_{\sigma\delta}$) and b) intensities ($I_0^{\sigma\delta}$), for an ensemble of 900 dipoles for different excitation-detection polarization combinations. The values are plotted as a function of the percentage of the dipoles at surface (in the air side, $\varepsilon = 1$), with respect to the amount embedded in the PSS/PAH matrix ($\varepsilon = 2.319$ at $\lambda = 633\,\text{nm}$). For simulation in either side, the dipoles were placed at 0.5 nm from the interface. In the simulation, the emitter parameters $\Delta\theta, \Gamma_{nr}$ and Γ_0 were taken as determined by the Polarization Combination Method (see chapter 4).

be considered. Hence, surface roughness and porosity may bring to possible chromophores diffusion and dipole position indetermination. In this respect, for an ensemble of dipoles at interface, an approximate picture of the real physical situation can be given allowing different amount of dyes to be in either side. Then the fluorescence radiation coming from the two regions can be summed. The theoretical fluorescence lifetimes and intensities of an ensemble of dyes in proximity of a polymer-air interface are reported in figure 5.2.3 a) and b), respectively. Data is for different excitation-detection polarization combinations. The values are expressed as a function of different percentages of emitters at surface (in the air side), with respect to the total number of dyes. For example 0% means all the chromophores are embedded in the PSS/PAH polymer matrix, 2% of dyes at surface means that the left 98% are within the polymer side and so on. The values in figures 5.2.3 are obtained by fitting the theoretical decay curves $D_e^{\sigma\delta}(t)$ in equation 5.2.2, calculated for an ensemble of 900 dipoles. In the simulation, the emitter parameters $\Delta\theta, \Gamma_{nr}$ and Γ_0 were taken as determined by the Polarization Combination Method (see chapter 4).

Figure 5.2.3 shows a smooth transition from an "in polymer" behaviour (0% of dyes in air) to the 100% "in air" behaviour (at surface), for all polarization combinations. In the polymer, the dipoles normal to the dielectric interface have greater lifetimes than the parallel dipoles ($\tau_{pp} > \tau_{ss}$). In air the opposite behaviour can be noticed ($\tau_{pp} < \tau_{ss}$), as indicated in figure 5.2.3 a). Also dipoles randomly oriented contribute to the values τ_{pp} and τ_{ss}, by their vector components perpendicular and parallel to the interface. The largest lifetime variation occurs for the *pp* polarization combination, due to the discontinuity of the electric field component normal to the interface. Whereas τ_{ss} has a slight change caused by the average process over the ensemble, i.e. the contributions from different dipole orientations are present. The simulated values for fluorescence intensities ($I_0^{\sigma\delta}$) are plotted in figure 5.2.3 b). Also here, according to the boundary conditions of the elctromagnetic field, the *pp* polarization undergoes a large change and in the medium with lower refractive index a higher intensity is obtained. On the other hand, the parallel component does not show any variation. As for the lifetimes, *ps* and *sp* polarization combinations represent dipoles not perpendicular or parallel and the change is driven from the *p* component (in excitation or detection). In figure 5.2.3 a) and b), for each percentage of dyes at surface, there is a determined ratio among different polarizations combinations. From a comparison with experiments, it is possible therefore to establish what kind of surrounding

the dye molecules experience or the percentage of dyes in polymer for a specific sample architecture. This may represent a useful tool for a successive quantitative analysis and possible applications will be discussed at the end of the chapter. A comparison between the classical model utilized for the simulation and the experimental results from a dyes ensemble may provide also a test about the validity of the model and some insights about the local electromagnetic field.

5.3 The quest for a good sample

The analysis of fluorescence in proximity to dielectric interfaces requests a good control over the organic dyes position, well defined sample architectures and a reliable fluorescence signal. On the other hand, the chromophores should be single entities on the surface (no clusters formation), to avoid static self-quenching [20]. As a consequence, a minimum distance among the dye molecules onto the sample is required. In this manner, fluorescence quenching effects are avoided and the organic dyes can be modeled as distinct point-like electric dipoles. Finally, the emitter should not be affected by photobleaching for the utilized excitation intensities.

5.3.1 How to recognize a good sample?

Intensity issue

To achieve control over dyes position, the samples surface should show roughness on the sub-nanometer range and be impermeable to dyes diffusion. Flat and compact substrates like glass or silica present ideal characteristics, but in general a surface functionalization is necessary to obtain sufficient dyes or polymer adsorption. The reference for a reliable fluorescence signal is set evaluating the background by the same setup configuration used for sample measurements. Then for each polarization combination, the photons are recorded by using a bare fused silica slide as a sample. A quantitative estimation for the minimum signal-background (S/B) ratio is not straightforward: the background is polarization dependent, while the S/B ratio is a function of time lag between a fluorescence photon and the excitation pulse (Micro Time). Fluorescence intensities ($I_0^{\sigma\delta}$, see section 5.2) are evaluated by a fit at time $t_0 = 3.8\,\text{ns}$, in the Micro Time scale: that is the estimated time of the "delta-like" excitation peak (see also chapter 2). On the other hand, to avoid eventual contribution of scattered light and make the fit more reliable, the data interval for the fit was chosen to begin at $t_b = 4.5\,\text{ns}$. A possible method to estimate a minimum signal-background ratio could be to calculate $\text{S}/\text{B}(t = t_b)$. Then the decay curves that (at this time) are at least ~ 5 times higher than background can be considered reliable[2].

In figure 5.3.1, a comparison between a reliable decay curve (a) and a critical one (c) is shown. The relative S/B ratios as a function of the Micro Time are plotted in b) and d), respectively.

The vertical dashed lines indicate $t_b = 4.5\,\text{ns}$: the beginning of the fit interval. At this time a value of $\text{S}/\text{B} \approx 20$ is obtained, for the reliable fluorescence signal in b). On the other side, the signal to background ratio is $\text{S}/\text{B} \approx 4$, for the decay curve with lower intensity, in c). It is believed in this last case the background may affect the fit results, therefore only samples providing $\text{S}/\text{B}(t_b) \gtrsim 5$ will be considered reliable for fits.

[2]The factor $\text{S}/\text{B}(t_b) \approx 5$ was arbitrarily chosen as minimum to achieve reliable measurements, after inspection of several experimental decay curves.

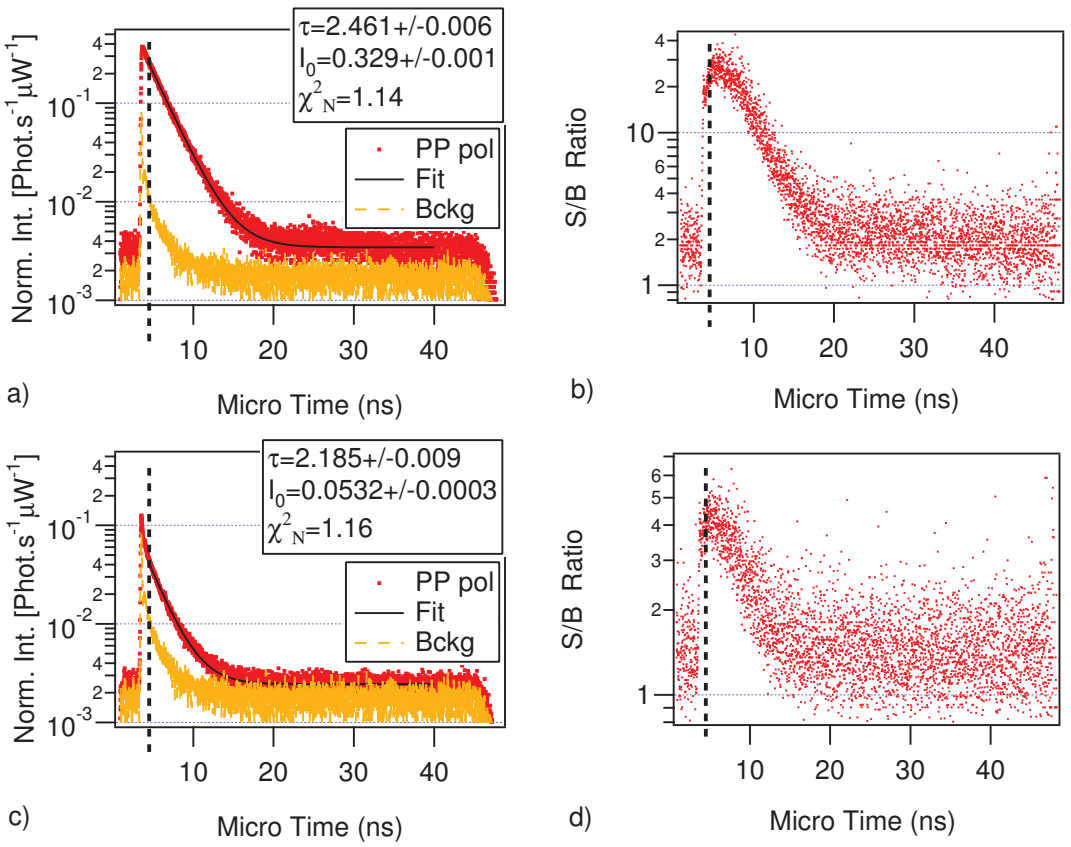

Figure 5.3.1: a) and c): fluorescence decay curves with fit and background (Bckg), for *pp* polarization combination. b) and d): signal-background ratios, respectively for a) and c). With vertical dashed lines the beginning of the fit interval is indicated, at $t_b = 4.5\,\text{ns}$. In the legends, the fit parameters are reported: excited-state lifetime (τ, in ns), intensities (I_0, in phot./$(\text{s}\cdot\mu\text{W})$) and χ^2_N values.

Dyes aggregation

Another essential characteristic for a good sample is the absence of dye aggregates: direct experimental evidence for single dyes on the substrate is not possible by far field techniques and indirect measurements are necessary. Cluster formation of organic dyes causes fluorescence self-quenching [20] and a reduction of lifetime. In detail, the relative fluorescence decay curve is no longer a single exponential and a faster decay is observed for short time after the excitation pulse [20]. On the other hand, no clear indications can be given about an absolute value for the expected lifetime. The exact dyes position across the interface in fact can not be known down to the sub-nanometer range and the surrounding environment may be not well defined. As an example, two fluorescence decay curves showing multi-exponential and single exponential characters are reported in figure 5.3.2 a) and b), respectively. The experimental data are for $\mathrm{DiIC}_1(5)$, deposited onto PSS/PAH polyelectrolyte substrates from two different concentrations of an aqueous solution. By a deposition solution with a concentration of 10^{-3} M, a multi-exponential curve with shorter excited-state lifetime is obtained, showing clusters formation. For much lower concentrations, in figure 5.3.2 b), the decay curve is approximately single exponential, as it is possible to notice from the fit and the associated χ^2_N value. The deviation from 1 is mainly due to the deviation of the fit from data in the background region (Micro Time $\gtrsim 20$ ns): i.e. if the fit is performed up to ~ 20 ns then a value of $\chi^2_N \simeq 1.16$ is obtained. The little bump seen in 5.3.2 a) and b) around ~ 25 ns is due to scattered light and it is present also in the background.

In figure 5.3.2 c) three calculated functions are plotted in logarithmic scale to show the difference between a single exponential curve (SE) and a multi exponential decay. There the multiexponential curves are plotted with 3 (ME3) or 5 (ME5) different decay constants.

The aggregation of fluorophores may occur in solution before deposition step or directly on the sample substrate: in order to identify the eventual presence of clusters, a study of the excited-state lifetime (τ) as function of the dyes concentration should be performed. In this way a suitable concentration value (i.e. c^*) may be found, below which no fluorescence quenching is detected. For higher concentration values than c^*, the detected decay curve should be multiexponential and the fitted τ small (with respect to the non-quenched value). Lowering the dye concentration, the multiexponential character of the decay curve should diminish and the fitted lifetime increases. Once the concentration is less than c^*, mostly non-interacting single dyes are present on the sample surface and the value of τ hits its maximum value and remains constant. In general, c^* is unknown and its value may be far beyond the fluorescence detection limit, for far field measurements and most of the organic dyes and solvents utilized. Anyway, during the dyes deposition, some process variables may be varied to maximize the fluorescence lifetime value and to work as close as possible to the c^* concentration. A possible alternative can be obtained by minimizing the χ^2_N values ($\chi^2_N \to 1$): in this manner a single exponential character of the decay curve is searched, within the range of accessible concentrations. Also here it is not possible to set a tight limit for χ^2_N values, due to the deviation in the curves tail (background, scattered lights, afterpulsing. See comments to figure 5.3.2). Strong deviation from single exponential behaviour (linear trend in log scale) can be detected also graphically by eye: this method will be used for quick checks in optimizing the sample preparation process. In summary for a good sample, it will be required:

- signal to background ratio $\mathrm{S/B}(t_b) \gtrsim 5$, where t_b is the lower limit of the fit interval.
- Single exponential fluorescence decay curve: $\chi^2_N \to 1$ (as close as possible).
- Maximization of excited-state lifetime (τ).

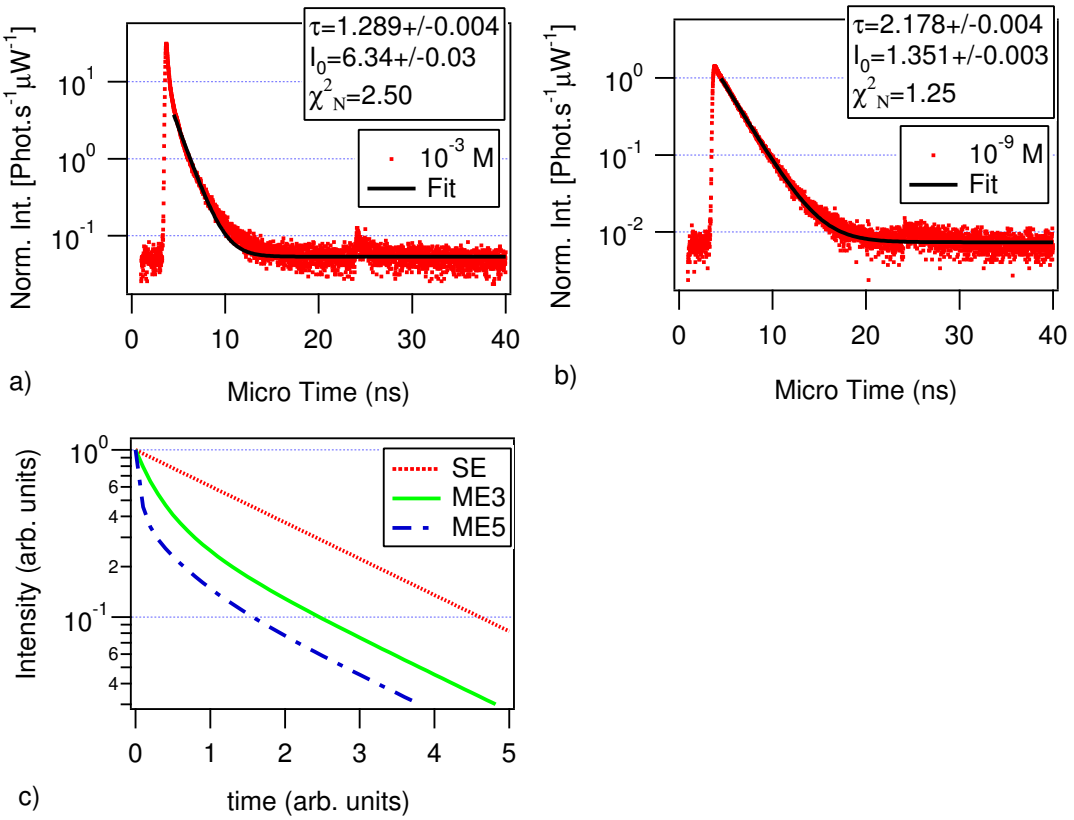

Figure 5.3.2: Experimental fluorescence decay curves of $DiIC_1(5)$ dye, deposited onto a PSS/PAH polyelectrolyte substrate from two different concentrations of aqueous solution: (a) 10^{-3} M and (b) 10^{-9} M. The measurements are for *ss* polarization combination. Sample in a) was prepared by dipping, while a flow cell was used for b). In the legends, the fit parameters are reported: excited-state lifetime (τ, in ns), intensities (I_0, in phot./$(s \cdot \mu W)$) and χ^2_N values. c) Calculated curves for: (SE) single exponential function with decay time of $\tau = 2$; (ME3) multi-exponential function with $\tau_1 = 2, \tau_2 = 0.5, \tau_3 = 0.2$; (ME5) multi-exponential function with $\tau_1 = 2, \tau_2 = 0.5, \tau_3 = 0.1, \tau_4 = 0.05$ and $\tau_5 = 0.02$. All decay constants are expressed in arbitrary units.

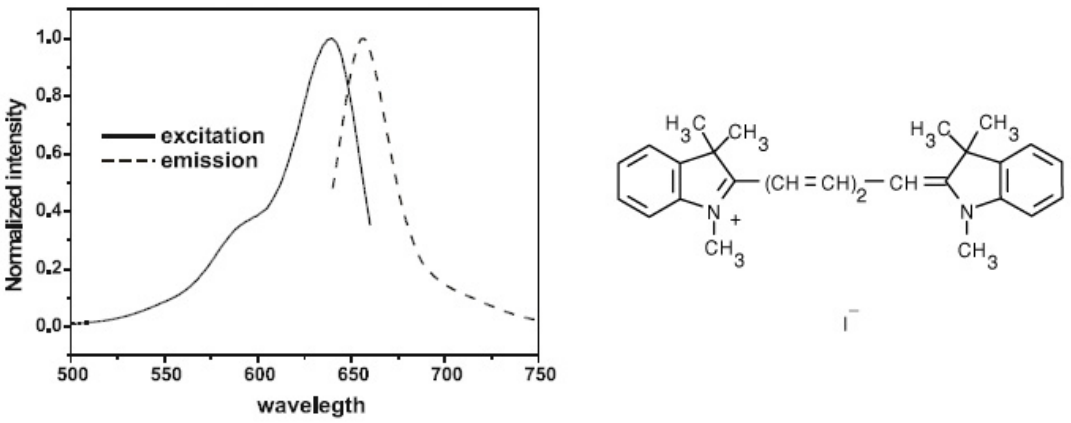

Figure 5.4.1: Fluorescence spectra of $DiIC_1(5)$ (from [12]) and its chromophore structure. The organic dye molecular formula is $C_{27}H_{31}IN_2$, while the molecular weight is 510.46.

In the following work, to achieve such requirements, several organic dyes, different substrate architectures, surface treatments and dye deposition protocols will be tested.

5.4 $DiIC_1(5)$

Figure 5.4.1 depicts the molecular structure of $DiIC_1(5)$ (1,1",3,3,3",3" - Hexamethylindodicarbocyanine iodide, Molecular Probe, Invitrogen Inc., prod. no. H14700). This is an organic dye having maximum excitation at $\lambda_{ex} = 638\,\text{nm}$ and fluorescence emission maximum at $\lambda_{em} = 670\,\text{nm}$ [12].

5.4.1 Sample Preparation

Glass surface treatment

UV-grade fused silica slides, both sides optically polished, with dimensions 25 mm x 25 mm x 1 mm (PGO GmbH) have been cleaned by a 2% detergent solution (Hellmanex - Hellma GmbH) in an ultrasound bath for 15 minutes and rinsed 20 times by ultrapure water (MilliQ resistivity, $18.2\,\text{M}\Omega\cdot$ cm). The cleaning process was applied two times. After successive rinsing by ethanol (Fischer Scientific) the slides were subsequently dryed by a N_2 flow and immersed in a bath of $H_2O_2 : NH_3 : H_2O$ (10 ml : 10 ml : 50 ml). An NH_3 solution of 32% and a H_2O_2 solution of 34% have been used. The slides were left in the solution for 45 minutes at 80Â°C. After 20 times rinsing with ultra pure H_2O and ethanol, the slides were dried by a N_2 flow and put in a closed flask (1000 ml volume) with 0.5 ml of (3-Aminopropyl)-triethoxysilane (3-APTES, CAS: 919-30-2, Sigma Aldrich Inc.). The closed flask was then put in an oven, under vacuum, at 130Â°C for 3 hours [24]. After the cooling-off period, the slides were rinsed two times with ethanol to remove possible silane aggregates from the surface and rinsed additionally 20 times with ultra pure water. The substrates were at the end dried by N_2 and used as first charged layer for polyelectrolyte deposition.

Polyelectrolyte deposition

The 3-APTE silanes provide a positively charged surface, covering the glass slide in a fairly uniform manner [25]. Hence to have a more uniform fully charged surface, a polymer spacer above the glass was used. The spacer was constituted by 2.5 bilayers of PSS/PAH [poly(styrene sulfonate) / poly(allylamine hydrochloride)], terminated by PSS. To prepare the PSS solution, 50 ml of ultrapure water (resistivity of $18.2\,M\Omega\cdot cm$) was thoroughly mixed in a flask with 4.049 g of $MnCl_2$ salt (Alfa Aesar). Thereafter, 0.207 g of PSS (CAS: $25704-18-1$, $M_w \sim 70000$, Sigma Aldrich) were added and the ultrasound bath was utilized for complete solubilizations of the polymer. The solution was then filtered in an empty slides-container (Faearbebox, Assistent) through a 200 nm pores size syringe filter. 0.5 ml of HCl 0.1 N was afterward added to bring the pH of the solution to 3. To prepare the PAH solution, 50 ml of ultrapure water thoroughly mixed in a flask with 10.29 g of NaBr (Alfa Aesar). Therefore, a 0.0935 g of PAH (CAS: $71550-12-4$, $M_w \sim 15000$, Sigma Aldrich) was added and the ultrasound bath assured complete solubilizations of the polymer in water. The solution was then filtered in an empty slides-container (Faearbebox, Assistent) through a syringe filter of 200 nm pores size. 0.5 ml of HCl 0.1 N was afterward added to bring the pH of the solution to 3. To deposit polyelectrolytes layers on the substrates, the fused silica slides were subsequently immersed in the PSS and PAH solution, each for 20 minutes. After each deposition step, the samples were rinsed 10 times with ultrapure water. At the end of the desired number of deposition cycles, the slides were dried by a N_2 flow and stored under room conditions.

Dyes deposition

After deposition of 2.5 PSS/PAH bilayers (PSS terminated), the $DiIC_1(5)$ chromophore was deposited on top of the substrate by a dye solution. Several solvents, concentration values, immersion times and different deposition techniques were tested to achieve the requirements for a good sample (see section 5.3).

5.4.2 Results and Discussion

DiIC1(5) in water

An initial dye solution in ultra pure water (MilliQ, resistivity of $18.2\,M\Omega\cdot cm$) was prepared at concentration of 10^{-3} M, in which several samples substrates were immersed with different deposition times. Successively the slides were rinsed in ultra pure water for 5 times and at the end dried by a nitrogen stream. In figure 5.4.2, the experimental decay curves are reported for *pp* polarization combination and several dipping times. It is possible to observe a strong multi exponential character of the decay curves, especially for longer deposition times. As highlighted in section 5.2, the slope differences due to different dipole orientations within an ensemble can not be observed. Therefore, the multi exponential character may indicate fluorescence self-quenching, as a consequence of dyes aggregation. The decay curves trend with deposition time in figure 5.4.2, could be explained with the formation of dyes clusters on the sample surface or with the slower diffusion toward the surface of larger aggregates pre-formed in solution. Additional investigations would be required in order to distinguish between the two mechanism of dye aggregation.

Using an ultra-sound bath overnight at room temperature and the next day for 15 minutes at ~ 50Â°C were not beneficial in removing the suspected aggregation from the dye solution. Thus lower concentrations of dye were tested. Based on figure 5.4.2, also a larger time window was suggested to

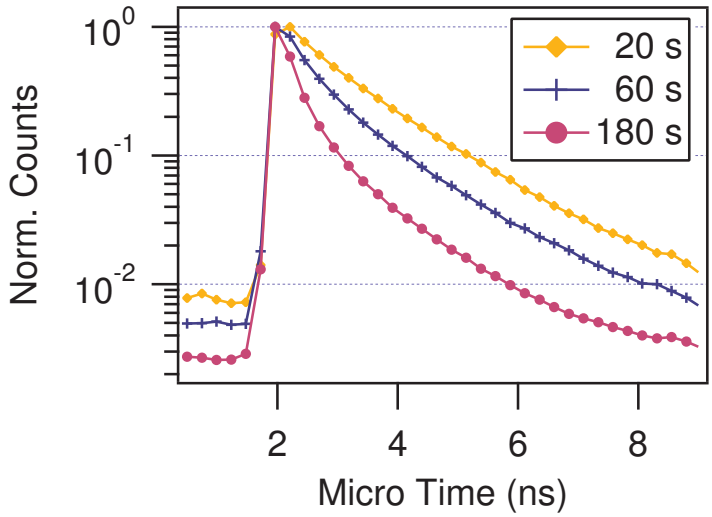

Figure 5.4.2: Normalized fluorescence decay curves for samples with different dipping time (in legend), in a dye solution of $DiIC_1(5)$ at 10^{-3} M in ultrapure water. Measurements are for *pp* polarization combination, a bin width of ≈ 122 ps was used to plot the decay curves.

detect completely the fluorescence decay process. Therefore the excitation repetition rate was lowered from 100 MHz to 20 MHz with an excitation intensity loss of factor ~ 5. As a consequence, the initial detector (Single Photon Avalanche Photodiode, SPAD), was replaced by a fast photomultiplier (PMT) with a larger detection area. As a drawback, the utilization of a PMT increased the amount of scattered light detected, therefore the fits of the decay curves were limited to micro time values larger than 4.5 ns.

Figure 5.4.3 shows the measured decay curves (*pp* polarization combinations), for three substrates dipped in ultrapure water solutions at different $DiIC_1(5)$ concentrations (deposition time 30 s). Afterward the samples were rinsed 5 times in ultra pure water and then dried by a nitrogen stream.

It is possible to observe a multi-exponential behaviour for all the concentrations studied, indicating a probable presence of dye aggregates on the samples substrates. An additional factor contributing to the fluorescence quenching could be given by the presence of residual water in the polyelectrolytes film [16]. A post deposition study was carried out to gain more insights about the aggregation of the dyes and the effects of residual water in the film.

Post deposition analysis Figure 5.4.4 a) and b) show the fluorescence decay curves measured after the chromophore deposition and after a post-deposition treatment, respectively. Initially a 2.5 bilayers PSS/PAH substrate was immersed in a dye solution at 10^{-3} M in ultrapure water (for 180 s) then rinsed 5 times, dried by a N_2 flow and the lifetime was finally measured ("no treat." in the legend). Successively the sample was immersed in a water solution containing 0.4 M of $MnCl_2$ salt and 0.1 N of HCl, for 25 minutes, rinsed 5 times in ultrapure water and dried by a nitrogen flow. Lifetime measurements were performed right after the drying step ("salty sol." in the legend). Figure 5.4.4 shows that the suspected dye aggregation is partially removed by the post-deposition treatment: a decrease of χ^2_N and a correspondent increase of lifetime are seen. The fluorescence intensity shows also an increase, confirming the partial reduction of the self-quenching effect.

Figure 5.4.5 shows the measured decay curves, for $DiIC_1(5)$ dyes deposited onto 2.5 PSS/PAH bilay-

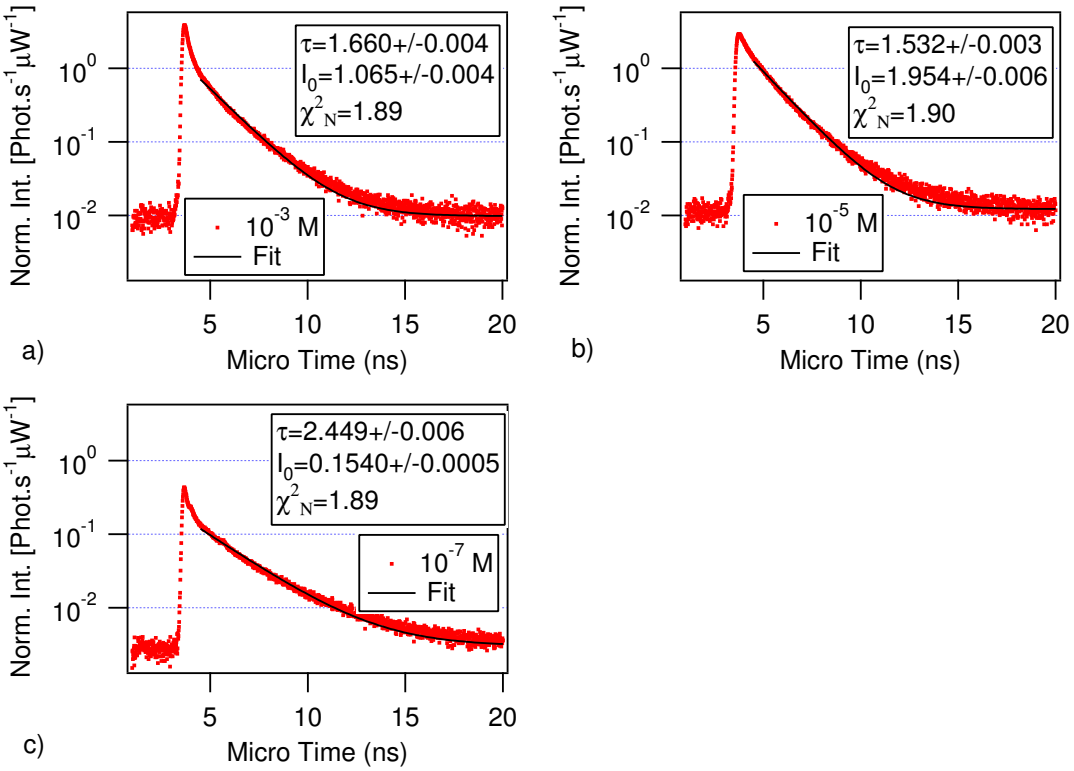

Figure 5.4.3: Fluorescence decay curves, for *pp* polarization combination, of $DiIC_1(5)$ deposited onto 2.5 bilayers PSS/PAH substrates by immersion in ultrapure water solutions at different dye concentrations (as indicated in legends). Fits and relative results are also shown: lifetime (τ, in ns), intensities (I_0, in phot./(s · μW)) and χ^2_N values. For all the samples the dipping time was 30 s.

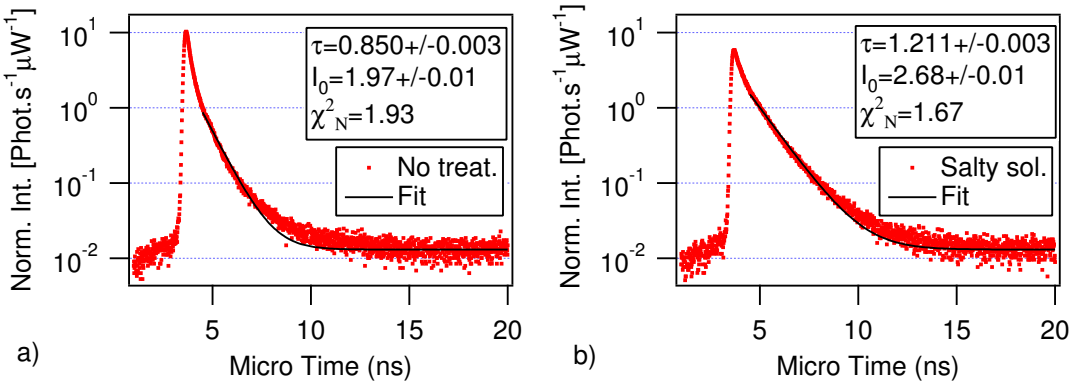

Figure 5.4.4: Fluorescence decay curves for *pp* polarization combination of $DiIC_1(5)$ deposited onto 2.5 PSS/PAH bilayers substrate. The slides were dipped in a dye solution at 10^{-3} M in ultrapure water, for 180 s. The curve indicated by "no treat." in a) was measured after dye deposition, while the decay curve in b) was obtained after leaving the sample for 25 minutes in a salty solution. Figure shows also fits and relative results: lifetime (τ, in ns), intensities (I_0, in phot./(s · μW)) and χ^2_N values.

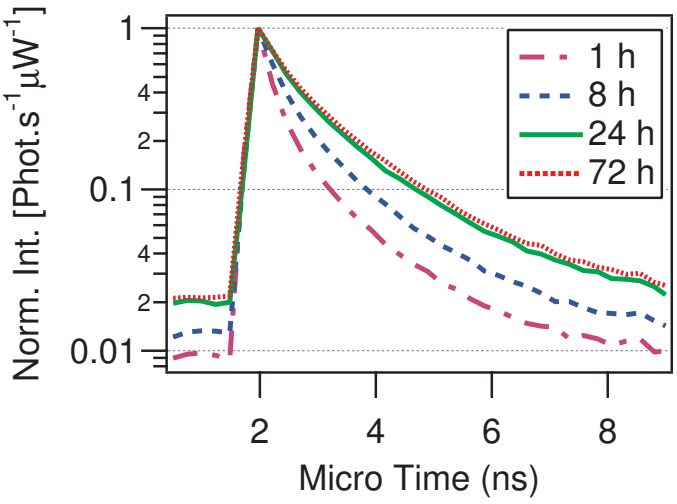

Figure 5.4.5: Fluorescence decay curves for *pp* polarization combination, as a function of the time lag after chromophore deposition on a 2.5 PSS/PAH bilayers substrate. The dye solution was constituted by $DiIC_1(5)$ at 10^{-5} M in ultrapure water. Deposition time was 60 s. The curves are plotted by using an histograms bin width of ≈ 122 ps.

ers substrate, as a function of the time lag after chromophores deposition step. The sample was left for 60 s in the dye solution, rinsed 5 times by ultra pure water and then dried by a nitrogen stream. The fluorescence decay curves, for *pp* polarization combination, were measured after $1, 8, 24$ and 72 hours, after leaving the sample at room conditions. From figure 5.4.5, it is possible to observe the change of the curve slope, with a limit value reached after about 1 day. A possible explanation could be given by the presence of different amount of residual water trapped in the polyelectrolytes film, as a function of the time. Fluorescence lifetime measurements of $DiIC_1(5)$ dyes in solution, at different concentrations, have actually shown that water is a strong fluorescence quencher. Lifetime values around ≈ 0.6 ns are obtained in solution (see also table 5.4.1), against a value of ≈ 2.4 ns from single molecule experiments at the dielectric interface [27]. Another possible hypothesis of this result could come from dye-polymer system re-arrangement with time: fluorophores mobility and polymer matrix relaxation may lead to larger dye-dye distances, reducing thus the number and the size of the aggregates. Nevertheless the multi-exponential character of the decay curves is still clear after the sample was stored at room condition for 3 days.

In summary, the results of figures 5.4.4 and 5.4.5 has shown that dye clusters formation and residual trapped water within the polymer susbtrate may prevent the utilization of dipping technique, for $DiIC_1(5)$ dye deposition by water solutions down to 10^{-5} M. It was not possible to determine if the dye clusters formation occured in solution or at the sample surface, since concentrations values lower than 10^{-5} M did not provide reliable fluorescence signals.

Different deposition technique In order to overcome the issue encountered by using the immersion technique, a flow cell was utilized for deposition. By a closed loop circulation system (0.4 ml/min.) and a water solution of $DiIC_1(5)$ at 10^{-9} M, the chromophores were deposited onto a 2.5 PSS/PAH bilayers substrate, by a circulation time of 3 hours. Afterwards the sample was rinsed 5 times by ultra pure water and then dried by a nitrogen stream. Figure 5.4.6 reports the fluorescence decay curves, for different polarization combinations, for $DiIC_1(5)$ dye deposited on top of the polyelectrolytes substrate by the flow cell. The aggregation appear to be largely reduced with respect to the immersion

technique at higher concentration values. This is can be observed from lifetimes and χ^2_N values in comparison with figure 5.4.3 (for *pp* polarization).

Evaluation By using the PCM (chapter 4), it is possible to compare theoretical calculations with the experimental data shown in figure 5.4.6. The comparisons for fluorescence lifetimes and intensities values are reported respectively in figure 5.4.7 a) and b). Simulated values are obtained for 900 dipoles embedded in a 6 nm thick polymer film (see the sample characterization section in chapter 4), at 1 nm from the air-polymer interface. The dielectric film (n = 1.523) in the model is placed on top of a semi-infinite fused silica substrate (n = 1.457) and a sketch of the multilayer system utilized for the simulation is reported in figure 5.4.7 c). The parameters used in the theoretical calculations are extracted from the PCM by fitting the experimental data (for details see chapter 4) and they are reported in the legend of the figure.

Figure 5.4.7 shows a good agreement between theory and experiment for both excite-state lifetime and intensities, when the fluorophores are considered embedded in the polymer matrix. This result indicates that the emitters experience the polymer as surrounding environment, suggesting a probable diffusion of the dyes into the PSS/PAH polyelectrolytes layers.

DiIC1(5) in Ethanol

Figure 5.4.8 a) reports the fluorescence decay curves for $\mathrm{DiIC}_1(5)$ chromophores, deposited on top of 2.5 PSS/PAH bilayers, for several immersion times. The samples were prepared by dipping the substrates into a dye solution at 10^{-5} M in ethanol, rinsed 5 times by ultra pure water and finally dried by a nitrogen stream. From comparison between figure 5.4.8 a) and 5.4.3 b), it is possible to notice that ethanol is a better solvent for the $\mathrm{DiIC}_1(5)$ dye (approximately single exponential character of the decay curves). In figures 5.4.8 b), c) and d), the curves in a) are plotted with relative fits and smaller histogram bin width. From the comparison among the excited-state lifetimes and the χ^2_N values in the legends (according to the criteria given in section 5.3), the sample with 30 s of dipping time represents the best choice for a theory-experiment comparison.

Evaluation Theoretical fluorescence lifetimes and intensities have been calculated for different polarization combinations and compared with the experimental data. The results of the comparison are shown in figure 5.4.9 a) and b) respectively. The theoretical values are obtained by considering the system in figure 5.4.7 c). The system parameters used in the theoretical calculations are extracted by PCM (for details see chapter 4) and are displayed in the legend of figure 5.4.9 a). The chosen experimental data are for the sample with deposition time of 30 s and the correspondent decay curves are shown, for different excitation-detection polarizations, in figures 5.4.9 c), d), e) and f).

Figure 5.4.9 a) indicates a quite good agreement for the excited-state lifetimes. For the fluorescence intensities in b), the theory deviates from measured data only for *pp* polarization combinations. In general, the field components perpendicular to an interface depend on the media refractive indices, while the parallel components are preserved according to boundary conditions (see also figure 5.2.1). In this regards, the discrepancy between experiment and theory may be caused by an incorrect estimation of the polyelectrolytes refractive index, in the model. For higher values of refractive index a slightly better agreement is achieved between theory and experiment (see as an example figure 5.4.10). For the comparison, the same model parameters were used for theoretical calculation as in figure 5.4.9 a): $\Gamma_{nr}/\Gamma_0 = 0.4, \Delta\theta = 0$ and $1/\Gamma_0 = 3.55$ ns. Nevertheless in spite of the better agreeement it was not possible to find a justification for a refractive index value of n = 1.70, since such higher value is not supported by any experimental data for thin PSS/PAH layers ($\approx$ 6 nm).

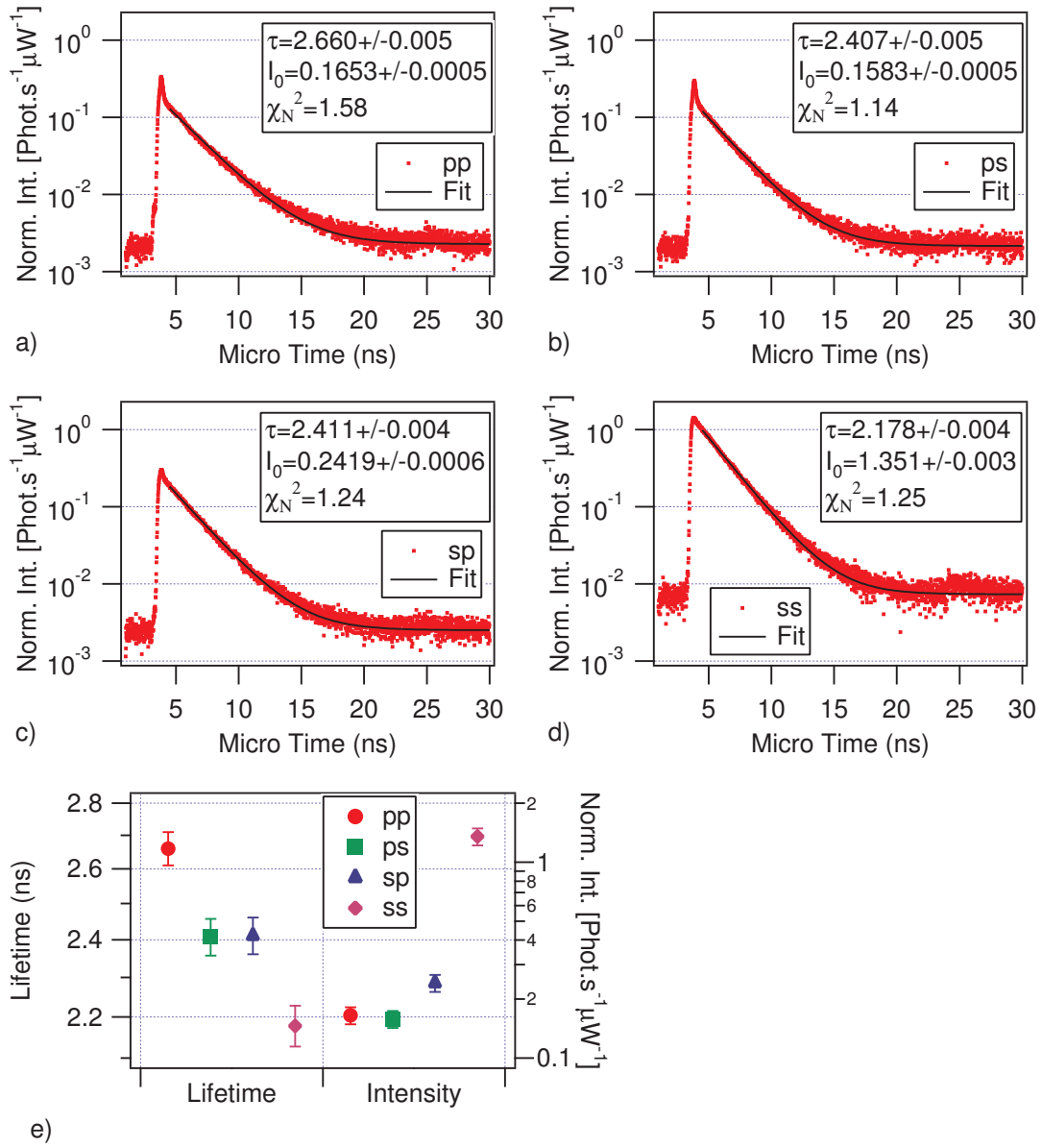

Figure 5.4.6: a)-d) Fluorescence decay curves for different polarization combinations for $DiIC_1(5)$. The dye was deposited on a 2.5 PSS/PAH bilayers substrate, by flow cell and 3 hours circulation (0.4 ml/min.). The dye solution used was at 10^{-9} M in ultrapure water. Figure shows also fits (between 4.5 ns and 40 ns) and relative results: lifetime (τ, in ns), intensities (I_0, in phot./$(s \cdot \mu W)$) and χ^2_N. e) Plots of lifetimes and intensity values from fits in a)-d). Experimental error for lifetimes it is ± 0.05 ns, while for intensities it is $\pm 10\%$.

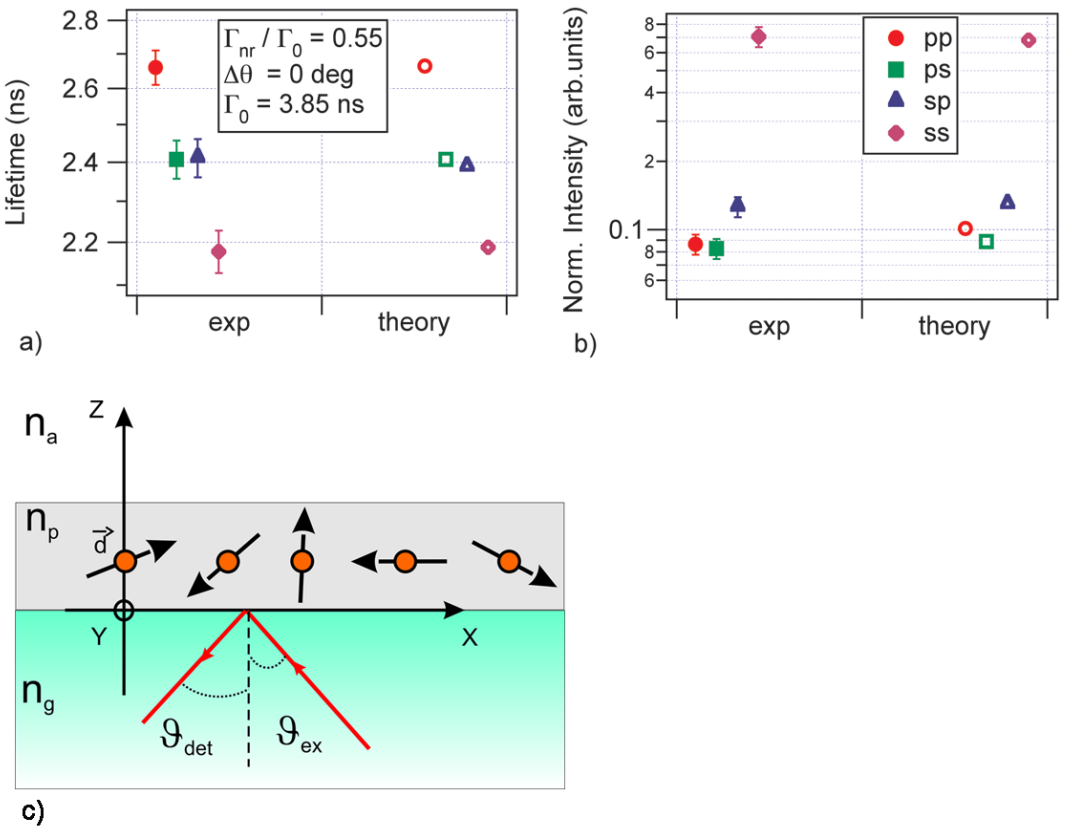

Figure 5.4.7: Comparison between experiment and theory, for excited-state lifetime (τ) a) and fluorescence intensity (I_0) b), for different excitation-detection polarization combinations. Measured data are for sample of figure 5.4.6, while the parameters used in simulation are shown in legend. Experimental error for lifetimes is ± 0.05 ns, while for intensities is $\pm 10\%$. c) Sketch of multilayer system used for theoretical calculations, with $n_a = 1$, $n_p = 1.523$ and $n_g = 1.457$. The polymer film (n_p) is 6 nm thick, while the dyes are at 1 nm from the air-polymer interface. Air (n_a) and glass (n_g) sides are semi-infinite. The excitation and detection angles are $\theta_{ex} = 41.1\hat{A}°$ (0.72 rad) and $\theta_{det} = 48.9\hat{A}°$ (0.85 rad) respectively.

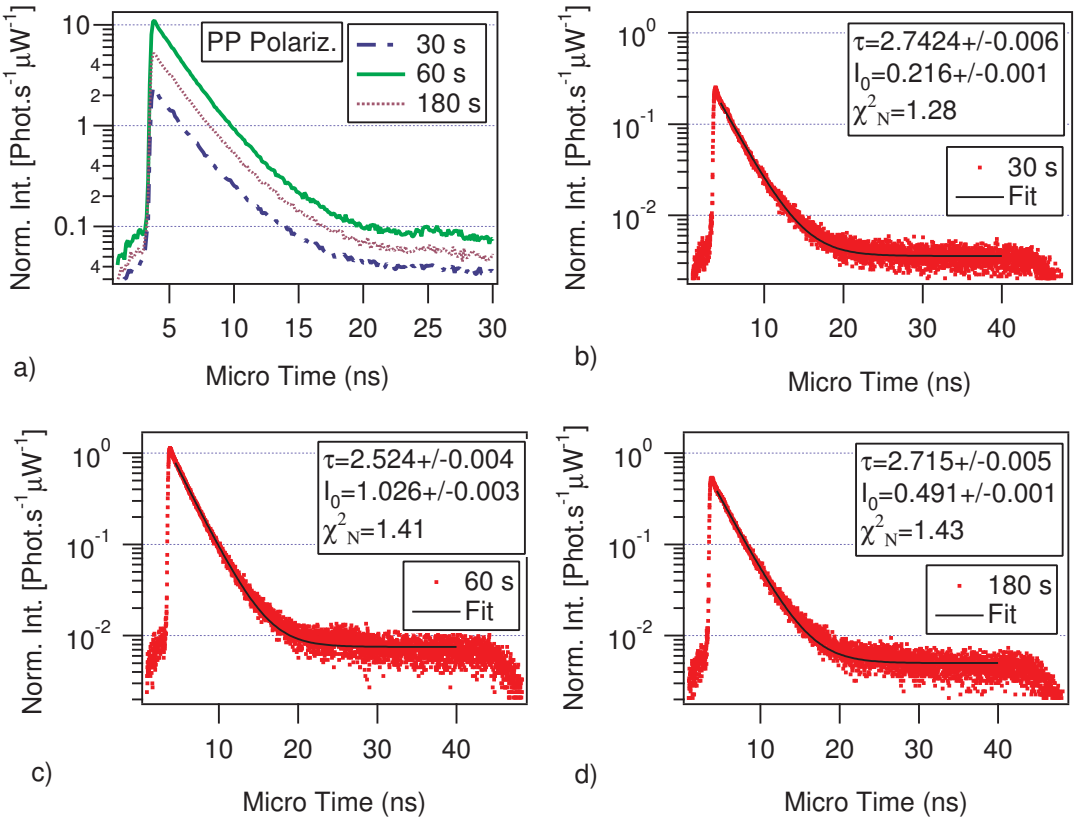

Figure 5.4.8: a) Fluorescence decay curves of $DiIC_1(5)$ deposited onto 2.5 PSS/PAH bilayers substrate by dye solution at 10^{-5} M in ethanol, for different deposition times. The measurements are for *pp* polarization combination by using an histograms bin width of ≈ 122 ps. b), c) and d): details for decay curves in a) with relative fits and histogram bin width ≈ 12.2 ps. In the legends the values of lifetime (τ, in ns), intensity (I_0, in phot./$(s \cdot \mu W)$) and χ^2_N are reported.

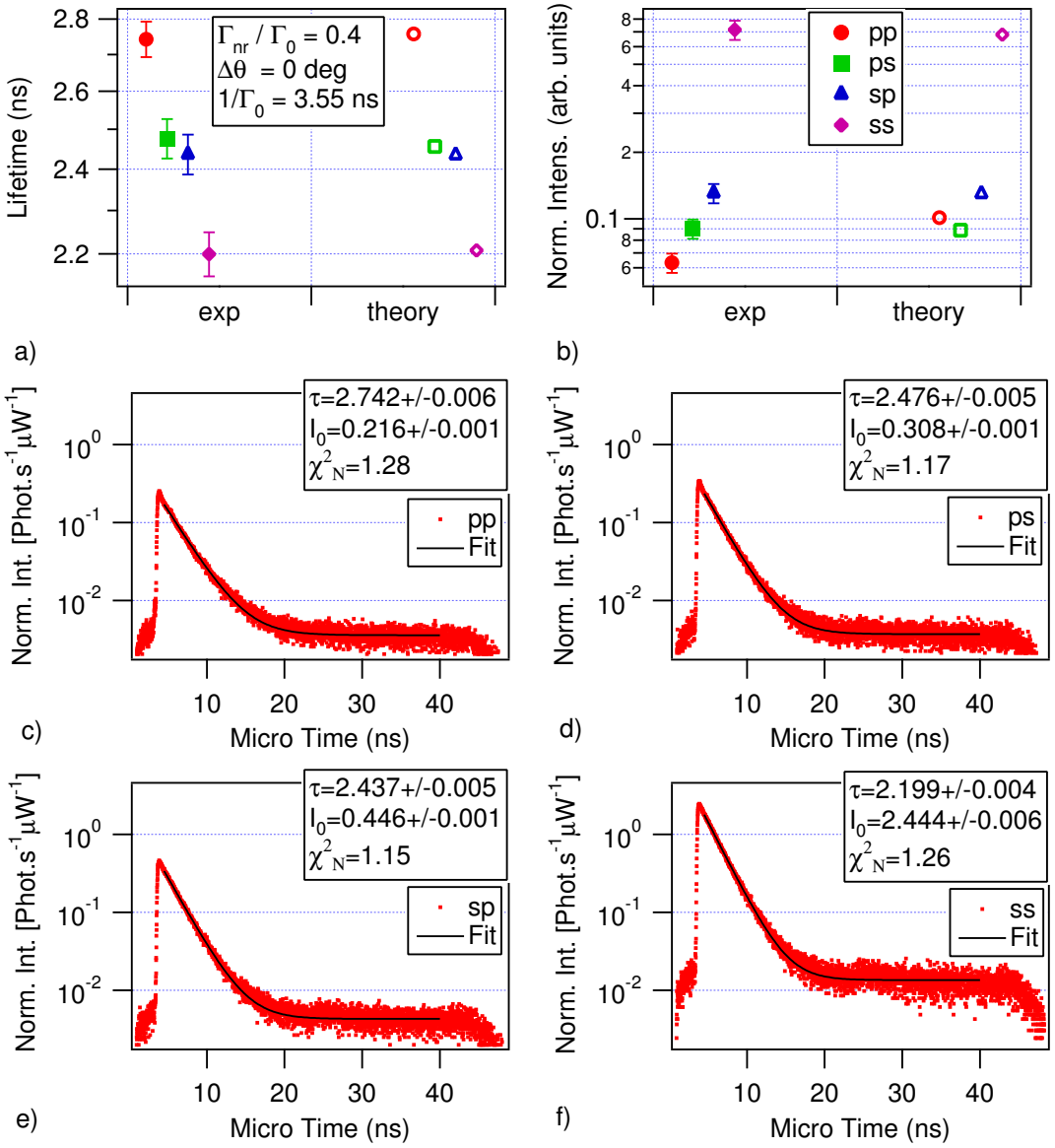

Figure 5.4.9: Comparison between experiment and theory, for excited-state lifetime (τ) a) and fluorescence intensity (I_0) b), for different excitation-detection polarization combinations. Experimental error for lifetimes is ± 0.05 ns, while for intensities is $\pm 10\%$. Measured data are for sample with 30 s of deposition time, while the parameters used in the simulation are shown in the legend of a). The multilayer system used for the calculations is sketched in figure 5.4.7 c). In c), d), e) and f) the measured decay curves with relative fits are reported for *pp, ps, sp* and *ss* polarization combinations, respectively. The values of lifetime (τ, in ns), intensity (I_0, in phot./$(s \cdot \mu W)$) and χ^2_N are also reported.

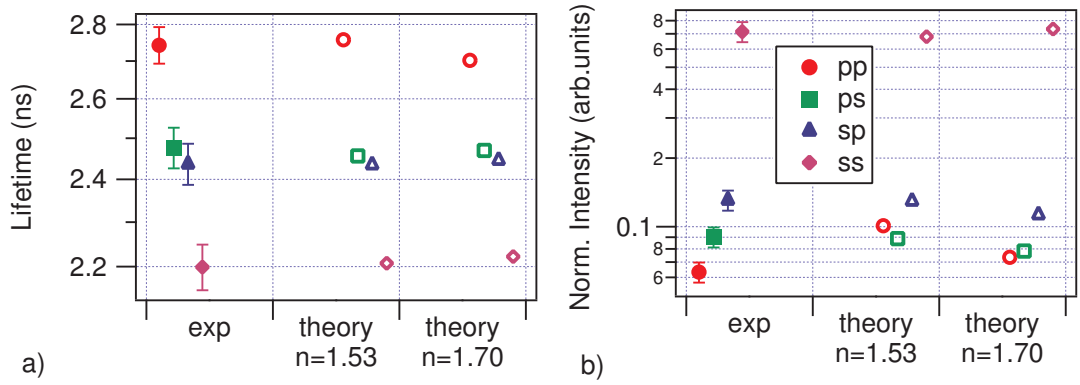

Figure 5.4.10: Comparison between experiment and theory for two refractive index values of the polymer spacer. Excited state lifetimes a) and fluorescence intensities b) are plotted for different excitation-detection polarization combinations. Experimental data and simulation parameters are like in figure 5.4.9 a). Experimental error for lifetimes it is ± 0.05 ns, while for intensities it is $\pm 10\%$.

On the other side, the introduction of the local field effects corrections based on the Lorentz model or the empty cavity model [8], do not provide any change for normalized intensities and for lifetimes.

The theory-experiment comparison indicates that the chromophores experience polymer as surrounding environment, even if the dye molecules were deposited on top of the polyelectrolyte substrate. The film porosity, in this respect, may promote the diffusion of the emitters [18] just below the air-polymer interface. Another hyphotesis could be that the polyelectrolytes collapse due to the different dielectric constant between water and ethanol, causing chains re-arrangement and holes formation [29] (where the fluorophores could diffuse into).

Different deposition technique Spin coating of $DiIC_1(5)$ dye solution at different concentrations in ethanol was also tested on a 2.5 PSS/PAH bilayers substrate (figure 5.4.11). The spin coating time was 60 s for all the samples, speed 4000 rpm for solution with 10^{-5} M and 10^{-7} M, while 2500 rpm spin coating speed was used for the sample at 10^{-3} M.

Figure 5.4.11 shows that aggregation is still present for all the concentration values, indicating that spin coating is not a suitable technique.

DiIC1(5) in Other Solvents

Utilization of other solvents, like Acetone, Methanol, Ethylene and Glycol, brought to aggregation or precipitation of the chromophores in solution (like in Toluene), for dye concentrations down to 10^{-7} M. The use of ultrasound or temperature to improve solubility or the mix of different solvents did not provide any significant improvement. The measurement of fluorescence lifetime in solution as a function of the concentration, for different solvents, did not add valuable information (see table 5.4.1).

5.4.3 Summary

Dye aggregation seems to be a major issue, for all concentrations investigated down to 10^{-5} M, while lower concentrations by dipping technique do not provide reliable fluorescence signal. Chromophores

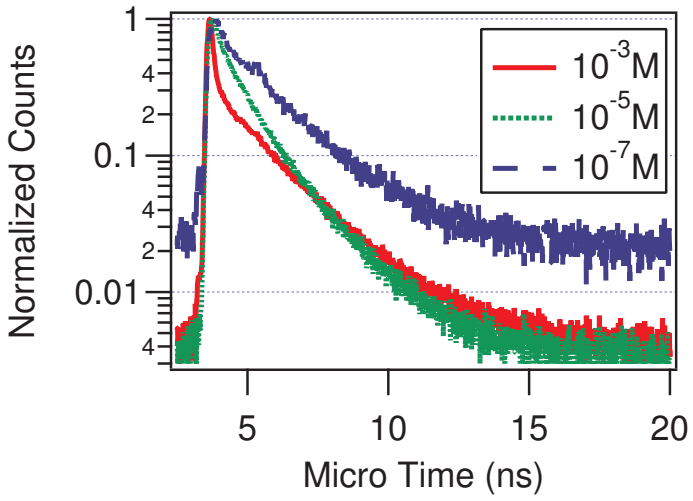

Figure 5.4.11: Fluorescence decay curves for $DiIC_1(5)$ chromophore on top of 2.5 PSS/PAH bilayers. The dye was deposited by spin coating a ethanol solution at different concentrations.

Solvent	10^{-3} M	10^{-5} M	10^{-7} M
H_2O	0.62	0.56	/
Ethanol	1.27	1.06	0.94
THF	/	1.25	/

Table 5.4.1: Fluorescence lifetimes in ns for $DiIC_1(5)$ dyes in solution, for different solvents and concentration values. Note: THF is Tetrahydrofuran.

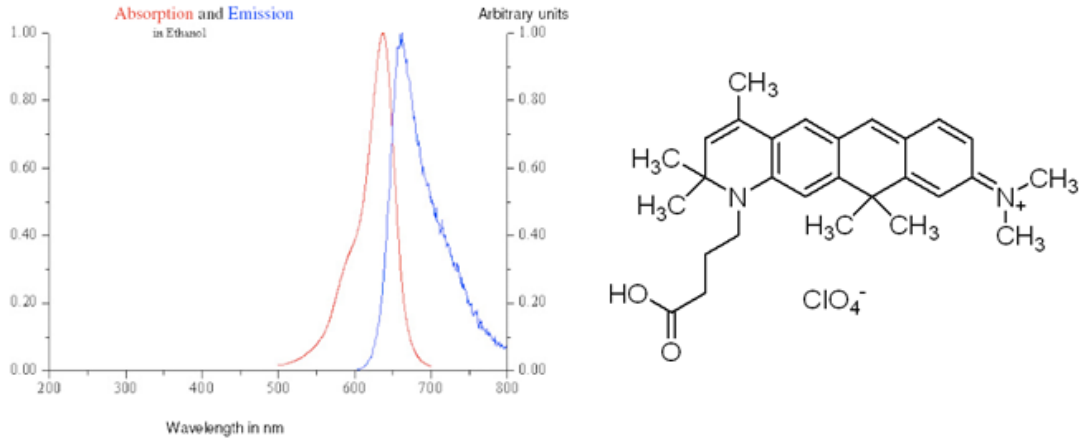

Figure 5.5.1: Fluorescence spectra and molecular structure of ATTO 635 dye. The organic dye molecular formula is $C_{28}H_{35}ClN_2O_6$, while the molecular weight is 531.1. Quantum yield 0.35. Data provided by the manufacturer [26].

deposition by a flow cell with a dye solution of 10^{-9} M in water, provided significant aggregation reduction and reliable fluorescence signal. A good agreement is found in the comparison between theory and experiment, suggesting the dye molecules may diffuse into the polyelectrolytes spacer. Ethanol turned to be a better solvent for $\mathrm{DiIC}_1(5)$, providing approximately single exponential decay curves already at 10^{-5} M, with same excited-state lifetime values obtained by the flow cell and a water solution at 10^{-9} M. The theoretical model reproduces well the experimental lifetimes and fairly good the measured fluorescence intensities, when ethanol and immersion technique are used for dyes deposition on top of polyelectrolytes layers. Deviations for intensities may be explained by an underestimation of the polymer layer refractive index of $\sim 10\%$, nevertheless no justification was found for higher refractive index values. As a general indication, the simulation results suggest an "in polymer" surrounding environment for the dye molecules. Different solvents or solvent mixtures lead to chromophore clusters formation, for the explored concentrations values.

5.5 ATTO 635

In figure 5.5.1, the molecular structure of ATTO 635 organic dye is reported (Fluka, Sigma Aldrich Inc., Prod. No. 08968). The chromophore has a maximum excitation at $\lambda_{ex} = 635$ nm and a fluorescence emission maximum at $\lambda_{em} = 659$ nm [26].

5.5.1 Samples Preparation

2.5 PSS/PAH bilayers (terminated by PSS) and 1 monolayer of PSS were deposited respectively on two different glass substrates (compare section 5.4.1). Afterward the ATTO 635 organic dye was deposited onto the samples by dipping the substrates in a water solution containing the chromophore, for different concentrations and immersion times.

5.5.2 Results and Discussion

2.5 PSS/PAH bilayers spacer

In figure 5.5.2 a), the fluorescence decay curves for *pp* polarization combination and several ATTO-635 dye concentrations are reported. The chromophore was deposited on a polymer film constituted by 2.5 PSS/PAH bilayers (PSS terminated), by dipping the substrate for 30 s in several aqueous solutions at different dye concentrations. Afterward the samples were rinsed 5 times in ultrapure water and then dried by a N_2 stream. Figure 5.5.2 b) shows the fluorescence lifetimes, for different polarization combinations, as function of the dye concentration, for the same samples discussed in a).

From figure 5.5.2 a), a strong dependence of the decay curves from dye concentration in the deposition solution is detected. The multi-exponential character may show the presence of dye aggregation on the substrates. In figure 5.5.2 b) as a general trend, it is possible to observe that the fluorescence lifetimes become smaller in a significant way as the concentration increases. This probably indicates that a fluorescence self-quenching mechanism is present. The sample prepared by the dye solution at 10^{-7} M shows the highest excited-state lifetime and a χ^2_N value close to 1. Thus it represents a good sample for a comparison with theoretical data. At higher concentrations the conclusions of the results are difficult to obtain. The suspected clusters formation prevents reliable evaluations of the ratios among different excitation-detection polarization combinations.

A comparison between experimental and theoretical data is reported in figure 5.5.3 a) and b), for fluorescence lifetimes and intensities, respectively. Data is shown for different polarization combinations. The measured data are obtained by using a sample prepared with a dye solution at 10^{-7} M. A sketch of the model used in the simulation is described in figure 5.4.7 c), while the parameters used in the software code are reported in the legend of figure 5.5.3 a). Normalized non-radiative decay rate (Γ_{nr}/Γ_0), excitation-emission dipoles relative angle ($\Delta\theta$) and vacuum lifetime ($1/\Gamma_0$), were extracted by the PCM (for details see chapter 4).

Figures 5.5.3 a) and b) indicate that the agreement with theory is poor for *pp* and *ps* polarizations, while smaller deviations are seen for the other combinations. Following the discussion of figure 5.4.9 b), the discrepancy may be explained by an underestimation of the polymer film refractive index. From a qualitative analysis of lifetimes ratios in figure 5.5.3 a), it is anyway possible to indicate most of the dyes experience the polymer as surrounding environment (compare section 5.2).

PSS monolayer as spacer

Figure 5.5.4 a) and b) show comparison between experimental and theoretical data, for different polarization combinations, for fluorescence lifetimes and intensities, respectively. The experimental data are for ATTO 635 dyes deposited on top of 1 layer of PSS, by dipping the substrate in a dye solution at 10^{-7} M, with 180 s of immersion time. After rinsing the slide was dried by a nitrogen flow. The model used in the simulation is described in figure 5.4.7 c), with the only difference that now the polymer film is considered 2 nm thick. The parameters utilized in theoretical calculations are reported in the legend of figure 5.5.4 a), as extracted by the PCM (for details see chapter 4).

There is a fairly good agreement between theoretical and experimental results, beside a deviation for I_{0pp}. This can be explained by an incorrect refractive index value used in simulation for the polymer layer (see also discussion of figure 5.4.10). An explanation for the mismatch between experiment and theory in τ_{ps} has not been found. In spite of the smaller film thickness ($\approx 1.5 - 2$ nm [39]) with respect to the 2.5 PSS/PAH bilayers (thickness ≈ 6 nm), the emitters still experience the polymer

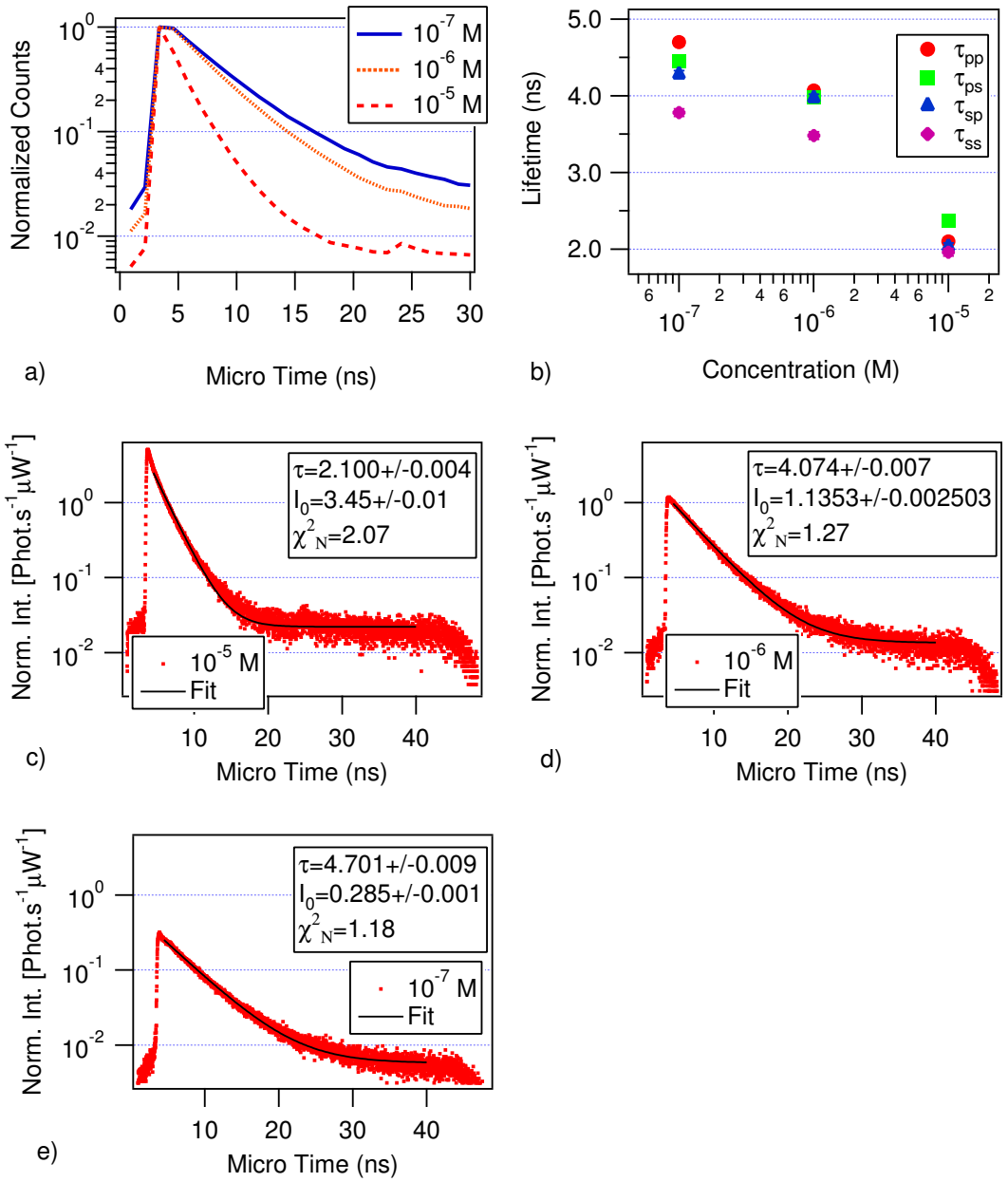

Figure 5.5.2: a) Fluorescence decay curves for *pp* polarization combination, for ATTO-635 dye deposited on a 2.5 PSS/PAH bilayers substrate. Dipping technique with 30 s of immersion time was used and several chromophore concentrations. An histogram bin width of ≈ 122 ps has been used for plotting. b) Fluorescence lifetimes for different polarization combinations, as a function of the dye concentration, for the samples in a) Experimental error for lifetimes is ± 0.05 ns and it is not plotted for clarity. In c), d) and e) the decay curves with fits are shown, for the samples in a). In the legends the values of lifetime (τ, in ns), intensity (I_0, in phot./$(s \cdot \mu W)$) and χ^2_N are reported.

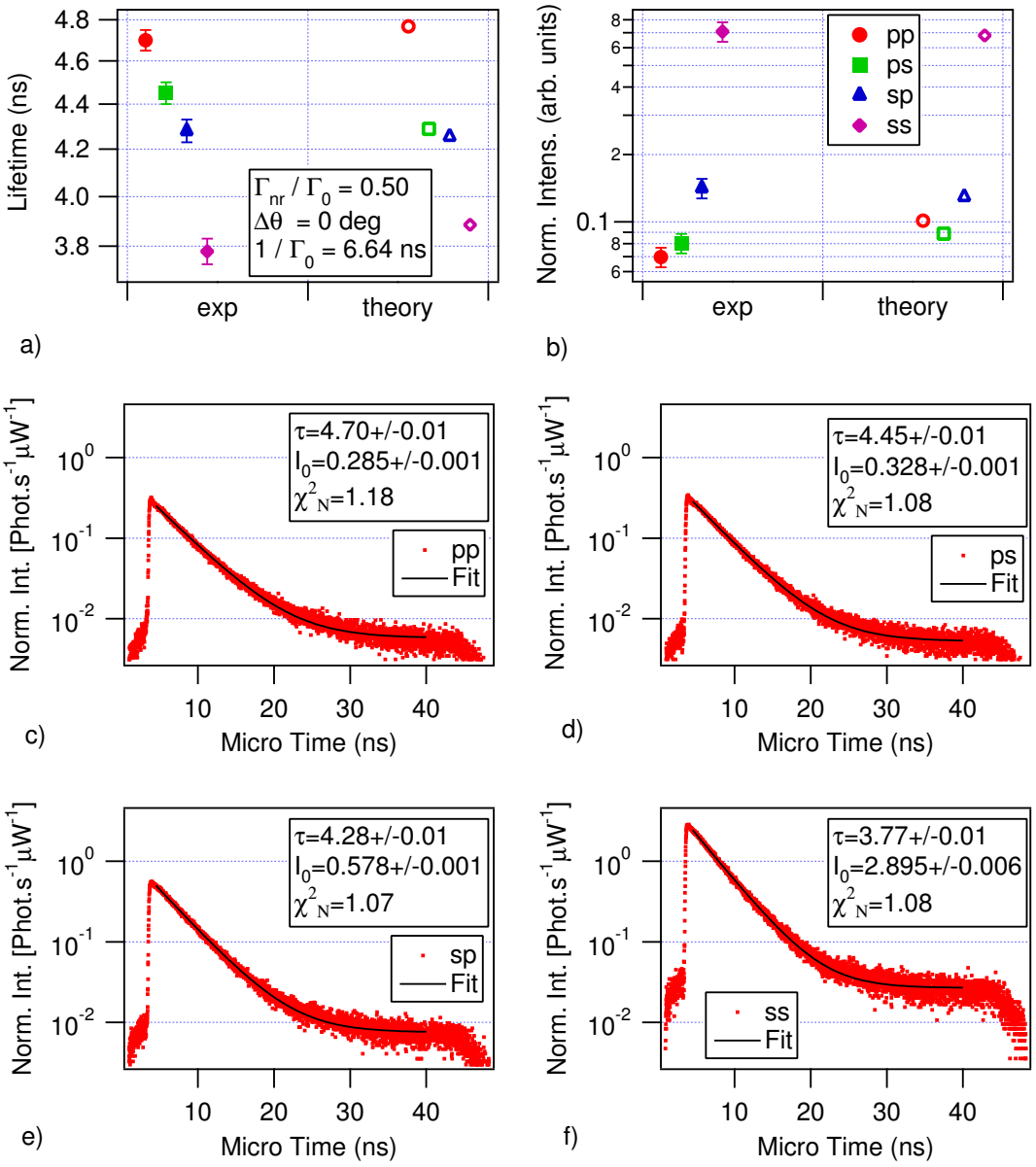

Figure 5.5.3: Theory-experiment comparison for excited-state lifetime (τ) a) and fluorescence intensities (I_0) b), as a function of different excitation-detection polarization combination. Experimental error for lifetimes is ± 0.05 ns, while for intensities is $\pm 10\%$. Experimental data are for ATTO 635, deposited onto 2.5 PSS/PAH bilayers (PSS terminated) by dipping the substrate for 30 s, in a 10^{-7} M water solution of dyes. c), d), e) and f) Measured decay curves and relative fits, for *pp, ps, sp* and *ss* polarization combinations respectively. In the legends, the values of lifetime (τ, in ns), intensity (I_0, in phot./$(s \cdot \mu W)$) and χ^2_N are reported.

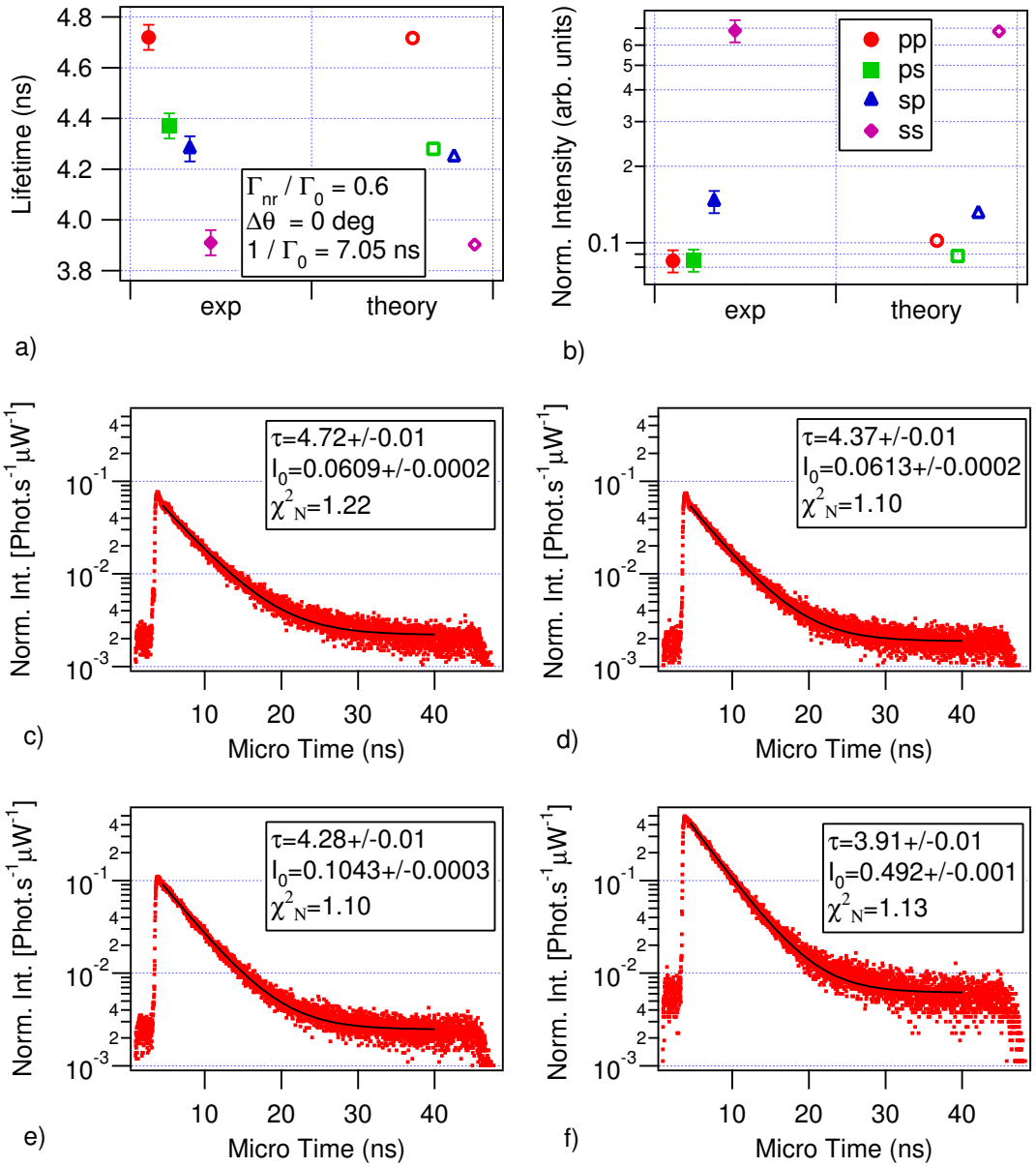

Figure 5.5.4: Comparison between theory and experiment for fluorescence lifetimes (τ) a) and intensities (I_0) b), for different polarization combinations. Measured data are for ATTO 635 dyes deposited on top of 1 monolayer of PSS. Experimental error for lifetimes is ± 0.05 ns, while for intensities is $\pm 10\%$. c), d), e) and f) Experimental decay curves for respectively *pp, ps, sp* and *ss* polarization combinations, with indication in the legends of the fitted lifetimes (τ, in ns) and intensities (I_0, in phot./$(s \cdot \mu W)$). Values for χ^2_N also reported.

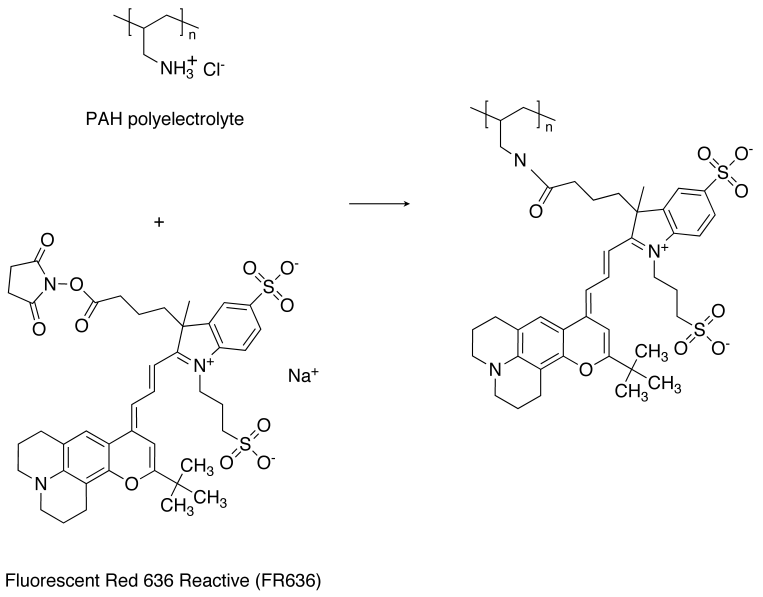

Figure 5.6.1: Schematic of PAH labelling by the FR636 chromophore.

matrix as surrounding environment ("in polymer" behaviour). In this case a role could be played also by the interaction between dyes and 3-APTE silanes, even if it was not possible to obtain a direct confirmation due to low intensitiy detected without the glass functionalization. On the other hand the addition of the 3-APTE layer in the theoretical model (2 nm thick, $n = 1.42$, [40]) resulted in a change of the simulated values around $\lesssim 0.1\%$, below numerical accuracy.

5.5.3 Summary

The ATTO 635 dye provides better results for cluster formation in water than $\mathrm{DiIC}_1(5)$ dye, allowing measurements down to 10^{-7} M (probably due to its higher quantum efficiency). Nevertheless similar results in term of "in polymer" behaviour are obtained, for emitters deposited on top of a 2.5 PSS/PAH bilayers polyelectrolytes substrate or more interestingly on top of one layer of PSS ($\approx 1.5 - 2$ nm [39]). Classical theoretical model provides a fairly good description of the real system, with small deviations for fluorescence intensities. No clear explanation was found for such theory-experiment discrepancies.

5.6 FR636 Covalently Bond to PAH

To reduce the mobility of the emitters on the samples surface, PAH chains were functionalized with an organic dye able to react with the amino group (NH_2) of the polyelectrolyte monomers.

In this manner the chromophore forms a covalent bond of few angstroms with the polymer chains (like in figure 5.6.1). It is therefore possible to determine the dye molecules position with respect to an interface, depending on the position of the PAH chains. The polymer loaded with the chromophores can be deposited onto a substrate by the layer-by-layer technique and therefore a certain control over emitters position is achieved. For this purpose a fluorescent organic dye with an active ester group was chosen (NHS-modified fluorescent red dye: FR636 Red Reactive organic dye - Sigma Aldrich

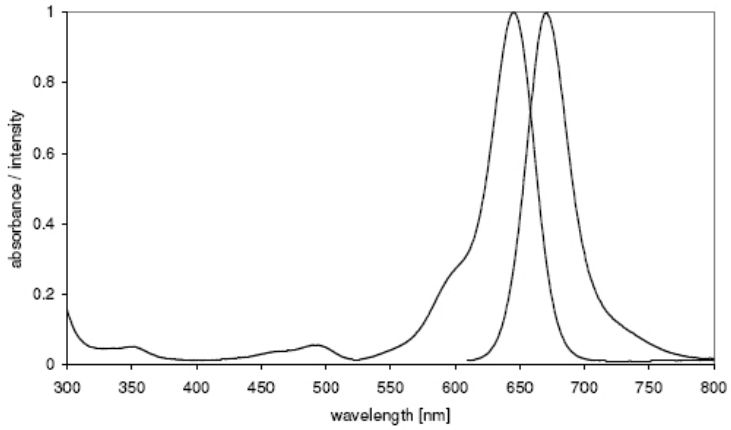

Figure 5.6.2: Absorption and fluorescence emission spectrum for the FR636 red reactive organic dye, as provided by the manufacterer (Sigma Aldrich).

Inc., product no. 69296). The dye has a molecular weight of 760.91 and a molecular structure as shown in figure 5.6.1. The associated fluorescence spectrum is reported in figure 5.6.2, as provided by the manufacturer.

The ratio between the polymer and the dye amount in the reaction leading to the functionalized polymer (condensation reaction) must be within a certain range. As it was tested by several experiments, a minimum PAH concentration is necessary for the condensation reaction to occur. On the other side, too high polymer concentration led to difficulties in the formation of single layers. Analogously, the upper limit for the dye concentration was established by clusters formation, while a minimum amount of the dye is required to avoid fluorescence detection problems. Several ratios of dye-polymer amount were tested to optimize the condensation reaction. In detail, the aim was to obtain an emitter concentration (c) on the sample surface, that provided:

- a minimum distance among dye molecules, preventing aggregates formation and dye-to-dye interaction ($c < c_{max}$).
- High fluorescence intensity with respect to the background ($c > c_{min}$).

It is important to highlight that the concentration limits (c_{min} and c_{max}) depend not only on the dye-monomer ratio as a result of the condensation reaction. The amount and the conformation of the polymer chains adsorbed onto the specific substrate play a role as well.

5.6.1 Dyes Aggregates in Solution

In order to meet the previous requirements on dye concentration, the right amount of chromophores and of PAH have to be mixed. With the purpose of testing the result for the different recipes, the final product was deposited by dipping technique on top of 2.5 PSS/PAH bilayers substrates (PSS terminated, prepared as explained in section 5.4.1) and the fluorescence was measured. In figure 5.6.3, experimental data for only two samples are shown as an example of analysis method: the aim is to find a range for the right amount of PAH and FR636.

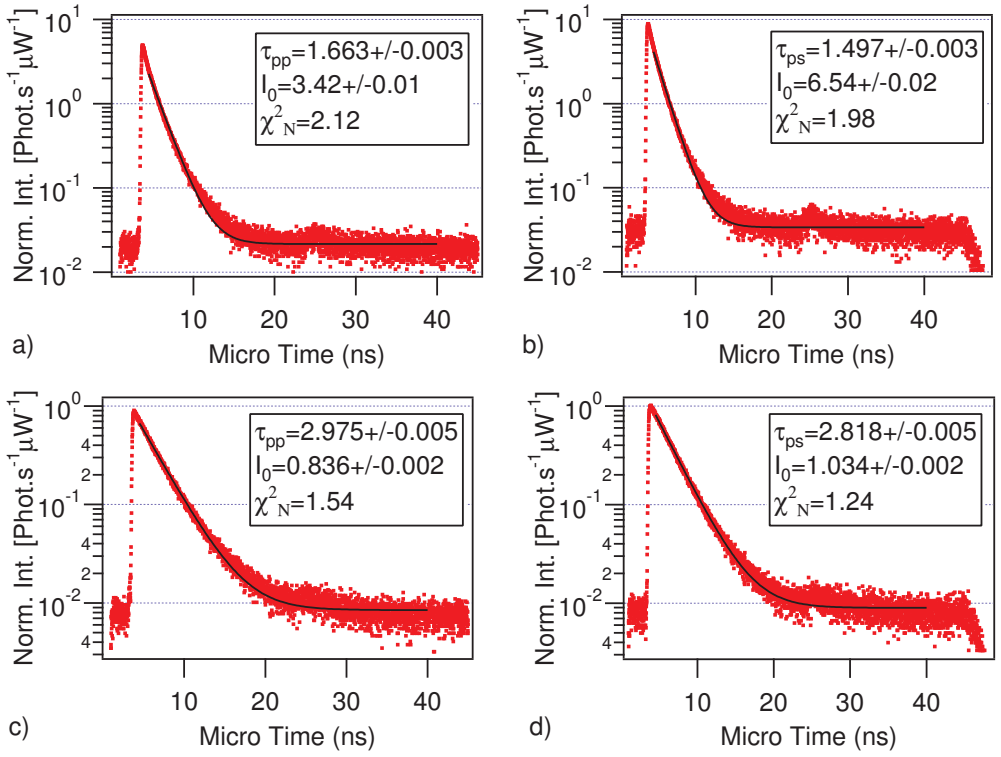

Figure 5.6.3: Fluorescence decay curves for dye FR636 covalently bound to PAH, deposited on 2.5 PSS/PAH bilayers (PSS terminated). Data in a) and c) is for *pp* polarization, while in b) and d) is for *ps* polarization. In the condensation recipe, 50 mg of PAH + 0.2 mg of FR636 dye were used in a) and b). 24.5 mg of PAH + 0.002 mg of FR636 dye were instead utilized in c) and d). In both cases the samples were dipped in the deposition solution for $\sim$ 1 hour. Afterwards the samples were rinsed 10 times in ultra-pure water, dried by N_2 stream. In the legends lifetimes (τ, in ns), intensities at time $t_0 = 3.8$ ns (I_0, in phot./(s $\cdot$ μW)) and normalized χ^2 values for the curve fitting (solid black lines) are reported.

Figure 5.6.3 shows the measured fluorescence decay curve, for *pp* and *ps* excitation-detection polarization combinations[3], as a comparison between two different polymer-dye ratios. Figures 5.6.3 a) and b) are for a recipe with 50 mg of PAH and 0.2 mg of FR636, while in figures 5.6.3 c) and d) 24.5 mg of PAH and 0.002 mg of FR636 dye have been used. Single exponential curve fits are plotted as black continue lines. In the legends, fluorescence lifetimes (τ_{pp} and τ_{ps}) and intensities at time $t_0 = 3.8$ ns (I_0) are reported[4]. Comparing the lifetimes and χ^2 values in figure 5.6.3, the recipe with higher FR636/PAH ratio (a and b) shows stronger deviation from single exponential behaviour and shorter lifetime, with respect to the other FR636/PAH ratio (c and d). This may be caused by chromophores self-quenching effect, leading to think of dye molecules aggregation. The recipe used for sample in figures 5.6.3 c) and d) may represent a reasonable compromise between single exponential behaviour (i.e. absence of dyes aggregates) and fluorescence intensity. Nevertheless, a key step for this work is the variation of the sample substrate and different substrates (like bare fused silica or sulfonatophenyl-silane groups) showed lower surface charge density than PSS/PAH. Hence, even using the recipe with higher FR636/PAH ratio (figure 5.6.3 c and d), fluorescence detection problems were experienced for substrates different from PSS/PAH (i.e. fluorescence signal was comparable to the background). To improve the detected signal, a direct increase of the FR636 dye concentration in the condensation reaction is not possible. In fact, as shown in figure 5.6.3, it leads to lifetime quenching as a consequence of the chromophores aggregation. In the same way, the increase of the functionalized polymer concentration in the deposition solution may bring large amounts of polymer not electrostatically adsorbed on the surface. In this situation, the formation of a single layer is not certain and the dye molecules may be partially embedded in the polymer film, preventing the study of fluorescence characteristics at the surface. It is therefore necessary to find first the highest dye concentration in solution that does not lead to chromophore clusters formation, successively it is possible to determine the right amount of PAH polymer which has to be added for the condensation reaction.

With the purpose of studying the aggregation effect, FR636 dye solutions with different concentrations were characterized by time resolved fluorescence and fluorescence spectra, in DMF (dimethylformamide) and water. The measurements results did not bring any valuable information, due to the strong fluorescence quenching in solution and to the difficult spectra interpretation: for data and discussion see Appendix A.3. The only technique providing some insights on dye solutions turned out to be dynamic light scattering.

Dynamic light scattering

Dynamic light scattering experiments for FR636 dye in aqueous and DMF solutions at different concentrations were performed. All the samples were prepared starting from an initial solution of FR636 dye at $1.31 \cdot 10^{-2}$ M in DMF.

Experimental Samples preparation and parameters used for measurements are described in chapter 2, in section 2.5.

Results and Discussion Figure 5.6.4 reports the dynamic light scattering results for FR636 dyes in aqueous solutions at different concentrations. All the samples were prepared diluting a dye solution at $1.31 \cdot 10^{-2}$ M in DMF. In figure 5.6.4 a), b) and d) the correlation intensity functions ($g_2(t)$) are

[3] Other polarization combinations have not been measured.

[4] For a definition of t_0 and an explanation of the fitting procedure for the lifetimes and the intensities, see chapter 4, section 4.4.2.

plotted as function of the time, respectively for pure water and free FR636 dye solution in water with concentrations of $\sim 10^{-5}$ M and $\sim 10^{-7}$ M. In c) and e), for the concentrations indicated in the legends, the associated particles size distributions calculated by data fit are shown.

The correlation curves in figure 5.6.4 b) and d) indicate that the chromophore aggregates diffuse in water within a time scale of few ms, while from c) and e) the corresponding apparent hydrodynamic radii distribution has a maxima around ≈ 100 nm. The peaks for larger radii values ($\approx 1-100\,\mu$m) are believed to belong to impurities (dust) present already in the cuvettes before the solution was added or to some "re-aggregation" of dyes in water, occuring after the filtration (filters pores size $0.22\,\mu$m). The structure appearing in the size distribution at very large radii (around ≈ 1 mm) are fit artifacts. Figure 5.6.5 shows the correlation intensity functions ($g_2(t)$) from dynamic light scattering data of FR636 dyes in DMF solutions for different concentrations. For all the samples there is no clear correlation regardless of concentration, indicating absence of dye molecules aggregates in DMF, above the experimental setup resolution ($\approx 2-3$ nm [22]). For single dyes an estimation of the size could be done directly from figure 5.6.1, leading approximately to $R_{app} \approx 1.5$ nm.

DMF appears to be a good solvent for the FR636 dyes for concentrations $\lesssim 10^{-5}$ M, while measurements in water show traces of chromophore aggregation at the same dilution degree. For experimental purposes the solutions were filtered by ~ 200 nm pores size syringe filters, as a consequence the radii distribution may be incomplete and larger aggregates be present in the original water solution (not filtered). Additional insights for the aggregation effect could be obtained from a dye solution at $\sim 10^{-7}$ M in water, but prepared from an initial chromophore solution at $\sim 10^{-5}$ M in DMF (for the last one the absence of aggregates has been already shown). The results for this experiment are displayed in figure 5.6.6: in a) the correlation intensity function is plotted as a function of the time, while b) shows the associate apparent hydrodynamic radii distribution.

Figure 5.6.6 a) and b) indicate the formation of aggregates, even if the starting solution ($\sim 10^{-5}$ M in DMF) did not show any evidence of chromophore clusters (see figure 5.6.5 b). Interestingly the correlation function and the the radii distribution reproduce quite well the results obtained from scattering of dyes in a water solution at $\sim 10^{-7}$ M, prepared from a solution at $1.31 \cdot 10^{-2}$ M in DMF: see figure 5.6.4 d) and e). Figure 5.6.6 may suggest the dye aggregation occurs in water (within the range of the concentration values explored).

The dye molecule was schematized in figure 5.6.7, to find a possible explanation for the results of dynamic scattering light experiments. In this figure, the chromophore molecule was sketched by a much simpler geometrical structure, highlighting the main charges, the hydrophobic part constituted by the aromatic rings and the hydrophilic parts represented by the polar groups.

With this scheme and the light scattering results, a hypothesis could be formulated on formation of micelles, tubular micelles or vesicles in water solution. Even stack-like structures have been shown to be possible for small molecular structures like hydrotropic compounds [23]. The broad size distributions in figures 5.6.4 c) and e), like in figure 5.6.6 b), may indicate the presence of some of these kind of aggregates.

Conclusions

Dynamic light scattering results suggest to dissolve the chromophore in DMF down to a concentration of at least $\sim 10^{-5}$ M and therefore add directly the dye solution to the buffer containing the PAH polymer. In the former protocols, the initial dye solution at $\sim 1.31 \cdot 10^{-2}$ M in DMF was diluted to $\sim 10^{-5}$ M in water before mixing with the buffer solution. A sketch of the initial protocol (old) and of the necessary changes (new) to avoid dye aggregation in solution is depicted in figure 5.6.8.

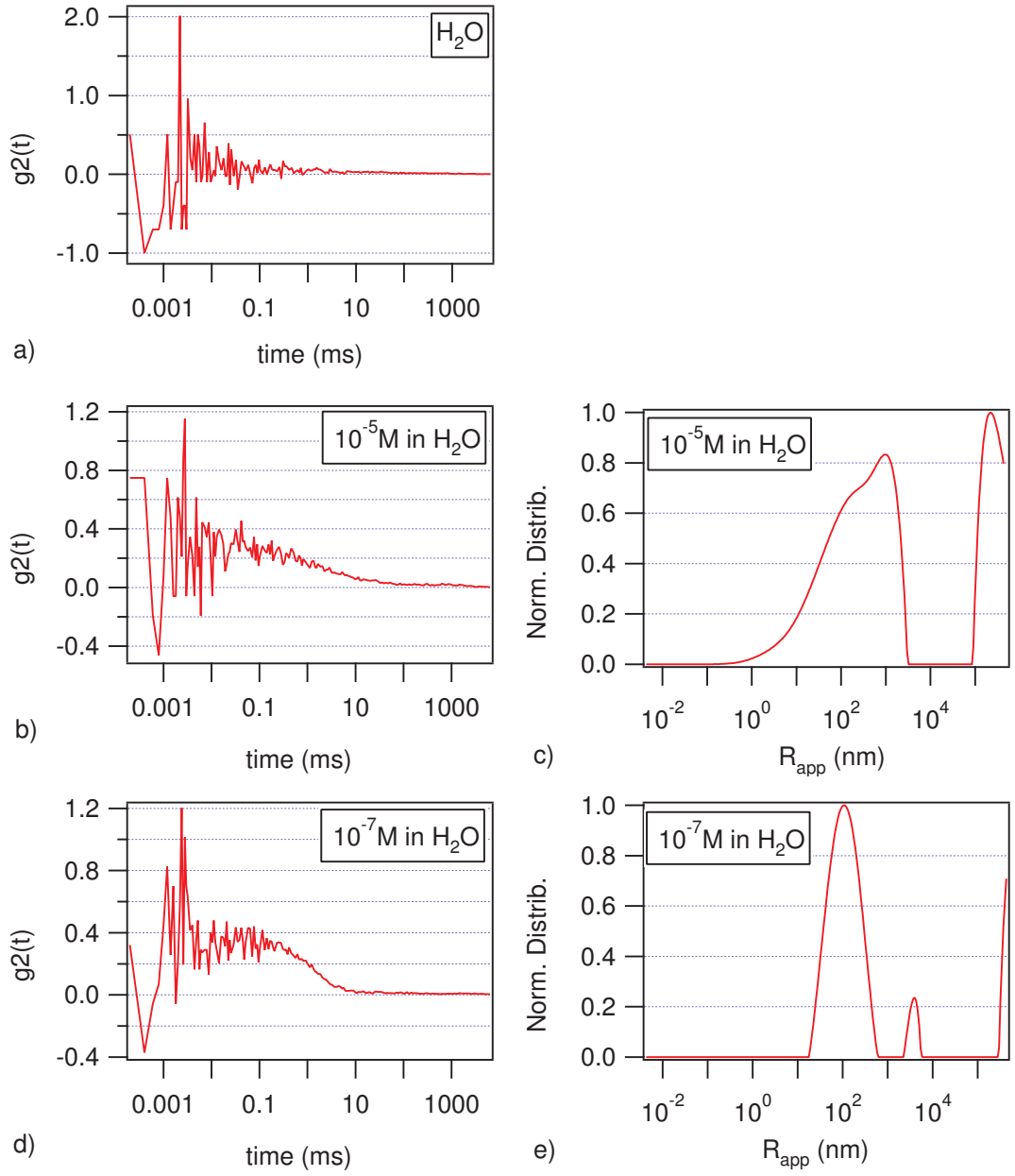

Figure 5.6.4: Correlation intensity function from dynamic light scattering data, for a) pure water, b) free FR636 chromophores in aqueous solution at $\sim 10^{-5}$ M, d) free FR636 chromophores in aqueous solution at $\sim 10^{-7}$ M. All the solutions were prepared diluting a dye solution $1.31 \cdot 10^{-2}$ M in DMF (dimethylformamide). In c) and e) the associated particles size distributions for the different concentrations (indicated in the legends) are shown.

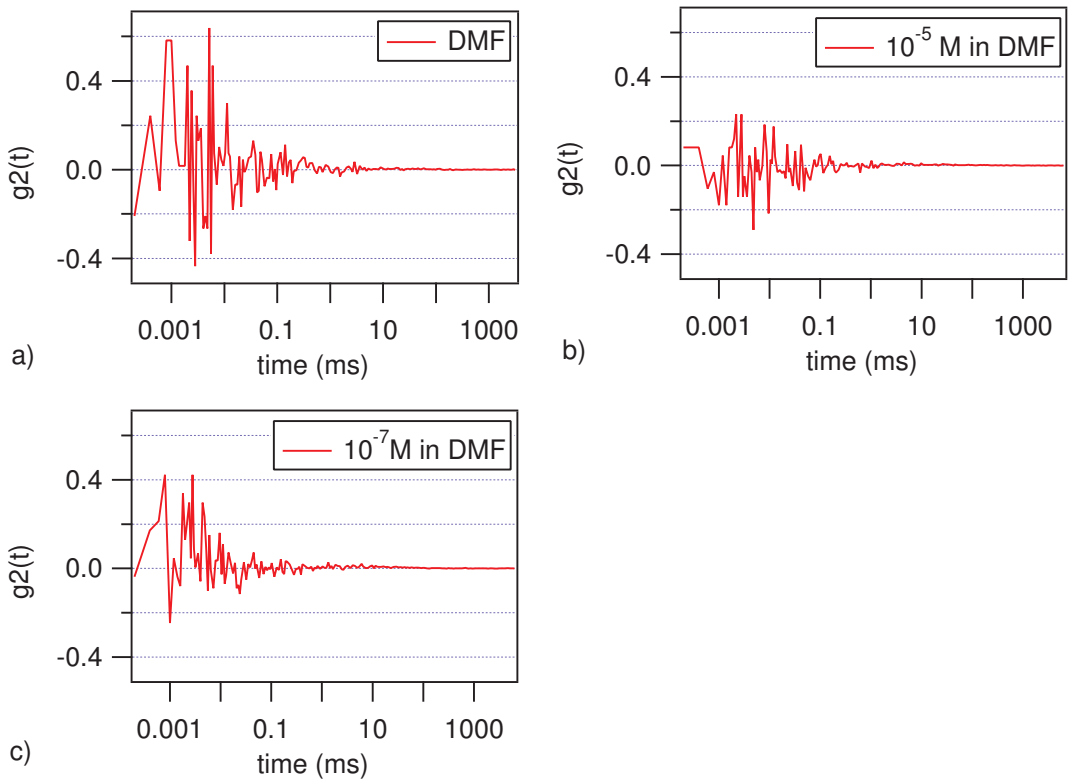

Figure 5.6.5: Correlation intensity function from dynamic light scattering data for: a) pure DMF (dimethylformamide), b) free FR636 chromophores in DMF solution at $\sim 10^{-5}$ M, c) free FR636 chromophores in DMF solution at $\sim 10^{-7}$ M.

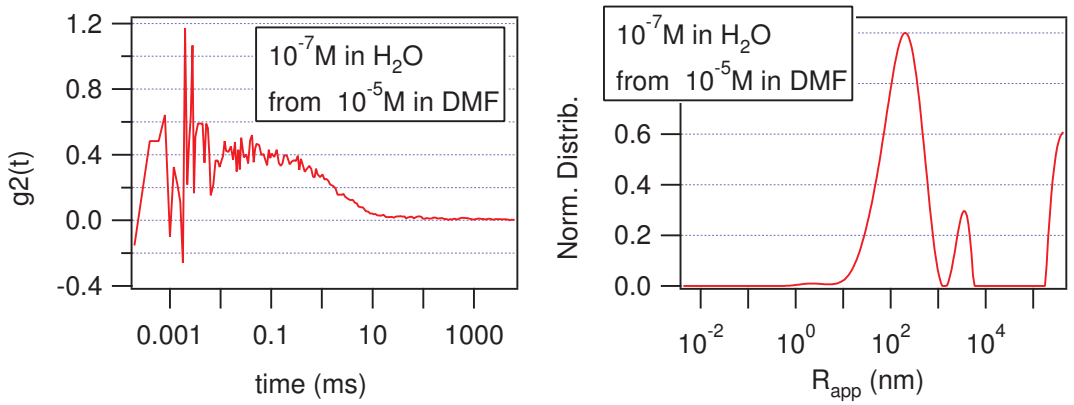

Figure 5.6.6: a) Scattering correlation intensity function, for free FR636 chromophores in water solution at $\sim 10^{-7}$ M, prepared by dilution from a solution in DMF at $\sim 10^{-5}$ M. b) Apparent hydrodynamic radius distribution for the sample in a).

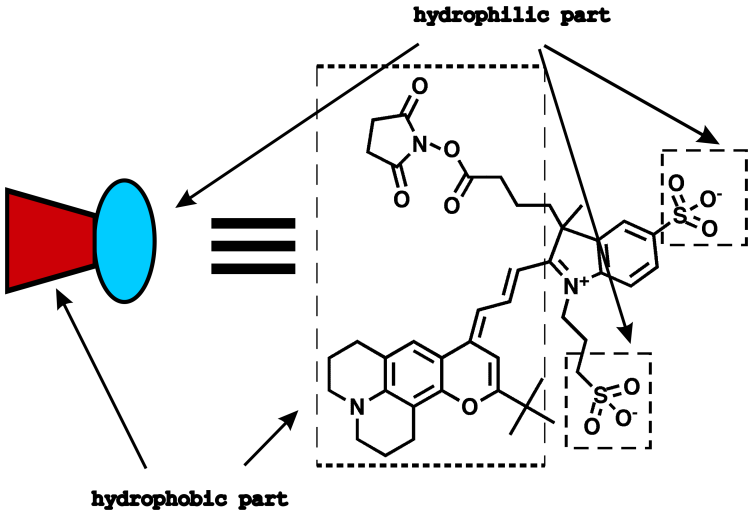

Figure 5.6.7: Schematization of FR636 dye molecule. Hydrophilic and hydrophobic parts of the structure are also shown.

The main difference is seen in the chromophore dilution in DMF, before mixing with the aqueous buffer solution containing the polymer. Due to the presence of PAH polyelectrolyte and bicarbonate, it was not possible to perform a dynamic light scattering experiment of the buffer solution after the addition of the dyes. Light scattering experiments in water in fact require extremely high purity of the solvent, in order to have reliable measurements, especially for small objects at low concentrations. The difference between the "old" and the "new" approach (see figure 5.6.8) can be thus evaluated only "a posteriori", by measuring the fluorescence lifetime and intensity for two samples prepared by the two procedures.

Figure 5.6.9 shows fluorescence decay curves of FR636 dyes covalently bonded to PAH polyelectrolyte, for *ss* polarization combination. The comparison is made between the "old" (5.6.9 a) and the the "new" dilution scheme (5.6.9 b), according to the sketch in figure 5.6.8. For both samples, the polymer is deposited by immersion on top of a plasma activated fused silica substrate, at pH $= 3$. The "new" dye dilution scheme (according to figure 5.6.8) provides better results in terms of single exponential behaviour (smaller χ^2 values), larger excited-state lifetime (τ) and higher fluorescence intensity (I_0).

5.6.2 Condensation Reaction

The PAH functionalization recipe for FR636 dye molecule was optimized, having the following constraints:

- Insolubility of PAH in DMF.
- Dye concentration in DMF $\lesssim 10^{-5}$ M, to prevent chromophore aggregation, based on light scattering results of the previous section.
- PAH concetration $\gtrsim 5 \cdot 10^{-6}$ M to make the condensation reaction possible (as it was verified by several tests).

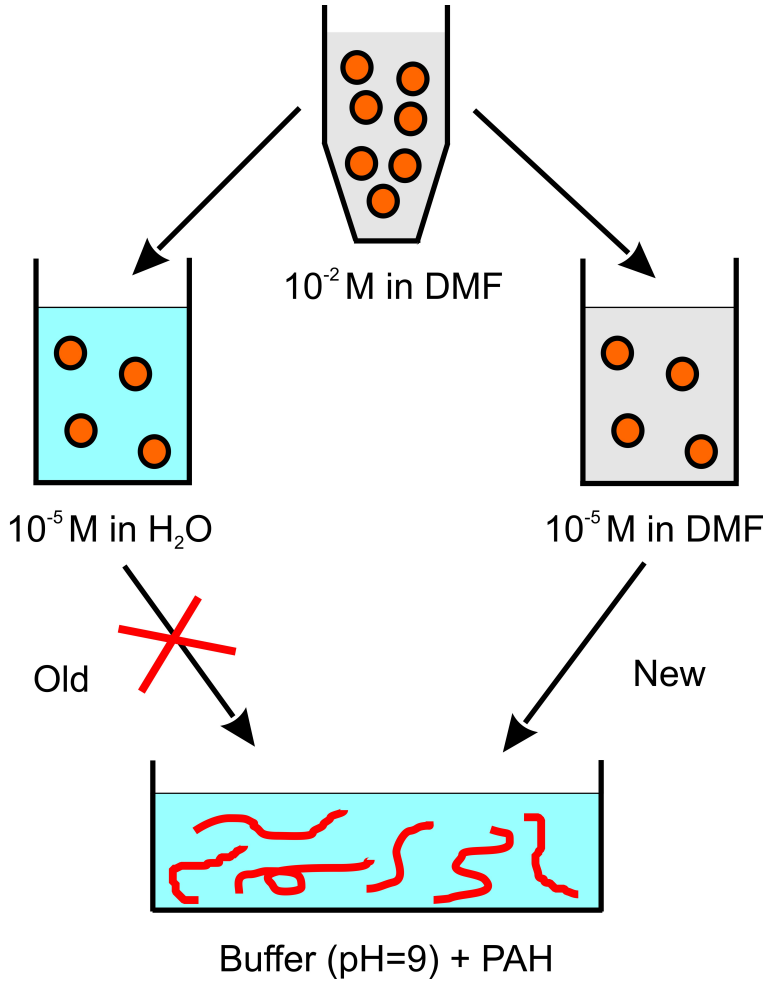

Figure 5.6.8: Schematization of main difference between process step in the former and new condensation recipes, according to light scattering experiments results.

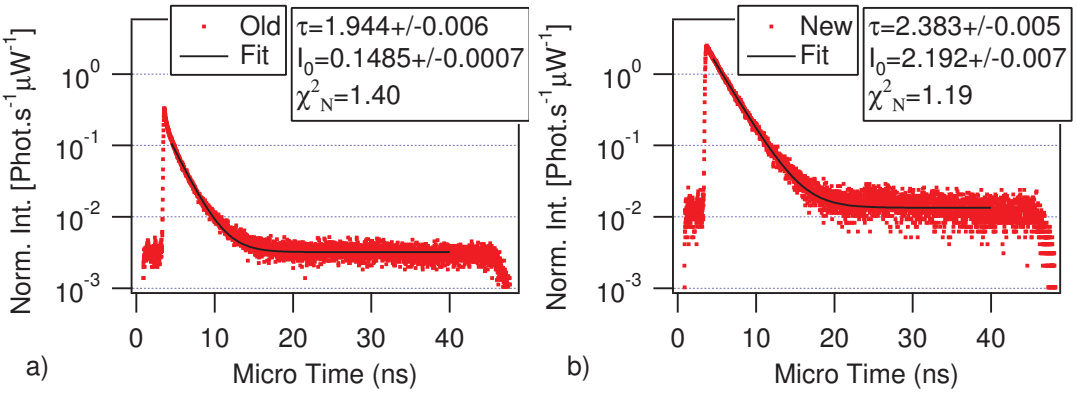

Figure 5.6.9: Fluorescence decay curves (*ss* polarization combination), for 1 layer of dye loaded PAH, deposited onto plasma activated fused silica substrate, at pH = 3. The polymer functionalization process was performed by the "old" scheme in (a) and by utilizing the "new" dilution scheme in (b), according to figure 5.6.8. Lifetimes (τ, in ns), intensities at time $t_0 = 3.8$ ns (I_0, in phot./(s $\cdot \mu$W)) and normalized χ^2 values for the curves fit are reported in the legends .

Experimental Details

Initially, 196 mg of PAH (CAS: 71550-12-4, $M_w \sim 15000$, Sigma Aldrich) were dissolved in 32 mL of a bicarbonate buffer solution previously prepared (420 mg of $NaHCO_3$ in 100 mL of ultra pure water: 50 mM, pH = 9.0). The solution was stirred to dissolve the polymer. The buffer solution gurantees that polymer monomers have mainly NH_2 groups instead of NH_3^+ groups. The NHS-modified fluorescent red dye FR636 (FR636 Red Reactive organic dye - Sigma Aldrich Inc., product no. 69296) was dissolved first in DMF (dimethylformamide) at a concentration of $5.24 \cdot 10^{-5}$ M and successively 8 mL of the dye solution were added dropwise to the stirring buffer solution. The dye addition was made only after the polymer was dissolved in the bicarbonate buffer. After mixing the components, the solution was kept stirring in the dark for 1 hour. Successively an Erlenmeyer flask was prepared with 400 mL of acetone and the incubated dye solution added by a Pasteur pipette while stirring. The purified FR-functionalized PAH was then collected by filtering the acetone solution and let the final product dry at $\sim 10^{-5}$ bar for about an hour. After drying, the polymer was diluted in ultra pure water to obtain a concentration of $\sim 1.2\,\mathrm{mg/mL}$. The pH was adjusted by adding HCl until the desired value. No salt was added.

Results and Discussion

PAH molecular weight In order to verify possible improvements in polymer functionalization process and polymer absorption onto substrates, a test was performed using PAH with molecular weight of 70 KDa. This was compared to PAH with a molecular weight of 15 KDa. To magnify the eventual differences between the two, a FR636 dye concentration of $\sim 1.5 \cdot 10^{-4}$ M was used in the functionalization recipe. In figure 5.6.10 the fluorescence decay curves for two ensembles of FR636 chromophores chemically bond to PAH chains having different molecular weights are plotted. The two different polyelectrolytes were deposited by dipping technique on top of a cleaned fused silica substrates. Dipping time was ~ 2 hours and the pH of the deposition solution was 3. Successively, the samples were rinsed 10 times with ultrapure water and then dried with a N_2 stream.

Figure 5.6.10 shows the average ratio between the two decay curves is ≈ 1.3 and the polymer with $M_w = 70$ KDa does not provide any improvement in the detected fluorescence intensity. The molecular weight is not a critical parameter for the condensation reaction (within the explored range) and the polymer absorption process on the surfaces. As a consequence, through all the following work, PAH polyelectrolyte with the lowest molecular weight (15 KDa) will be used in the experiments.

Recipe characterization The described process provides a certain ratio (r) between chromophores and PAH monomers, which can be calculated knowing the molecular weights of the dye ($M_w = 760.91$) and of the PAH monomer ($M_w = 92$), (see also figure 5.6.1):

$$r = \frac{92}{760.91} \cdot \frac{amount\ of\ FR636(g)}{amount\ of\ PAH(g)} \approx \frac{1}{5000} \tag{5.6.1}$$

The PAH utilized has an average molecular weight of $M_w \sim 15000$ and therefore for each polyelectrolyte chain there are about $15000/92 \simeq 160$ monomers. Then the equation 5.6.1 indicates that one chromophore every $5000/160 \simeq 30$ polymer chains is approximatively obtained, by the final recipe. It is important to observe that equation 5.6.1 fixes at the same time: the amount of dye molecules and the amount of PAH polymer used in the condensation recipe. Though these two variables can not be freely varied, due to the constraints given at the beginning of the section 5.6.2, different ratios

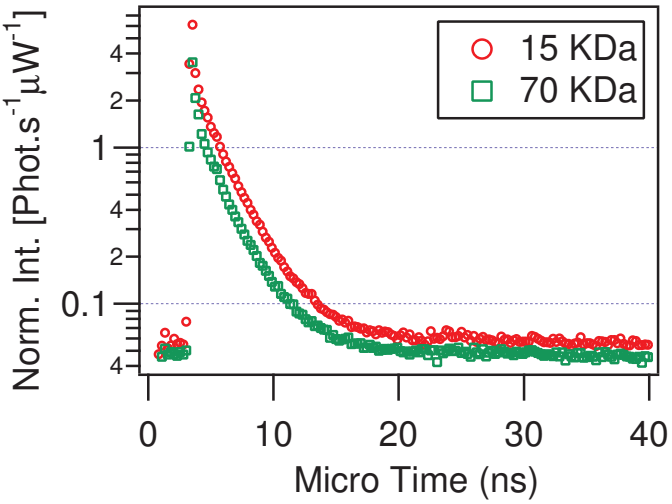

Figure 5.6.10: Fluorescence decay curves of FR636 dye chemically bond to PAH chains having molecular weight 15 KDa and 70 KDa. The functionalized polymer is then deposited on top of a cleaned fused silica substrate.

were tried in order to find optimum conditions. The optimized condensation reaction was tested by depositing the functionalized polymer directly on plasma activated fused silica cover slips, by dipping the slides for ~ 1.5 hours in the dye loaded polymer solution, at pH ~ 3. For the glass surface activation the plasma recipe number 4 in table A.5.1 (Appendix A.5) was utilized . The samples were rinsed once in ultrapure water and afterwards dried with a N_2 stream. Figure 5.6.11 shows a comparison among fluorescence intensities, for different polarization combinations and several condensation recipes used. The recipes are specified by two main parameters:

- the dye-monomer ratio r (equation 5.6.1).
- The amount of functionalized PAH dissolved in 1 mL of ultra-pure water, in the solution used for polymer deposition.

In figure 5.6.11 a) the optimized recipe ($r = 1/5000$, final product dilution of 1.2 mg/mL) provides better results for *pp* and *ps,* being those the polarization combinations critical in terms of intensities during measurements. Figure 5.6.11 b) depicts the fluorescence intensity for *pp* polarization (I_{0pp}) plotted against the lifetime (τ_{pp}): it is possible to observe the optimized recipe shows the highest intensity and the largest lifetime, indicating a smaller influence of the self-quenching effect. In figure 5.6.12 the fluorescence decay curves for the four different recipes compared in figure 5.6.11 are reported, for *pp* polarization combination. The optimized recipe guarantees the highest intensity and a better single-exponential behaviour.

Once the recipe was set, some optical properties of the dye loaded polymer were investigated. In figure 5.6.13 the comparison between the fluorescence spectra of the free dye and of the dye covalently bond to PAH is reported, both in an ultra pure water solution. For the measurements an excitation wavelength at 610 nm and slits aperture of 2 mm were used for the dye free in solution. Excitation wavelength was 620 nm and slits aperture of 4 mm for the functionalized polymer in water. The measurements were performed by a fluorescence spectrometer Spex Fluorolog II - 212.

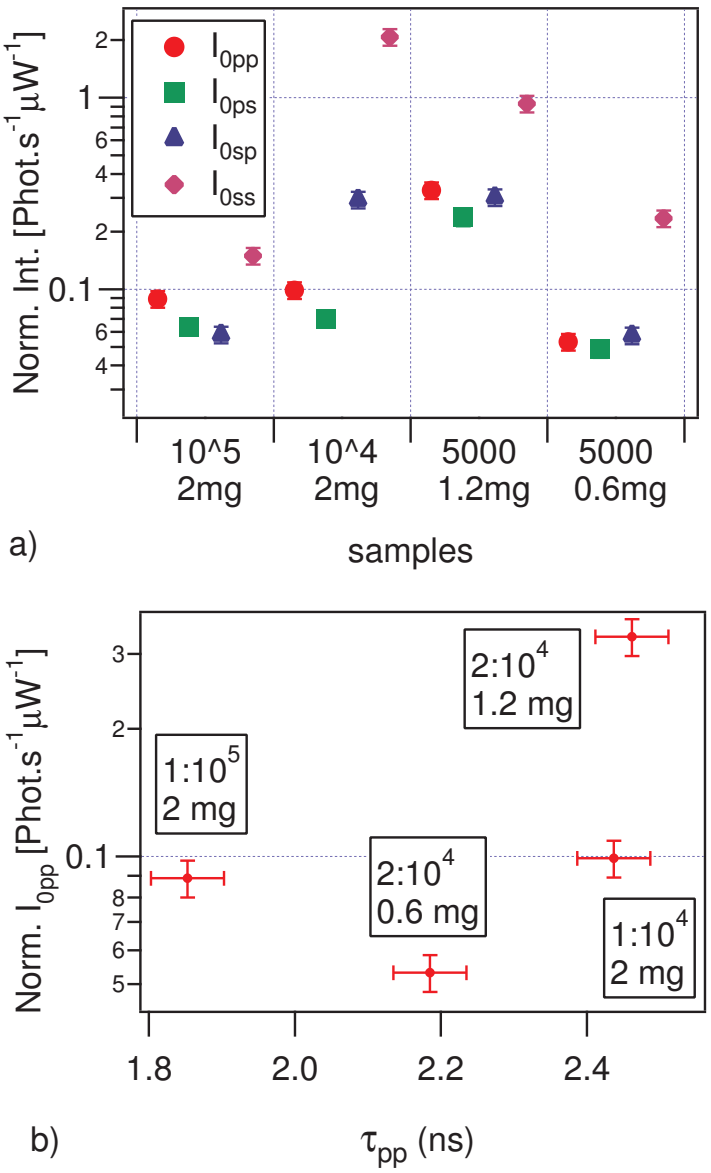

Figure 5.6.11: a) Fluorescence intensities for different polarization combinations and different condensation recipes for PAH functionalized with FR636 chromophore. The first row in abscissa reports the estimated number of PAH monomers between two dyes, while the second row in abscissa indicates the amount of functionalized polymer dissolved for 1 mL of the deposition solution. The markers represent an error on intensity of 10%. b) Fluorescence intensity plotted against the lifetime for recipes in a), for *pp* polarization combination. The main recipes parameters are reported in the text boxes: the estimated ratio dye-monomer *r* (according to eq. 5.6.1) and the amount of functionalized polymer (in mg) for 1 ml of the deposition solution. Error on lifetime is ±0.05 ns, while error on intensity is 10%.

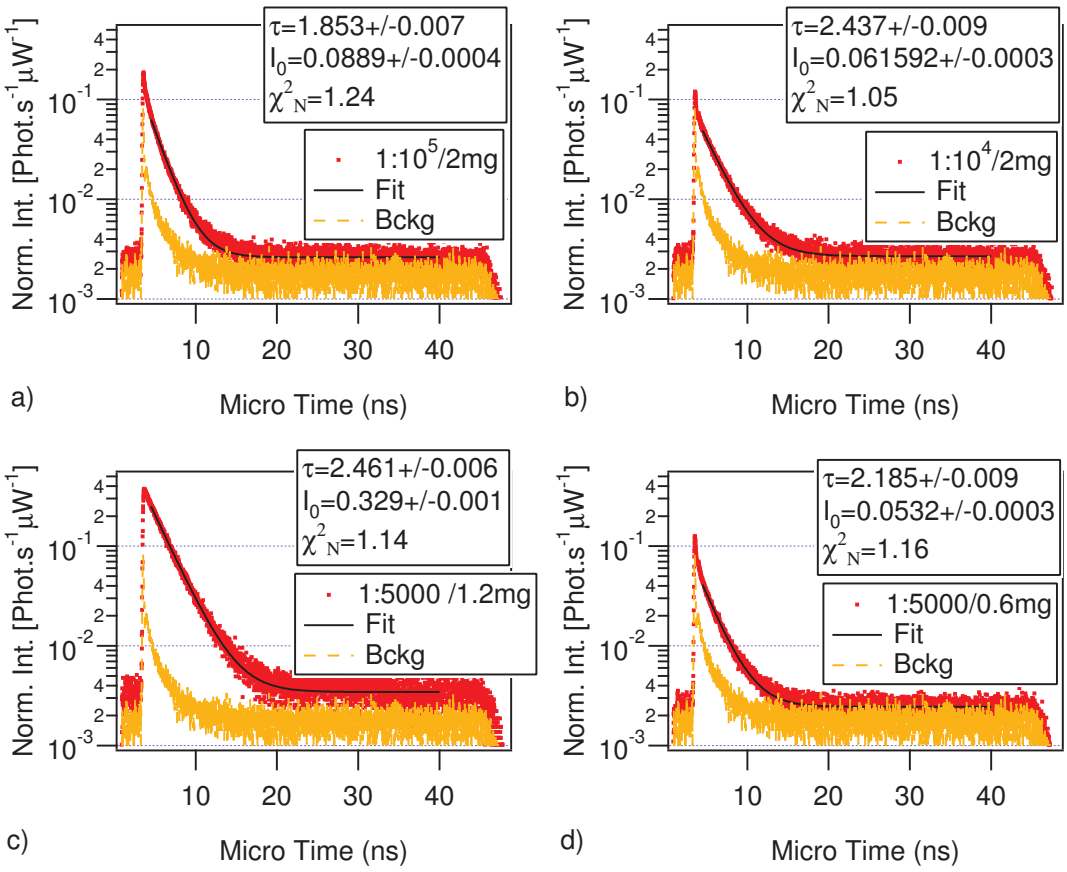

Figure 5.6.12: a)-d) Fluorescence decay curves of the several condensation recipes utilized for PAH functionalized with FR636 chromophore (for *pp* polarization combination). The estimated ratio dye-monomer r (according to eq. 5.6.1) and the amount of functionalized polymer (in mg) for 1 mL of the deposition solution are reported in the legend. The fit curves and relative fit results (lifetime τ in ns, intensities I_0 in phot./$(s \cdot \mu W)$ and χ^2_N) are shown for each single recipe, together with the setup background (Bckg).

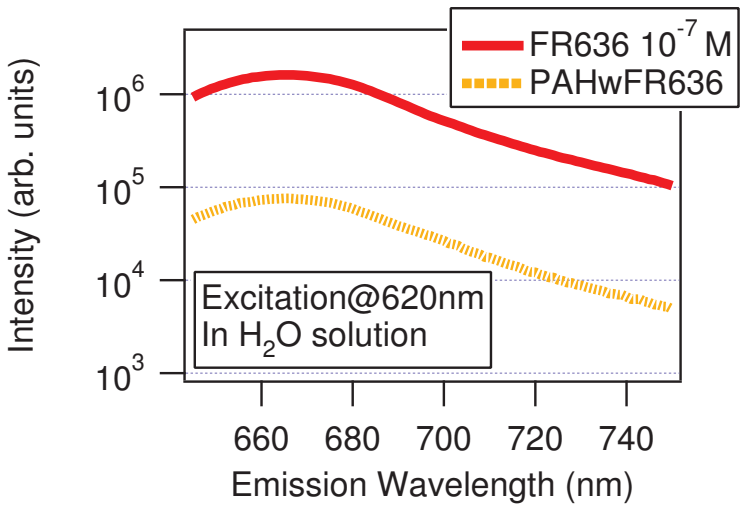

Figure 5.6.13: Fluorescence spectra of FR636 dye molecules in solution at $\sim 10^{-7}$ M and covalently bond to PAH chains in ultrapure water, by using the optimized recipe ("PAHwFR636" in the legend).

In figure 5.6.13 there are not significant spectra changes and it is possible to conclude that the functionalization process does not alter the fluorescence properties of the chromophore.

Conclusions

A functionalization reaction to covalently bind the FR636 organic dye to PAH polyelectrolyte chains was set. The estimated ratio is of one chromophore each ≈ 30 polymer chains. The designed condensation reaction provides samples, for which high fluorescence intensity (with respect to the background) and single exponential decay curves are detected in the far field. The specific functionalization process maximizes the measured excited-state lifetime and it does not alter the optical properties of the chromophores.

5.6.3 Post-deposition variables

The final polymer-interface structure is driven not only by deposition conditions (like pH [41] or ionic strength [44]) but also by post-deposition treatments, like rinsing, drying and storage. In particular for layer-by-layer technique applied to polyectrolytes deposition, a large amount of non specific adsorbed polymer (not elecrostatically bond) may be present at the surface. This would lead to a poor control of the deposition process and of the interface architecture. On the other hand, to study optical properties of dyes at interfaces, an accurate definition of the surface geometry is needed. Therefore a rinsing step after deposition has to be performed in order to remove non specific absorption of functionalized PAH onto the substrate [42]. Moreover from fluorescence lifetime measurement of dyes in solution, it was observed that water represent a strong quencher for fluorescence emission, in the case of the FR636 chromophore (see figure A.3.1 in Appendix A.3). PAH and PSS are polyelectrolytes well soluble in water and making use of the layer-by-layer technique for deposition, residual trapped water within the polymer matrix may represent an issue [16].

In this respect, a study of fluorescence characteristics was performed, as function of the rinsing steps and of the time lag between the dye-loaded polymer deposition and the measurements (for discussion and results see Appendix A.4). As a result: to obtain reliable measurements of excited-state lifetimes and fluorescence intensities, after the functionalized polymer deposition, the samples were rinsed 5 times (minimum), dried by a nitrogen stream and left at room condition for at least ~ 6 hours.

5.6.4 Variation of the Substrate

Sample surface plays a relevant role in the polymer absorption process and different substrates may provide interesting information about the fluorescence characteristics of dye loaded chains on the surface. For instance, changes in fluorescence as a function of the functionalized PAH chains morphology could be revealed. A comparison with theory for the two limit situations of dyes “in air” and “in polymer” can be done and thus microscopic electromagnetic phenomena investigated.

The PSS polyelectrolyte constitutes an optimum substrate due to high surface charge density and entanglement properties (i.e. high amount of polymer adsorbed). On the other hand the surface roughness and inhomogeneity may constitute a source of indetermination on the chromophores exact position. Other susbstrates with lower roughness properties, like fused silica, show a smaller surface charge density and the amount of adsorbed polymer can be an issue for the fluorescence detection. To solve this, a surface treatment or functionalization (i.e. silanization) is necessary. As a consequence,

larger amounts of adsorbed polymer are needed to obtain the surface charge inversion (overcompensation) and therefore to stop layer deposition. In the following, the substrates constituted by PSS/PAH polyelctrolytes, bare fused silica and sulfonatophenyl-silane groups will be studied.

PSS/PAH Polyelectrolytes Substrate

Samples preparation 2.5 PSS/PAH bilayers, terminated by PSS, were deposited on glass according to the method described in section 5.4.1. Fluorophores were successively added onto the substrate by dipping the glass slides for 45 minutes in a water solution containing dye-loaded PAH chains at pH = 3. Sample was rinsed 5 times with ultra pure water and dried with nitrogen stream.

Characterization It is possible to have an estimation of the PSS surface charge density, considering that the amount of material for an adsorbed polyelectrolyte layer is typically $\approx 1 \div 5\,\mathrm{mg/m^2}$ [17] and the PSS $M_w \sim 70000$. Therefore the weight of a single chain is $\sim 1.2 \cdot 10^{-19}\,\mathrm{g/chain}$. For an average surface coverage of $\approx 2.5\,\mathrm{mg/m^2}$, a chain density as high as $\approx 2 \cdot 10^{12}\,\mathrm{chains/cm^2}$ is obtained. Considering each chain having $70000/206 \simeq 340$ monomers, the monomer density for PSS is $\approx 10^{14}\,\mathrm{monomers/cm^2}$. Other authors report a monomer density $\approx 10^{16}\,\mathrm{monomers/cm^2}$ [21]. The PSS is classified as strong polyelectrolyte and in the explored pH range $(3 \div 9)$ its ionization degree is constant (pKa $\simeq 1$, [28]). With the assumption that all the monomers carry a negative charge, the surface charge density is between $\approx 10\,\mu\mathrm{C/cm^2}$ and $\approx 1\,\mathrm{mC/cm^2}$ for a PSS substrate.

For PAH the weight for single chain is $\sim 2.5 \cdot 10^{-20}\,\mathrm{g/chain}$ with $15000/92 \simeq 163$ monomers for each chain. Thus the monomer density is again around $\approx 10^{14}\,\mathrm{monomers/cm^2}$ (always considering an average absorption amount of $\approx 2.5\,\mathrm{mg/m^2}$). The optimized condensation recipe (section 5.6.2) provides roughly one dye every 5000 monomers[5], therefore in the case of dye loaded PAH deposited above PSS layer it could be possible to estimate $\approx 10^{11}\,\mathrm{dyes/cm^2}$.

Results and Discussion In figure 5.6.14 the comparison between theory and experiment for fluorescence lifetimes a) and intensities b) is plotted for different excitation-detection polarization combinations. The measured values are for PAH chains functionalized with FR636 dyes and depositd on top of 2.5 PSS/PAH bilayers, PSS terminated ($\approx 6\,\mathrm{nm}$, see chapter 4). The theoretical values are calculated for two different cases:

- for an ensemble of 900 dye molecules, that are located 0.5 nm above a 6 nm polymer film with a dielectric constant $\varepsilon = 2.319$ (i.e. “in-air”).
- for the same dyes embedded in the polyelectrolytes matrix at 0.5 nm from the polymer-air interface (i.e. “in-polymer”).

In the simulation, $\Delta\theta, \Gamma_{nr}$ and Γ_0 parameters as determined by the Polarization Combination Method (see chapter 4) have been used.

From figure 5.6.14 a) a good agreement between experimental lifetimes and simulated values for the case of chromophores embedded in polymer is observed. Fluorescence intensities in figure 5.6.14 b) give instead a poor agreement. Figures 5.6.14 a) and b) indicate that the emitters experience the same surrounding optical environment as when embedded in the polymer side. This occurs even if they are

[5] Condensation yield is not considered.

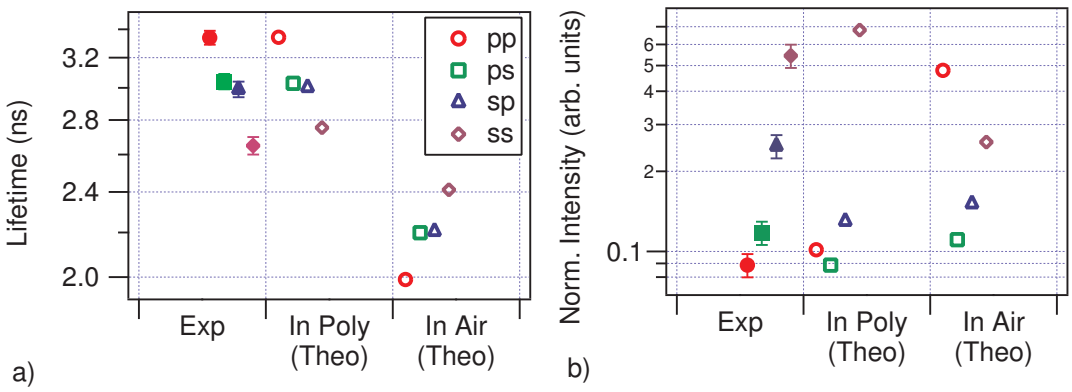

Figure 5.6.14: a) Comparison between simulated (*Theo*) and experimental (*Exp*) fluorescence lifetimes, for different excitation-detection polarization combinations. The simulations are for an ensemble of 900 dye molecules above 2.5 PSS/PAH bilayers (*In Air*) and embedded in the polyelectrolytes matrix (*In Poly*), at 0.5 nm from the air-polymer interface in both cases. b) Same comparison than in a) but for fluorescence intensities. In the simulation, the physical parameters of FR636 have been determined by PCM in chapter 4. Experimental error for lifetimes is ± 0.05 ns, while for intensities is $\pm 10\%$.

covalently bonded to the uppermost PAH layer. Such effect may be due to the specific nature of PAH and PSS polyelectrolytes films: they consist of stratified structures in which polyanions and polycations of individual layers interdigitate one another intimately, with an interface roughness between adjacent layers up to $\sim 2 \div 3$ nm [30]. It is interesting that the analysis of polarized fluorescence confirms this stratified nature, providing an indication for the chromophores position in the range of very few nanometers.

Conclusions Functionalized PAH chains were deposited on top of a PSS/PAH polyelectrolytes spacer and fluorescence characteristics were analyzed. The covalently bond organic dyes experience an "in polymer" surrounding environment, in spite of the surface roughness and the interdigitation depth are of the same order of magnitude of the chromophores size (i.e. $\approx 2 \div 3$ nm). Numerical simulations indicate a quite good agreement between theory and experiments, for excited state lifetimes, thus confirming the "in-polymer" behaviour of the emitters. It is interesting to note that the classical model used for calculations did not include any local field correction. Deviations for fluorescence intensities are believed to be a consequence of approximations in system modelling: dyes position within the multilayer system and refractive indices values. A contribution may be also coming from a non ideal behaviour of optical components utilized in the measurements (filters, polarizers, lens).

Fused Silica Substrate

Sample preparation UV-grade fused silica slides were cleaned and treated with the chemical treatment explained in section 5.4.1.

Characterization and optimization Figure 5.6.15 shows a comparison between the decay curves of FR636 dye, covalently bond to PAH chains, deposited directly on top of a bare glass slide and on top of 2.5 PSS/PAH bilayers (PSS terminated). In both cases, the fluorophores were deposited

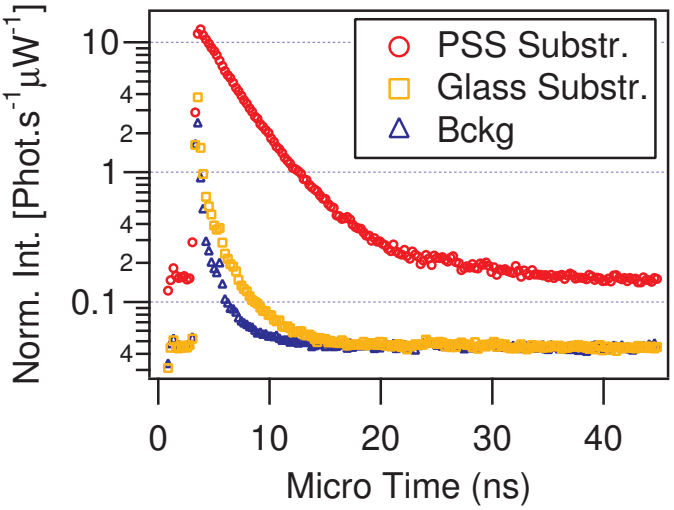

Figure 5.6.15: Fluorescence decay curves comparison for FR636 dye covalently bond to PAH chains, deposited directly on fused silica cover slip and above 2.5 PSS/PAH bilayers spacer, PSS terminated, by using ~ 1 hour as immersion time and pH $= 3$. The setup background ("Bckg" in the legend) is also plotted. Data is for *pp* excitation-detection polarization combinations, other polarization combinations provide same results in terms of intensities comparison and are not reported here.

by immersing the substrates for ~ 1 hour in a water solution containing the dye-loaded polymer, at pH $= 3$. Successively the samples were rinsed 10 times in ultra pure water and dried by a N_2 stream.

Figure 5.6.15 indicates that the total fluorescence intensity (area integral under the decay curve) is much higher for the PSS substrate, with respect to the fused silica. In this latter case the signal detected is comparable with the background, indicating that the amount of functionalized PAH adsorbed is too low to be detected by far field measurements. The difference in surface charge density between PSS and fused silica substrates may represent the main cause of the large intensity variation in figure 5.6.15. In general surface charge density values for fused silica range from $\sim 0\,\mu C/cm^2$ at pH $\simeq 2$ to $\sim 24\,\mu C/cm^2$ at pH $\simeq 9$ [43], while if all the monomers carry a negative charge, the surface charge density for PSS is between $\approx 10\,\mu C/cm^2$ and $\approx 1\,mC/cm^2$. A different glass surface treatment was tested in order to increase the substrate charge density (see Appendix A.5), but no significant improvements were observed.

Conclusions Fused silica glass constitutes an ideal substrate for the extremely low fluorescence background and surface roughness (RMS ~ 0.5 nm). Nevertheless due to the lower surface charge density with respect to PSS substrate and the strong dependence of surface charges to pH, fluorescence intensity issues were encountered. The surface charge density of fused silica does not guarantee a sufficient amount of polymer adsorbed, therefore a rinse step after deposition process may wash most the polyelectrolyte chains away.

$SiSO_3^-$ Substrate

The PSS susbstrate guarantees an high surface charge density (up to $\approx 1\,mC/cm^2$) but surface roughness is around 2 nm, moreover the chains interpenetration effect represents a limit to study fluorescence of dyes on the surface. On the other hand, fused silica shows good flatness (~ 0.5 nm)

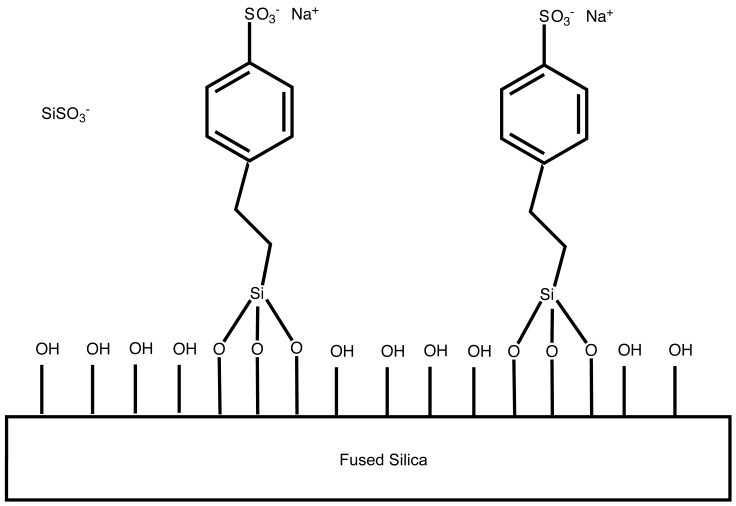

Figure 5.6.16: Sketch of the fused silica substrate functionalized by sulfonatophenyl groups ($SiSO_3^-$).

and porosity at the angstrom level [35], but lower surface charge density (maximum $\sim 24\,\mu C/cm^2$). Fused silica substrate modified by sulfonatophenyl groups ($SiSO_3^-$) may represent a compromise between high amount of adsorbed polymer (i.e. high fluorescence intensity) and weak dependence of the ionization degree from pH. This kind of silane are typically $\approx 1\,nm$ long (see figure 5.6.16) and therefore, the resulting substrate roughness should not represent an issue for the chromophores with an average size $\approx 3\,nm$.

Sample preparation After standard cleaning procedure (see section 5.4.1), the substrates were immersed in a Piranha solution ($H_2O_2 : H_2SO_4$ and $3:7$ relative amount ratio). H_2SO_4 solution $95-97\%$ (Fluka - Sigma Aldrich) and H_2O_2 solution 35% (Sigma Aldrich) have been used. The slides were dipped in the solution for 3 hours, successively rinsed 20 times by ultra pure H_2O (MilliQ, resistivity: $18.2\,M\Omega\cdot cm$) and finally left in a desiccator a $10^{-5}\,bar$ for an hour. By using extra dry toluene (Acros Organics, 99.85%, extra dry, water $< 30\,ppm$) a solution at 1% v/v of 2-(4-Chlorosulfonylphenyl)ethyltrichlorosilane ($C_8H_8Cl_4O_2SSi$, CAS: 79793-00-3, ABCR GmbH & Co. KG, prod. AB129108) was prepared and the glass substrates immersed for 2 hours [36]. The glass container was filled by Argon and wrapped with parafilm to minimize solution exposition to environmental moisture. The fused silica slides were afterwards rinsed 3 times in tetrahydrofuran (THF, Sigma Aldrich) by using ultrasounds for 15 minutes and then dried with N_2 gas. The substrates were then treated with a 2N solution of H_2SO_4 ($95 \div 97\%$ Fluka - Sigma Aldrich) for 12 hours at 80Â°C [38]. After rinsing 20 times with ultra pure H_2O (MilliQ, resistivity: $18.2\,M\Omega\cdot cm$), the glass slides were left in a 1 M NaCl solution for about 1 hour and successively in a 0.1 M NaOH solution to restore the pH to neutral values. As final step, the samples were rinsed 20 times with ultra pure H_2O and kept under ultrapure water. To deposit the dye loaded polymer above the silanes, the samples were left in the polymer solution overnight, without salt added. The following day the substrates were rinsed 10 times and dryed with a N_2 stream. Afterwards, the slides were left for 1 day at room temperature for complete residual water removal and the fluorescence was successively measured.

Characterization and optimization of $SiSO_3^-$ substrate For the used silanes some authors assume a surface density of $4\,molecules/nm^2$, that is the experimental value for the monolayer of 2-(4-cholorosulfonylphenyl)ethyltrimethoxysilane on a water surface [36], [37]. Fused silica does not have

	$SiSO_3^-$	PAH + FR636 (on $SiSO_3^-$)
angle (Â°)	12.1	50.2

Table 5.6.1: Contact angles values for $SiSO_3^-$ silane substrate and for 1 monolayer of dye loaded polymer, deposited onto the $SiSO_3^-$ surface.

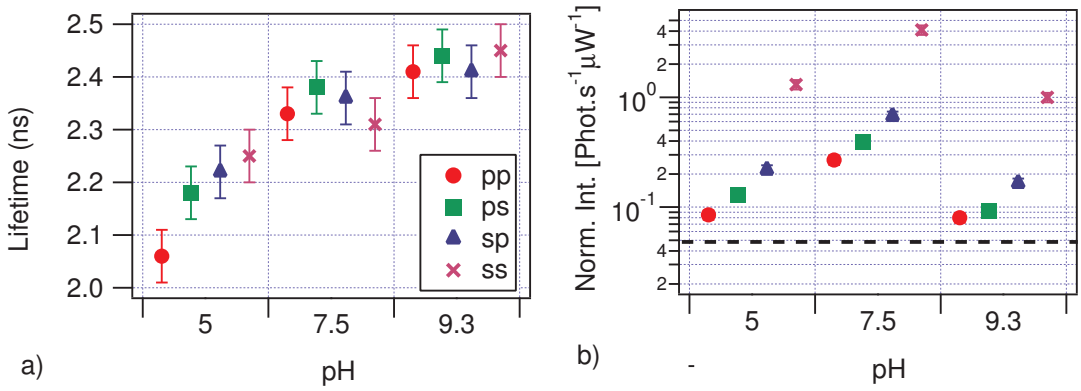

Figure 5.6.17: Measured fluorescence lifetime (a) and intensities (b) for different polarization combination and different pH values of the deposition solution. The dye loaded PAH is deposited on top of a $SiSO_3^-$ substrate. The samples were rinsed 10 times and dried by nitrogen, then they were left for 1 day at room conditions. The different solutions containing the functionalized polymer are without any salt. Error on lifetime it is ± 0.05 ns, while error on intensity it is 10%. An estimated fluorescence detection limit, for reliable measurements, is also reported in figure by a dashed horizontal line (see also section 5.3).

the same OH groups density of water and during the silanization process, two ion exchange steps are involved to reach the final structure on the surface. Therefore the expected number of sulfonatophenyl groups on the surface is less than 4 molecules/nm^2. Nevertheless, even considering the same density of OH groups on a water surface, then the maximum charge density would be $\sigma \approx 10\,\mu$C/cm^2. A first surface characterization can be done by contact angle measurements to check the substrate hydrophilicity. In table 5.6.1 the contact angle data are shown: for a bare $SiSO_3^-$ substrate and for a surface constituted by 1 monolayer of functionalized PAH polymer deposited on top of $SiSO_3^-$ silanes.

Table 5.6.1 indicates that the used silanes are hydrophilic, while dye loaded polymer adsorption changes the surface toward a more hydrophobic substrate. This could be due to carbon chains of the polyelectrolyte. The hydrophilicity degree of $SiSO_3^-$ surface is comparable with the values for bare silica glass (see table A.5.1 in Appendix), but stability of the carried charges against pH changes is much higher than for glass.

Results and discussion Figure 5.6.17 reports measured lifetimes (a) and intensities (b), for FR636 dye chemically bonded to PAH chains onto $SiSO_3^-$ substrate. Data are for different polarization combinations and different pH values of deposition solution[6].

A first qualitative analysis of figure 5.6.17 a) shows that, at low pH, most of the chromophores experience "air" as optical environment (compare with figure 5.2.2). This result agrees with the picture of

[6]For these set of measurements a new glass polarizer was used in front of PMT. Detected intensity was reduced about a factor ~ 3 but better selectivity among different polarization combinations was achieved.

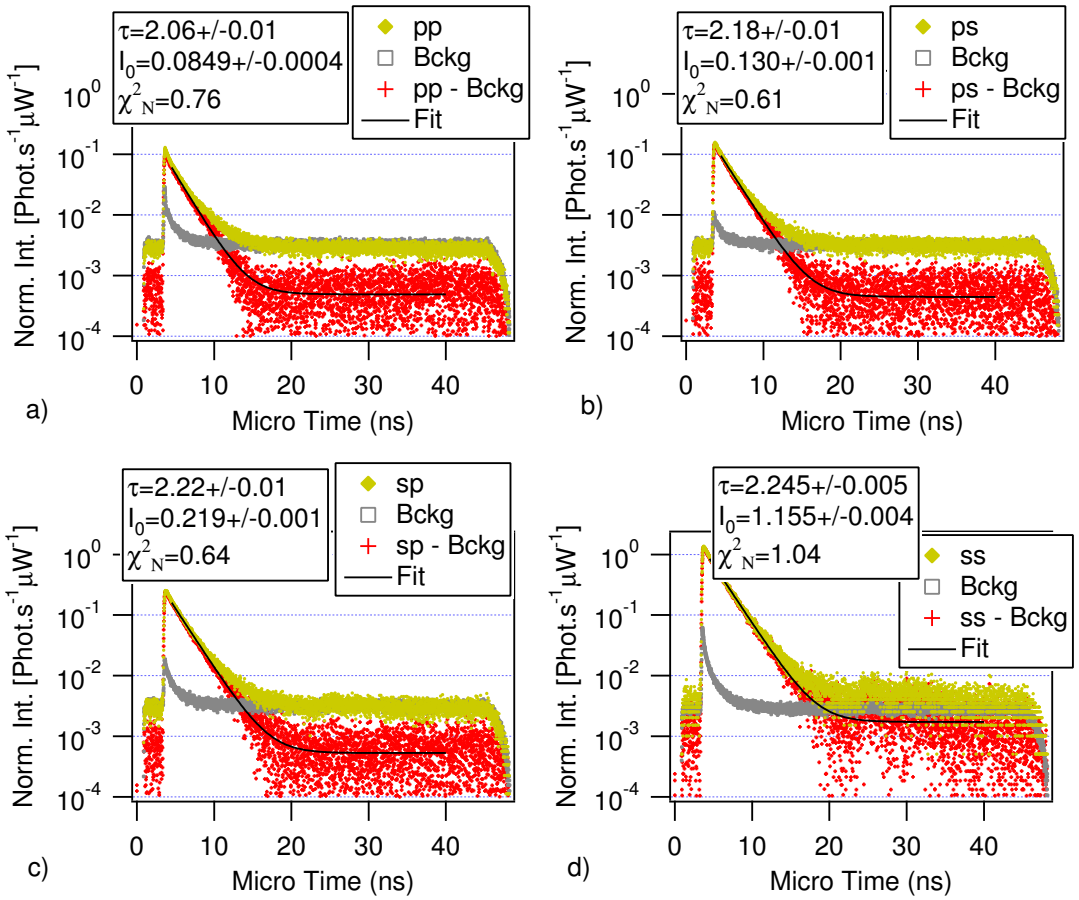

Figure 5.6.18: Measured fluorescence decay curves (rhombi) for dye loaded PAH, deposited at pH = 5, onto $SiSO_3^-$ substrate. Different excitation-detection polarization combinations are considered, as indicated in the legends. Instrument background (squares), experimental data with background subtracted (crosses) and correspondent fits are also reported. Lifetimes (τ, in ns), intensities at time $t_0 = 3.8$ ns (I_0, in phot./(s · µW)) and normalized χ^2 values for the curves fit are shown.

chains deposited as trains (rod-like shape) on the substrate, in acid environment (because of the high ionization degree of the monomers). On the other hand, at higher pH (i.e. lower degrees of ionization) the polymer has mostly a loop-like conformation, after deposition on the surface. In this latter situation, the polyelectrolyte chains may constitute themselves the environment surrounding the dyes and thus many more chromophores may experience "polymer" as optical environment. Vice versa, the fluorescence intensities in figure 5.6.17 b) indicate a physical situation where most of the dyes should be fully embedded in the polymer matrix (compared to figure 5.2.2), in complete opposition to the excited-state lifetimes behaviour.

Figures 5.6.18, 5.6.19 and 5.6.20 show the measured decay curves for dye loaded PAH, deposited on $SiSO_3^-$ substrate, at pH = 5, pH = 7.5 and pH = 9.3 respectively. The fits were performed on the experimental data after the instrument background subtraction. Consequently, the tails of the curves for larger micro time values are widely spread, leading to χ^2_N values smaller than 1. For instance, if the fit in figure 5.6.18 a) is limited to ~ 14 ns then $\chi^2_N \simeq 1.11$, with negligible deviations for fitted lifetime and intensity ($\triangle\tau \simeq 0.06$ ns and $\triangle I_0 \lesssim 3\%$).

From raw data for pH = 5, the ratios between fluorescence signal and background at $t_b = 4.5$ ns are: $S/B(t_b) \sim 8.9$, 12.2, 20.4 and 117.5 respectively for *pp*, *ps*, *sp* and *ss* polarization combinations.

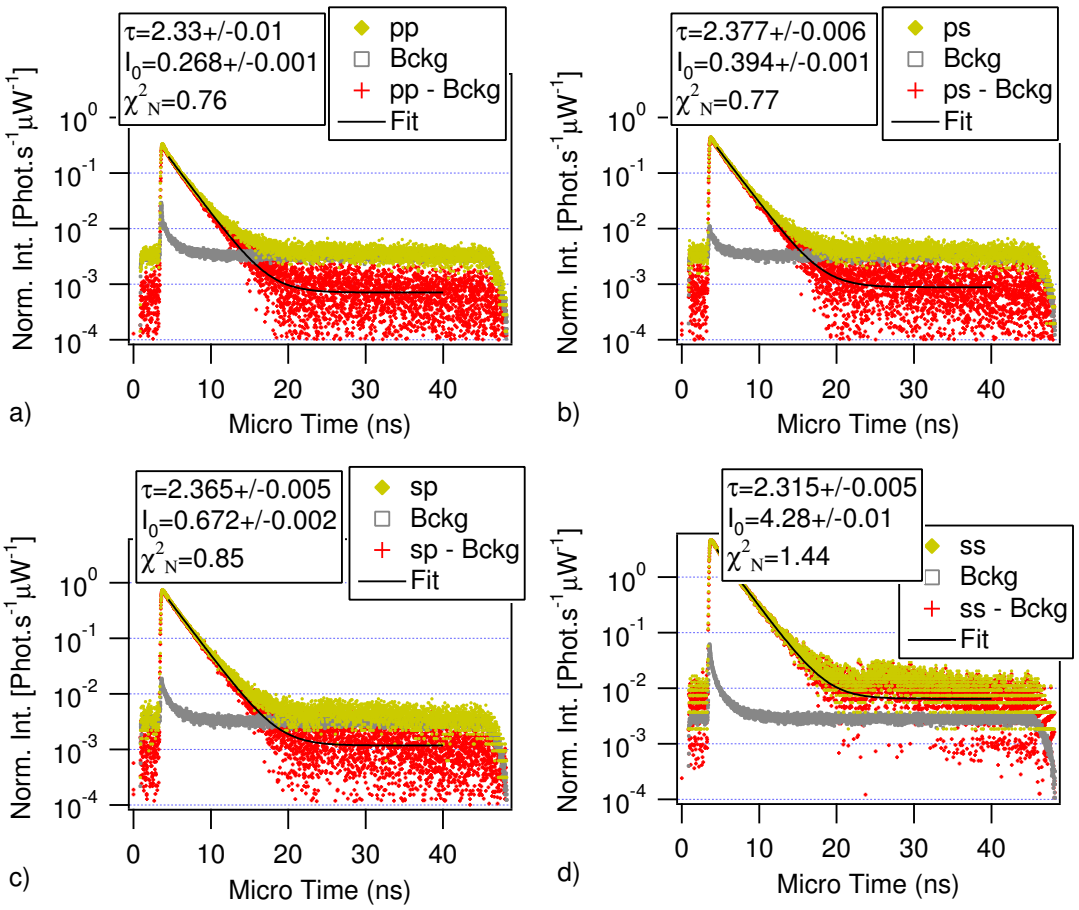

Figure 5.6.19: Measured fluorescence decay curves (rhombi) for dye loaded PAH, deposited at pH = 7.5, onto $SiSO_3^-$ substrate. Different excitation-detection polarization combinations are considered, as indicated in the legends. Instrument background (squares), experimental data with background subtracted (crosses) and correspondent fits are also reported. Lifetimes (τ, in ns), intensities at time $t_0 = 3.8$ ns (I_0, in phot./(s · μW)) and normalized χ^2 values for the curves fit are shown.

Analogously for pH = 7.5: $S/B(t_b) \sim 28.1$, 35.7, 61.0 and 384.7, while for pH = 9.3 the values are $S/B(t_b) \sim 8.9$, 9.6, 16.2 and 93.4. According to section 5.3, the measured data for all the samples and all the polarization combinations are reliable for fits.

For a more quantitative data analysis, fluorescence intensities and lifetimes were simulated for an ensemble of 900 dye molecules on a substrate constituted by a polymer film, with thickness of 3 nm ($SiSO_3^-$ substrate and PAH chains) and dielectric constant $\varepsilon = 2.319$. The dielectric constant chosen was identical to the value used for PSS, due to the presence of the sulphonic groups in the silanes. The theoretical values were calculated for different ratios between the number of chromophores sitting on top of the film and the number of the ones embedded in the polyelectrolytes matrix. In either side the dye molecules were placed at 0.5 nm from the polymer-air interface. In the simulation, the emitter parameters $\Delta\theta = 0, \Gamma_{nr}/\Gamma_0 = 0.56$ and $\Gamma_0 = 4.9$ ns were taken as determined by the PCM (see chapter 4), for the same dye molecule embedded in a PSS/PAH film. The choice of these parameters may be justified by the presence of sulphonic groups (identical to PSS) in the silanes structure. The comparison was then carried out with the experimental data in figure 5.6.17.

Figures 5.6.21 a), b) and c) represent, for different pH values, the least mean square curves of lifetimes

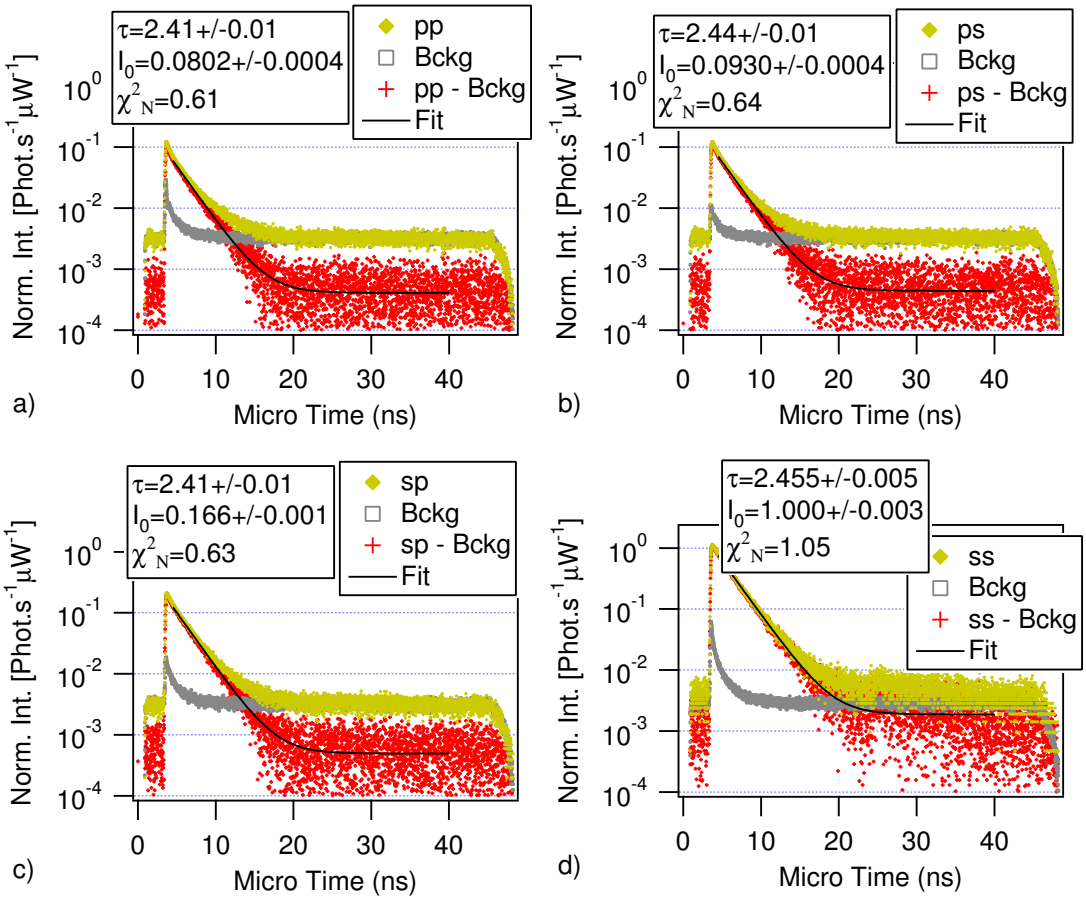

Figure 5.6.20: Measured fluorescence decay curves (rhombi) for dye loaded PAH, deposited at pH = 9.3, onto $SiSO_3^-$ substrate. Different excitation-detection polarization combinations are considered, as indicated in the legends. Instrument background (squares), experimental data with background subtracted (crosses) and correspondent fits are also reported. Lifetimes (τ, in ns), intensities at time $t_0 = 3.8$ ns (I_0, in phot./$(s \cdot \mu W)$) and normalized χ^2 values for the curves fit are shown.

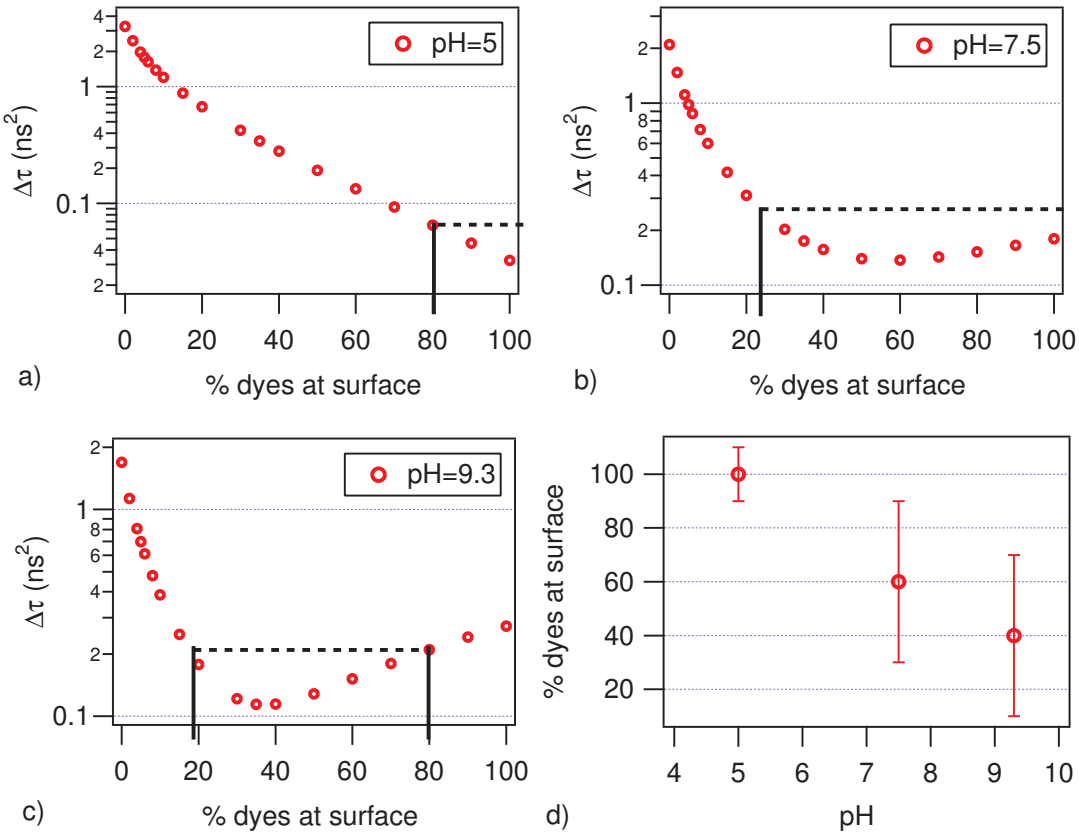

Figure 5.6.21: a)-c) Least squares sums for lifetimes over different polarization combinations, according to equation 5.6.2, for several pH values (in the legends). Horizontal dotted lines represent 2 times minima ordinate. The associated abscissa interval around the minima is $\sim 2 \cdot \sigma$ wide. d) Minima of curves in a)-c) as a function of the correspondent pH values. Error bars are $\pm\sigma$.

plotted as a function of the percentage of dyes at surface, according to the following equation:

$$\Delta\tau(\%\,at\,surface) = \sum_{pol} \left[\tau_{pol}^{theo}(\%\,at\,surface) - \tau_{pol}^{exp}\right]^2 \tag{5.6.2}$$

The sum is over all the polarization combinations, while τ_{pol}^{exp} and τ_{pol}^{theo} are the experimental and the simulated lifetimes respectively. Abscissae of minima in equation 5.6.2 provide the most probable values for the percentage of dyes on the surface, for different experimental data sets. It is also possible to evaluate the associated standard deviation σ by statistical consideration (see section A.2 in Appendix A).

Figure 5.6.21 d) shows the least squares curves minima in a), b) and c), as a function of the pH of the deposition solution. Although large errors are present, it is possible to notice a trend indicating that a larger number of dyes experience the polymer as optical environment, when the pH increases (i.e. chains modify their conformation from train-like to loop-like). In figure 5.6.22 a comparison between theory and experiment for fluorescence lifetimes (a, c, e) and intensities (b, d, f) is shown. Different polarization combinations and different pH values of the deposition solution are taken into account. The mesaured data are taken from figure 5.6.17, while the abscissae for these experimental data are taken from curves minima in figure 5.6.21.

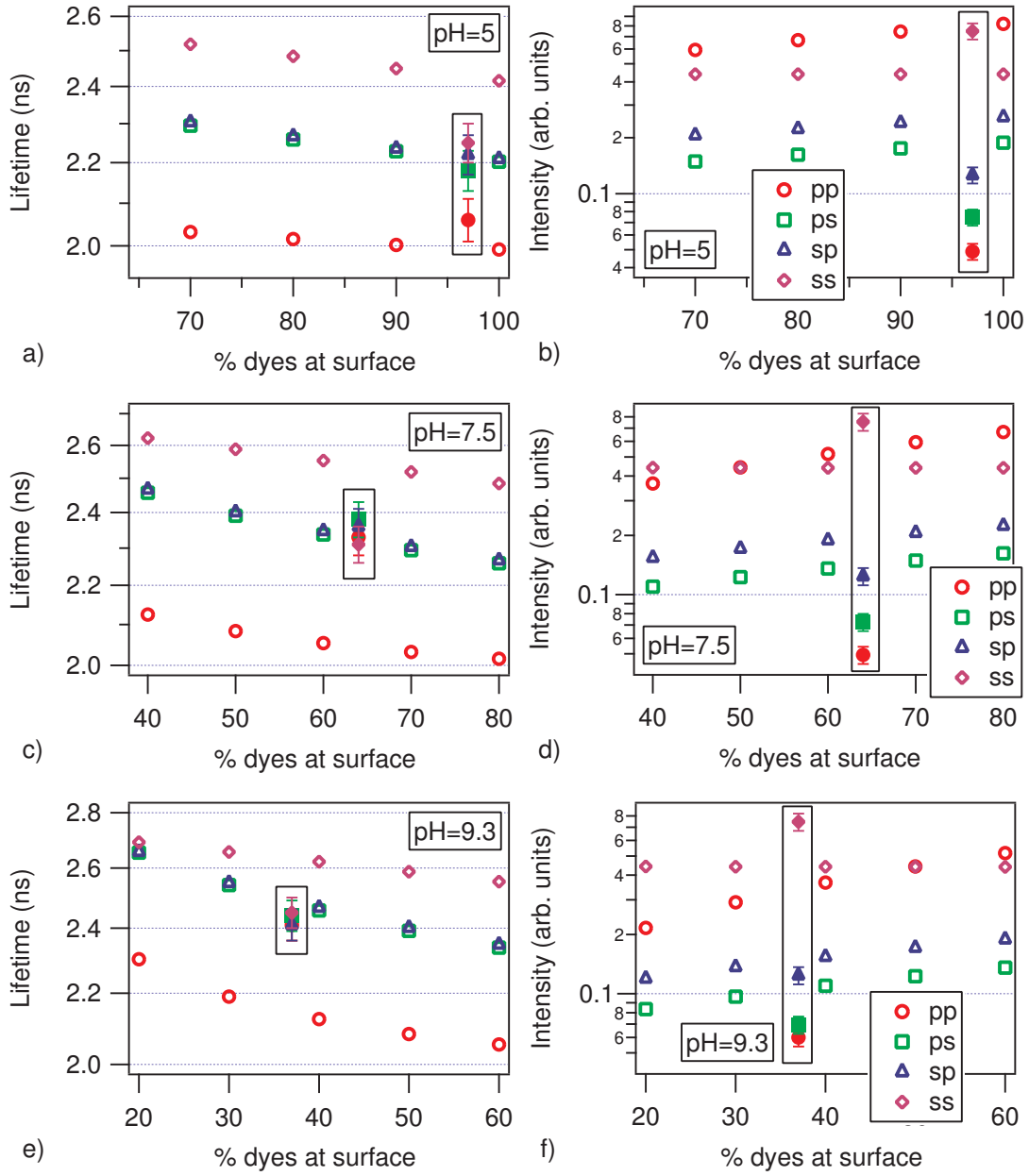

Figure 5.6.22: Fluorescence lifetime (a, c and e) and intensities (b, d and f) of functionalized PAH deposited onto $SiSO_3^-$ substrate, for several pH of the deposition solution. The experimental data (full markers) are compared with simulation (open markers), as a function of the percentage of the chromophores at surface. The abscissae of measured data are taken from the minima of the curves in figure 5.6.21. The parameters used for simulation were: $\Delta\theta = 0, \Gamma_{nr}/\Gamma_0 = 0.56$ and $\Gamma_0 = 4.9\,\text{ns}$, as determined by the Polarization Combination Method (see chapter 4).

Figure 5.6.22 a), c) and e) indicate that an agreement between theoretical and experimental excited-state lifetimes is not achieved, especially at high pH values. The ratios among different polarization combinations for simulated values are larger than for measured data, with a mismatch of $\lesssim 10\%$. The comparison is more critical when, in the calculations, an approximately equal amount of dye molecules is considered either side of the polymer-air interface (i.e. for higher pH values).

When looking at intensities, the differences between deviations are much larger and in particular for *pp* combination. The reason is found in the abscissae of experimental data in figure 5.6.22 b), d) and f). These were chosen according to curves minima in figure 5.6.21 a), b) and c) respectively. The minima are the results of a least squares minimization for lifetimes, as indicated in equation 5.6.2: therefore the percentage of dyes at surface used in the simulation are set from the experimental lifetimes. Nevertheless, as already discussed in figure 5.6.17, the lifetimes values show mainly an "in-air" behaviour, while the fluorescence intensities indicate an "in-polymer" behaviour for the dye molecules (i.e. 0% of dyes at surface). Consequently, the theoretical calculations can not take into account the different ratios among the polarization combinations, for lifetimes and intensities, at the same time.

It is useful at this point to summarize some of the assumptions used to model the real system and hypothesize about the eventual failures of the model itself:

- the non radiative contribution Γ_{nr} used in the simulation it has been calculated for chromophores fully embedded in the polyelectrolyte matrix and it was supposed to be polarization independent (see chapter 4). Close to an interface (for dyes-interface distances comparable with the dyes size) the non radiative contribution could be different and it could depend also on the polarization. More investigations would be needed for an experimental proof of such hyphotesis.
- The assumption of uniform distribution for the dipoles may be not satisfied, bringing different intensity contributions for different polarization combinations, which are not included in the model. In this respect, the experimental I_{0ss} is always larger than the simulated value, regardless of the percentage of dyes at the surface.
- The definition of dielectric constant, used in theoretical calculus, may be not appropriated for dielectric films $\lesssim 2-3\,$nm thick (i.e. experimental I_{0pp} is always much smaller than simulated value).
- The theoretical values are obtained by adding the decay curves of different amounts of dyes inside and outside the dielectric film. In the model, this implies a sharp interface definition and a clear discontinuity for the electromagnetic field normal component across the interface (as the boundary conditions impose). In reality, the interface may be not well defined on the scale of the interface roughness and due to the dye molecular size, the point-like dipole approximation may fail. As a consequence, an indetermination on the position of chromophore is present with respect to the definition of "in-air" or "in-polymer".

Conclusions Deposition of dye loaded PAH polyelectrolyte on top of $SiSO_3^-$ substrate, provides evidence of an "in air" behaviour of chromophores on the surface. Changes in the excited state lifetime, as a function of deposition solution pH, confirm polymer morphology transition from train-like (acid environment) to loop-like (neutral-basic environment) chains. It is also believed (see also section 5.6.3) that the rinse steps lead to a monolayer formation. The thickness of bilayers assembled from fully charged polyelectrolyte in the absence of any added salt is known to be small (about $\approx$ 1nm, [39]). From this perspective, it is remarkable that a PAH monolayer constitutes sufficient

material to change the optical properties of the emitters surrounding environment, depending on the chains morphology. A rough estimation of the percentage of dyes on the surface as a function of deposition solution pH is given.

Quantitative anaysis is believed to suffer from approximations used in the model: non-radiative contribution, uniform distribution of dipoles orientations, dielectric constants for ultra thin layers, sharp interface definition. As a consequence, discrepancies between theoretical and experimental data are observed, especially for fluorescence intensities.

5.7 Applications

5.7.1 Polyelectrolytes Morphology versus pH

Polystyrene sulfonate (PSS) is classified as strong polyanion and the monomers constituting the polymer chains possess in solution a negative charge, quite stable over a wide range of pH values. Polyallylamine hydrochloride (PAH) on the other side is a weak polycation and its degree of ionization is strongly dependent from the acidity of the solution where it is dissolved. As a consequence, by changing the pH, it is possible to activate-deactivate a different number of charges along the PAH polymer chains [31]. In general the pKa of a weak polyelectrolyte can be a complex function of the degree of ionization [32] but, according to J. Choi and M. F. Rubner [31], it is possible to use the common â€œpKa" value to indicate the pH at which 50% of the polymer functional groups are ionized. By this definition, the pKa of PAH was estimated to be between 8.0 and 9.0 (see [31] and reference therein).

Figure 5.7.1 represents schematically two samples with functionalized PAH chains deposited, as last layer, on top of 2.5 PSS/PAH bilayers (PSS terminated). The two samples in figure 5.7.1 are prepared by two different deposition solution conditions: a) low pH ($\sim 3 \div 5$, higher ionization degree) and b) high pH ($\sim 8 \div 9$, lower ionization degree). For high ionization degree the chains have a “train-like" shape due to electrostatic repulsion and therefore they are adsorbed in a flat conformation (molecularly thin layer, fig. 5.7.1 a). For low ionization degree, most of the groups are not charged: the weak polycation chains adopt a conformation of dense loops that extend away from the surface (molecularly thick layer, fig. 5.7.1 b). By changing pH thus, it is possible to modify the average distance between emitter and the polymer-air interface, within a certain range. Limitations may be related to polymer chains length, chemical affinity with the substrate and chains entanglement.

From step profiler measurements (see section 4.5 in chapter 4) the thickness of 3 PSS/PAH bilayers above a fused silica substrate is $\sim 6\,$nm, while from the molecular structure of the FR636 dye (see figure 5.6.1) an estimation of the molecule size could be done, leading to values around $\sim 2-3\,$nm.

Results and Discussion

Figure 5.7.2 shows the experimental fluorescence lifetimes and intensitites for the samples depicted in 5.7.1 and prepared according to the procedure in section 5.6.4. From figure 5.7.2 a), it is possible to observe a clear shift of the lifetimes for the *pp* polarization combination, as pH varies. τ_{ss} is not affected within the experimental error, while minor changes are present for τ_{ps} and τ_{sp}. The fluorescence intensities in figure 5.7.2 b) indicate a significant change for I_{0pp} but a less clear trend over the other polarization combinations. Figures 5.7.2 c), d), e) and f) show the measured decay curves for the sample deposited at pH = 3, respectively for *pp, ps, sp* and *ss* polarization combinations. Whereas, the experimental data for the sample deposited at pH = 9 are indicated in figure 5.7.3.

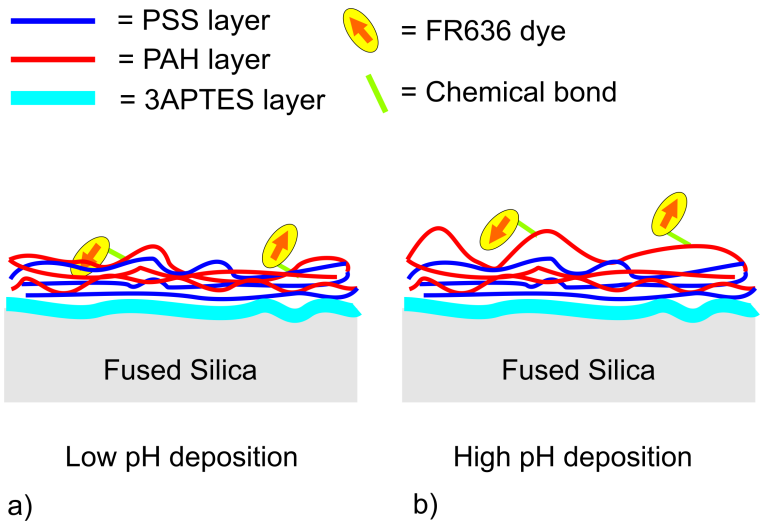

Figure 5.7.1: Schematic representation of samples with PAH chains loaded by FR636 dyes, deposited on top of 2.5 PSS/PAH bilayers by (a) pH $\sim$ 3 and by (b) pH $\sim$ 9 water solutions.

To explain the trends in figure 5.7.2 a) and b), fluorescence intensities and lifetimes have been theoretically calculated as a function of the percentages of dyes at the vacuum side. The results were compared with the two experimental cases for pH = 3 and pH = 9 and the comparison is displayed in figure 5.7.4. For the experimental data in all the cases, the abscissae are taken from the minima of the curves in figures 5.7.4 e) and f), for pH = 3 and pH = 9 respectively. In detail, in the figures 5.7.4 a) and b) a comparison between theory (empty markers) and experiment (full markers) is shown for lifetimes. In figures 5.7.4 c) and d), the experimental (full markers) and the theoretical (empty markers) fluorescence intensities are compared. The comparison is done between normalized theoretical and normalized experimental fluorescence intensities, as explained in section 4.6.3.

In the figures 5.7.4 e) and f), the least mean squares curves are plotted as function of the percentage of dyes at surface, with respect to the amount embedded in the polymer matrix, according to the following equation:

$$\Delta\tau(\%\ at\ surface) = \sum_{pol} \left[\tau_{pol}^{theo}(\%\ at\ surface) - \tau_{pol}^{exp}\right]^2 \tag{5.7.1}$$

The sum is over all the polarization combinations, while τ_{pol}^{exp} and τ_{pol}^{theo} represent respectively the experimental and the simulated lifetimes. By using equation 5.7.1, it is possible to consider the percentage of the dyes at the surface as the fit parameter and the abscissae of minima in the $\Delta\tau$ function provide the most probable value. By statistical consideration (see section A.2 in A), it is also possible to evaluate the associated standard deviation σ. In this way for pH = 3 about 0.2% of dyes are found at surface with an error of $\sigma \sim 0.4\%$, while at pH = 9 about 4% of chromophores are outside the polymer matrix, with an an error of $\sim 2\%$. The mean values for percentages are then used in figures 5.7.4 a), b) c) and d) to determine the abscissae of experimental data.

In figure 5.7.4 a) a fairly good agreement between theory and experiment is reached for pH = 3. Here, the simulation with the parameters derived by the PCM (see chapter 4) indicates that more than $\sim 99\%$ of chromophores experience a surrounding polymer environment. The agreement with data for pH = 9 in figure 5.7.4 b) is not as good as for pH = 3. This may confirm the failure of the model when already a small percentage of the dye molecules ($\sim 4\%$) are on the surface and

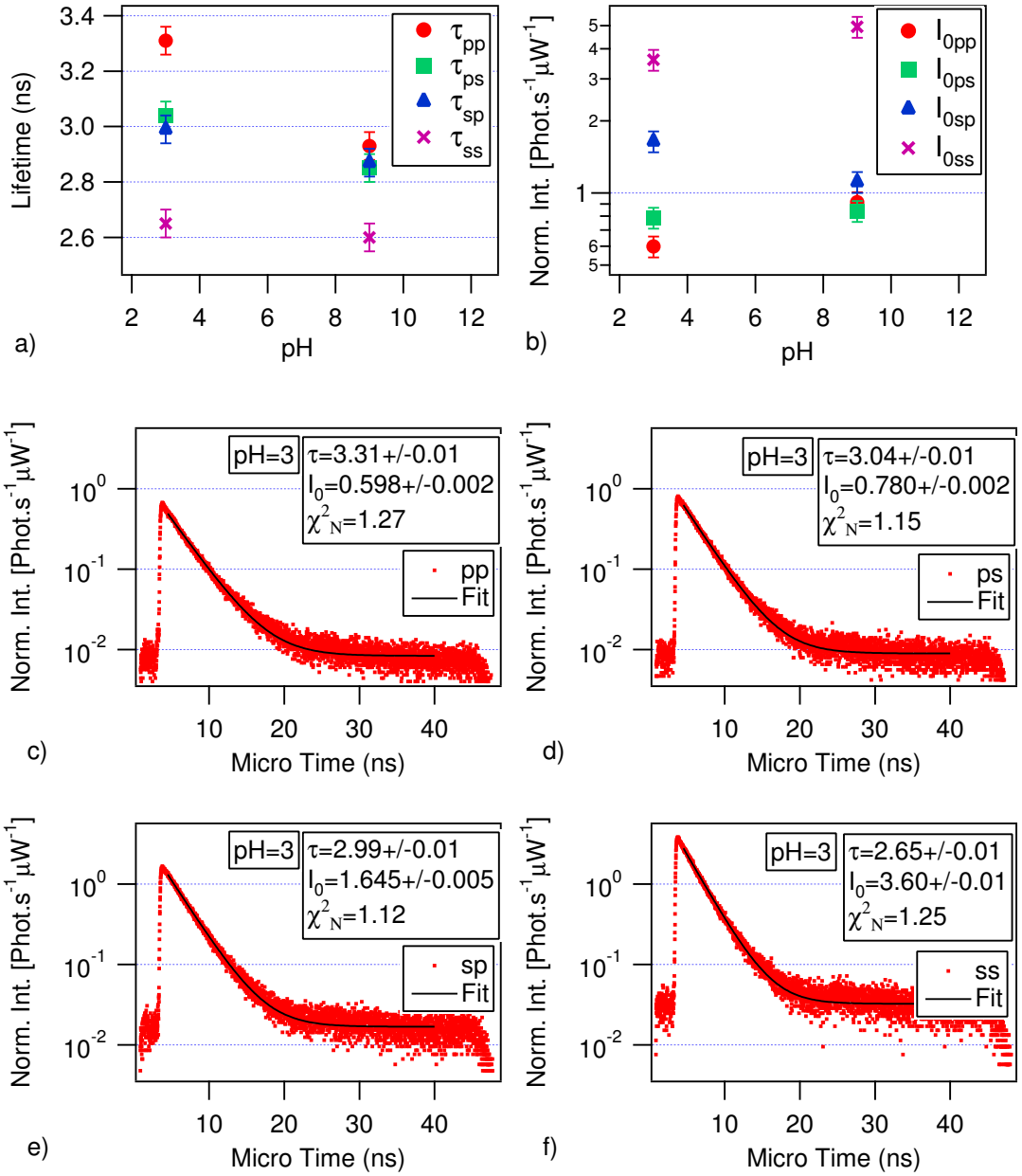

Figure 5.7.2: Experimental fluorescence lifetime a) and intensities b), for the two samples depicted in figure 5.7.1 a) with pH = 3 and 5.7.1 b) with pH = 9. Experimental error for lifetimes is ± 0.05 ns, while for intensities is $\pm 10\%$. c), d), e) and f) Measured decay curves for the sample deposited at pH = 3 condition, respectively for *pp, ps, sp* and *ss* polarization combinations. Lifetimes (τ, in ns), intensities at time $t_0 = 3.8$ ns (I_0, in phot./(s $\cdot \mu$W)) and normalized χ^2 values for the curves fit are reported in the legends.

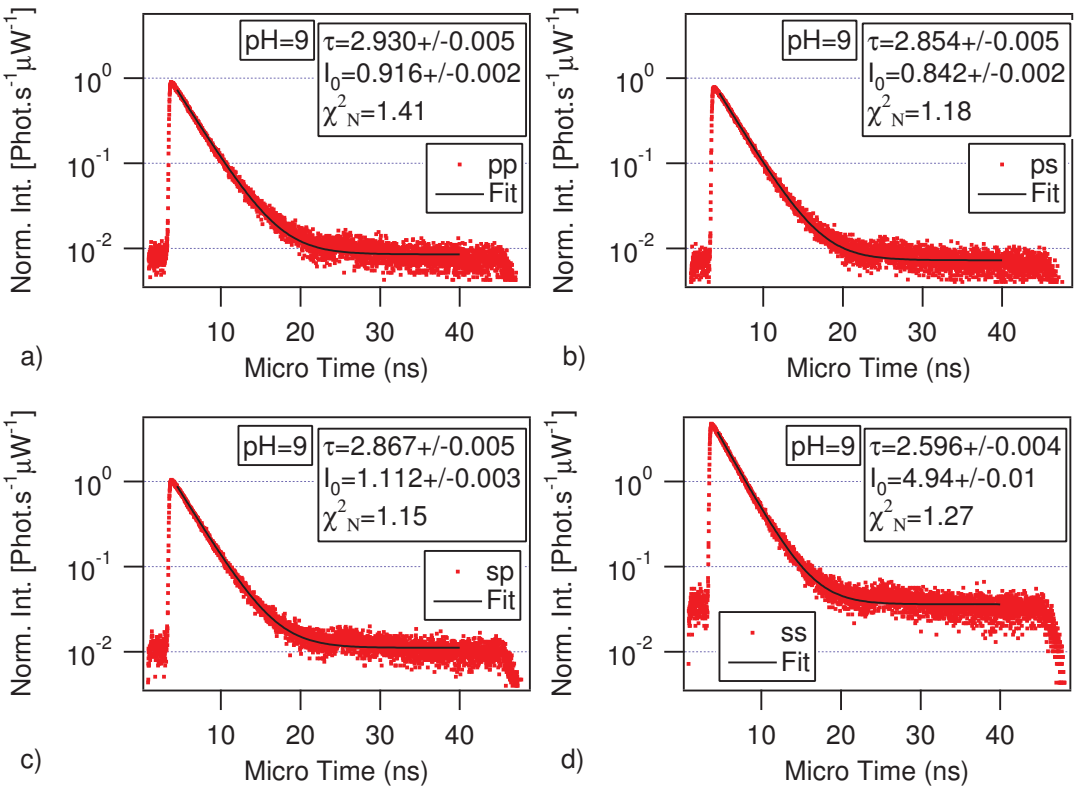

Figure 5.7.3: a), b), c) and d) Measured decay curves for the sample deposited at pH = 9 condition, respectively for *pp, ps, sp* and *ss* polarization combinations. Lifetimes (τ, in ns), intensities at time $t_0 = 3.8$ ns (I_0, in phot./(s $\cdot \mu$W)) and normalized χ^2 values for the curves fit are reported in the legends.

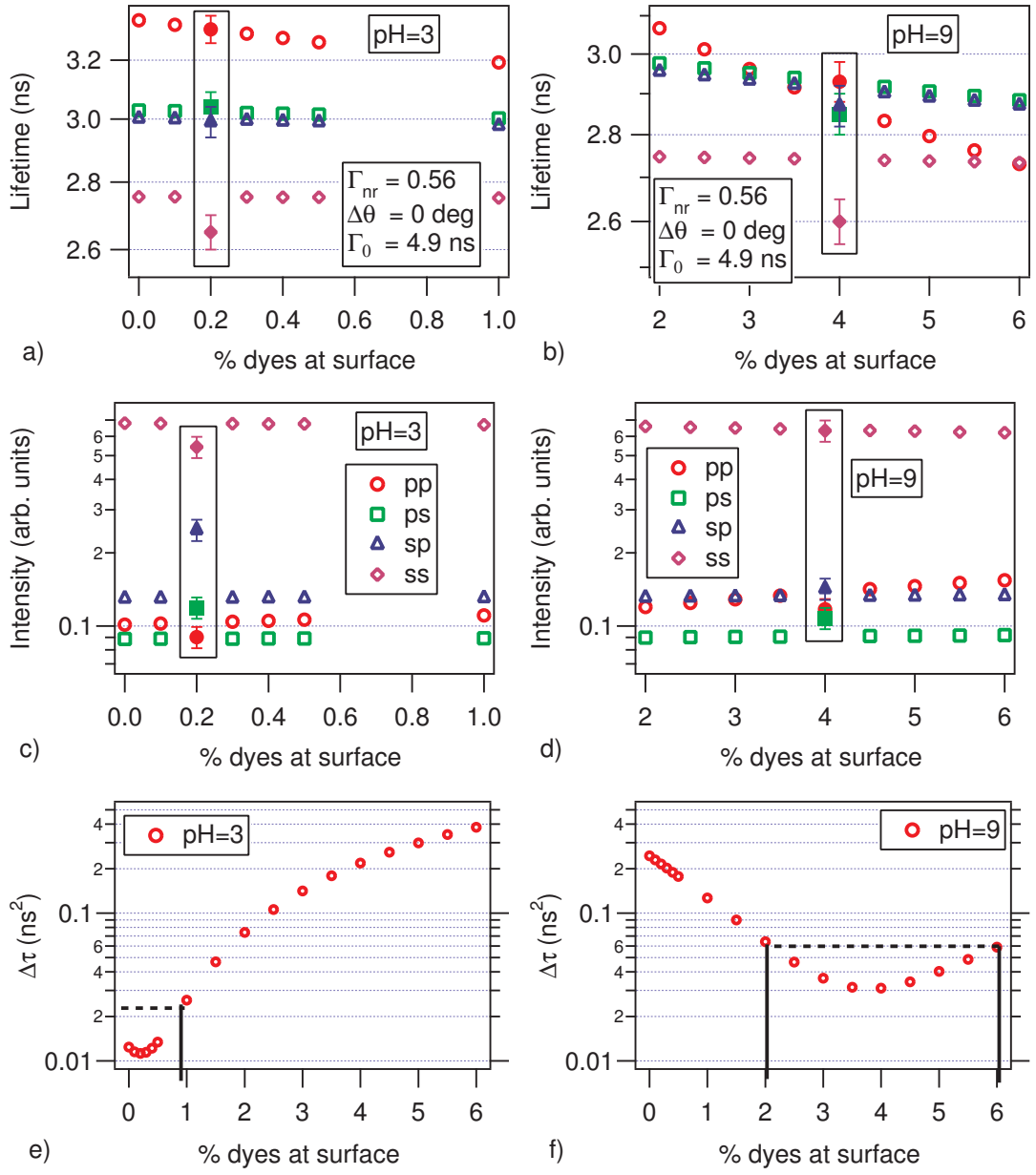

Figure 5.7.4: Comparison between simulation (empty markers) and experiment (full markers), for fluorescence lifetimes τ (a and b) and normalized intensities I_0 (c and d). Values for different polarization combinations are reported as a function of the percentage of dipoles onto a 2.5 PSS/PAH bilayers film (see figure 5.7.1). The parameters used for simulation are indicated in the legends in a) and b). The pH of the deposition solution used for experimental data is also displayed in the legends. e) and f) least squares sums for lifetimes as a function of the percentage of dipoles on top of the 2.5 PSS/PAH bilayers film, according to equation 5.7.1. Horizontal dotted lines represent 2 times minimum value ordinate, while the associated abscissa interval represents a deviation around the minima of $\sim 2 \cdot \sigma$.

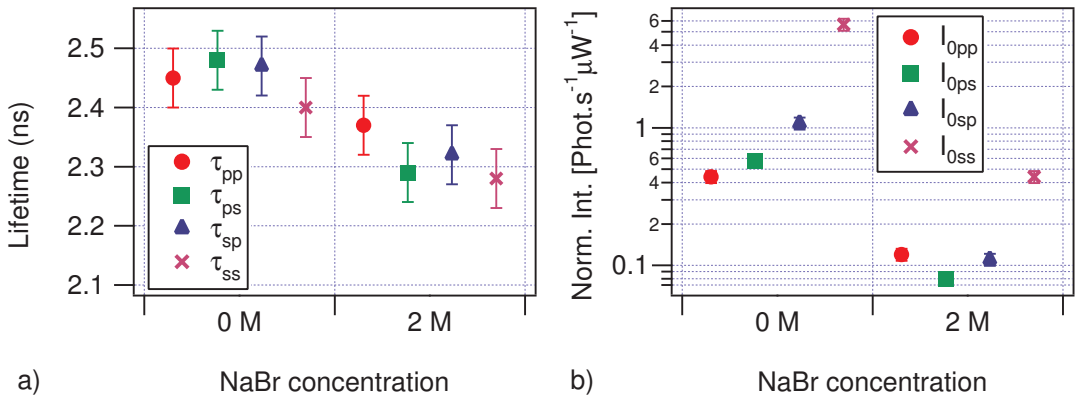

Figure 5.7.5: Measured fluorescence lifetime (a) and intensities (b) for samples with $SiSO_3^-$ substrate, after ~ 6 hours drying process at room conditions, as function of NaBr salt concentration for the deposition solution. In both cases the pH value was 9.35 ± 0.10. Errors on lifetime it is ± 0.05 ns, while error on intensity it is 10%.

therefore not embedded in the polymer matrix. In figures 5.7.4 c) and d), the comparison between theory and experiment for fluorescence intensities shows a reasonable agreement for pH $= 9$, while some deviations are found at pH $= 3$. In the case of I_{0sp} an explanation has been not found.

Conclusions

The fairly good agreement between experimental and theoretical data support the hyphotesis of different polyelectrolytes chains conformation, depending on the pH of the deposition solution. In detail, for a deposition in an acid environment the polymer chains have mainly train-like shape, while for basic deposition solution the chains have a loop-like conformation. In the first case all the dyes ($\sim 99.8\%$ from fitting the experimental data) are embedded in the polymer, probably due to the chains interdigitation. In the latter case, the chain adsorption occurs in a "frustrated" way and the chains interpenetration is reduced, leaving more dyes at the surface in the air ($\sim 4\%$ from fit). An approximative sketch of the two possible scenarios, it is depicted in figure 5.7.1. The fairly good agreement between experiment and theory also indicates that the PCM may be a useful tool to investigate polymer layers conformation, after adsorption onto a surface.

5.7.2 Polyelectrolytes Morphology versus Salt Concentration

The results from the previous section show the pH plays a major role in the polyelectrolytes adsorption process onto a surface, modifying the polymer conformation as a consequence of the change of the chains ionization degree. Presence of salt in the deposition solution has analogous effects, shielding the monomers charges and thus altering the chains conformation. Moreover, since salt is composed by small ions with respect to the polymer chains, their adsorption onto a charged substrate is favorite for kinetic and entropic reasons. In this way, the amount of polyelectrolytes adsorbed from solution onto a surface is highly affected by the salt concentration ([17, 45], [44] and [33]).

Analysis of fluorescence characteristics from dye loaded PAH chains adsorbed onto a charged substrate provides confirmation of salt effects. Figure 5.7.5 reports lifetime (a) and intensities (b) for

functionalized PAH deposited onto $SiSO_3^-$ substrate in a basic environment (pH ~ 9.3), for two different concentration of NaBr salt (for sample preparation procedure see 5.6.4). Figure 5.7.5 a) indicates that salt addition slightly modifies lifetimes, as a consequence of a change in adsorbed polymer chains morphology. From figure 5.7.5 b), it is observed that an addition of salt lead to a large intensity decrease, probably due to either shielding of the charges on the substrate and lower ionization degree of PAH chains. The results are in a good agreement with general theory of polymer absorption at interfaces [33]. It is interesting to notice that from polarized fluorescence study, some information on the adsorption process can be obtained. Moreover, it is also possible to gain insights about the structure of the polyelectrolytes-air interface.

5.8 Summary

Polarized fluorescence studies of organic dyes in proximity of a dielectric interface provided qualitative information about microscopic electromagnetic effects. Quantitative analysis suffered from approximations of the theoretical model, from a degree of uncertainty in the system geometry and in the emitters position. In this regards, the use of free organic dyes presented limitations due to chromophores aggregation and diffusion, for the concentrations range explored. At lower concentration values, fluorescence detection problems were experienced for the kind of substrates tested. To overcome these limitations, a PAH chain functionalization process was designed. Polyelectrolytes, deposited with layer-by-layer technique, provided an accurate control of the film thickness down to a few nanometers and an interface roughness on the scale of the chromophore size ($\approx 2-3\,\mathrm{nm}$). By varying the deposition solution properties (i.e., pH and ionic strength), the conformation of the adsorbed polymer on top of different substrates was changed and the effect on the emission of the chromophores was tested. By changing the degree of ionization of the chains, it was possible to modify the characteristics of the fluorescence emission: from an "in air" behaviour to a situation where many organic dyes experienced the polymer as surrounding optical media ("in polymer"). It was remarkable to observe that one monolayer of PAH constituted a sufficient amount of material for such a "in air"-"in polymer" transition.

Free organic dyes behaved as emitters embedded in a polymer matrix, even if the fluorophores were deposited on a thin polyelectrolyte spacer ($\approx 6\,\mathrm{nm}$), suggesting the diffusion of the dye molecules into the polyelectrolyte. The same results applied for a very thin polymer spacer ($\approx 2\,\mathrm{nm}$ thick). As a consequence, a monolayer of polyelectrolyte appeared to be sufficient to define the optical environment surrounding the chromophores. For the dyes investigated, a good agreement between theory and experiment was achieved, showing the validity of our model based on classical electromagnetism without any local field correction.

For functionalized chains deposited at low pH, on top of the polyelectrolyte spacer, the fluorescence showed the characteristics of emitters embedded in a polymer matrix. For deposition at high pH a different behaviour was obtained: it could be modelled by assuming that some fraction of the molecules experience fields as calculated for the low refractive index side (air). At low pH, chains entanglement between the dye-functionalized chains and the polyelectrolyte of the spacer may bring most of the dyes inside the polymer. Therefore, the fluorophores may experience the polymer as surrounding environment. On the other hand, for high pH values the dye-loaded chains adsorbed have a conformational arrangement of dense loops that extend away from the surface. In this case, a larger fraction of fluorophores may experience the air as surrounding environment. A good agreement was achieved between experimental and theoretical data for fluorophores covalently bound to PAH chains and deposited onto the polyelectrolyte spacer.

Deposition on glass substrates, functionalized with a negatively charged silane, at different pH values was also performed. The silane provided higher surface charge density than a bare glass slide and reliable measurements were achieved. For the negatively charged substrate the fluorescence intensities indicated the behaviour of emitters embedded in a polymer matrix, regardless of the pH value. On the other hand, for low pH values, the excited-state lifetimes showed that the emitters behaved as in air. For higher pH values, lifetimes indicated an intermediate behaviour between fluorophores located within and above of a dielectric film. For these samples, discrepancies were found between theory and experiment, even if a qualitative trend could be observed. The poor agreement may be due to the simplified model used, by which the dipoles are assumed either in one side or in the other with respect to the interface. A more defined system geometry and precise dyes position knowledege may be necessary to check the model assumptions and to introduce opportune modifications accordingly.

Finally, from a qualitative point of view, far field polarized fluorescence may be considered as a useful tool for surfaces characterization. In particular, in combination with PCM (see chapter 4), the technique could be applied:

- to test monolayer vs. bilayers formation.
- to study very first adsorption of polymers onto a surface.
- to test chains flatness (morphology studies in general).
- for surfaces investigation (roughness, porosity, surface charge density).
- to check the percentage of dyes on one side of a interface between two dielectric media, with respect to the total amount of chromophores. In this regards, possible applications could be in the field of biology, such as transfection of plasmid DNA, microsomes or nanoparticles.

Bibliography

[1] R.A.L. Vallee et al., *Phys. Rev. Lett.*, **91**, No. 3, 038301 (2003).

[2] R.A.L. Vallee et al., *Chem. Phys. Lett.*, **372**, 282-287 (2003).

[3] R.A.L. Vallee et al., *J. Chem. Phys.*, **122**, 114704 (2005).

[4] R.A.L. Vallee et al., *Chem. Phys. Chem.,* **6**, 81-91 (2005).

[5] R.A.L. Vallee et al., *J. Am. Chem. Soc.*, **127**, 12011-12020 (2005).

[6] R.A.L. Vallee et al., *Chem. Phys. Lett.,* **348**, 161-167 (2001).

[7] N. Tomczak, *Private Communication*.

[8] S. M. Barnett, *J. Phys. B: At. Mol. Opt. Phys.,* **29** 3763â€“3781 (1996).

[9] Kreiter M. et al., *J. Chem. Phys.*, vol. 117, **20**, (2002).

[10] J. J. Macklin, J. K. Trautman, T. D. Harris, and L. E. Brus, *Science* 272, 255 (1996).

[11] N. Danz et al., *Phys. Rev. A*, **66**, 063809 (2002).

[12] K. Vasilev, *PhD Thesis*, Martin Luther University, Halle Wittenberg (2004).

[13] Lvov, Y.; Haas, H.; Decher, G.; Mohwald, H.; Kaladev, A. *J. Phys. Chem*. 1993, **97**, 12835. Schmitt, J.; Grunewald, T.; Decher, G.; Pershan, P. S.; Kjaer, K.; Losche, M. *Macromolecules* 1993, **26**, 7058. Decher, G.; Lvov, Y.; Schmitt, J. *Thin Solid Films* 1994, **244**, 772. Ferreira, M.; Cheung, J. H.; Rubner, M. F. *Thin Solid Films* 1994, **244**, 806. Ferreira, M.; Rubner, M. F. *Macromolecules* 1995, **28**, 7107. Fou, A. C.; Rubner, M. F. *Macromolecules* 1995, **28**, 7115.

[14] M. Toda et al., *Langmuir*, **24**, 3191-3198 (2008).

[15] Yang M.H. et al., *Phys. Rev. Lett.*, 96, 066105 (2006).

[16] T. Farhat et al., *Langmuir*, 15, 6621-6623, (1999).

[17] S. A. Sukhishvili and S. Granick, *J. Chem. Phys.*, vol. 109, No. **16**, (1998).

[18] Regine v. Klitzing and Helmuth Moehwald, *Macromolecules*, **29**, 6901-6906 (1996).

[19] Born M. and E. Wolf, *Principles of Optics*, Oxford: Pergamon, 6th edn. (1970).

[20] B. Valeur, *Molecular Fluorescence*, Wiley-VCH (2002).

[21] Y. Lvov et al., *Langmuir*, **9**, 481-486 (1993).

[22] Steffen Werner, *private communication*.

[23] D. Balasubramanian et al., J. Phys. Chem., **93**, 3865-3870 (1989).

[24] W. J. Zhu, T. Song J.Q., Liu Z.F. *Thin Solid Films,* **327**, 591 (1998).

[25] M.C. Alvarez, private communication.

[26] http://www.sigmaaldrich.com/fluka/product%20information%20sheet/08968dat.pdf

[27] F. Stefani et al., *New Journal of Physics*, **9**, 21 (2007).

[28] Z. Mao et al., *Journal of Controlled Release*, **104**, 193-202 (2005).

[29] Wen-Fei Dong et al., *Chem. Mater.* , **17**, 4992-4999 (2005).

[30] Loesche et al. *Macromolecules*, Vol. 31, No. **25**, 8893 (1998).

[31] J. Choi and Michael F. Rubner, *Macromolecules*, **38**, 116-124 (2005).

[32] M. Mandel, *Eur. Polym. J.*, **6**, 807 (1970).

[33] G.J. Fleer, M.A. Cohen Stuart, J.M.H.M. Scheutjens, T. Cosgrove, B. Vincent, *Polymers at Interfaces*, Chapman & Hall (1998).

[34] S. S. Shiratori and M. F. Rubner*, Macromolecules*, **33**, 4213-4219 (2000).

[35] L. A. Ageev et al., Optics and Spectroscopy, vol. 102, no. 3, 442 (2007).

[36] S. Yamamoto at al., *Macromolecules*, **33**, 5608-5612 (2000).

[37] Takeshi F., *Japanese Polymer Journal*, (2005) and private communication from Hiroaki Benten.

[38] Yanlong Gu et al. , *Angew. Chem. Int. Ed.*, **45**, 7217 â€“7220 (2006).

[39] G. Decher, J. D. Hong and J. Schmitt, *Thin Solid Films*, **210/211** 831-835 (1992).

[40] Sigma Aldrich Inc., Material Safety Data Sheet, Prod. No. A3648.

[41] J. Dejeu et al., *Colloids and Surfaces A: Physicochem. Eng. Aspects*, **288**, 26-35 (2006).

[42] G. Decher, Science, **277**, 1232 (1997).

[43] R. K. Iler, *The Chemistry of Silica*, N.Y. Wiley (1979).

[44] C.C. Buron et al., *J. Colloid and Interface Science*, **314**, 358-366 (2007).

[45] H.G.M. van de Steeg et al., *Langmuir*, **8**, 2538-2546 (1992).

Chapter 6

Summary

The correlation between the orientation and the excited-state lifetimes of organic dyes close to dielectric interfaces was studied. For this purpose, an experimental setup was designed and built, based on a Surface Plasmon Fluorescence Spectroscopy apparatus, in the so called Kretschmann configuration. The experimental concept is based on the determination of averaged excited-state lifetimes, as a function of the excitation and detection polarizations. Working close to the total internal reflection angle, the experimental differences between polarization combinations were enhanced. In this way, the contributions from differently oriented dipoles could be clearly distinguished. The new optical investigation method, analogous to polarized fluorescent emission in solvent, was called Polarization Combination Method.

Free organic dyes and organic dyes covalently bound to polyelectrolyte chains were used. All molecules under investigation exhibited cluster formation in most of the solvents utilized, down to a concentration of 10^{-7} M. At lower concentrations for all the substrates tested, the signal-to-background ratio was too small to obtain reliable measurements. A dye with an active ester group was covalently bound to polyelectrolyte chains, through a condensation reaction, to solve this problem. The polymer functionalization process avoided aggregation and provided control over the dyes position, within a few nanometers to the interface ($\sim 2-3$ nm). Moreover, by varying the pH, the polymer chains could be deposited on different substrates with different conformations and the fluorescence characteristics analyzed. In general, for low pH values the chains are deposited on a substrate in a train-like conformation. For high pH values, the chains are deposited in a loop-like conformation.

A numerical method to model the excitation and emission of the dye molecules embedded in a multilayer system was developed, by which a full simulation of the time resolved fluorescence experiments was achieved. The method models the chromophores as a couple of point-like electrical dipoles, relying on the equivalence between the radiated power of an electrical dipole and the fluorescence decay rate of a molecule. Local electric fields within a multilayer system were calculated using of the Transfer Matrix Algorithm, by which the excitation rate was evaluated. The calculation of the dipole emission into space was then accomplished by exploiting the symmetry properties of the electromagnetic field, as indicated by the reciprocity theorem. The method was numerically implemented by a software code, specifically built for a five layers system and with the purpose of simulating the experimental conditions met during the measurements. The numerical convergence of the integrals involved in the theoretical calculations was explored and verified for the discretized variables. The code was also optimizated in order to reduce computational time. This algorithm can be easily extended to multilayer systems with an arbitrary number of layers and provides the theoretical fluorescence decay curve for a single dye or for an ensemble of embedded dyes, within a multilayer system.

For dyes embedded in a polymer matrix, fluorescence as a function of the distance between the fluorophores and the polymer-air interface was initially studied. It was thus possible to obtain a value for the non-radiative decay rate, the vacuum decay rate and the relative angle between the excitation dipole and emission dipole of the chromophores, without any adjustable parameters. The model calculation, assuming all dyes placed in the high refractive index medium, reproduces well the experimental data, even for distances between the emitter and the air-polymer interface down to $\approx 2-3\,\mathrm{nm}$. As a result, only a few layers of polyelectrolytes are sufficient for the dye molecule to behave as predicted by point-like dipoles, embedded in a medium which is described by its refractive index.

With the aim to explicit the discontinuity of the electromagnetic field at the dielectric interface, several fluorophores were also deposited onto different substrates and the fluorescence characteristics measured. Different free organic dyes ($\approx 2-3\,\mathrm{nm}$ size) behaved as emitters embedded in a polymer matrix, even if the fluorophores were deposited on a thin polyelectrolyte spacer ($\approx 6\,\mathrm{nm}$). This suggests diffusion of the dye molecules into the polyelectrolyte. Interestingly, the same results were valid for a very thin polymer spacer ($\approx 2\,\mathrm{nm}$ thick), deposited onto a fused silica substrate functionalized with 3-APTE silane. As a consequence, a monolayer of polyelectrolyte appeared to be sufficient to define the optical environment surrounding the chromophores. For the dyes investigated, a good agreement between theory and experiment was achieved, showing the validity of our model based on classical electromagnetism without any local field correction.

When functionalized chains were deposited at low pH, on top of the polyelectrolyte spacer, the fluorescence had the characteristics of emitters embedded in a polymer matrix. Surface deposition at high pH showed a behaviour, which could be modelled by assuming that some fraction of the molecules experience fields as calculated for the low refractive index side (air). At low pH the functionalized polymer strongly interdigitates with the polyelectrolyte chains of the spacer, bringing most of the dyes inside the polymer. Thus, the fluorophores may experience the polymer as surrounding environment. On the other hand, for high pH values the dye-loaded chains adsorbed have a conformational arrangement of dense loops that extend away from the surface. Therefore a larger fraction of fluorophores may experience the air as surrounding environment.

Deposition on glass substrates, functionalized with a negatively charged silane, at different pH values was also performed. Here, the experimental lifetimes and intensities showed contradictory results. The fluorescence intensities indicated the behaviour of emitters embedded in a polymer matrix, regardless of the pH value. On the other hand, for low pH values, the excited-state lifetimes showed that the emitters behaved as in air. For higher pH values, lifetimes indicated an intermediate behaviour between fluorophores located within and above of a dielectric film. Here, the dielectric film is constituted by the functionalized polymer chains themselves and for adsorbtion in a loop-like conformation, many dyes may be surrounded by the polymer. At low pH, the electrostatic interaction between the fully ionized chains and the substrate lead to the formation of a thin monolayer, thus the dye molecules are placed at surface, in the air side. Discrepancies were found between theory and experiment, probably due to the simplified model used, by which the dipoles are assumed either in one side or in the other with respect to the interface.

These experiments suggest that, polarized fluorescence studies of organic dyes in proximity of a dielectric interface provide information about microscopic electromagnetic effects. They may be used as tool to probe the local field and gain insights about the nano-environment surrounding a fluorescent emitter. Nevertheless, a well defined geometry down to the nanometer scale and impurity-free samples are required to extract useful information from the comparison between simulation and experimental data. On the lenght-scale of a few nanometers, the chromophore sizes, the interface roughness and the exact position of molecules with respect to the interface may play a relevant role thus limiting the accuracy of the analysis. Quantitative analysis suffered from approximations of the

theoretical model and from a degree of uncertainty in the system geometry. It is believed that more comprehensive models have to be developed to explain the microscopic electromagnetic phenomena for dyes at either side of a dielectric interface.

On the other hand, from a qualitative point of view, far field polarized fluorescence may be considered a useful tool for surfaces characterization. In particular, the technique could be applied to the study of the very first steps in the adsorption of polymers onto a surface, revealing details of their chain morphology. Surfaces properties like roughness, porosity and surface charge density can be investigated, by discriminating between the different fluorescence behaviour of the emitters in air and within polymer. By dye-labelling, it would be possible in general to apply the developed method to the area where it is important to verify the position of nano-objects with respect to a dielectric interface.

Appendix A

A.1 Experimental decay curves

Figures A.1.1, A.1.2, A.1.3, A.1.4 and A.1.5 show the fluorescence decay curves, for FR636 dyes covalently bonded to PAH chains and covered by 2, 4, 6, 8 and 10 PSS/PAH bilayers, respectively. In every picture, the experimental data is reported for all different excitation-detection polarization combinations. The preparation of the samples is described in chapter 4, section 4.3.

A.2 Statistical error evaluation for $\Delta\theta$

To evaluate $\Delta\theta$ for each sample, the sum over the polarization combinations of the squared differences between experimental and simulated intensities is minimized. According to the equation 4.6.4 in section 4.6.1, the expression used was:

$$\triangle I(\triangle\theta,\alpha) = \sum_{pol} \triangle I_{pol} = \sum_{pol} (I_{0exp}^{pol} - \alpha \cdot I_{0sim}^{pol})^2 \rightarrow minimum \tag{A.2.1}$$

Also, according to equation 4.6.9 in section 4.6.1, it was possible to determine (Γ_{nr}/Γ_0) by the same principle applied to lifetimes:

$$\triangle\tau(\frac{\tau_0}{\gamma},\Gamma_{nr},\triangle\theta) = \sum_{pol} (\tau_{exp}^{pol} - \frac{\tau_0}{\gamma} \cdot \tau_{sim}^{pol})^2 \rightarrow minimum \tag{A.2.2}$$

In general for a finite number of observations of a variable x the variance can be calculated by:

$$\sigma = \sum_{\substack{all \\ measurements}} p_i \cdot (x_i - \mu)^2 \tag{A.2.3}$$

where μ is the mean value of the measurements and p_i is the frequency (number of occurence) relative to each experimental point x_i. In the limit of infinite number of measurements, considering the statistical error as casual variable, the number of occurence tends to the normal distribution and μ to the real value of the variable. In this regards, as a consequence of the Central Limit Theorem, it is possible to represent the probability distribution of a x variable by a Gaussian with mean value μ and variance σ,

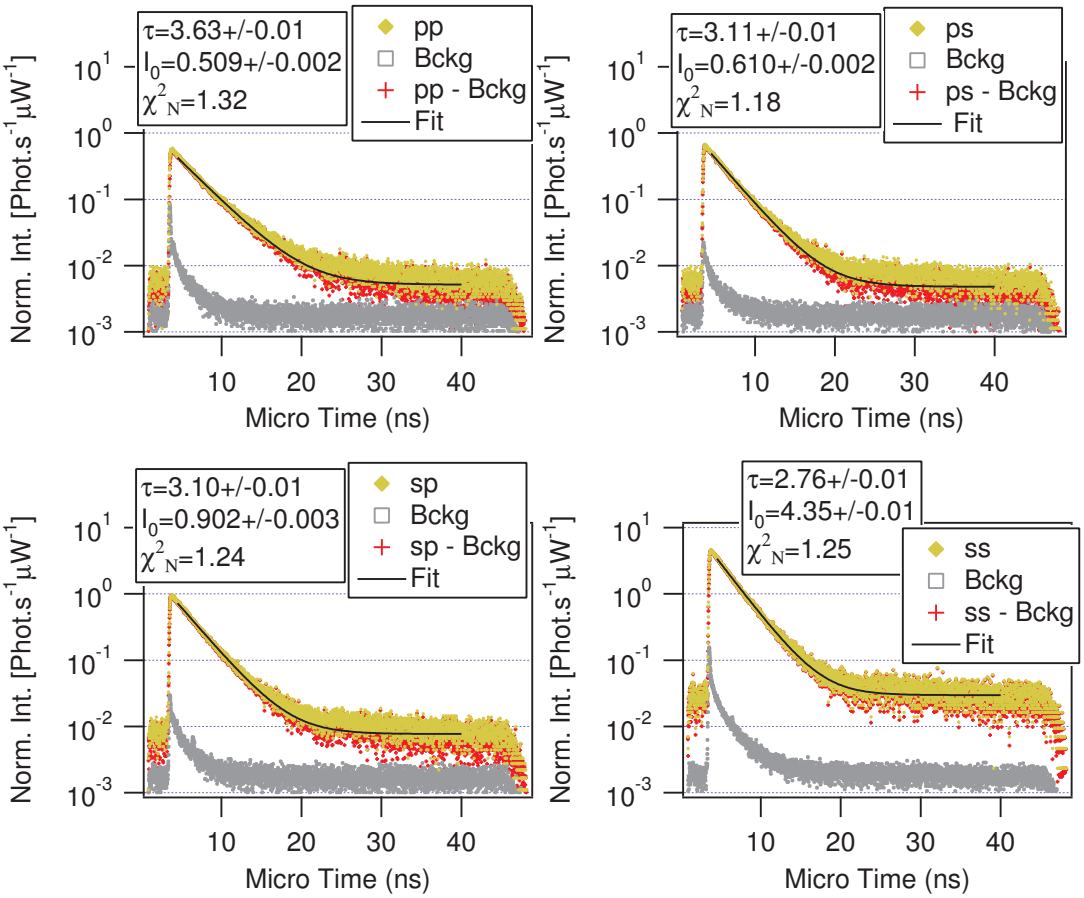

Figure A.1.1: Experimental fluorescence decay curves for FR636 dyes covalently bonded to PAH chains and covered by 2 PSS/PAH bilayers. Different excitation-detection polarization combinations are considered, as indicated in the legends. Instrument background (squares), experimental data with background subtracted (crosses) and correspondent fits are also reported. Lifetimes (τ, in ns), intensities at time $t_0 = 3.8\,\text{ns}$ (I_0, in phot./(s $\cdot\,\mu$W)) and normalized χ^2 values for the curves fit are shown.

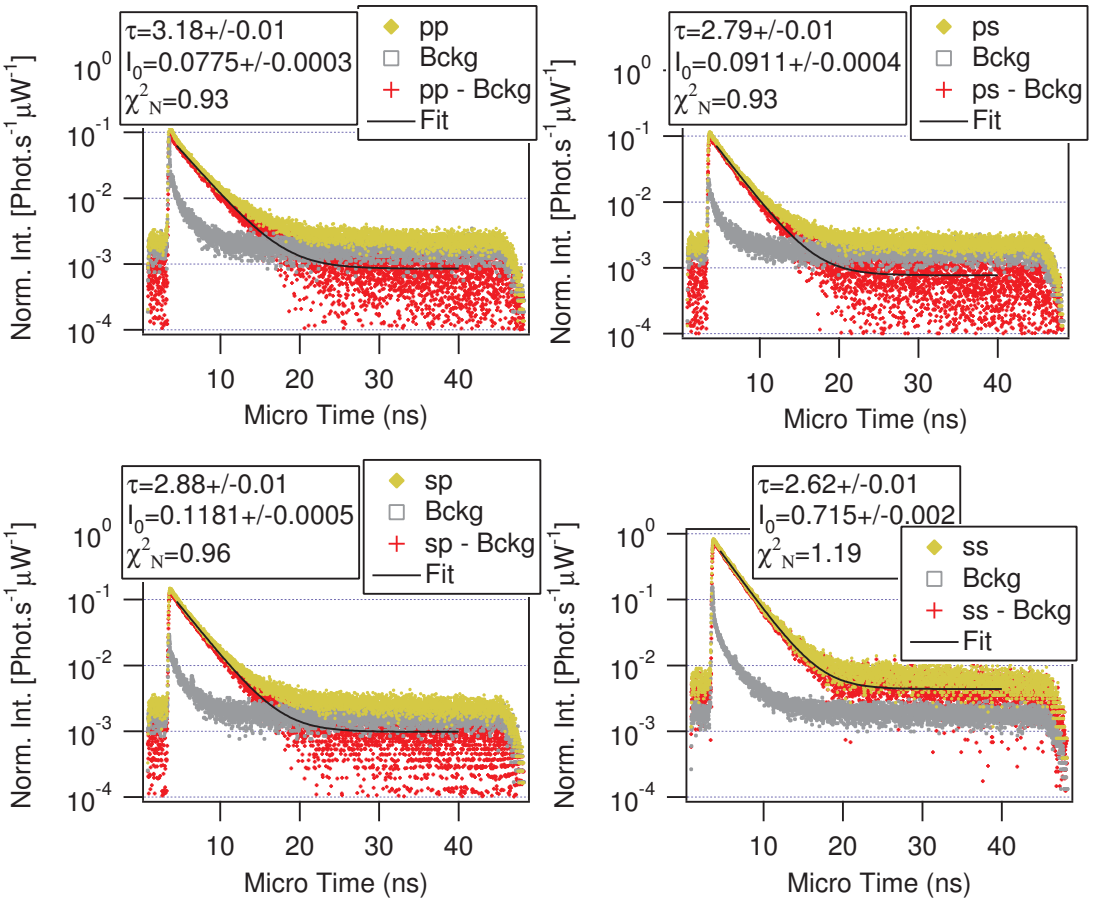

Figure A.1.2: Experimental fluorescence decay curves for FR636 dyes covalently bonded to PAH chains and covered by 4 PSS/PAH bilayers. Different excitation-detection polarization combinations are considered, as indicated in the legends. Instrument background (squares), experimental data with background subtracted (crosses) and correspondent fits are also reported. Lifetimes (τ, in ns), intensities at time $t_0 = 3.8\,\text{ns}$ (I_0, in phot./$(\text{s}\cdot\mu\text{W})$) and normalized χ^2 values for the curves fit are shown.

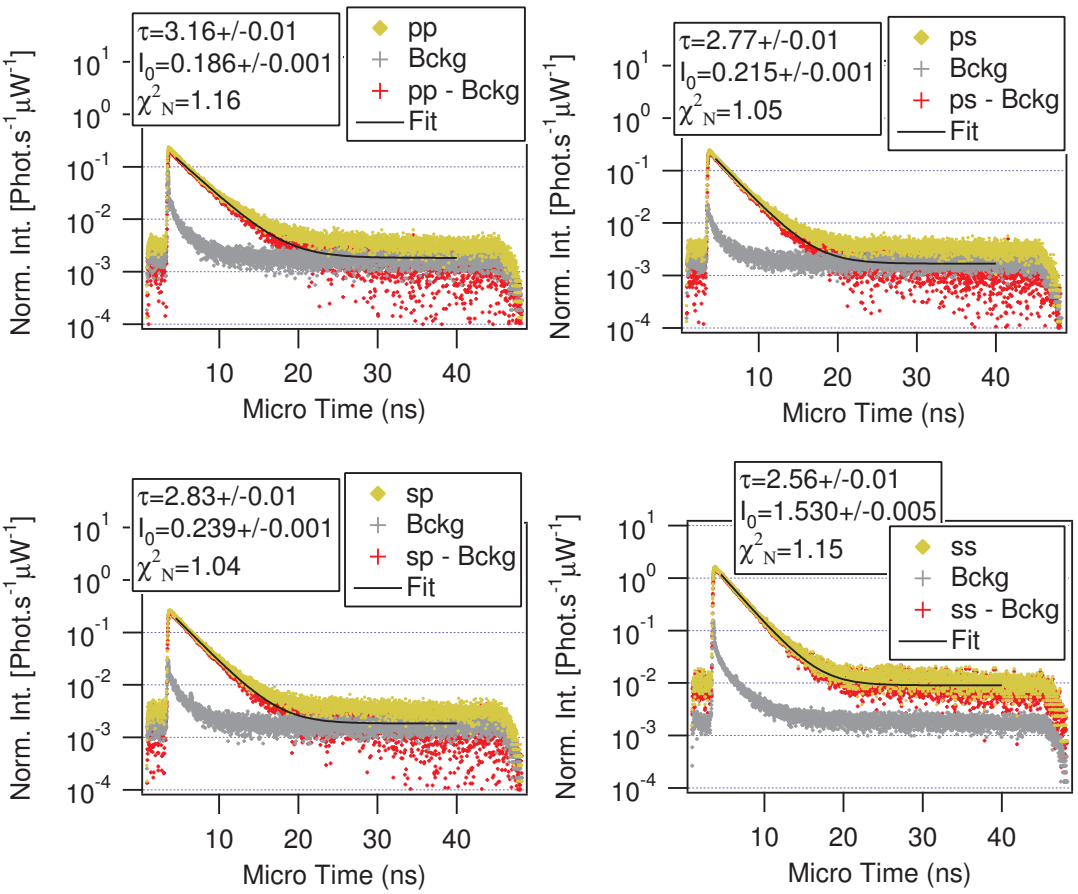

Figure A.1.3: Experimental fluorescence decay curves for FR636 dyes covalently bonded to PAH chains and covered by 6 PSS/PAH bilayers. Different excitation-detection polarization combinations are considered, as indicated in the legends. Instrument background (squares), experimental data with background subtracted (crosses) and correspondent fits are also reported. Lifetimes (τ, in ns), intensities at time $t_0 = 3.8\,\text{ns}$ (I_0, in phot./$(\text{s}\cdot\mu\text{W})$) and normalized χ^2 values for the curves fit are shown.

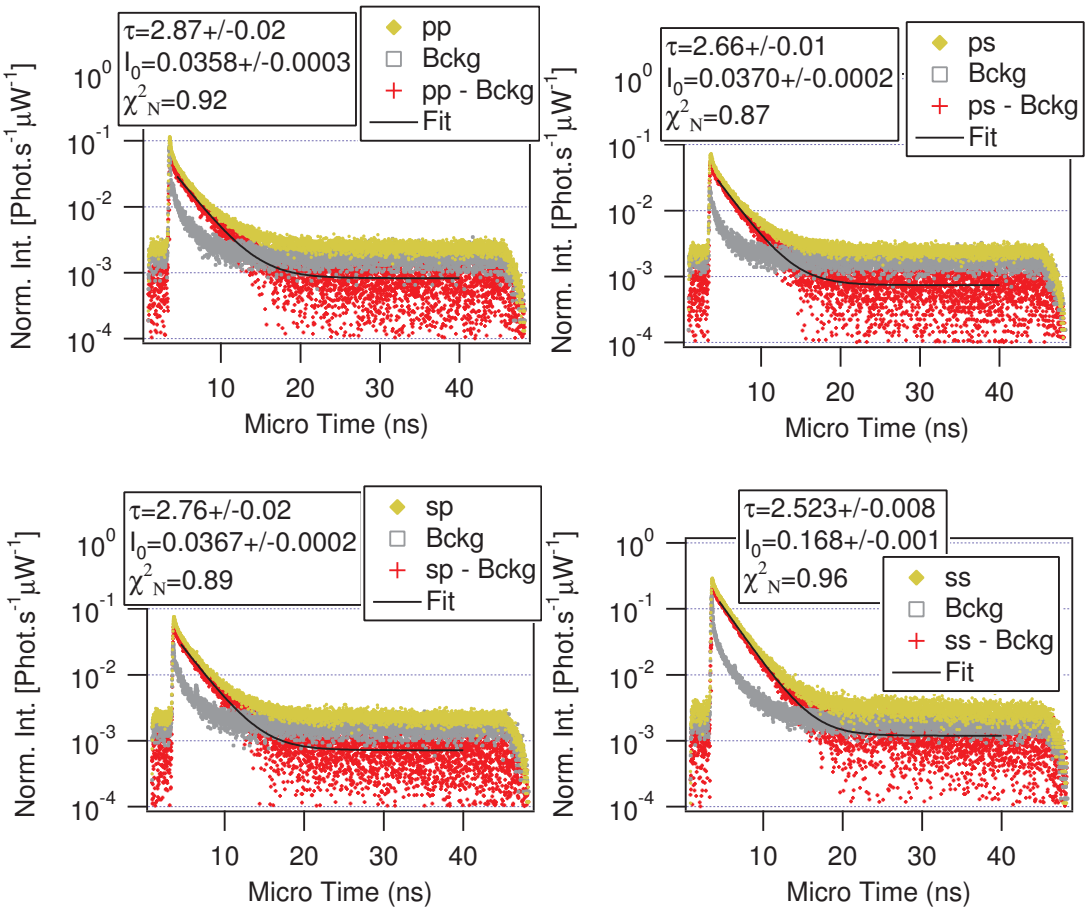

Figure A.1.4: Experimental fluorescence decay curves for FR636 dyes covalently bonded to PAH chains and covered by 8 PSS/PAH bilayers. Different excitation-detection polarization combinations are considered, as indicated in the legends. Instrument background (squares), experimental data with background subtracted (crosses) and correspondent fits are also reported. Lifetimes (τ, in ns), intensities at time $t_0 = 3.8\,\text{ns}$ (I_0, in phot./$(\text{s}\cdot\mu\text{W})$) and normalized χ^2 values for the curves fit are shown.

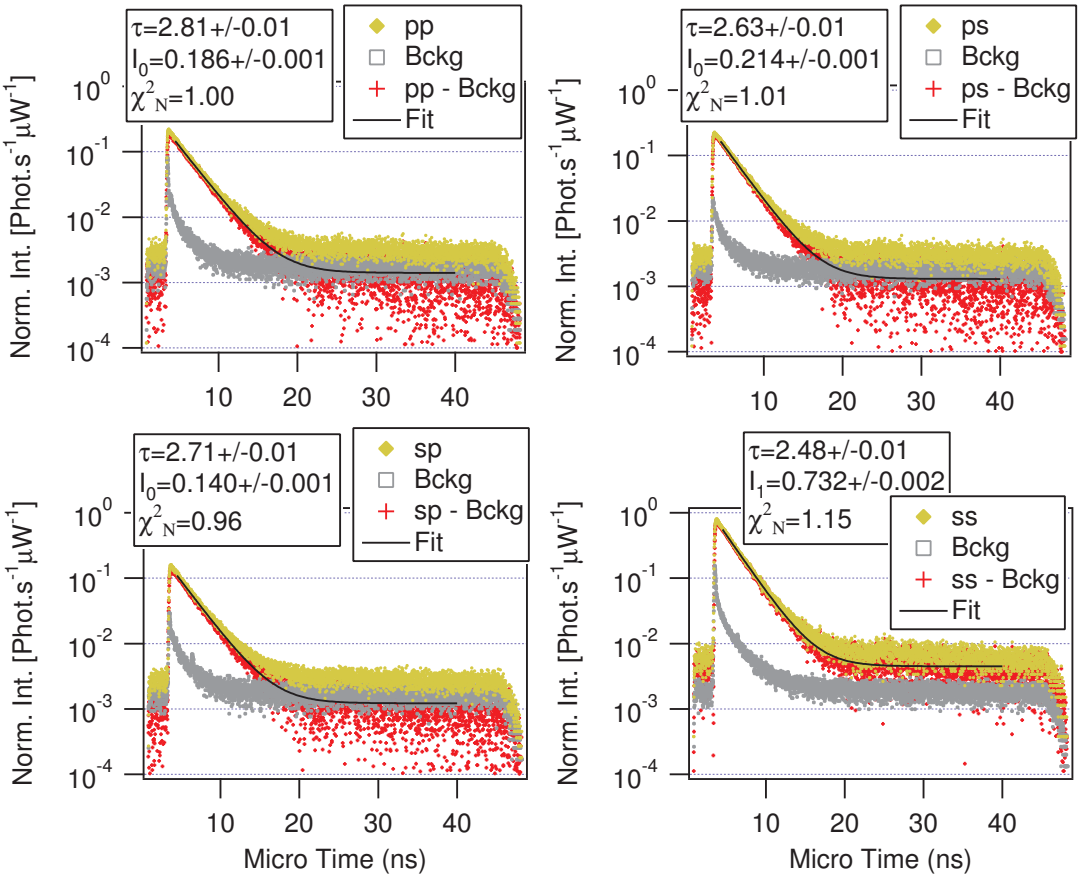

Figure A.1.5: Experimental fluorescence decay curves for FR636 dyes covalently bonded to PAH chains and covered by 10 PSS/PAH bilayers. Different excitation-detection polarization combinations are considered, as indicated in the legends. Instrument background (squares), experimental data with background subtracted (crosses) and correspondent fits are also reported. Lifetimes (τ, in ns), intensities at time $t_0 = 3.8$ ns (I_0, in phot./(s $\cdot \mu$W)) and normalized χ^2 values for the curves fit are shown.

$$F(x) = \frac{1}{\sigma\sqrt{2\pi}} \cdot e^{-\frac{(x-\mu)^2}{2\sigma^2}} \tag{A.2.4}$$

By definition, the variance for a distribution of events is given by the second central moment:

$$\sigma^2(\mu) = \int_{-\infty}^{+\infty} dx\,(x-\mu)^2 \cdot F(x). \tag{A.2.5}$$

The variance is the area under the curve $G(\mu,x)$:

$$G(\mu,x) = \int dx\,(x-\mu)^2 \cdot F(x). \tag{A.2.6}$$

The function $G(\mu,x)$ in equation A.2.6 represents the distribution of the squared differences for the entries with respect to the real value and a generalization of equation A.2.3 to the case of continuum (infinite number of measurements). From equation A.2.6 it is possible to evaluate the ordinate $G(\mu,\mu)$ and $G(\mu,\mu+\sigma)$ and thus obtain in the most general case:

$$\frac{G(\mu,\mu+\sigma)}{G(\mu,\mu)} \cong 2. \tag{A.2.7}$$

Therefore for a variable with Gaussian probability distribution like in equation A.2.4, the distribution of the associated squared differences $G(\mu,x)$ (eq. A.2.6) has a minimum for $x=\mu$ and a value $\simeq 2$ times higher for an abscissa value as far as σ from μ.

For each polarization combination a single measurement was performed and therefore only a rough comparison cen be done between equations A.2.1, A.2.2 and equation A.2.6. In addition, each term in the sums A.2.1 and A.2.2 contains different experimental values (i.e. different μ values), each one for different polarization combinations. Nevertheless, by making use of the scaling factors α and $(\frac{\tau_0}{\gamma})$, it is possible to consider such differences only with respect to one mean value (like in eq. A.2.6). In this way the minimization process is reduced to one mean value and 4 experimental entries. Figure A.2.1 depicts a sketch of this reduction process to one mean value (for intensities).

Moreover, in the case of the evaluation of $\Delta\theta$ and (Γ_{nr}/Γ_0), it assumed that the experimental measurements are close to the correspondent real physical values. It is also assumed that the intensities and liftimes are distributed around the real values following a Gaussian distribution in the limit of infinite measurements. In this way an equivalence between equations A.2.1, A.2.2 and A.2.6 is restored. As a consequence, the abscissae of the intersections between the $\triangle I(\triangle\theta,\alpha)$ and $\triangle\tau(\frac{\tau_0}{\gamma},\Gamma_{nr},\triangle\theta)$ curves and an ordinate value larger than two times the curves minima are separated by an abscissa value as large as σ.

A.3 FR636 dye solution characterization

A.3.1 Fluorescence lifetime in solution.

In figure A.3.1, the experimental fluorescence decay curves are plotted for the FR636 organic dye dissolved in DMF (dimethylformamide) solvent (a) and in ultra pure H_2O (b), for different dye concentrations. The curves are normalized to the excitation intensities and to the collection time. The

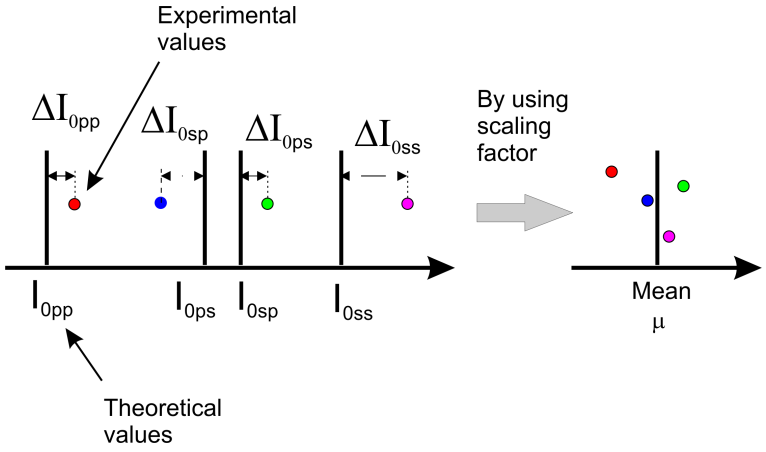

Figure A.2.1: Equivalence of the minimization process schematization by making use of the α parameter in equation A.2.1.

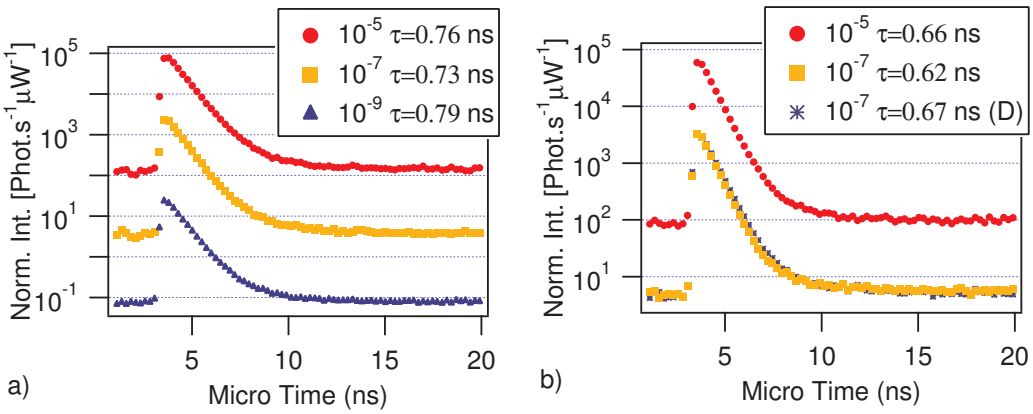

Figure A.3.1: Fluorescence decay curves for different concentrations of FR636 in DMF solution (a) and in ultra pure H_2O (b). The curve labelled with D in the legend in (b) is for a concentration in water of $\sim 10^{-7}$ M, but prepared by diluting a dye solution in DMF at $\sim 10^{-5}$ M. In the legends the lifetimes coming from a fit of the curve are indicated.

curve labelled with D in the legend in (b) is for a dye concentration in water at $\sim 10^{-7}$ M, but prepared by diluting a dye solution in DMF at $\sim 10^{-5}$ M.

From figure A.3.1 a clear difference among the samples is not detected: it may be blurred by the interactions dye-solvent which dominate. Moreover, the excited-state lifetime values are concentration independent and much smaller than within a solid matrix. As a conclusion, the fluorescence lifetimes measurements in solution for different solvents and different dye concentrations do not provide discriminating information on eventual chromophore clusters formation.

A.3.2 Fluorescence spectra

Figure A.3.2 shows the excitation fluorescence spectra (EX) detected at 740 nm and the emission fluorescence spectra (EM) obtained by excitation wavelength of 610 nm, for FR636 dye molecule dissolved in H_2O and DMF. The spectra for different dilution concentrations are reported, with indication of the maxima position in nanometers for absorption and emission peaks. The measurements were performed by a fluorescence spectrometer (Spex Fluorolog II - 212) by using slits aperture of 2 mm for the samples at 10^{-5} M, while the value was set to 8 mm for samples at 10^{-7} M. In figure A.3.2 d) a comparison between two solutions in water at 10^{-7} M is displayed: one is obtained by diluting an aqueous solution with a dye concentration of 10^{-5} M, while the other (curves labelled with *D* in legend) is obtained by diluting a DMF solution at 10^{-5} M.

Figures A.3.2 a) and c) show that for a dye concentration of 10^{-5} M, the excitation and emission efficiency are slightly higher in DMF than in H_2O. Figures A.3.2 b) and d) indicate that the opposite situation occurs, when going down to a concentration of 10^{-7} M. In water, it is possible to notice a small blue shift going from 10^{-5} M to 10^{-7} M, with the absorption and the emission processes showing a comparable efficiency. For DMF the lowest concentration does not provide a clear spectrum, while at 10^{-5} M an overall red shift of excitation and emission peaks with respect to the water case occurs. At the end no clear conclusions could be taken from spectra analysis, also due to lack of information for DMF at 10^{-7} M. Based on the other spectra the interpretation is not straightforward and univocal.

A.4 Samples post-deposition treatment

A.4.1 Rinsing Step

In figure A.4.1 fluorescence lifetime and intensity trends as a function of samples rinsing mode are plotted. The functionalized polymer was deposited by a pH ~ 7 water solution onto a $SiSO_3^-$ substrate, without any salt addition, by a two step process: initially the sample was immersed in the dye loaded solution for ~ 70 minutes, then rinsed once by ultra pure water and dried by a N_2 stream. Afterwards, the sample was dipped again in the same solution and left there overnight. The following day different rinsing steps in ultra pure water were applied and the fluorescence was measured. It was tested that this kind of deposition process guarantees a higher amount of non specific adsorbed polymer and therefore a reliable fluorescence signal can be detected by far field measurements.

From figure A.4.1 it is clear that the fluorescence intensity decreases with successive rinsing steps, even if a partial contribution from photobleaching should be considered, being the same sample utilized in the study. A possible hyphotesis could be that initially there is no monolayer formation and the non-specific adsorbed polymer is removed from the surface by successive rinsing steps. The fluorescence lifetime in figure A.4.1 increases and apparently hits a limit value already after roughly

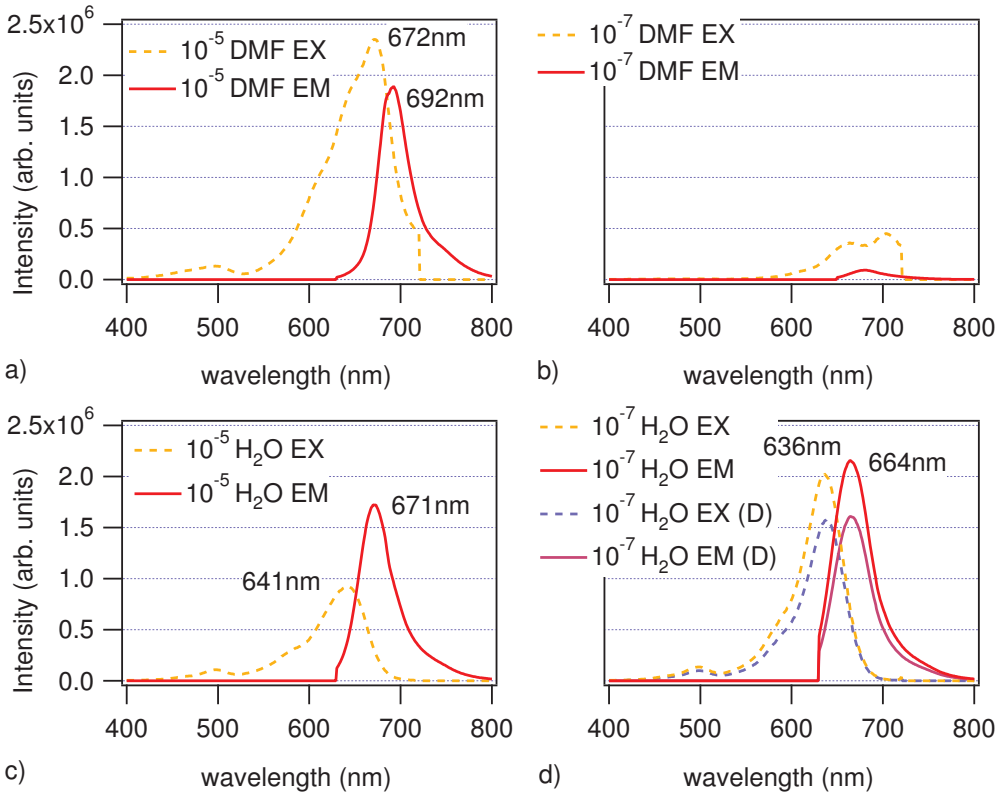

Figure A.3.2: Excitation fluorescence spectra (EX) at 740 nm and emission fluorescence spectra (EM) obtained by excitation at 610 nm, for FR636 dye molecules in H_2O and DMF solvents. In the figures the correspondent peaks maximum position is also indicated. The spectra are for different dilution concentrations, as indicated in the legends. For the samples at 10^{-7} M in b) and d), the spectrometer slits aperture was changed from 2 mm, used for a) and c) measurements, to 8 mm. The curves in d) labelled by D indicate samples prepared by diluting a dye solution in DMF at 10^{-5} M.

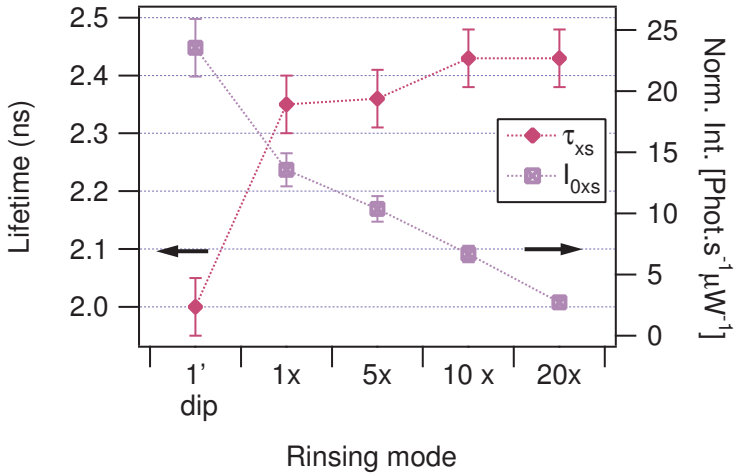

Figure A.4.1: Fluorescence lifetime and intensity for unpolarized excitation (x) and *s* polarized detection, as a function of the samples rinsing mode in ultrapure water, after two successive depositions of the dye loaded polymer on a $SiSO_3^-$ substrate. The lines between the points are meant just as a guide to the eye. The rinsing steps are cumulative for the same sample. The abscissa shows the different rinsing modes: 1 minute by immersion and $1, 5, 10, 20$ times rinsing by shaking the sample in water. The experimental error of the lifetime is ± 0.05 ns, while for intensity it is 10%.

$\sim 5-10$ rinses: the constant lifetime value may indicate absence of dye-dye interaction on the substrate and therefore larger average distances among the chromophores. This may support the picture of polymer chains removal from the surface by progressive rinses. Qualitative fluorescence intensity trends as a function of the number of rinsing steps and for different surface charge densities are shown in figure A.4.2. The skecth may provide a picture of the physical effect behind the rinsing effect (in figure A.4.1) and explain the differences in detected fluorescence intensities for different substrates (like in figures 5.6.15).

The purpose of figure A.4.2 is to provide an approximative idea of the physical variable involved in the samples preparation procedure, making clear the necessity to have as much high as possible surface charge density (in figure indicated by $n_{0-PSS}, n_{0-SiSO3}$ and $n_{0-Fused\,Silica}$). In this way it could be possible to obtain a reliable fluorescence intensity and at the same time a single monolayer of polymer on the substrate, after the necessary rinsing steps.

The curves in figure A.4.2 depend also on pH and salt concentration in the deposition water solution, but a detailed analysis as a function of those parameters is beyond the purposes of this work. It is interesting to notice that the curves in figure A.4.2 provide a reasonable justification for the differences in fluorescence intensity detected by different substrates and at the same time explain in a consistent way the trends obtained in figure A.4.1.

A.4.2 Residual Water Issue

In figure A.4.3 experimental lifetimes (a) and intensities (b) are reported for *ss* polarization and different pH values of the deposition solution, without addition of salt except for pH = 9.4 (2 M of NaBr). The samples are constituted by FR636-dye loaded PAH chains deposited onto a $SiSO_3^-$ surface, by dipping the substrates overnight in the functionalized polymer solution. The next day the samples were rinsed once by ultrapure water, dried by an N_2 stream and successively lifetime and intensities

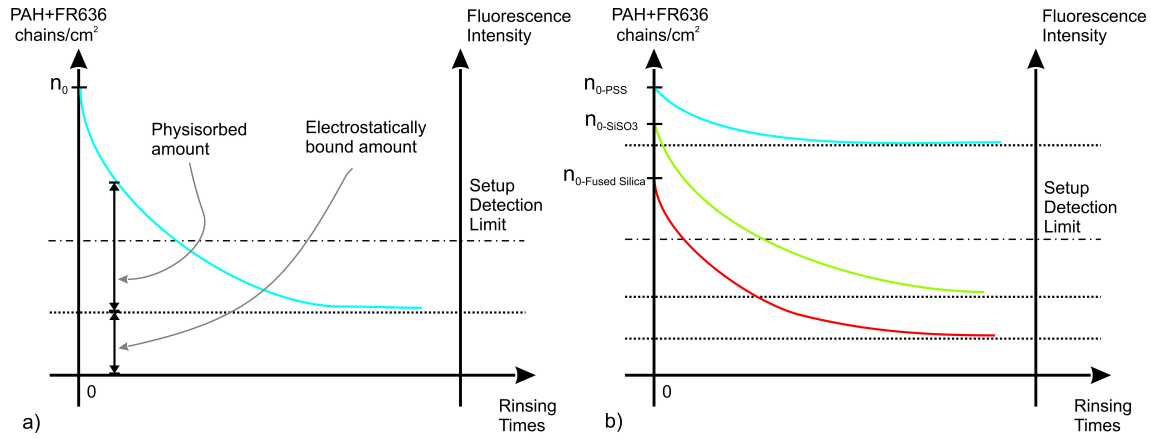

Figure A.4.2: a) Qualitative sketch of the functionalized polymer chains density on a generic sample substrate and related fluorescence intensity detected, as a function of the number of rinsing cycles. n_0 represents the maximum density of chains on the generic surface after deposition, without any rinse. b) Same qualitative plot as in a) for three different substrates: PSS polyelectrolyte, $SiSO_3^-$ and fused silica. The dashed-dotted horizontal line indicates a hypothetical value for the setup detection limit (instrument sensitivity).

were measured. The slides were afterward left at room conditions for ~ 6 hours and measurements were repeated on the same sample spot.

Figure A.4.3 a) and b) show remarkable differences after ~ 6 hours from the first measurement for low values of pH, while for higher pH the effect is small for the lifetimes and negligible for the intensities. The variations could be caused by the presence of residual water in the substrate, acting as a quencher for fluorescence. Therefore lower lifetimes and intensities values are obtained. For basic deposition solution or with high concentration of salt added, the charges shielding effect may reduce the amount of trapped water (reduced electrostatic trapping and hydrogen bonds formation with polymer chains and substrate).

Figure A.4.4 reports a detail of the decay curves measured right after polymer deposition and after ~ 6 hours, keeping the substrate at room conditions, for the sample with pH $= 7.5$ (see also figure A.4.3). Comparing the two decay curves in figure A.4.4, it is possible to observe the large variation in total intensity (integral under the curve) and lifetimes (reciprocal of slope). The curves detail also shows the multi-exponential character of the decay curve, for measurements performed right after polymer deposition. By the vertical dashed line in figure A.4.4, approximatively two fluorescence regimes were identified: before ~ 4 ns the signal contribution comes mainly from dyes having a very short lifetime ($\lesssim 0.3$ ns), while for micro time values larger than ~ 4 ns, fluorescence is generated mainly by chromophores having a lifetime of ~ 2 ns. The large difference of slopes between the two parts of the curve (in a ratio ≈ 7), can not be explained by different dipole orientations (see section 5.2). Thus, the reasons of such a decay trend have to be searched in the interaction of the dyes with the external environment.

From figure A.4.4 the single exponential behaviour of the decay curve is found after ~ 6 hours. For this sample the fluorescence intensity is higher. From the almost single exponential characteristic of the decay curve and considering that the PAH layer has a thickness of ≈ 2 nm, it is believed that the decay curve after ~ 6 hours represents an equilibrium condition of the sample.

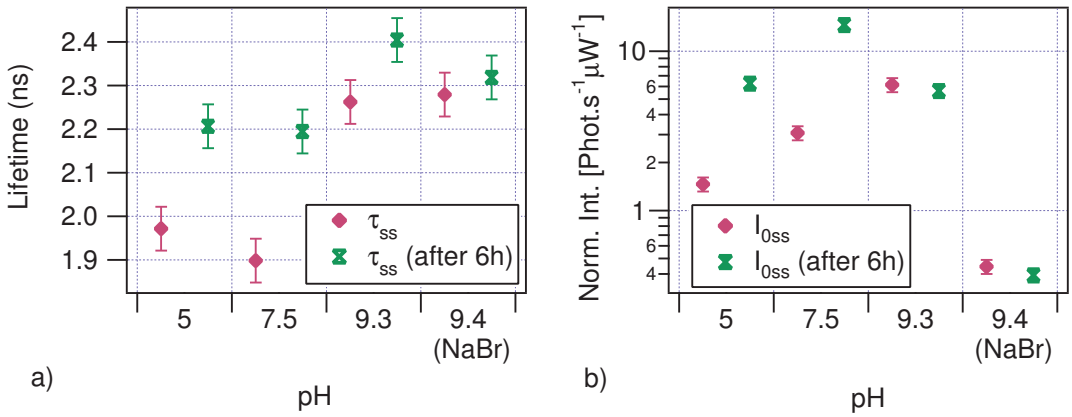

Figure A.4.3: Fluorescence lifetimes (a) and intensities (b) for *ss* polarization as a function of the pH value of the deposition solution, onto a $SiSO_3^-$ substrate. The different solutions containing the functionalized PAH are without any salt, except for the sample at pH = 9.4, containing 2 M of NaBr. The samples are measured directly after polymer deposition and after $\sim$ 6 hours, keeping the substrates at room conditions. Error of the lifetimes is $\pm$0.05 ns, while the error on intensity is 10%.

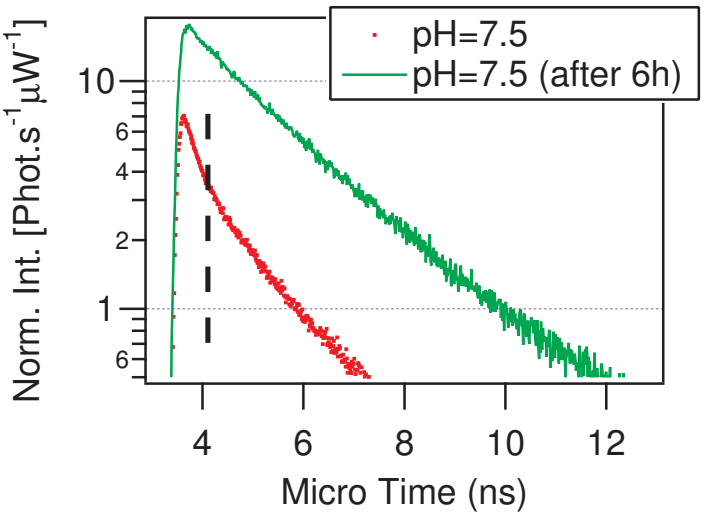

Figure A.4.4: Fluorescence decay curve for *ss* polarization, right after polymer deposition and after $\sim$ 6 hours, with the substrate stored at room conditions. Sample details are in the text.

Sample	Ar(mbar)	O_2(mbar)	Power(W)	Time(s)	C.A.(Â°)	C.A.(Â°) 1d	RMS(nm)
1	0.9	0.2	150	600	12	20	0.655
2	0.9	0.2	300	600	<5	23	0.687
3	1.5	0.2	300	600	<5	18	0.462
4	0.2	0.1	150	600	<5	<5	0.468

Table A.5.1: Plasma recipes for fused silica glass surface activation. The relative contact angles measurements (C.A.) right after the treatment and 1 day later (1d) are shown. The angles values are the average over two different spots on the samples surface. Surface roughness values (RMS) obtained by AFM are also displayed.

A.5 Surface Activation by Plasma Process

Four plasma recipes were created like described in table A.5.1 and applied to cleaned fused silica slides (for cleaning procedure see section 5.4.1) by a plasma reactor (Tepla GmbH, 200-G Plasma System). Right after the process and also the following day, the samples were characterized by contact angle measurements to test the surfaces hydrophilicity degree. The results are shown in table A.5.1.

The fused silica surfaces were investigated, after the plasma treatment, by AFM (Dimension 3100 CL NS IV Controller - Cantilever Typ: Olympus non-contact mode OMCL-AC160TS-W2 $K = 42\,N/m$, range: $33.5 \div 94.1\,N/m$), to check the surface average roughness and possible defects formation. The AFM images did not show any presence of defects for any sample. The relative root mean square values (RMS) for glass surface flatness are reported in table A.5.1. The plasma recipe applied to sample 4 presents the best results in term of hydrophilicity (number of OH^- groups activate onto the surface), charge stability in time and average roughness: as it is possible to notice from table A.5.1.

In figure A.5.1 a comparison is shwon among the fluorescence decay curves for FR636 dyes chemically bond to PAH chains. The functionalized chains are deposited respectively on a blank fused silica substrate on a plasma activated and on a chemically activated fused silica substrates. The chemical treatment is the one used for the substrate preparation in the section 5.4.1. All the glass slides before treatment underwent the standard cleaning procedure described in the same section. In all cases the functionalized PAH was deposited by the dipping technique using ~ 1 hour as immersion time and a $pH = 3$ solution. Finally, the samples were rinsed 10 times in ultra pure water and successively dried by a N_2 stream.

The data shown in figure A.5.1 are for *pp* excitation-detection polarization combinations, other polarization combinations provide same results in terms of intensities comparison and are not reported here. In the case of plasma activation, figure A.5.1 indicates an increase of the fluorescence signal up to a factor $\sim 2-3$, most probably related to a larger amount of polymer adsorbed on the fused silica cover slip.

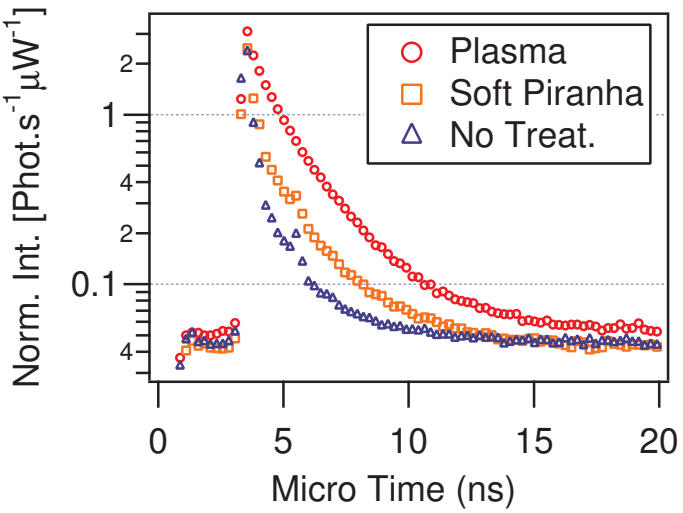

Figure A.5.1: Comparison of the decay curves for PAH chains functionalized by FR636 dye and deposited directly on a glass substrate (No Treat.), on a glass surface chemically treated (Soft Piranha) and on a glass surface activated by plasma process (Plasma). The data is shown for the *pp* excitation-detection polarization combination.

A.5.1 Silanization Optimization by Plasma Treatment

A test was performed to optimize the glass activation before the silanization process. The chemical treatment reported in section 5.4.1 was compared with a plasma treatment (recipe no. 4 in table A.5.1), based on the of fluorescence characteristic of the dye loaded polymer (deposited above the $SiSO_3^-$ silanes). Figure A.5.2 depicts the comparison based on fluorescence lifetime and intensity of dyes chemically bond to PAH and deposited onto a $SiSO_3^-$ surface for two different glass substrate treatments (piranha treatment and plasma treatment). After silanization, the dye loaded polymer was deposited at pH = 7.5 on top of both samples. Then, the slides were rinsed once in ultrapure water and dried by N_2. The fluorescence was measured directly afterwards.

From figure A.5.2 it is possible to conclude that the two glass activation methods provide similar results for lifetimes. An improvement of a factor ~ 2 in the intensity for the plasma process is present.

A.6 Igor Routines

Several routines were written by using the software package IGOR (Ver. 5.05, WAVEMETRICS Inc.) to:

- calculate theoretically the excited-state lifetime and fluorescence intensity values, for an ensemble of dye molecules in stratified media.
- extract, analyze and fit the measured data, as collected from the TCSPC card.

Due to the large number of routines and to the length of each single procedure, the sources codes have not been included here for practical reasons. The source codes can be obtained, by sending an e-mail to: pomozzi@mpip-mainz.mpg.de

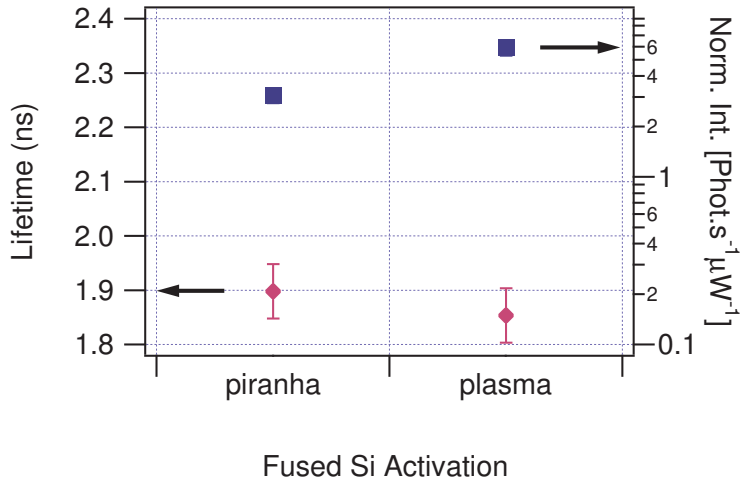

Figure A.5.2: Measured fluorescence lifetime and intensity for *ss* polarization combination, as a function of the glass activation procedure used. The different solutions containing the functionalized polymer are without any salt at pH = 7.5. The recipes details are in the text. Errors on lifetime is ± 0.05 ns, while error on intensity is 10%.

A.7 Acronyms and Symbols

3-APTES	(3-Aminopropyl)-triethoxysilane
CPS	Chance-Prock-Silbey theory
c	concentration
$\Delta\theta$	Excitation-emission dipoles relative angle
DMF	Dimethylformamide
ε	Dielectric constant
FWHM	Full Width Half Maximum
Γ_0	Decay Rate in Vacuum
Γ_r	Radiative Decay Rate
Γ_{nr}	Non-Radiative Decay Rate
Γ_{tot}	Total decay rate
$\Gamma_\perp$	Decay rate for a perpendicular orientation with respect to an interface
$\Gamma_\parallel$	Decay rate for a parallel orientation with respect to an interface
I_0	Fluorescence intensity evaluated at time t_0
IRF	Instrument Response Function
M_w	Molecular Weight

n	Refractive Index
PAH	poly(allylamine hydrochloride)
PCM	Polarization Combination Method
PMT	Photomultiplier
PSS	poly(styrene sulfonate)
RMS	Root Mean Square
S/B	Signal to Background Ratio
SPR	Surface Plasmon Resonance
t_0	Micro time of excitation δ-like pulse
t_b	Micro time of beginning of the fit interval
τ	Excited state lifetime
TCSPC	Time Correlated Single Photon Counting
TE	Transverse Electric
TIR	Total Internal Reflection
TM	Transverse Magnetic

Acknowledgments